BRNO UNIVERSITY OF TECHNOLOGY
VYSOKÉ UČENÍ TECHNICKÉ V BRNĚ

FACULTY OF MECHANICAL ENGINEERING
FAKULTA STROJNÍHO INŽENÝRSTVÍ

INSTITUTE OF SOLID MECHANICS, BIOMECHANICS AND MECHATRONICS
ÚSTAV MECHANIKY TĚLES, BIOMECHANIKY A MECHATRONIKY

STRESS-STRAIN ANALYSIS OF CAROTID ARTERIES WITH ATHEROMA
DEFORMAČNĚ-NAPĚŤOVÁ ANALÝZA KAROTICKÝCH TEPEN S ATEROMEM

DOCTORAL THESIS
DIZERTAČNÍ PRÁCE

AUTHOR — **Ing. Ondřej Lisický**
AUTOR PRÁCE

SUPERVISOR — **prof. Ing. Jiří Burša, Ph.D.**
VEDOUCÍ PRÁCE

BRNO 2022

Abstrakt

Kardiovaskulární příhody byly a jsou rozšířenou příčinou úmrtí ve většině zemí. Ateroskleróza karotických tepen mnohdy vedoucí k mrtvici je jejich nedílnou součástí. Včasná a vhodně mířená diagnostika rizikových lézí může vést ke snížení kritických příhod, a tím potenciálně snížit počet úmrtí. Porušení nestabilního aterosklerotického plátu je ovlivněno působením sil od proudící krve. V biomechanice měkkých tkání je využíváno výpočtového modelování jakožto potenciálního ukazatele, díky němuž by bylo možné odhalit nestabilitu plátu u pacientů podstupujících pravidelná kontrolní měření. Mechanické veličiny bývají spojovány s klinicky dostupnými ukazateli jako jsou například podstatné rozměry léze nebo přítomnost rizikových komponent. Komplexita a malé rozměry tkáně ovšem stále omezují možnosti tvorby výpočtových modelů a existuje tedy spousta faktorů, které je před možnou implementací do klinických postupů potřeba řádně vyšetřit. Tato práce je členěna do kapitol shrnujících aktuální stav řešené problematiky. Kapitoly jsou doplněny o komentář autorova příspěvku k dané problematice a odkaz na originální práci. Studium problematiky naznačilo velké množství potenciálních směrů výzkumu, což by ovšem nebylo možné zahrnout do jediné práce. Řešená témata se dají rozdělit na: (i) ověření možnosti tvorby 3D výpočtového modelu ze snímků aterosklerotického plátu s následným rozšířením na výpočtovou studii zahrnující řadu faktorů pro ověření vlivu na napjatost, (ii) studium mechanických vlastností aterosklerotických plátů odebíraných z endarterektomie během celé doby řešení, (iii) možnosti analýzy deformačního pole u experimentů zahrnujících měkké tkáně a (iv) experimentální a výpočtovou studii zbytkové deformace, potažmo napětí v souvislosti s karotickými tepnami. Výsledky jednotlivých částí jednoznačně poukázaly na problémy spojené s výpočtovým modelováním jako například časté opomíjení přítomnosti komponent stěny tepny při modelování aterosklerotického plátu, nutnost správného pochopení mechanického chování, ale také na způsob vyhodnocení experimentů s vyšším počtem vzorků. V neposlední řadě bylo ukázáno, že zbytkové napětí nemusí být podstatným faktorem u aterosklerotických plátů karotických tepen.

Summary

Health risks associated with cardiovascular diseases are apparent in many countries' high mortality rates. Atherosclerosis in carotid arteries can cause a stroke and contributes thus in a large extent. Early detection of risky lesions is substantial to prevent an incident. The forces from the blood flow influence a rupture of a vulnerable plaque. The biomechanics of soft tissue is often incorporated with computational modelling as a potential tool to predict the plaque vulnerability for patients who underwent screening. Mechanical characteristics can then be correlated with clinical biomarkers such as crucial plaque dimensions or the presence of some risky component. However, the plaque complexity, together with a small size, influences a proper model creation leading to simplifications with an unknown effect on the mechanical characteristics. To incorporate computational modelling as a potential diagnostic tool, this is to be solved. The thesis is structured into chapters describing state of the art in computational modelling of atherosclerotic tissue. Relevant chapters are completed with a description of the author's contribution with references to the original works. Many possible directions were discovered during the literature review, although their inclusion was possible only partly as it would require more than one thesis. The main topics of interest were: (i) creation of 3D models from imaging and their subsequent use in computational study augmented by other factors, (ii) study of mechanical properties of endarterectomy samples during the study period, (iii) study of full-field strain detection methods for soft biological tissue and (iv) experimental and

computational study of residual deformations and stresses of carotid arteries. The results of each part indicated problems related to computational modelling of atherosclerotic tissue, like omission of the arterial wall when the plaque stress-strain analysis is performed, the necessity of a proper understanding of mechanical responses, and its evaluation for more samples. Last but not least a negligible influence of layer-specific residual stresses for carotid plaques.

Klíčová slova
Ateroskleróza, karotida, konstitutivní modely, mechanické vlastnosti, výpočetní modelování, zbytková deformace, zbytkové napětí

Keywords
Atherosclerosis, carotid artery, constitutive models, mechanical properties, computational modelling, residual deformation, residual stress

LISICKÝ, Ondřej. *Deformačně-napěťová analýza karotických tepen s ateromem.* Brno, 2022. 94 s. Dizertační práce. Vysoké učení technické v Brně. Fakulta strojního inženýrství. Thesis supervisor Jiří BURŠA.

Prohlašuji, že jsem disertační práci *Deformačně-napěťová analýza karotických tepen s ateromem* vypracoval samostatně pod vedením prof. ing. Jiřího Burši, Ph.D., s použitím materiálů uvedených v seznamu literatury. Práce je psána v anglickém jazyce.

Ing. Ondřej Lisický

Rád bych poděkoval svému školiteli prof. ing. Jiřímu Buršovi, Ph.D.za odborné vedení, rady a profesionální přesto přátelský přístup během mého postgraduálního studia. Děkuji také svému školiteli specialistovi ing. Pavlovi Skácelovi, Ph.D. za cenné rady a připomínky k řešeným tématům. Poděkování patří také lékařům z II. chirurgické kliniky a I. patologického ústavu, bez jejichž pomoci by tato práce nebyla možná.
Velmi děkuji svým rodičům za jejich podporu během studia a také přítelkyni Míši, která mi byla po celou dobu nepředstavitelnou oporou. Dále děkuji všem kolegům a přátelům z fakulty za zpříjemnění celého studia a spoustu zábavy, které jsme si za tu dobu užili.
Tato práce vznikla za podpory projektu Grantové Agentury České Republiky 18-13663S a 21-21935S.

Ing. Ondřej Lisický

Contents

Introduction

Contemporary lifestyles with unhealthy eating and predispositions often result in health problems like cardiovascular diseases, leading causes of death in many countries. The global trend seems to decrease, which can be attributed partially to increasing causes of malignant neoplasms (cancer) but a more accurate diagnostics may help significantly. For asymptomatic patients, it is under coincidence whether problems are detected. Atherosclerosis affects most of arteries all along the body, e.g., coronary, carotid. Advanced plaques may rupture, resulting in clot formation with serious health problems. Early detection via imaging (computed tomography, magnetic resonance, ultrasound) provides a visual control where a level of stenosis (restriction in a blood flow) can be determined. Stenosis severity is still a primary factor for treatment guidance as it is easy to analyse its level and progression by frequent screening. Subsequently, the patient is advised to undergo carotid endarterectomy or stenting to prevent complete artery blockage or even plaque rupture, which might otherwise lead to fatal consequences. A closer examination of recent clinical trials indicates that current risk prediction is imprecise.

Consequently, patients (often +70 years) are exposed to risk during intervention even though they would not have gone on to have a stroke. Of course, it is unclear what risk would weight more, promoting and active research in this field. In order to enable early prediction of acute events, more accurate screening methods are necessary, introducing a variety of biomarkers. The role of mechanical forces is generally agreed in plaque progression and plaque rupture, although biomechanical stress-based indicators were not confirmed yet clinically to predict possible rupture. Our knowledge is based chiefly on ruptured plaques, which inspires geometry models and factors but the question whether these models can help us to predict future events is still far from being answered.

Nevertheless, we are still learning about new mechanisms inspiring experimental investigations. Moreover, the progression in imaging methods enables reconstruction of more complex computational models from *in vivo* data where we can benefit from the already gained knowledge, e.g., based on *ex vivo* inspired models. It would be ridiculous to believe that such a complex problem is solvable with a simple model. However, one should believe that every contribution could lead to a better understanding of disease plaguing us for a long time. As accurate predictive methods have not been established yet, the clinician has to decide about the treatment based on information from available technologies. We have to face this challenge and do our best to improve our methods and technologies.

The presented doctoral thesis was written as a commented collection of the author's publications and prepared works put into the state of the art of arterial biomechanics with atherosclerosis. The thesis is structured into chapters providing an insight into the specific fields related to the computational modelling of the plaques. The author's original contribution is incorporated with relevant chapters as a description of the author's contribution.

1.1. Motivation

The motivation for this study is to thoroughly investigate the up-to-date biomechanical problems related to atherosclerosis of the carotid artery and to contribute as much as possible to the project from Czech Science Foundation no. 18-13663S solved in the Institute of Solid Mechanics, Mechatronics and Biomechanics in cooperation with the St. Ann's Faculty Hospital in Brno. Endarterectomy, an invasive treatment performed daily in this hospital, emerges typically from acute (symptomatic) cases and may also be indicated during preventive imaging, where only stenoses satisfying current criteria are taken into consideration for intervention. Computational modelling may contribute to decision making and bring another insight into the problem. However, modelling is related to many factors such as geometry model or mechanical behaviour and the related constitutive description, which should be considered for an appropriate description of stress-strain states in arteries. Even though this problem is still related to the primary research, the practical impact on clinical practice is not negligible. It may extend the clinicians' expertise in further intervention or pre-operative detection.

1.2. Goals of the thesis

1. To perform a thorough literature search on up to date problems solved within the biomechanics of atherosclerotic plaque.
2. To develop a methodology for plaque reconstruction from medical images.
3. To perform a sensitivity study of factors influencing stress in computational modelling of atherosclerotic plaques.
4. Experimental investigation of mechanical behaviour of carotid plaque and wall components and its appropriate constitutive representation.
5. Experimental investigation of layer-specific residual deformation of carotid arteries.

Atherosclerosis - clinical view

A brief clinical introduction is presented in this chapter for better orientation in the problem. As the study focuses mainly on the diseased arterial tissue, an explanation of the cardiovascular system and healthy arterial tissue is not presented. However, many works discussed it extensively, see, e.g., Humphrey et al. (2002) and also in many dissertations (Man, 2018; Novák, 2018; Polzer, 2012) from the institute of the author.

2.1. Trigger for atherogenesis

Two contradictory hypotheses were proposed in the 1970s to explain the distribution of atherosclerotic lesions. Fry (1969) hypothesized a direct endothelial injury and denudation, caused by high shear stress (40 Pa), as a trigger for atherogenesis. On the other hand, Caro et al. (1971) suggested low shear stress as a more important attribute. Experimental study Zarins et al. (1983) with non-stenotic carotid bifurcations investigated the role of flow velocity profiles and shear stresses. Though very sensitive to Reynolds number, results indicated the low shear stress and complex flow profile were always found in regions where intimal thickening was detectable. Regions with negligible intimal thickening were followed mainly by high shear stress (up to 60 Pa) with an axially aligned, unidirectional flow profile. The low shear stress hypothesis was then validated by multiple studies as summarized in review Malek et al. (1999) suggesting that low hemodynamic shear stress (< 0.4 Pa) is prevalent to atherosclerosis-prone sites of an artery, stimulating an atherogenic phenotype. At the same time, higher shear stress (> 1.5 Pa) induces endothelium quiescence and athero-protective gene expression. Figure 2.1 indicates risky areas around arterial bifurcation.

The knowledge of endothelial phenotype is an essential tool that may help one to guide future therapeutic strategies. Data from experimental study Tardy et al. (1997) indicated that local shear stress gradients rather than shear stress magnitude might play a vital role in the morphological remodelling of endothelial cells. However, regions related to the critical shear stress gradients were again associated with the areas with an unsteady disturbed flow profile, indicating the arterial layout may highlight dangerous positions, important when locating possible low shear regions. Cecchi et al. (2011) suggested the uniform regions of the arterial tree, exposed to a unidirectional and constant flow, determine physiologic shear stress. In contrast, regions, where oscillatory and disturbed flow may occur are exposed to lower, non-physiologic shear stress. During built up of a plaque, the vessel wall enlarges, maintaining standard lumen dimensions up to about 40 % of a relative plaque area (Glagov et al., 1987). Slager et al. (2005) followed up this idea and proposed a hypothesis that maintenance of a proper lumen dimensions by wall remodelling may help to prevent plaques from intruding into a lumen but also preserve conditions for their growth. Haemodynamic shear stress may be an essential feature when

an advanced atherosclerotic lesion is treated by stent deployment, and re-stenosis should be considered as proposed by Koskinas et al. (2012). The stent adds a restriction to the blood flow, disturbing its profile in usually safe regions. Non-uniform shear loading may cause separation of the endothelial cells creating gaps as recently simulated in Escribano et al. (2019) which allows lipid to migrate into the sub-endothelial space with consequent atherogenesis and atheroma development.

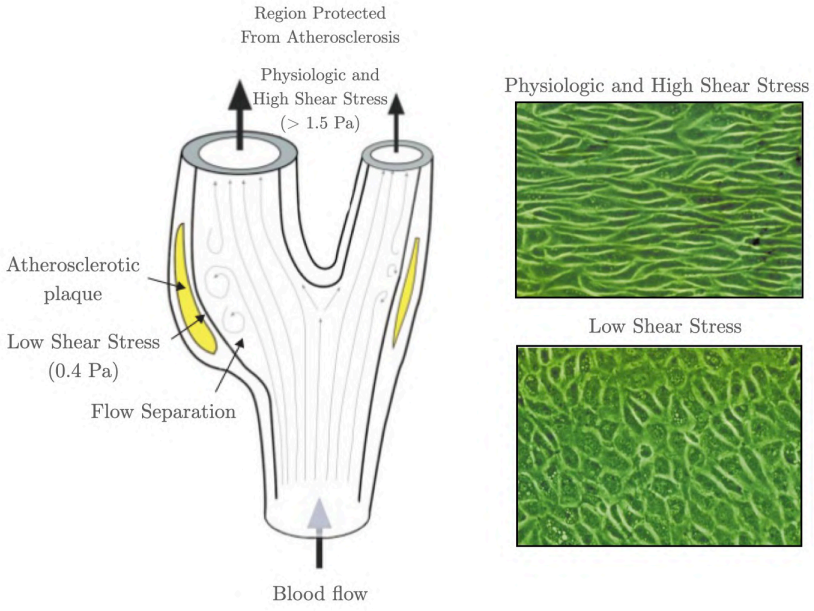

Figure 2.1: Schematic illustration of the most frequent location for atherosclerosis creation in the bifurcation of the artery (left). Bovine aortic endothelial cells exposed to physiologic shear stress show good alignment in a blood flow while those exposed to low shear stress do not (right). Reprint from Malek et al. (1999).

2.2. Pathogenesis of atherosclerosis

The name atheroma was firstly used in 18^{th} century, describing a thickened area in the vessel wall exuding yellow lipids. An effort to describe a possible mechanism of atherosclerotic plaque development started in the 1980s. Despite the complexity of the plaques in histological sections, most of the lesions contained lipids, primarily cholesterol ester. Goldstein and Brown published multiple studies with a low-density lipoprotein pathway as a possible description of atherogenesis where human cells, including smooth muscle cells (SMC), are protected from the cumulation of sterols (Brown et al., 1976; Brown et al., 1975; Goldstein et al., 1977). Severe lesions may grow under conditions of violation of this regulatory mechanism (e.g. patients with genetic disorders such as diabetes). The response-to-injury hypothesis firstly mentioned by Ross et al. (1976) and then modified in Ross (1986) suggests that the primary event causing the growth of the plaque is an endothelium damage. Early and advanced lesions consist of SMCs and macrophages. Macrophages predominate in fatty streaks while proliferated SMCs, macrophages, and leukocytes are present in advanced lesions, indicating possible defensive responses that have progressed to a pathological response. A thorough investigation in Ross (1993) brought more description of

early, intermediate and advanced atherosclerotic lesions where a presence of monocyte-derived macrophages, SMCs and T-lymphocytes (Gown et al., 1986; Libby et al., 1991) was confirmed, pointing out the fundamental role of inflammation in atherogenesis. Cathcart et al. (1985) and later Rosenfeld et al. (1990) showed a primary role of oxygenized low-density-lipoproteins(oxLDL); their formation may cause migration of monocytes and T-lymphocytes into the sub-endothelial space. In Ross (1999) the atherosclerosis was accepted as an inflammatory disease. Moreover, the author suggested that an advance in molecular genetics will help to determine the role of various genes with possible success in further prevention or healing. Atherosclerosis does not result simply from the accumulation of lipids. In contrast, other factors need to be taken into account.

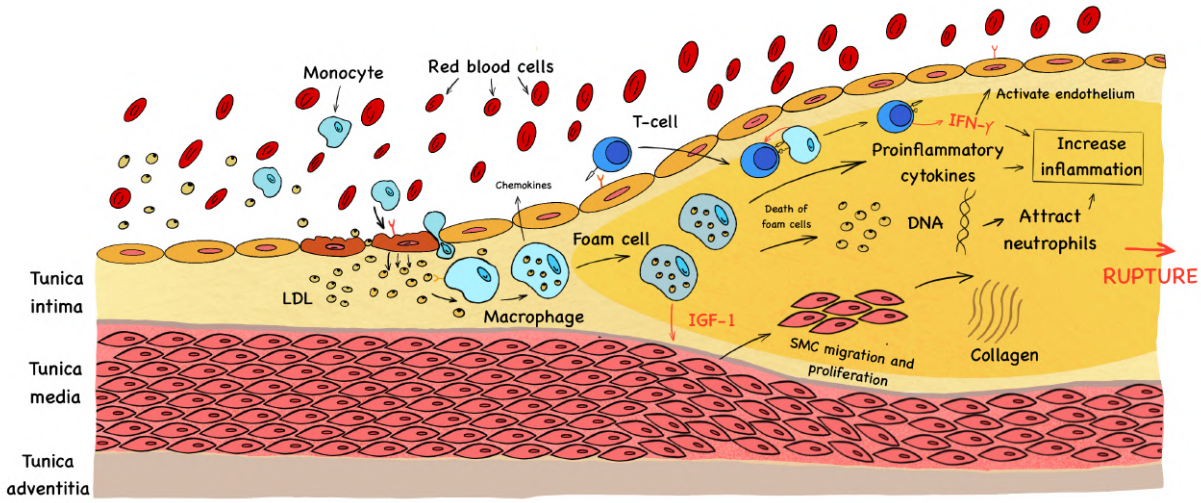

Figure 2.2: Stages in the development of atherosclerosis. Disruption of endothelial cells leads to a lipid migration into the tunica intima layer, starting the inflammatory reaction. Cell migration, proliferation and subsequent apoptosis form a plaque that may advance up to its rupture.

The research of last few decades led to a globally accepted paradigm on the pathogenesis of atherosclerosis. A high amount of circulating LDLs (together with other lipoproteins in blood plasm) is cumulating in critical regions. Due to their increased amount, LDLs can deposit in the tunica intima through dysfunctional endothelium. LDLs are oxidized to oxLDLs in the tunica intima by action of enzymes released by the endothelium. Once LDLs are oxidized, it cannot leave the intima. The oxLDL activate the endothelial cells causing the expression of receptors for white blood cells. Adhesion of leukocytes allows monocytes and T-cells to move into the tunica intima layer. During the movement of monocytes from the vessel to the tissue, they become macrophages (monocyte-derived). Once the macrophages, also known as scavenger cells, are in the tunica intima, they take in the oxLDLs and become foam cells. Foam cells are a critical factor in atherogenesis. They promote the migration of the SMCs from tunica media into tunica intima and promote SMC proliferation by releasing an IGF-1 growth factor.

Moreover, foam cells heighten collagen synthesis in the tunica intima, causing wall hardening. During this process, the foam cells die and release their lipid content and DNA materials, which attract neutrophils. Foam cells also release pro-inflammatory cytokines, which, together with neutrophils, will increase the inflammation in the area, driving the growth of the plaque. After plaque rupture, the plaque content is released into the blood flow. The ruptured plaque causes a thrombus formation due to blood coagulation and is

covered with a clot. The already narrowed vessel is blocked, even more, impeding thus the blood flow to organs. It is important to note that all the above processes run in parallel.

2.3. Plaque vulnerability

The knowledge of the pathogenesis of atherosclerosis is fundamental for further treatment or prevention. However, this is a problem to be solved mainly by genetic engineers. The process of plaque formation is a long term problem. Foam cells form at a juvenile age (Napoli et al., 1997) and gradually grow. Until the prevention is available, detection of advanced plaques suspected of health troubles, is required. In the last decades, the interest in plaque ruptures ran together with pathogenesis research. The first rupture of the plaque as a cause of the death was mentioned in 1844 (Falk, 1992). The rupture itself was then neglected for an extended period until an explosion of research about plaque pathogenesis in the 1980s (Finn et al., 2010). Researchers found that the instability of plaque often leads to rupture. In the 1990s, the concept of "vulnerable plaque", as an indicator of problematic lesions, started to be used, and it was terminologically unified in 2003 in the guide for clinicians dealing with patients with a higher risk of plaque rupture (Schaar et al., 2003). The vulnerable plaque was defined by Grønholdt et al. (1998) as an advanced lesion with a large necrotic/lipid core (LC), thin fibrous cap (FC) and possible thrombosis. A presence of calcification should also be taken into consideration, as it may cause a discontinuity of FC as mentioned in Virmani et al. (2000). Burke et al. (1997)

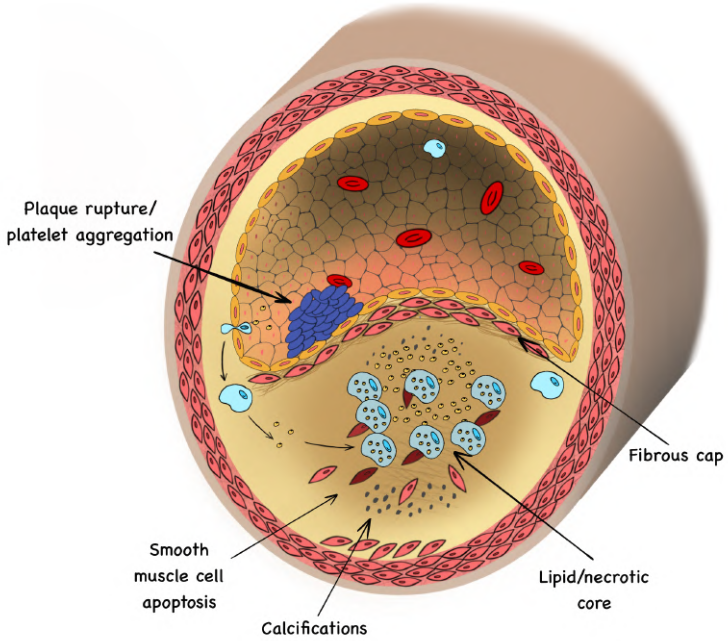

Figure 2.3: Fibrous cap rupture of advanced plaque forming a clot of platelets. The rupture is located near the shoulder region, a specific location from an autopsy and computational studies.

analyzed ruptured coronary plaques and identified the limit FC thickness $<65\ \mu m$ being critical in vulnerable plaques. Cumulation of information about atherosclerosis inspired Libby et al. (2015) to evaluate the concept of vulnerable plaque even though it served for

years as a guide for identification and treatment. The post mortem analyses of ruptured plaques supported this paradigm despite the lack of information on non-ruptured plaques, which would suit the vulnerability definition. Monitoring of lesions with *in vivo* imaging methods e.g., ultrasound (Rioufol et al., 2002) indicated that rupture occurs in lesions, though they should not be labelled as vulnerable. In the PROSPECT study, Stone et al. (2011) used the "virtual histology", which showed that only about 5 % of thin-capped plaques caused coronary events during 3.4 years. These exciting findings indicate that global interest based on plaque vulnerability could be inadequate. Its further refinement might decrease fatal cases. An extensive review of findings from several clinical studies on detection of high-risk or vulnerable plaques was proposed by Fleg et al. (2012). The study summarized available techniques, findings from patient follow-up studies and, more importantly, proposed possible future directions. The grand challenges arisen are (i) finding more sensitive and predictive risk factors, (ii) developing new screening tools, (iii) identifying more vulnerable patients for plaque rupture and associated clinical events such as stroke and heart attack, and (iv) recommending a proper treatment plan to prevent a plaque rupture. From this perspective, biomechanics of atherosclerotic plaques may contribute to establishing the association of mechanical risk factors with biological/clinical events. Nevertheless, the level of stenosis is still the primary factor used as guidance for treatment decisions in practice.

2.4. Surgical treatment of atheromas

The above-mentioned plaque growth and artery lumen narrowing (see Figure 2.4) may bring severe troubles for a patient's health. Depending on the artery, symptoms may differ. In the case of a coronary artery, the blood full of oxygen is usually carried to the cardiac muscle cells, however, the plaque disables the proper delivery of blood, and, as a consequence, the cardiac muscle cells are deprived of oxygen (ischemia), causing angina pectoris or even heart attack. A similar scenario may occur in different locations, e.g. in the aorta, femoral, iliac, renal, or carotid arteries. The treatment will then depend on the specific case. This section will discuss common treatments of atherosclerosis within the carotid artery.

2.4.1. Carotid endarterectomy

Carotid endarterectomy (CEA) is an invasive, most commonly used treatment procedure (see figure 2.5) to prevent stroke (Rothwell et al., 2004); it was subjected to several randomized trials. For example, Rothwell et al. (2003) compared results from randomized clinical trials Europen Carotid Surgery Trial (ECST) and North American Symptomatic Carotid Endarterectomy Trial (NESCET) to unify inconsistent results and recommendations. CEA was found highly beneficial for 70-99 % stenosis and moderately for 50-69 % stenosis. According to the ESVS Guidelines (Liapis et al., 2009), the CEA is recommended in symptomatic patients with >50 % stenosis if the perioperative stroke/death rate is < 6 %; in case of asymptomatic men < 75 years old with 70-99 % stenosis if the perioperative stroke/death risk is < 3 %. The benefit of CEA is insignificant for women globally and is preferable only for younger, fit women. Carotid artery stenting (CAS) should be performed only in patients with high risk for CEA. The vulnerable plaques, if detected, are evaluated separately.

Figure 2.4: MRI representing a patient with severe stenosis in *internal carotid* artery which appears completely closed (100 % stenosis).

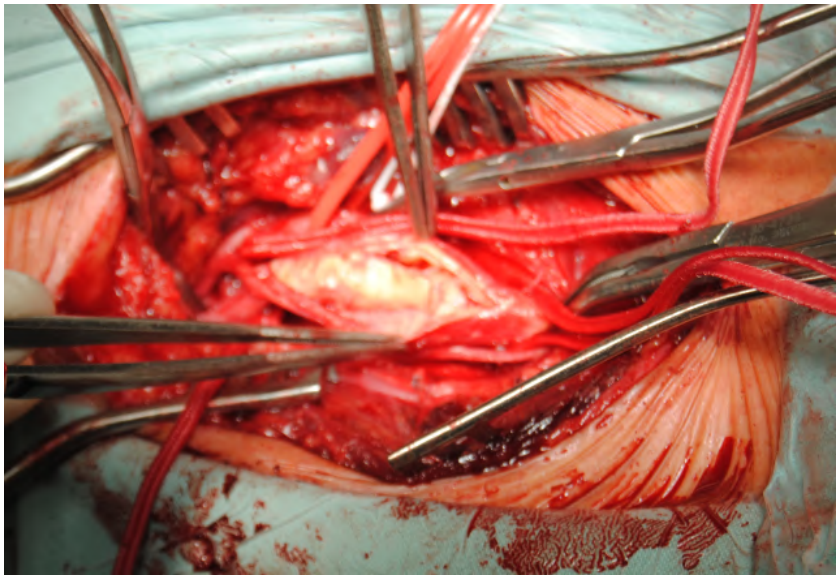

Figure 2.5: An image was taken during CEA in St. Ann's Hospital. The artery is cut, and plaque is carefully separated from the adventitia od media-adventitia bilayer, depending on lesion severity. Opening originated from the cut is overlaid mainly with a bio-compatible material during angioplasty.

2.4.2. Carotid artery stenting

During CEA, the plaque is removed from the artery leaving only the outer layer tunica adventitia and partly the middle layer tunica media. The latter mentioned CAS is an alternative less-invasive procedure. A vascular surgeon inserts a slender, metal-grid tube called a stent, which expands inside a carotid artery to increase lumen and consequently the blood flow in the area stenosed by the plaque. Randomized trial study "Stent-Protected Angioplasty versus Carotid Endarterectomy (SPACE)" Eckstein et al. (2008) tested the hypothesis that CAS is not inferior to CEA for treating patients with severe symptomatic carotid artery stenosis. The incidence of recurrent ipsilateral ischemic stroke was found similar for both groups. However, the incidence of recurrent carotid stenosis is significantly higher after CAS. Therefore, the long term efficacy of CAS and less specific experience in clinical practice is influencing the procedure, as debated in Nallamothu et al. (2011). Application of stent is associated with a relatively high risk of restenosis (Iqbal et al., 2013) which is partly related to wall damage during stent deployment. Usage of stents might seem only as a temporary solution. However, there are cases where the CEA might be problematic or even impossible, i.e. a plaque in an unapproachable location or applications for other arteries. Moreover, the development of drug-eluting stents in combination with biodegradable materials showed promising results for coronary arteries in reducing restenosis risk (Schmidt et al., 2018) and is also promising for a carotid artery and future studies. Interested reader about randomized studies for carotid artery is referred to Morr et al. (2014).

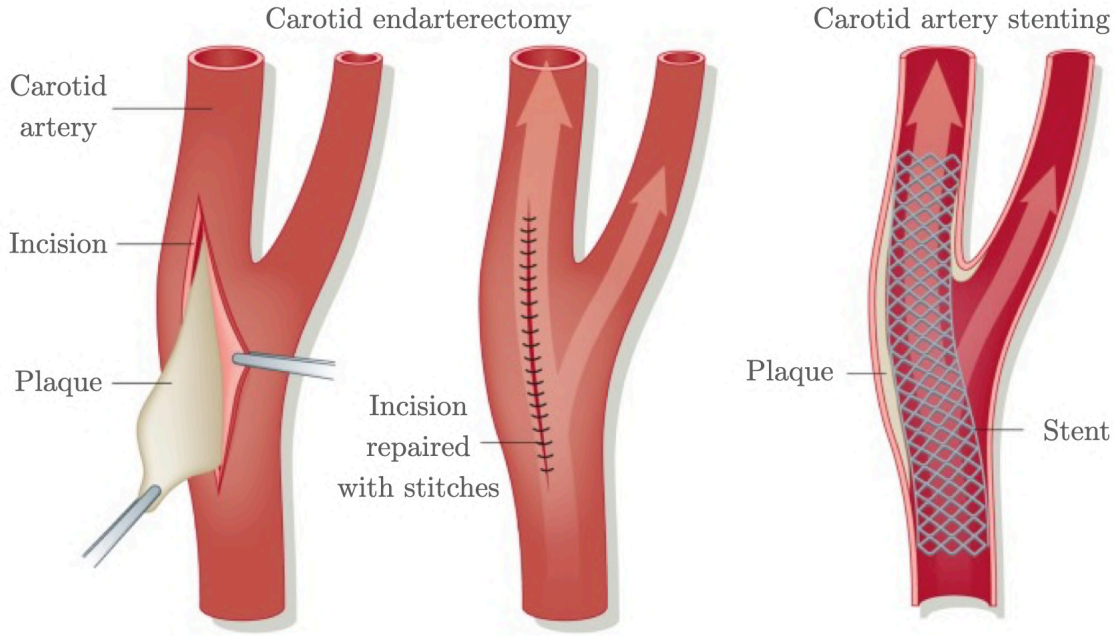

Figure 2.6: Two different treatments of a carotid artery with atherosclerosis. The plaque is removed during a carotid endarterectomy while compressed by metal or plastic material during carotid artery stenting. Reprint from Fernández-Ruiz (2016).

In 2017, according to statistics in the U.S., stroke was the fifth most common cause of death according to Kochanek et al. (2019). Compared to the year 2000, when the stroke was in third place, the results seem relatively positive (Miniño et al., 2002). According to

European statistics in Europe, the cerebrovascular disease was the second most common cause of death in 2016. However, the first place was occupied in all the latter mentioned statistics by heart disease where atherosclerosis strikes a great deal in coronary arteries. An additional point of view, offered by biomechanics, may result in a more accurate risk assessment of patients with the degree of stenosis, generally excluded from intervention planning or for those who do not need the intervention yet as the rupture risk is low. An investigation of patient-specific mechanical properties and its specific computational model can be used to design patient-suited stents, possibly decreasing the incidence of plaque recurrence.

Biomechanics - general overview

It is fundamental to identify how the tissue structure behaves *in vivo* in order to prevent serious events. Correspondingly, *in silico* physiology may help by developing computational models that can predict a basic functionality. Computational modelling brings a powerful tool to integrate *ex vivo* (experimentally observed mechanical properties and tissue structure) and *in vivo* characteristics (model geometry, boundary conditions). The iterations between model and experiments provide an opportunity for numerical testing of hypotheses. Validated models have various applications in surgery, diagnostics or bioengineering showing their importance.

Development in computing allows researchers to simulate complex non-linear boundary values in all engineering aspects in the last decades. It, therefore, enables a simulation of various problems in biomechanics related to hard tissue like bones and teeth and soft tissue like skin, muscle, blood vessel and lungs. All the latter mentioned fields bring many possibilities for computational modelling but are rarely investigated together by a single researcher. A general overview of biomechanics of soft tissue in the cardiovascular system is well described in the book Holzapfel et al. (2014a) describing the research directions up to the year 2014. A reader can see the complexity of the whole problem. Hence, it is common to follow one direction, as is atherosclerosis in a carotid artery in the case of this study.

From an engineering point of view, a plaque rupture is an event where a mechanical failure occurs, possibly due to stresses exceeding the FC strength. Therefore, one should be looking for maximal stresses within the cap, the so-called peak cap stress (PCS). Ideally, this value would be used as a simple indicator for plaque vulnerability for subsequent decision-making during a patient screening. Mechanical loading from a blood flow acting on an advanced plaque can be taken into account not only for vulnerable but also stable lesions. Unfortunately, plaque stress cannot be measured directly and hence another approach is needed. Modelling of underlying physics is one of the available possibilities. First computational studies began to appear in the late 80s and early 90s to investigate the characteristics of atherosclerotic plaque using 2D structure-only models. Richardson et al. (1989) analysed coronary plaques from 85 patients who died from coronary thrombosis and investigated the plaques which had fissured. They found a correlation between high circumferential stresses with a site of intimal tears found at necropsy. Plain strain idealized section of the diseased artery was investigated by Loree et al. (1992) by using the finite element (FE) method. Reduced FC thickness increases circumferential stresses within the plaque, strengthening thus the paradigm of vulnerable plaque characterization. The following study Cheng et al. (1993) compared the lesions causing lethal myocardial infarction with the stable lesions. The use of patient-specific (PS) histology-based plane strain models pointed out an essential role of stress concentrations in plaque rupture. These initial studies showed the importance of computational modelling and inspired many researchers.

Artery narrowing affects the blood flow and oxygen delivery. Therefore, computational fluid dynamics (CFD) or even fluid-structure interaction (FSI) analyses appear frequently when dealing with atherosclerosis. CFD is mainly used in terms of wall shear stress; their extremes may indicate the sites of artery more prone to plaque developments (Markl et al., 2010; Milner et al., 1998; Prosi et al., 2004; Yang et al., 2007) as described in Trigger for atherogenesis. The use of CFD in advanced plaques is debatable when the lesion is already present, and a possible invention is planned. However, it can be helpful in preliminary stages or assessments whether restenosis can occur. In the case of FSI, the benefits of solid and fluid states are exploited together, resulting in a more advanced investigation (Cilla et al., 2015; Tang et al., 2004, 2009; Yuan et al., 2015). However, a recent study Huang et al. (2014b) showed that even though the FSI analysis may slightly differ from the solid only, it is very time consuming and sometimes even not feasible with more sophisticated models as shown by Teng et al. (2015). Therefore, it is reasonable to focus on the FE method in rupture risk assessment when identifying essential factors for plaque rupture. The FE method is mainly used in biomechanics and is available in commercial software like ANSYS, ABAQUS, NASTRAN, EPYLISIS. Its fundamentals are well known, and homemade applications can also be seen, although they may lack validation. Nevertheless, it does not change the fact that this method enables to solve very complex three-dimensional non-linear problems in biomechanics.

Most computational studies aimed to investigate the stress distribution within the so-called vulnerable plaques. With information summarized in section Plaque vulnerability, the research should focus not only on those particular lesions but also on less severe cases. If it was possible to establish traceability of the most common principles leading to a higher rupture risk, further implementation into clinical practice would be more beneficial. The biomechanics may contribute to various problems that should be solved to understand the mechanism of plaque rupture. However, it is, unfortunately, impossible to fulfil all problems within this study. Therefore, specific problems defined by the author during a literature review will be further described in separate chapters. All parts as model creation, acquiring of mechanical properties, and residual deformations should contribute to computational modelling, which is of interest to help in research.

Geometry models

4.1. Higher dimension

As mentioned earlier, the first appearance of computational models of atherosclerotic plaques began around the 1990s as plane strain models of idealized shape (Loree et al., 1992; Richardson et al., 1989) followed by histological sections reconstruction (Cheng et al., 1993). It was reasonable to use 2D models in those days due to computational requirements. As results indicated a possible connection between clinical and mechanical manifestations, they inspired further research in this field. One would expect that the development in computation will gradually lead to higher three-dimensional (3D) models capturing the geometrical complexity of atherosclerotic plaques. However, plain strain models can still be found in literature nowadays.

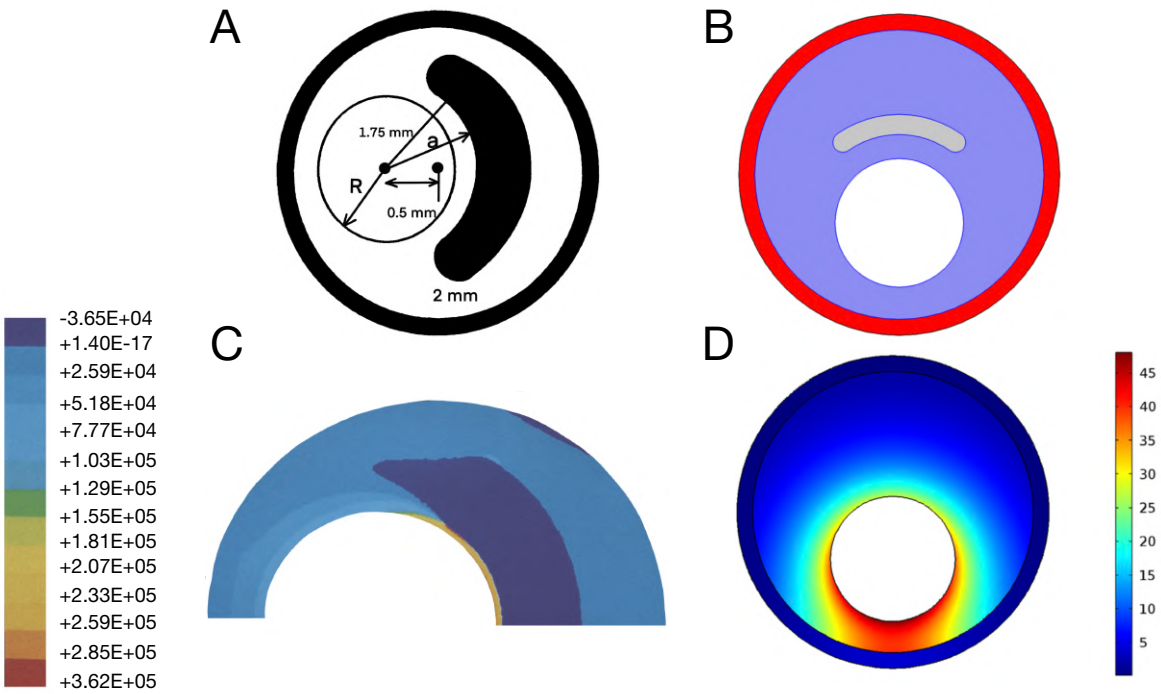

Figure 4.7: One of the first idealised 2D models introduced for atherosclerotic arterial tissue reprinted from Loree et al. (1992). Figure A shows the used geometry with lipid pool to analyse the impact of FC thickness while C represents contours of circumferential stress in pascals for this model. As it can be seen in figure B, almost the same idealised model was used for the analysis of different factors more than 20 years later; contours in figure D represent the first principal stress in kPa. Reprinted from Buffinton et al. (2014).

The usage of 2D models is mainly connected with histological sections, which provides the best structural information (Akyildiz et al., 2018; Chau et al., 2004; Gijsen et al., 2015; Nieuwstadt et al., 2014; Ohayon et al., 2007; Riou et al., 2014; Speelman et al., 2011). An image quality benefit in histological sections can be improved to create a higher-dimension model. However, this will be discussed separately as it is a new problem, including other approaches. Histological sections are sometimes combined with an idealized[1] 2D models (raw reproduction of the plaque shape) while enable, e.g., parametric analyses with a possibility to investigate more geometrical combinations (different thickness of FC) (Akyildiz et al., 2011; Buffinton et al., 2014). Akyildiz et al. (2016) proposed an exciting framework for local mechanical characterization of atherosclerotic plaques. The authors combined information from the histological section used for 2D model creation with ultrasound displacement measurements for an inverse FE analysis. Another exciting application of the 2D model was presented in Gijsen et al. (2021) combining a thorough analysis of histological sections investigating a collagen fibre distribution around calcifications with subsequent implementation into a computational model. Since collagen fibre distribution is extremely challenging itself, not to mention for atherosclerotic tissue, the analysis is often possible only in planar sections. Both the latter mentioned studies developed a fascinating approach that would be very challenging for 3D models, showing that the research still relies partly on simple planar analyses. It might be misleading to introduce mere 2D histology-based models because also, e.g., a single MRI image can be used to create a 2D model with fundamental structural components (Sadat et al., 2010; Teng et al., 2010).

An overestimation of stresses of an idealized 2D model was found in study Huang et al. (2014b) where authors performed a comparison between 2D and 3D structure-only and 3D FSI analysis. It was concluded that further research should focus on 3D models as also mentioned in the review paper Holzapfel et al. (2014b). Both studies were published in 2014, and as it was shown in the previous paragraph, 2D models are still of interest. The proportion of 3D models is gradually growing (Gao et al., 2009; Holzapfel et al., 2002, 2005a; Iannaccone et al., 2014; Kaazempur-Mofrad et al., 2003; Lisický et al., 2020; Nieuwstadt et al., 2015b; Tang et al., 2005, 2017) but their usage can be seen in parallel with 2D models. However, the level of these models varies. PS models are preferred nowadays, although they lack geometrical data (highly influenced by insufficient resolution of the image acquiring method). Hence, simpler models with idealized geometry are used to consider the heterogeneous structure of the atherosclerotic plaque (Cilla et al., 2012, 2015; Huang et al., 2014b; Tang et al., 2004; Teng et al., 2015; Wong et al., 2012; Yuan et al., 2015). Although created artificially, these models enable us to investigate a variety of possible important mechanical factors, which can be of interest in the case of PS analysis. There are, of course, many other studies which were not mentioned here, but their complete list would go beyond this section. This brief overview of level of the occurring geometry models introduces another critical field, based on obtaining accurate PS information to create mainly 3D models.

[1]Idealized in the content of this work describes a model which was created without any knowledge of patient data or sometimes created from average measurements and aims to distinguish this type of models from PS ones which are primarily created from medical images. This notion is taken from the literature.

4.2. Image acquisition and patient-specific modelling

Development in *in vivo* imaging methods enables to use more accurate PS models based on high-quality medical images. There are several methods available, but their suitability might be sometimes questionable. One of the main disadvantages is a relatively tiny dimension of atherosclerotic tissue which varies among arteries, e.g., carotid plaque is approximately 30 mm long with a diameter of 10 mm. A model reconstruction from medical images is done by a segmentation process where specific areas (often related to some level of image intensity) are assigned to components. The process is not described here as many free and commercial software packages are available for this purpose.

4.2.1. Magnetic resonance

From clinical studies, magnetic resonance imaging (MRI) seems the most promising, in visualizing the critical plaque components (FC, LC, calcifications), see e.g. (Hatsukami et al., 2000; Saam et al., 2005). However, the distance between images (transversal resolution) is still far from in-plane resolution. The typical clinical device can obtain in-plane resolution of around 0.5 mm, while traversal resolution can exceed 3 mm. This can lead to a relatively inaccurate approximation in reconstructing the model geometry between slices. It might be improved with specialized carotid coils (Balu et al., 2009; Coolen et al., 2016; Van Wijk et al., 2015) but their price is very high, and hence they are not that widespread. Nevertheless, some improvements in image quality are awaited for *in vivo* MRI because excellent resolution has already been achieved, e.g., in Benitez et al. (2021) where the authors obtained the transversal resolution 0.625 mm after resampling original images. The image quality is influenced by the measurement time for each slice, which demands a patient capable to stay without any movement. This is, of course, almost impossible, resulting in different image quality even for a single patient. Consequently, every missing information influences the quality of the model reconstruction, see Figure 4.8.

Nieuwstadt et al. (2015b) found the importance of an anisotropic resolution with a relatively better in-plane resolution to improve carotid plaque quantification. However, the same authors had reported that a decreased number of axial images might lead to the overestimation of some plaque components included in a computational model (Nieuwstadt et al., 2013). A decrease in slice thickness may not improve plaque quantification, although it is an important parameter for 3D PS models (Lisický et al., 2020). Nevertheless, *in vivo* MRI scanning is used very often in computational studies and can be considered as the most suitable in this field when combined with a proper device (carotid coil). Early applications showed rather reconstructions of carotid lumen only for young patients (Kaazempur-Mofrad et al., 2003) and lately also for older patients (Kaazempur-Mofrad et al., 2004) where a plaque was already present in the artery. Although the lumen information is important for CFD studies, the main focus was already directed at plaques because the *in vivo* MRI proved the capability to distinguish plaque components. Yang et al. (2007) compared FSI analysis with wall-only to confirm the importance of complex FSI modelling in this field. Their results indicated that the maximum stress (first principal stress) within the wall is about 145 % higher in the FSI than wall-only. Such difference seems very important but it was not confirmed in a later study by Huang et al. (2014b) who confirmed statistical significance though the difference was only about 2 %. Therefore, they concluded that 3D structure-only analyses should be of interest mainly

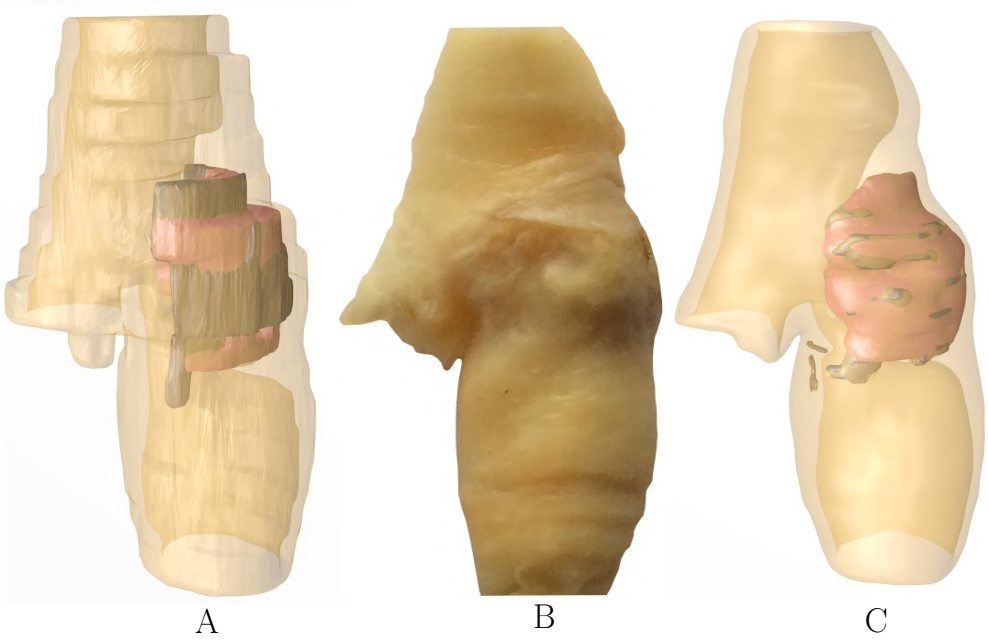

Figure 4.8: 3D plaque model. Red: lipid core; grey: calcification region. (A) shows a non-smoothed model based on 1.5 mm slice thickness; (B) shows the MRI image of carotid plaque sample recorded ex vivo; (C) shows a smoothed model based on 0.25 mm slice thickness. Picture adapted from Lisickỳ et al. (2019).

due to their lower computational complexity and negligible differences. There are many studies using the combination of *in vivo* MRI with FSI (Benitez et al., 2021; Chen et al., 2021; Gao et al., 2009; Kock et al., 2008; Tang et al., 2008, 2009, 2017; Yang et al., 2007). It is clear that FSI analyses are very prevalent, and their use depends on the researcher's preferences because of the high complexity and additional factors influencing the analysis. The research dealing with the *in vivo* plaque characterization (mainly done by the group of professor Dalin Tang and his collaborators) until 2014 is well documented in Tang et al. (2014) listing their achievements in obtaining a proper 3D FSI model from *in vivo* MRI and the necessary translation into clinical practice. Their contribution to 3D modelling is indisputable and one can look forward to future work possibly filling the missing gaps. Most of the latter mentioned studies created their 3D model on the basis of a minimal number of MR images with limited ability of tissue recognition. Even though it might provide some information about clear structures as LC or calcifications, it often requires an artery wall omission leading to oversimplified modelling where the wall is modelled as the fibrous tissue (FT). Nevertheless, *in vivo* MRI shows its benefits and is a dominant approach in computational modelling of carotid atherosclerotic plaques.

The patient's movement can be avoided though it requires a sample extraction from the body e.g., during *ex vivo* imaging. However, for the atherosclerotic tissue, it can be obtained relatively easily because a plaque extraction is a natural outcome from CEA, as mentioned in 2.4.1. Therefore, it can be imaged independently on time with a higher image quality. Also, *ex vivo* devices are often more robust as they are not in direct contact with a living body. There are also other approaches of how to improve the MR image quality, as used e.g., in Lisický et al. (2020) where the authors imaged the sample two times with inter-slice gaps equalling to the slice thickness, which were then completed in the second measurement. *Ex vivo* MRI was used in many studies (Groen et al., 2010; Moerman et al., 2019; Tang et al., 2005; Van Engelen et al., 2011) mainly of

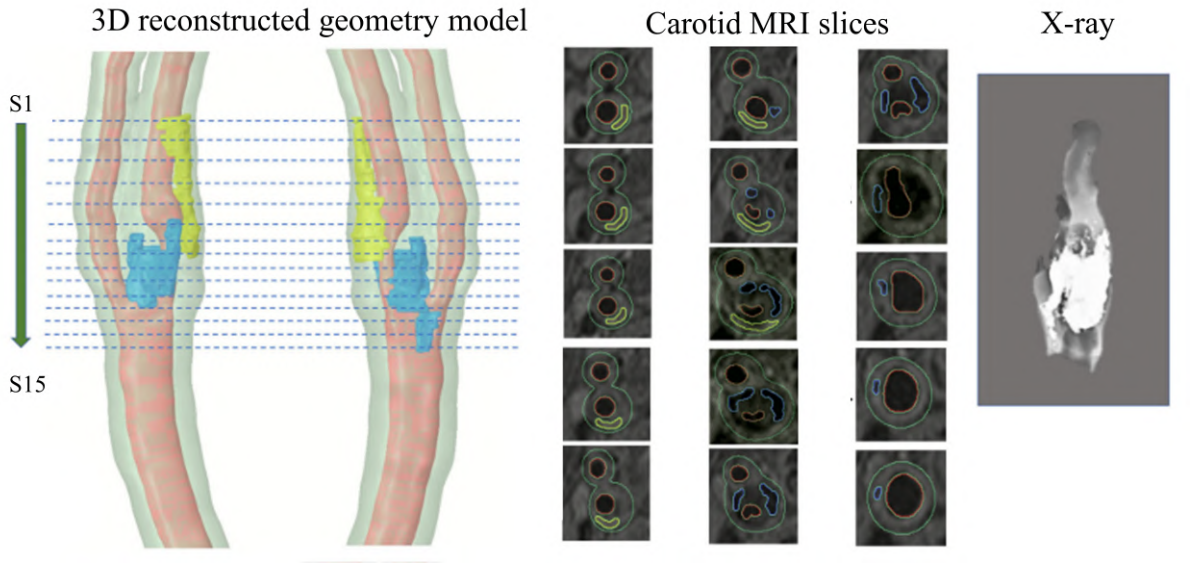

Figure 4.9: Model creation from *in vivo* MRI with very good resolution after resampling of 0.17 mm x 0.17 mm x 0.625 mm reprinted from the very recent study Benitez et al. (2021). Despite the very decent resolution, it is not clear to the author how the segmentation was performed because some visible areas were omitted. However, the presented image is too small for proper evaluation, and it is only the author's personal opinion.

CEA sample; especially Holzapfel et al. (2002) is of interest because the authors showed that there is a possibility to reconstruct various structural components, which were then also investigated experimentally for their mechanical behaviour. This unparalleled study brings a challenge for future studies to confirm the results. They also showed another possible source of samples for *ex vivo* imaging, and that is from the autopsy, which was scanned also in, e.g., (Huang et al., 2014a, 2016; Yang et al., 2007).

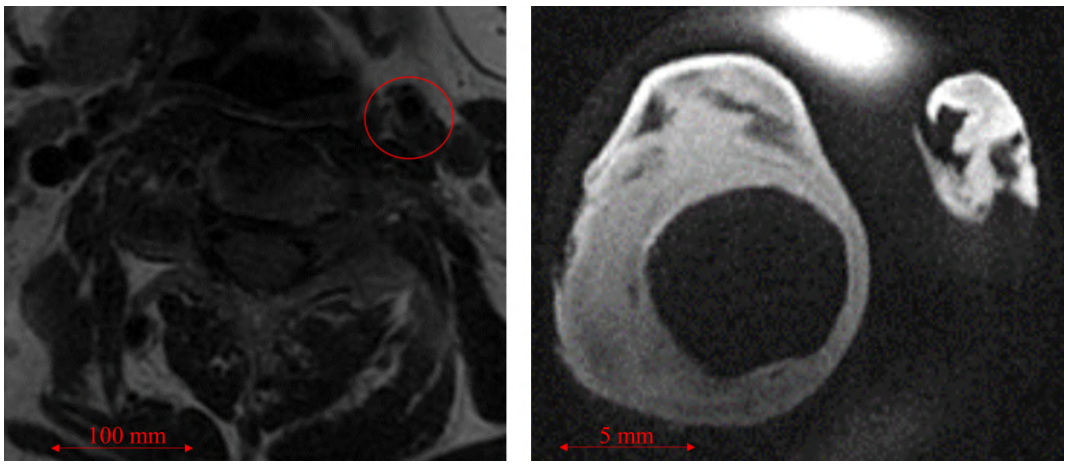

Figure 4.10: Comparison between *in vivo* MR image acquired at St. Anne´s University Hospital Brno (left) with a standard device without the carotid coil and *ex vivo* MR image acquired at Institute of Scientific Instruments in Brno with 9.4 T Bruker BioSpec 94/30 USR device. The region of interest in the left figure shows a location of the carotid artery, which is almost undetectable. It is, therefore, tough or even impossible to use such data for model reconstructions. On the other hand, the right image shows the section of a carotid artery with even more details.

4.2.2. Computed tomography

Despite the above comprehensive section related to the MRI, many readers may be more familiar with *in vivo* computed tomography (preferably angiography) CT-A. CT has an excellent isotropic resolution, necessary for proper modelling. Therefore, it is a frequently used method suitable for model reconstruction but dominantly for bone tissue or arterial lumen[2]. The visualization of lumen requires additional contrast material[3] which is injected into the blood vessel of a patient. However, it is not capable to visualize structural components of the soft tissue of atherosclerotic plaque, such as LC or FT. It is therefore impossible to reconstruct the model with complexity such as from MRI.

There are, of course, areas of soft tissue research where this information is sufficient if the imaged artery, e.g., aorta, is quite large. Moreover, they often focus on aneurysm[4] which may have some common risk factors with atherosclerosis (Kent et al., 2010) but the main focus is on the aneurysm wall. Despite some limitations for smaller arteries affected with atherosclerosis, *in vivo* CT can also be found (Auricchio et al., 2011; De Wilde et al., 2016; Huang et al., 2014b; Jonášová et al., 2018; Salvucci et al., 2010), although the application may differ because the information on lumen geometry is essential for flow simulations near the plaque and calculation of the corresponding indicators as, e.g., wall shear stress mentioned in 2.1. Moreover, it was used for simulation of artery stenting in Auricchio et al. (2011) where the authors followed an approach typical in aneurysm modelling and assigned a wall thickness to their lumen geometry following a suggestion from Sommer et al. (2010). This sounds like a straightforward approach, but the primary problem is that an atherosclerotic arterial wall forms the plaque mainly inwards, reducing thus the lumen but most notably increasing the thickness of the wall (plaque formation). The authors solved it by interpolating the outer wall mean thickness from a non-diseased distal and proximal location. That formed and increased wall thickness in the area of significant stenosis, simulating in the volume of the atherosclerotic plaque. The authors omitted the plaque complexity and modelled it as a healthy carotid wall, influencing thus the results as shown in Lisický et al. (2020). It is evident that *in vivo* CT-A is not able to provide essential information for plaque models and thus it is not frequently applied. Fekkes et al. (2016) created a 3D computational model from CT-A data, including calcifications, fatty plaque regions and the wall. As they could not detect soft tissue from CT data, regions with stenosis were manually adjusted to a healthy diameter by using the same diameter as the artery without atherosclerosis. The volume in between was then denoted as fatty region.

It might seem that CT is not well suited for acquiring geometries and structural components related to atherosclerosis. However, *ex vivo* variant is often used mainly due to an excellent (very often isotropic) resolution. *Ex vivo* CT is often denoted as μCT or even nano-CT depending on image resolution. This indicates that the pixel/voxel size is at least one order lower than that of common clinical devices[5] enabling a more comprehensive analysis of the underlying structure. This resolution was found very important in the

[2]Inside space of a tubular structure such as artery through which the blood flows.

[3]Contrast agent can be, e.g., an iodine-based compound that changes the appearance of blood in the CT image and resembles the density of bone. The blood vessel lumen can be then tracked and segmented. The material absorbs in the body after some time.

[4]An outward bulging of a blood vessel caused by a wall weakening. The enlargement may cause a rupture risk accompanied by severe health problems depending on aneurysm location.

[5]The development in imaging is, of course, rapid, and the resolution reaches still better values. (Boyd et al., 2006; MacNeil et al., 2007)

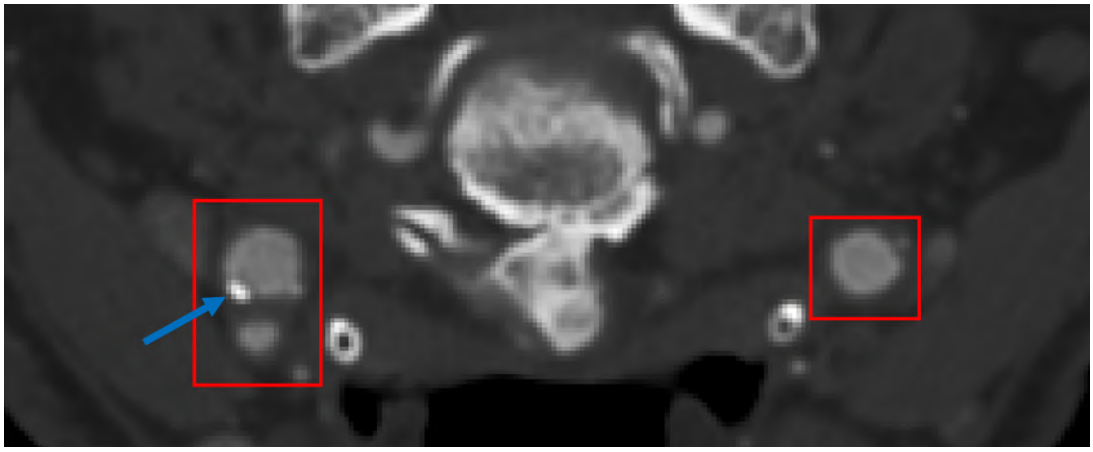

Figure 4.11: *In vivo* CT image. Red rectangles show areas of the carotid artery, which is recognizable only due to contrast agent making the intensity very close to a bone. The Blue arrow indicates a location of calcification which is very well detectable using CT but often appears as one big stone while it may be present as a grouping of micro-calcifications.

analysis of the influence of micro-calcifications in the plaques published by Kelly-Arnold et al. (2013) and Maldonado et al. (2012). The images enabled them to reconstruct a model of FT geometry with calcifications. As a very unusual use of a model from a μCT can be considered the one in the O'Reilly et al. (2020) who scanned each endarterectomy sample before a mechanical experiment and, on the basis of the scans, they decided which area of the sample is without calcifications and thus suitable for testing. Generally, CT applications are limited compared to MRI. This does not mean that it should be excluded from potential research in atherosclerosis; it brings a potential to find proper applicability for modelling of plaque geometries.

4.2.3. Optical coherence tomography

The previous two sections summarized the primarily used *in vivo* approaches for creating the geometry and structure for computational modelling of a carotid artery. However, other methods are also suitable for this purpose, such as optical coherence tomography (OCT). OCT requires catheterization, which increases the risk to the patients and is mainly used to model coronary arteries. However, Dohad et al. (2017) published recently a feasibility study where OCT is used during CAS showing the potential also in modelling the carotid artery. Therefore, it is crucial to introduce this technique and its possibilities. In Chau et al. (2004) the authors compared stress and strain distribution within 2D plaque models created firstly from OCT and secondly from a corresponding histology section, see Figure 4.12. The study did not find significant differences between both approaches and suggested that since OCT can be performed *in vivo* it might be a powerful tool in indicating vulnerable plaques in combination with FE analysis. However, OCT has a lower sensitivity for plaque components (compared to histology sections) as reported in Manfrini et al. (2006). Misinterpretations were mainly caused by low signal penetration in some areas as a thick FC covered LC. That was concluded as potentially beneficial as OCT might indicate relatively stable lesions. However, possible missing information of an underlying lipid/necrotic core was investigated in Kok et al. (2016) where a missing area was approximated by average information showing high correlation to the ground truth data from histological sections and improving thus the stress predictions. The use

of OCT is not as limited as it might seem, but the applications related to computational modelling are still relatively rare compared to other methods.

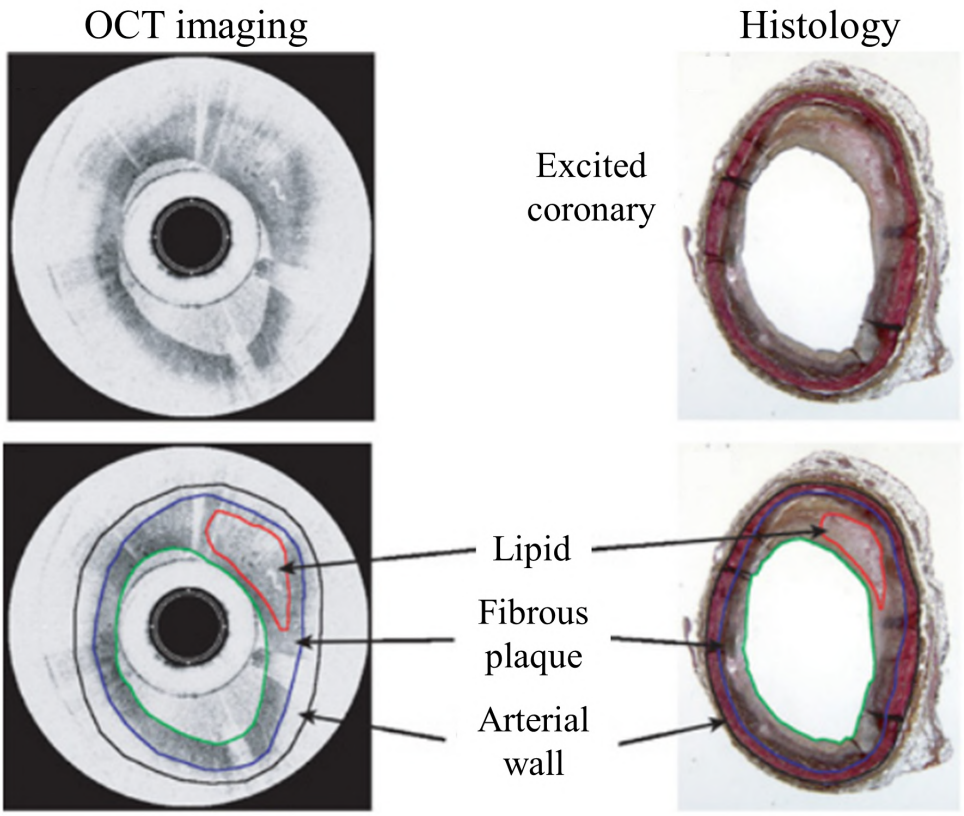

Figure 4.12: An example of OCT image acquired during the screening compared with histology. Reprinted from Chau et al. (2004). The authors show similar boundaries for common plaque components, which can be distinguished from the OCT. Boundaries for the arterial wall are not clear enough, but this is comparable with a standard MRI output.

4.2.4. Intravascular ultrasound

Similarly to OCT, an intravascular ultrasound (IVUS) requires catheterisation and might be thus risky. However, some applications can be found among computational studies too. The applicability of *in vivo* IVUS for a geometry model creation was already shown in Ohayon et al. (2001) indicating a perfect match between maximal circumferential stresses analysed by the FE model with locations observed in post angioplasty where a coronary plaque rupture was initialised by balloon angioplasty. Afterwards, Ohayon et al. (2005) investigated differences between 2D and 3D FE models where geometry was reconstructed from IVUS images. Even though their results indicated that 2D models were not always suitable for proper investigation of rupture sites, they were used in their subsequent studies (Floc'H et al., 2009; Ohayon et al., 2008) to investigate plaque vulnerability concerning necrotic core area and plaque morphology. They distinguished four different components (adventitia, media, cellular fibrosis and dense fibrosis). The possibility to model more plaque components was also confirmed in Yamashita et al. (2014) who successfully recognised fibrous, lipid, necrotic and calcified tissue. Similarly to OCT, the IVUS has a background in coronary arteries, although it showed positive results also

in stent deployment during CAS Clark et al. (2004). It might be interesting to attempt a model reconstruction for FE analysis of a carotid artery.

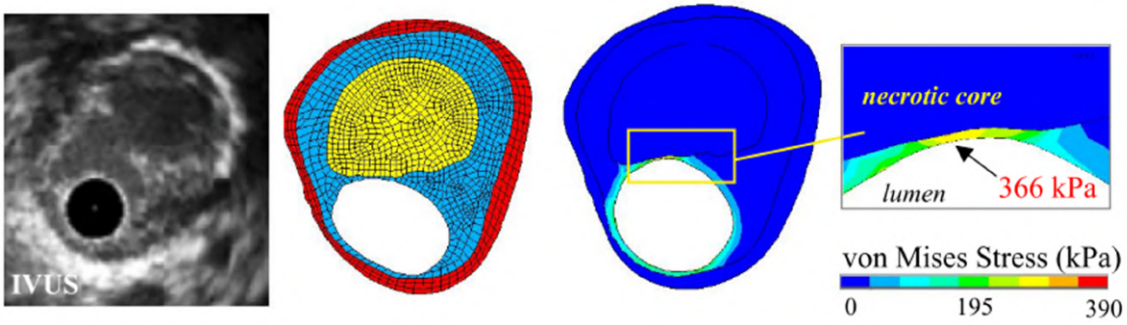

Figure 4.13: An example of 2D model reconstruction from IVUS image of the diseased coronary artery. Contours were discretized for FE analysis showing peak cap stress of 366 kPa. Reprinted from Ohayon et al. (2008).

Both OCT and IVUS provide essential information about the plaque composition *in vivo* what is necessary for possible predictions of the vulnerability in combination with computational modelling. It is very challenging to reconstruct the whole 3D model as both require continuous pull-back motion of the catheter accompanied by tissue movement and hence inaccuracies in the model. Moreover, both methods might be combined and thus exceed their capabilities as suggested, e.g., in Garcia-Garcia et al. (2009).

4.2.5. Histology

Histology is without dispute the most general approach for acquiring images that form a basis not only for computational models but also for experiments in the field of soft tissue biomechanics. Classical microscopic analyses of stained histological sections are slowly replaced by other methods discussed above, but they are still often used as a so-called "golden standard" or "ground truth" when verifying new approaches. They provide excellent resolution and enables distinguishing various components of atherosclerotic plaques (not limited only to atherosclerotic tissue). However, the key disadvantage compared to the above approaches is that they cannot be used *in vivo* and disables possible applicability in predictions of rupture risk. Additionally, the preparation of the sample brings a risk of section distortion (Groen et al., 2010) influencing the resulting geometry. Last but not least disadvantage is the restriction for 2D only models, which can be overcome as discussed in the next chapter. Nevertheless, histology sections and the subsequent 2D models are still valid to this day as they enable incorporation of structural analysis into the computational models as discussed in section 4.1.

4.2.6. Combination in modalities

It would be a shame to miss out on the benefits of the significant level of details of histological sections limited to 2D models only. Hence, researchers try to obtain spatial information making the 3D reconstructions possible. Pichat et al. (2018) presented a thorough survey on methods for 3D histology reconstruction. Several approaches are suitable for this, but each incorporates advantages and disadvantages. The easiest one is to stack histological sections on the top of each other with proximate spatial resolution

noted during histology. In this case, algorithms try to restore continuity smoothly across the volume from a set of slices (with appropriate spacing). However, one must bear in mind that there is no unique way to do it, and the final shape can be very different from the original. This was illustrated, e.g., in Malandain et al. (2004) on a reconstruction of bananas resulting in ellipsoid rather than the original fruit, sometimes referred to as the "banana effect". A similar effect might occur in (Nieuwstadt et al., 2013; Nieuwstadt et al., 2015b) where the authors aligned vertically the centres of gravity of lumen area of atherosclerotic histology sections (coronary artery) to obtain the 3D model. Even though it enabled them to study a 3D plaque with excellent structural knowledge, the applied procedure omitted its spatial shape and possible curvature (this can lead to misleading geometry models).

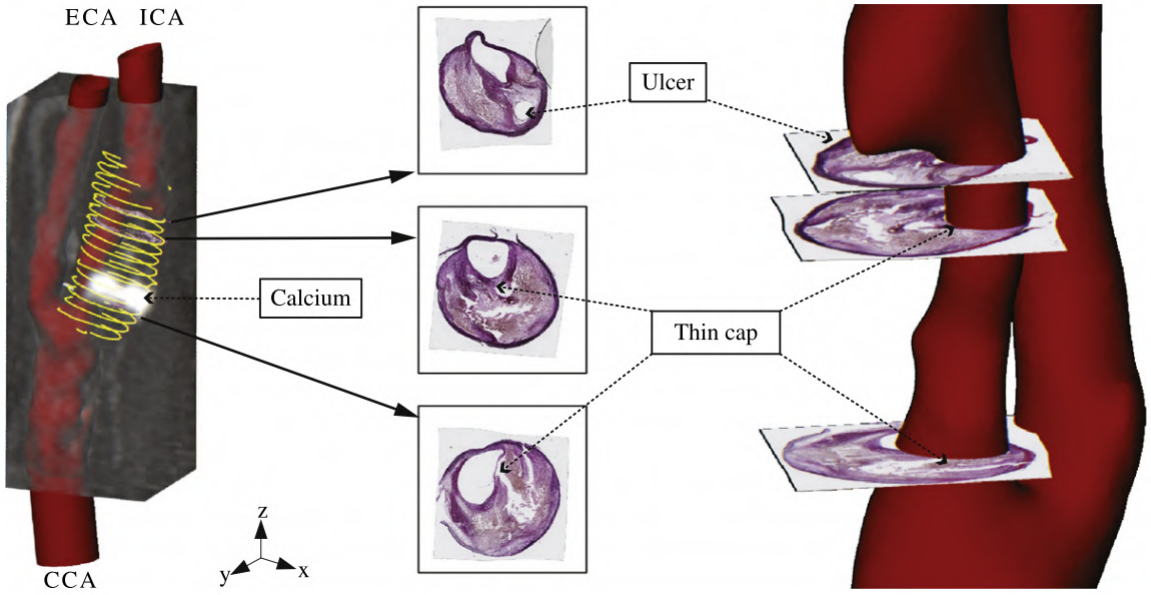

Figure 4.14: Combination of *in vivo* CT images with an information about structure from histology. Originally distorted histological sections were registered to *ex vivo* images. Reprinted from Groen et al. (2010).

The most direct way of reconstructing volume model from 2D sections is by optimizing the spatial alignment of each image by registration techniques[6]. The alignment is done to some reference images where the spatial information is well known, such as the mentioned MRI or CT techniques, refining the space of possible solutions. Therefore, it is possible to align histological sections with, e.g., MRI data to form a proper ground for subsequent segmentation and model creation. There are many approaches like 2D-2D, 2D-3D, 3D-3D or histology to 3D medical images using blockface photographs as proposed by Groen et al. (2010) for human atherosclerotic carotid plaques. Here, a paraffin block with the sample was photographed after having cut each section for histology. Moreover, the authors added also *in vivo* CT, *ex vivo* MRI and μCT which served as a base for subsequent image registration, see Figure 4.14. First, the authors confirmed the well-known fact that

[6]Image registration is an important tool in the field of medical imaging for combining patient data from the same device (mono-modal) or different sources (multi-modal: e.g., a combination of CT and MRI). For this reason, a one-to-one spatial mapping is performed using fixed (reference) and moving images.

histological sections are significantly distorted Lowder et al. (2007) (this is an important information because a simple reconstruction of the histological section would lead to an influenced model). Second, Groen et al. (2010) indicated an exciting way how to create a 3D model using histology data. This opens a new avenue in biomechanics, providing a technique for 3D "ground truth" modelling. Their work was then extended in Van Engelen et al. (2011) and recently in Moerman et al. (2019) where it was enriched by investigation of a possible correlation between wall shear stress and plaque composition of carotid endarterectomy sample. To increase the quality of the image registration, a similar resolution is required. Since *in vivo* imaging methods are mostly limited in this way (except for *in vivo* μCT which is capable of a great in-plane resolution), there is a need to use *ex vivo* imaging methods. Khimchenko et al. (2016) extended 2D histological information into the third dimension with the use of μCT by the slice to volume image registration. Their results showed that μCT could localize a certain cell type, enabling exploitation of micro-CT as a faster "virtual histology" solution.

The combination of modalities brings new possibilities how to improve the model reliability. The mentioned approach combining histology with 3D reconstruction still requires a sample to be excised and hence it disables any pre-surgery diagnosis. However, the image registration can also be applied to *in vivo* images to combine advantages of various methods. Guvenir Torun et al. (2021) combined ultrasound and MRI[7] to better characterize the plaque composition for an inverse FE analysis.

This section summarized current approaches in generating geometry models for atherosclerotic plaques, focusing primarily on the carotid artery. MRI seems the most suitable for this purpose from the author's perspective because it showed promising results *in vivo* when using the dedicated carotid coil. However, this is not a standard equipment of imaging centres, but this will change soon, hopefully. Nevertheless, it was shown that also *ex vivo* data provide a valuable input enabling more complex modelling, which can be slowly incorporated into clinical applications. On the other hand, CT is frequently used for patient screening to provide good information about artery stenosis used for subsequent intervention decisions, though the limited information about the soft tissue almost disables a proper geometry reconstruction. Additional adjustments are needed to overcome the need of artificial creation of the plaque if CT is used for the solid part model of an FSI analysis.

4.3. Author's contribution

The cooperation with the Institute of Scientific Instruments of The Czech Academy of Science and St. Ann's hospital enabled an investigation of image resolution for creating geometry models for computational modelling. Primarily, an axial resolution was thoroughly investigated as it was identified as a potentially critical factor for 3D modelling. Appendix A introduces an initial study where an endarterectomy sample of atherosclerotic plaque was scanned multiple times on high-resolution MRI (9.4 T) with slice thickness 0.25 - 1.5 mm. The results indicated that a smoothing process (a necessary part when triangulation is done on segmented areas with insufficient slice thickness) does not influence the models unduly. Nevertheless, considerable differences were found in

[7] Images were recorded during *ex vivo* inflation-extension test. However, the approach might be possibly applied *in vivo* as the carotid artery is well accessible for the ultrasound.

the outer surface comparison between 0.25 and 1.5 mm. The same applies to volume comparison of each considered plaque component (calcifications, LC and FT). However, these results only indicated that the resulting model might differ topologically, though the influence on computational modelling was not considered here. A robust methodology for surface reconstruction and subsequent volume creation was introduced, enabling an inter-slice gap during imaging to increase the image resolution. The follow-up study (Appendix B) included the axial resolution as one of the five factors in a computational study. Additionally, mechanical properties (FT and LC), media layer anisotropy and arterial wall thickness were used as varying factors for computational modelling. These factors were indicated on the basis of literature review. The use of Design of Experiment approach enabled a thorough study and incorporated interactions of all the factors. Overall, there were one hundred computational models prepared. Results showed that consideration of realistic mechanical properties of the arterial wall (for more details, see the wall thickness factor) is decisive for stress evaluation in the FT. Moreover, the impact of MRI slice thickness (axial resolution) was found to play a crucial role when a locally thin FC is presented. Also mechanical properties of FT and LC were found essential though in interaction with the above mentioned factors. Therefore, extreme mechanical responses for plaque components from experimental studies might interfere with the studied factors in computational works and influence the results significantly. Although *ex vivo* imaging was used here, it was pointed out that studies based on *in vivo* MRI, with slice thickness up to 3 mm, may inadvertently result in misleading stress concentrations. Other factors like the wall thickness can be easily incorporated, either using the process proposed here or differently, but their inclusion is necessary. The use of high-resolution MRI is, however, limited to extracted samples only, and all the discussed problems should be incorporated in *in vivo* models.

CT was already discussed as rather a rare modality for creation of computational models of a carotid artery with plaque (see 4.2.2). Nevertheless, images of a 63 years old female patient were used in our pilot study (see Appendix C) to reconstruct healthy-like arteries for the CFD study. The computed results are in agreement with physiological data see 2.1 showing that locations with low wall shear stress magnitude (<0.4 Pa) correspond to locations where the plaque was initially present. This confirmation inspired another study that is still in process as a large cohort of patients is needed. In this large study, the author is preparing geometry models and discretization. Moreover, complex models presented in the first paragraph are being prepared for FSI analysis to complete this problem.

Mechanical characterization

Computational modelling was presented to this point as an essential alternative for assessing plaque vulnerability and approaches to obtain a model geometry were introduced. Knowledge of the underlying mechanical behaviour is therefore essential. The credibility of computational models is contingent on a realistic geometrical model considering also appropriate material models for the atherosclerotic plaque components. They are mostly modelled as isotropic (Akyildiz et al., 2011; Teng et al., 2015); this simplification may be caused by missing direction-dependent experimental results, as well as a lack of structural information on collagen fibre distribution. Comparison of plaque responses in the longitudinal and circumferential directions may help us to describe better its behaviour and indicate the necessity of its more complex modelling and testing. Even though we know quite a lot about the mechanical behaviour of a healthy arterial wall (Holzapfel et al., 2014a; Humphrey et al., 2002) which comprises of three more or less homogenous layers (tunica adventitia, tunica media and tunica intima), the atherosclerotic tissue is a heterogeneous structure which influences its mechanical response.

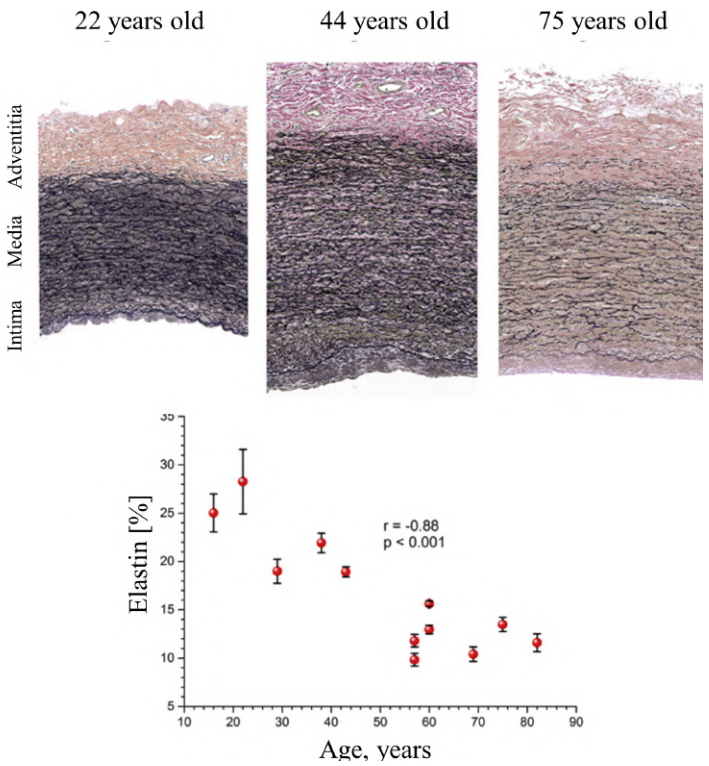

Figure 5.15: Transverse histological sections of the common carotid artery show a continuous decrease in elastin during ageing. Verhoeff-Van Gieson staining, with elastin stained black and collagen stained red. Reprinted from Kamenskiy et al. (2015).

Mechanical properties of arterial wall depend on its various micro-constituents. Their specific mechanical behaviour forms the final response, which can be measured. SMCs show the elastic modulus in their passive state on the order of 10^4 Pa while it can be increased significantly by means of their active contraction. In contrast, passive properties are controlled by an extracellular matrix formed by elastin with elastic modulus in order of 10^5 Pa and collagen with elastic modulus in the order of 10^9 Pa as summarized in Matsumoto et al. (2012) for wall layers[8]. However, when dealing with atherosclerotic plaques, one needs to take into account also lipids with elastic modulus ranging from 50 to 300 Pa (Loree et al., 1994) and other components such as calcifications. Calcifications were tested, e.g., in Ebenstein et al. (2009) showing a vast range of modulus from 100 MPa up to 21 GPa. The authors presented the average-mean values as 0.7 ± 2.2 GPa, which would mean that a significant portion of the calcifications had negative elastic modulus. This would be probably caused by non-symmetric outliers which make the standard deviation unrealistic.

Nevertheless, it can be concluded that calcifications can be very stiff. The geometry and mechanical responses of the carotid artery are changing during ageing, see Figure 5.15 which is inflicted by the irreversible degradation and fragmentation of intramural elastin (Kamenskiy et al., 2015). As elastin cannot be produced in adult age and is replaced by collagen, it is believed that collagen might emphasize the anisotropic mechanical response[9] of artery layers and atherosclerotic plaques.

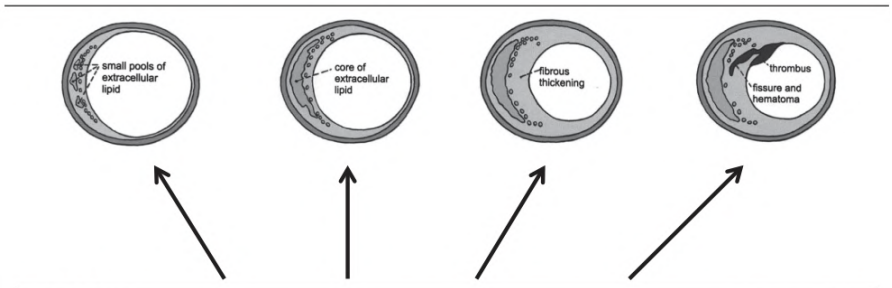

Plaque Type	III	IV	V	VI	VII	VIII
Description	Pre-Atheroma	Atheroma	Fibro-atheroma	Ruptured lesion	Calcified	Fibrous
SMC	-	-/+	+	-/+ or +	-/+	-/+
Collagen	-	-/+	+	-/+ or +	-/+	+
Stiffness	-	-	-/+	- or -/+	+	+
Homogeneity	-/+	-	-	-	-	-/+
Anisotropy	-	-/+	+	-/+ or +	-/+	-/+

Figure 5.16: Relations between the content and composition, relative stiffness, homogeneity, and anisotropy of different plaque types. Symbols "-", "±", and "+" indicate absence (or low amount), intermediate amount, and presence of a high amount, respectively. Reprinted from Akyildiz et al. (2014).

Akyildiz et al. (2014) proposed a summary table with a plaque classification from the American Heart Association based on the work of Stary et al., see, e.g., (Stary, 2000; Stary et al., 1992). Moreover, they introduced estimation of mechanical characteristics as relative stiffness, homogeneity but also anisotropy, see Figure 5.16. However, it is not clear how the level of anisotropy was estimated as the authors did not provide any

[8]Elastin fibres are nearly perfectly elastic and rather compliant while collagen fibres are much more rigid

[9]Collagen fibres are wavy and transmit a higher percentage of load after they were straightened; thus they cause strain stiffening of the mechanical response. As they are often modelled with dominantly circumferential orientation, the responses in different directions differ, causing an anisotropy.

relevant examples of mechanical studies of all plaque classes with corresponding directional information. Therefore, the author believes it was only expected due to a possible increase in collagen content, but it was not yet confirmed experimentally.

5.1. General overview on mechanical experiments for atherosclerotic tissue

Testing of a heterogeneous atherosclerotic tissue can be considered as a relatively complex process as it is hard to obtain a proper worthwhile specimen[10] from a tissue sample. Moreover, the thickness of the plaque varies considerably within the sample, so the tested specimen might not have a constant thickness which influences the computed stresses. It is often possible to separate more than one test specimen from the plaque sample obtained; for instance, a single sample of iliac artery with atheroma from autopsy could be divided into eight different components (Holzapfel et al., 2002). This data was expanded in their subsequent study Holzapfel et al. (2004) where nine iliac arteries were tested in circumferential and longitudinal directions and fitted with an anisotropic material model. Their results show such a large inter-patient variability; thus, the benefits of such a complex division and modelling cannot be proven without comprehensive statistical analyses.

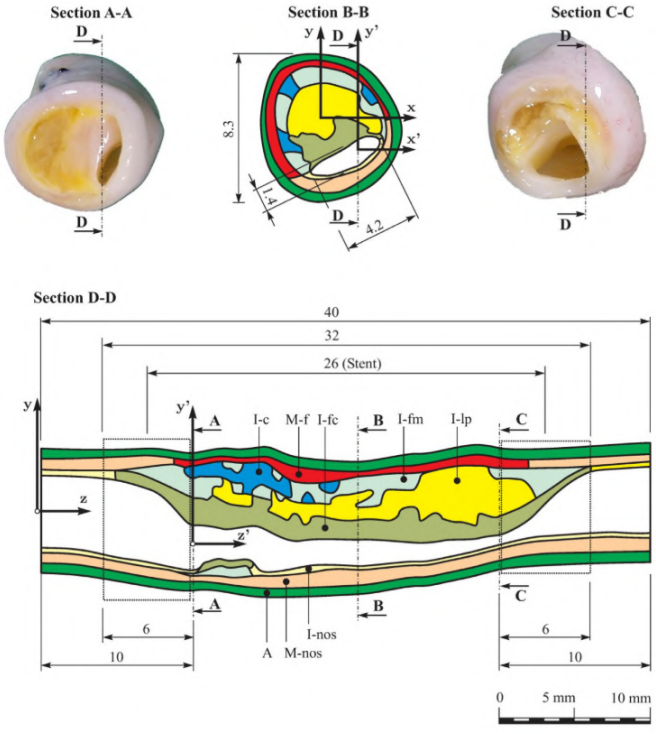

Figure 5.17: Sections of an iliac artery with atherosclerosis are incorporated with the segmentation of plaque components. Most of them were also mechanically tested but unparalleled among other studies. The components are adventitia (A), nondiseased media (M-nos), nondiseased intima (I-nos), fibrous cap (I-fc), lipid pool (I-lp), calcifications (I-c), fibrotic intima at the media border (I-fm) and diseased media (M-f). Reprinted from Holzapfel et al. (2005a).

[10]In the context of this work, a specimen is considered as a piece of an extracted sample (e.g., during endarterectomy) used for mechanical testing.

However, the majority of studies investigating mechanical behaviour of a fresh plaque from endarterectomy were not capable of dividing the samples for testing into such a large number of components, see Table 5.1. In contrast, most studies tested only a single circumferential specimen from each sample. Information on directional-dependency of carotid artery appeared recently in O'Reilly et al. (2020) where the authors used non-calcified samples for uniaxial tension testing in longitudinal and circumferential directions. Here, μCT was included in the measurement protocol before and after the experiment. This enabled the authors to use only non-calcified specimens, which is unique for experimental testing mainly due to the high costs of the scanning. Another disadvantage arises from the time the specimen cannot be immersed in saline solution, but this is believed to have only a minor influence on the mechanical response. Otherwise, only inverse FE analyses of indentation tests (Barrett et al., 2009; Chai et al., 2013, 2015) were performed. Therefore, few studies are available to assess tissue anisotropy.

Moreover, most of the presented comparisons of different plaque or wall components are based on a single parameter, e.g. initial modulus (Chai et al., 2013; Hoffman et al., 2017) which cannot describe the non-linear behaviour of the tissue. The reviews (Akyildiz et al., 2014; Walsh et al., 2014) showed a considerable variation among a large number of experimental studies focused on the mechanical response of atherosclerotic plaques in different arteries. However, the comparison was performed at a few specific levels of deformation and suffered from different test conditions in the compared studies. The authors suggested that a further post-operative plaque classification (e.g., from American Heart Association (AHA)) is needed to reduce the variation.

The idea of plaque classification is fundamental as it might show some unknown factors causing significant differences among studies and maybe even among specimens within a single study. The AHA classification focuses on the whole plaques, which are heterogeneous and can hardly describe an extracted specimen. Therefore, it is reasonable to evaluate every specimen with as many factors as possible, including, e.g., presence of calcification, macrophages, or location. In computational modelling, the FC is the most interesting to assess the plaque vulnerability. However, it is often impossible to test the cap itself, and other fibrous parts or components are evaluated instead. However, most studies model the plaque as a single component - FT - with the same mechanical behaviour, see (Gao et al., 2009; Huang et al., 2014a; Huang et al., 2014b; Kok et al., 2017; Tang et al., 2017). Moreover, Teng et al. (2014) confirmed that FC and FT (noted as media in the article) have similar average behaviour, confirming this way of modelling. Nevertheless, the classification should not be ignored. Although the underlying analysis might be tricky and expensive, somebody might attempt to do so. Based on structural data from electron microscopy, the findings in Mulvihill et al. (2013a) show a significant relationship between the presence of calcifications and the stress/stretch values at rupture.

When using pre-operative ultrasound to divide endarterectomy samples into three groups, the stiffest compressive behaviour was reported for the calcified group (Maher et al., 2009); however, the authors evaluated the mean material response by averaging the parameters of a chosen constitutive model for individual samples without any statistical analysis, not even considering the dispersion and hence it is hard to confirm the actual value of the classification. Teng et al. (2014) has shown that behaviour of media is comparable with the FC but showed that these components are significantly different from that of the tissue with intraplaque haemorrhage which might be identified during screening. These results indicate that the description of atherosclerotic plaque in biomechanical

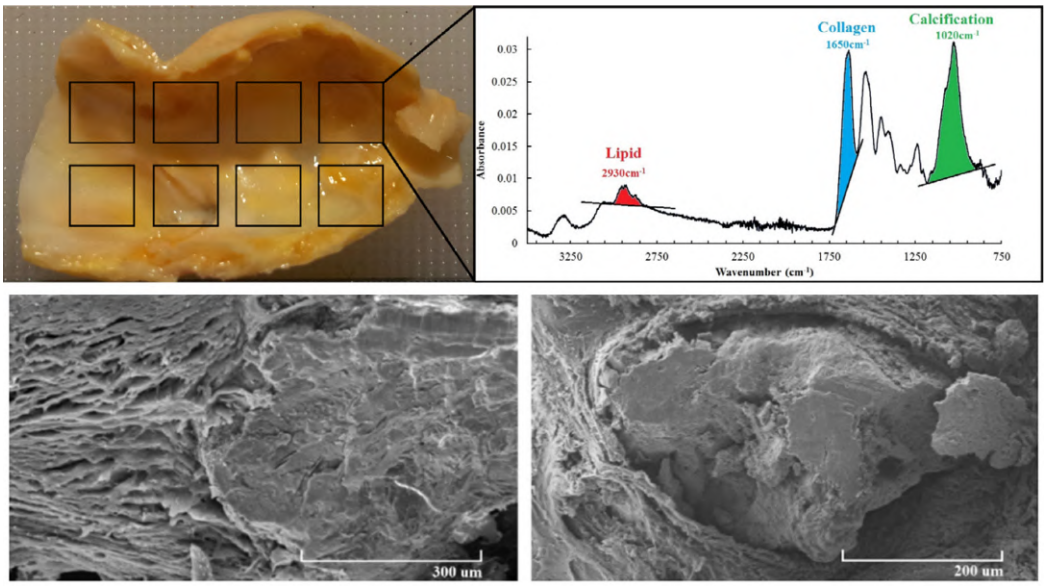

Figure 5.18: An example of structural analysis performed using FTIR (top row), identifying several components within the analysed area, which was then enhanced by SEM imaging (bottom row). Reprinted from Mulvihill et al. (2013a).

studies should be improved using suitable constitutive models with parameters based on the criteria disposable *in vivo*.

Although a more sophisticated investigation of the plaque structure might enable us to sort the results into more groups with lower dispersion, such more focused models cannot be exploited in computational predictions where the choice of the material model needs to be based on data obtainable *in vivo*. However, we might find that some factors are unimportant for plaque characterization while some others might be of interest. Then it will be essential to find a way how to detect them *in vivo* for a more suited constitutive model. This idea may be still too far from the current knowledge, and more data is required. As it is still almost impossible to combine a contribution of all structural components to estimate a global response of the tissue, it is preferentially separated into tiny specimens being homogenous as much as possible. Nevertheless, there are also other approaches to test the atherosclerotic tissue without the necessity of tiny specimens.

5.2. Testing approaches for atherosclerotic tissue

Investigation of mechanical properties in arterial biomechanics is mainly connected with a macroscopic response of arterial tissue like wall or components being characterized with tests like uniaxial, biaxial tension in different physiologically-relevant directions and inflation test (optionally with tension). These tests are recently followed with microscopical analysis, revealing the tissue microstructure and inspiring the structure-based constitutive models. In order to have comparable results among multiple studies, it is always important to keep the conditions similar as much as possible. There is no direct guidance for this purpose, but there were some attempts for atherosclerotic tissue (Walsh et al., 2014). One should keep in mind that experimental investigation of the atherosclerotic tissue might differ from a more standard test of the arterial wall itself. At the beginning of this section, three basic tests were mentioned. Among them, only the uniaxial test is feasible for the atherosclerotic tissue. However, *in vivo* the artery is loaded under condi-

tions similar to planar biaxial tension or, more closely, inflation test. However, both are not feasible because the planar biaxial test requires a relatively big square specimen while the tension-inflation test requires the whole tube such as a vessel wall.

Nevertheless, there is an unparalleled study Kural et al. (2012) who tested diseased carotid wall in the biaxial tension. However, except for one of the three patients who had moderate atherosclerosis, it is not clear whether the wall was influenced by atherosclerosis or not. Therefore, this study is assumed to focus on the healthy carotid wall and is not discussed here. However, there are other tests connected with atherosclerotic tissue. An interested reader is referred to literature review analyzing the methods in mechanical testing of arterial tissue (Macrae et al., 2016) where a thorough information can be found on biaxial and inflation tests. Table 5.1 also shows the specific type of test used in the particular study and the follow-up description, pointing out only the essential features related to the test.

5.2.1. Uniaxial tension

This is the most common approach in determination of biological material behaviour and involves elongating a rectangular specimen (or a dogbone-shaped specimen, as will be more discussed in the ultimate value section). It can be tested in multiple directions but preferably in circumferential and sometimes in longitudinal direction based on the sample size. The sample's radial dimension is insufficient for uniaxial tension test. As mentioned before, thickness is a critical component when calculating first Piola-Kirchhoff stress in axial and circumferential directions using

$$\sigma = \frac{F}{w \cdot t}, \tag{5.1}$$

where F is the measured force during the experiment at a given displacement, w is the width of the specimen, and t is the thickness; both of these undeformed dimensions form the initial cross-section of the specimen. Nevertheless, it is a required approximation for obtaining stresses. Of course, there are also other types of stress like Cauchy, and these can be found too, sharing the same problem, however. It is clear from the equation that one needs to measure only force and deformation to specify the stress-stretch response. The deformation is often tracked from mutual movement of two or more markers and can be then expressed as

$$\lambda_i = \frac{x_{i1} - x_{i0}}{X_{i1} - X_{i0}}, \tag{5.2}$$

where $x_{i1} - x_{i0}$ is a final distance between two tracked points, $X_{i1} - X_{i0}$ is a initial distance and i indicates the loading direction. An important assumption is that even though the specimen is rectangular and not dog-bone shaped, the deformation field is uniform in the measured area. Mulvihill et al. (2013b) published an interesting study showing that some atherosclerotic tissue might not be even suitable for a standard uniaxial tension test. Therefore, they specified that the width-to-length ratio should be lower than 1:1 for the sample to suit the tension test. Ratios more than 2:1 were found suitable for planar shear tension, as will be discussed later. This is an important finding for further studies that are not sure about their samples. Although uniaxial data is insufficient to describe a three-dimensional state of the artery, it still provides important information about the tissue and enables a comparison among specimens in the same type of test. Moreover, it provides a simple method of assessing the ultimate characteristics of the tissue.

Table 5.1: Summary table for experimental studies dealing with carotid atherosclerotic tissue.

Sample (year)	Test type (direction)	Number of patients	Number of specimens and description	Constitutive model	Ultimate stress [kPa]	Ultimate strain
Ebenstein et al. (2002)	nano-indentation (radial)	3*	NA; calcifications, partially calcified, FTe, hematoma	NA	NA	NA
Maher et al. (2009)	uniaxial tension (circumferential)	14	16; 8 calcified, 4 echolucent, 4 mixed	2nd order polynomial	NA	NA
Maher et al. (2009)	indentation (radial)	14	44; 16 calcified,5 echolucent, 23 mixed	2nd order polynomial	NA	NA
Barrett et al. (2009)	indentation (radial)	8	49 atherothrombotic	single term Ogden	NA	NA
Ebenstein et al. (2009)	nano-indentation (radial)	10	744; hematoma, FT, partially calcified, calcification	linear Young's modulus	NA	NA
Maher et al. (2011)	compression (radial)	8	21; 8 calcified, 8 mixed, 5 echolucent	Demiray	NA	NA
Lawlor et al. (2011)	planar tension (circumferential)	14	14 whole plaques; 2 hard, 6 mixed, 6 soft	3rd order Yeoh	366.67 ± 220.5	0.497 ± 0.088
Mulvihill et al. (2013a)	planar tension (circumferential)	23	25 whole plaques; 8 calcified, 17 lipid dominant	NA	618 ± 230 342 ± 160	0.631 ± 0.17 0.927 ± 0.26
Chai et al. (2013)	indentation (axial)	8	214; 29 SC/Mid; 36 SC/Sh, 54 SC/Intima, 14 UC/Mid, 25 UC/Sh, 36 UC/Intima, 20 CP/LRNC	neo-Hooke	NA	NA
Heiland et al. (2013)	indention-bending	2	9; NA	GOH, polynomial	NA	NA

Sample (year)	Test type (direction)	Number of patients	Number of specimens and description	Constitutive model	Ultimate stress [kPa]	Ultimate strain
Teng et al. (2014)	uniaxial tension (circumferential)	21	181;65 media, 59 FC, 36 lipid, 21 intraplaque haemorrhage	modified Mooney–Rivlin	NA	NA
Teng et al. (2015)	uniaxial tension (circumferential)	24	105;35 media, 32 FC, 26 lipid, 12 intraplaque haemorrhage	NA	247.6[169.0, 419.9] 158.3[72.1, 259.3] 68.8 [48.5, 86.6] 83.0 [52.1, 124.9]	0.21[0.17, 0.32] 0.18[0.10, 0.27] 0.25[0.11, 0.30] 0.20[0.17, 0.44]
Chai et al. (2015)	micro-indentation (axial)	5	28;11 intima, 7 middle FC, 10 shoulder FC	Holzapfel 2000	NA	NA
Barrett et al. (2015)	planar tension (circumferential)	6	6 whole plaques; 3 low stiffness, 2 medium stiffness, 1 high stiffness	NA	400 ± 90	0.44 ± 0.13
Davis et al. (2016a)	uniaxial tension (circumferential)	8	34; FC	2nd order polynomial	NA	NA
Cunnane et al. (2016)	planar tension (circumferential)	24	24 whole plaques	NA	490±230	0.89±0.36
Barrett et al. (2016a)	planar tension (circumferential)	17	17 whole plaques; 2 speckled, 9 diffuse tissue, 4 concentric, 2 diffused necrotic core	NA	470[413, 529] 970[962, 984] 486[457, 581] 269[219, 289]	1[0.95, 1.06] 1.03[0.87, 1.2] 1.49[1.19, 1.67] 0.72[0.68, 0.8]
Barrett et al. (2016b)	toughness (radial)	21	62; low, high combination, generally high	NA	NA	NA
Barrett et al. (2017)	planar tension (circumferential)	16	17 whole plaques; 2 speckled, 2 diffuse tissue, 4 concentric, 9 diffused necrotic core	NA	NA	0.74 ± 0.17 1.04 ± 0.17 1 ± 0.06 1.43 ± 0.26

Sample (year)	Test type (direction)	Number of patients	Number of specimens and description	Constitutive model	Ultimate stress [kPa]	Ultimate strain
Cahalane et al. (2018)	nano-indentation (axial)	10	NA; A,B and C based on Hounsfield Unit	linear Young's modulus	NA	NA
O'Reilly et al. (2020)	uniaxial tension + relaxation (circumferential, longitudinal)	22	32; 17 circumferential 15 axial	3rd Yeoh	242[189, 310] 209[166,265]	NA
Lisický et al. (2021b)	uniaxial tension (circumferential, longitudinal)	44	141; longitudinal, circumferential, calcified, non-calcified, <70, >70, out of LC, near LC, women, men	3rd Yeoh, Holzapfel 2005	337[227,535] 355[229,595] 323[220,504] 365[244,605] 351[221,578] 329[231,573] 432[261,626] 297[212,517] 282[210,525] 366[231,581]	0.15[0.12,0.21] 0.20[0.12,0.30] 0.15[0.11,0.22] 0.18[0.12,0.28] 0.14[0.11,0.22] 0.19[0.14,0.31] 0.20[0.13,0.31] 0.16[0.10,0.22] 0.12[0.09,0.16] 0.18[0.13,0.29]
Johnston et al. (2021)**	uniaxial tension (circumferential)	20	20; 12 axial dominant, 8 circumferential dominant	NA	307 ± 183 872 ± 632	0.13 ± 0.04 0.10 ± 0.04

NA: not applicable, * fixed in formaldehyde, ** it is not clear from the article whether the specimens were tested in circumferential or axial direction as images goes against the text, SC: structured, UC: unstructured, CP: collagen poor, Min: middle of FC, Sh: shoulder of cap, LRNC: lipid rich necrotic core, GOH: Gasser, Ogden and Holzapfel model Gasser et al. (2005)

5.2.2. Planar shear test

The width-to-length ratio mentioned in the previous sub-section (Mulvihill et al., 2013b) is indeed essential when assessing mechanical properties. The main loading direction of atherosclerotic plaques is generally considered to be circumferential. Therefore, most experimental studies are testing only this type of specimen. However, if we would like to estimate the mechanical behaviour of FC using, e.g., uniaxial tension, it would be almost impossible for a proper ratio of below 1:1 as the FC covers only a limited area. Sure, it is not a rule, and some plaques might have large LC covered by a large FC as might be in Teng et al. (2014) who tested incredible 59 FC specimens from 14 samples in the circumferential direction. This is though very rare[11]. Nevertheless, the ratio is essential when the endarterectomy sample is tested as a whole in the circumferential direction; with their size and width-to-length ratio, most of these samples correspond rather to planar tension test, see Figure 5.19.

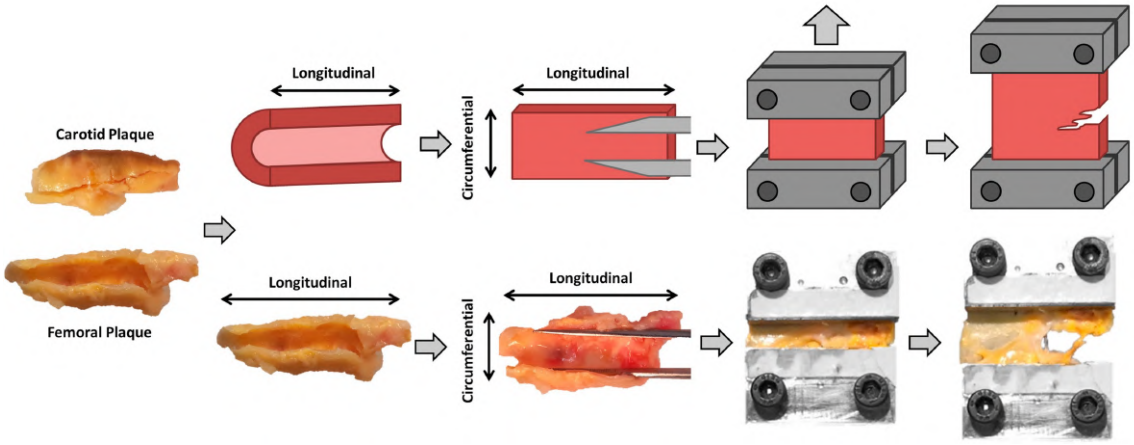

Figure 5.19: Sample preparation for planar tension test of femoral and carotid plaques in the circumferential direction. Reprinted from Cunnane et al. (2016).

Testing of large and wide specimens might sound confusing as the atherosclerotic plaque was described as very complex with varying thickness until now. Nothing has changed, and this remains very curious about studies that tested whole samples in planar tension. Almost all studies which used a planar tension test for the whole sample come from the same research group (Barrett et al., 2016a; Cunnane et al., 2016; Mulvihill et al., 2013a) except for Lawlor et al. (2011) who do not report the test as planar shear but as uniaxial tension and do not consider limitations for the width-to-length ratio; the authors probably did not realize a possible problem. Generally speaking, this type of test is going in the opposite direction, given that local mechanical properties are essential to describe better the atherosclerotic tissue behaviour. All this despite the fact that studies from the same research group introduced also a very sophisticated way of plaque classification using scanning electron microscopy with subsequent vibrational spectroscopy (Fourier transform infrared). Therefore, they were able to quantify the amount of collagen, calcification, and lipid, but all this information would hardly help to decrease the variability with additional factors for the whole sample being highly non-homogeneous.

[11]The author of this thesis tested endarterectomy samples with colleagues from almost 60 patients and suitable circumferential FC specimens were counted in units.

5.2.3. Compression test

Compression of the specimen is one of the tests which is not expected as, e.g., uniaxial or biaxial tension in arterial biomechanics. However, it brings a vital information to find the relation between the underlying structures. It can provide a stress-stretch response needed for constitutive modelling and a stiffness-dependence when the loading frequency is changed as shown long time ago in LEE et al. (1991). They found that the stiffness increases with presence of calcifications, which is an expected result for the compression test. The continuous compression can be achieved, e.g., as shown by Maher et al. (2009) who placed a specimen between two platens for compression. Their protocol included both pre-cycling to 10 % with subsequent static loading up to 60 % deformation. The authors then expanded the work also for cyclic compression test to identify a potential inelastic behaviour of carotid plaques (Maher et al., 2011) which though did not confirm significant differences between the measurements with a more extended periods (frequencies) between cycles. All the above studies have something in common. They investigated relatively large samples where it would be impossible to distinguish and therefore relate the responses with the underlying structure properly.

To improve this disadvantage, the solution is almost offered. Why we should compress the whole sample when it can be compressed locally with a micro-indenter, see Figure 5.20. Of course, this is nothing new and applications for atherosclerotic plaques already exist (Barrett et al., 2009; Chai et al., 2013, 2015). The approach is described and validated in Cox et al. (2008). Generally, a ball indenter is pressed towards the tissue while the force and depth of indentation are continuously measured.

Moreover, the bottom of the specimen is screened by a confocal microscope to see the underlying structure. However, it is impossible to extract the elastic parameters directly, and inverse FE analysis is required. This brings an additional variance, but the approach was already tested and showed that it could describe local non-linear and anisotropic behaviour of the specimen (Cox et al., 2008). The research went even further and introduced nano-indentation (Cahalane et al., 2018; Ebenstein et al., 2009). The output of this approach is a local mechanical characteristic such as Young's modulus.

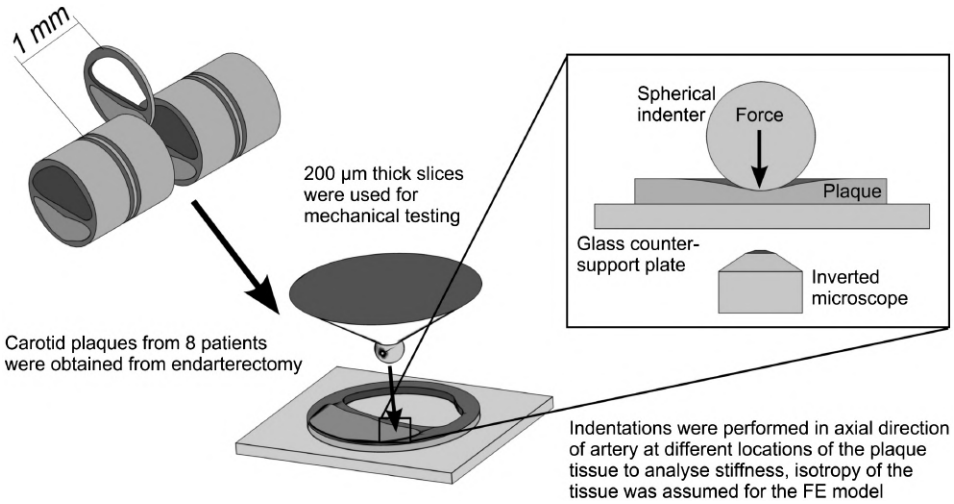

Figure 5.20: 200 μm slices prepared with cryotome for compression test of carotid plaques. This process enables preparation of multiple specimens of a single plaque. Reprinted from Chai et al. (2013).

A different approach of indentation was proposed in Heiland et al. (2013). Their novel approach enables investigation of the viscoelastic behaviour of carotid plaques through dynamic testing. Specimen of 3-6 mm width is glued to the testing base so that a part of this width laps over the base while the indenter moves in parallel with the base edge and induces bending of the specimen. Images, force and indenter displacement, were continuously recorded and exploited in a subsequent inverse FE analysis. Otherwise, it would be impossible to estimate mechanical properties.

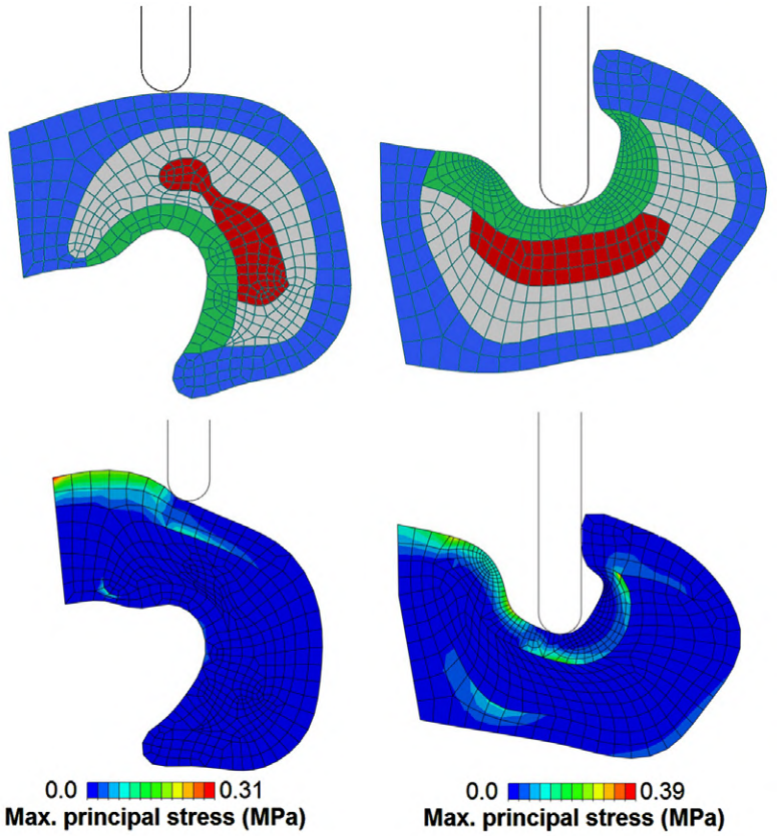

Figure 5.21: FE model for inverse analysis based on experimental setup of indentation test with a plaque section causing a bending. The model is fixed (glued during experiment) on the left site. Reprinted from Heiland et al. (2013).

Moreover, histological sections were also prepared to help with the segmentation of different plaque components. An essential thought behind this approach is the consistency of the plaque components during the test, thus their separation does not influence the underlying behaviour. The authors reported that they could obtain comparable responses as some experimental studies published previously. As there is a very high variation among them, it is not surprising to fit some of them; nevertheless, it does not diminish the potential of this study.

5.2.4. Mechanical toughness

Another mechanical characterisation of atherosclerotic plaque can be assessed through toughness tests being performed very rarely, though. It was shown that the toughness[12] differs among the different parts of the carotid artery, namely the common, bifurcation

[12]Calculated as the energy required for a controlled cut to propagate through the plaque.

and internal parts, whereby the tougher response was found in the last two aforementioned (Barrett et al., 2016b). It is not surprising since the plaque in the carotid artery is mostly localised in the bifurcation to the internal carotid artery, as illustrated in Figure 1 in that study.

5.3. Full-field measurement

Most of the experimental studies investigating the mechanical properties of atherosclerotic tissue assume a uniform response for the whole specimen. Therefore, the strains are analysed globally by tracking the displacement of, e.g., two markers resulting in average deformation in between. With this approach, it is straightforward to translate it into the stress-strain relationship, which can be then approximated by a constitutive model[13]. However, the assumption of homogeneous strain and thus stress fields in the analysed area might not be robust in biomechanics.

Moreover, this average response is then transferred into a computational model. This does not result from computational or theoretical limitations but rather from a lack of experimental quantification of possible local variations. The recent development of CCD cameras leads to their price decrease and thus in more frequent applications. The regional characterisation of strain can be addressed by a full-field method, namely digital image correlation (DIC)[14] which is used frequently in many research fields but also in the industry (Zhao et al., 2019).

Consequently, the deformation of a specimen is known in multiple points of the image, enabling a local investigation. Applicability of DIC for soft tissues was shown for human skin (Ní Annaidh et al., 2012), thigh muscle (Affagard et al., 2015), human ascending thoracic aneurysm wall (Cavinato et al., 2019) or recently for biaxial stress relaxation of a tissue of vaginal mucosa (Pack et al., 2020) and many others, confirming the advantages of evaluation of full-field deformation. The method has many variations enabling more complex analyses, e.g., a 3D DIC where two cameras are used to track surface deformation. This variant enables also to reconstruct the surface (rather than a simple plain field only (Davis et al., 2015, 2016a), or even a volume expansion as shown for biological tissues (Acosta Santamaría et al., 2018; Bersi et al., 2020; Dall'Ara et al., 2014; Di Giuseppe et al., 2020). The mentioned volume digital correlation brings unbelievable information about the whole 3D structure providing thus a potential for more complex analyses. However, it requires a special treatment of the samples in order to obtain a suitable speckle pattern within the whole volume as it is a very important factor to analyse the deformation field (Lionello et al., 2014). Nevertheless, 2D or 3D DIC is easily accessible with a proper device as it is possible to analyse the results by open-source algorithms like Ncorr within the Matlab interface (Blaber et al., 2015) or (Solav et al., 2018) or, e.g., Py2DIC in Python (Belloni et al., 2019).

To the best of the author's knowledge, there is only a single study analysing the strain field of atherosclerotic tissue, namely of the FC and it was published very recently by Johnston et al. (2021). The authors combined the complete field information on strains with collagen fibre orientation (average from a whole specimen). They were, therefore,

[13]Parameters of a constitutive model are optimised by using the experimental stress-strain characteristics and minimising the differences between the computed and measured stresses at specific deformations. Linear and non-linear methods are used here, most frequently the least-squares method.

[14]There are also other possible approaches like moiré, speckle interferometry and other grid methods, but DIC can be considered as the most used.

able to analyse stress-strain characteristics with strains evaluated locally in points near the rupture, which is only possible with full-field measurements. It would also be interesting to correlate the rupture location with local fibre orientation or other structural information. This brings more possibilities for further research in this field as atherosclerotic tissue (often tested in the form of large specimens) can exhibit heterogeneous strain fields due to the underlying structure, influencing the obtained characteristics. However, the full-field information alone would not be sufficient if the stresses were averaged through all the section. Therefore, it is crucial to introduce another concept of identifying the material model. As there are many alternatives, only two basic concepts will be discussed here. In case of greater interest, the reader is referred to the thorough literature review on this topic in Avril et al. (2008).

5.3.1. Finite element method updating

Finite element method updating (FEMU) or, in other words, inverse FE analysis was already mentioned in the context of indentation tests of atherosclerotic tissue. The name itself implies that the numerical solution is obtained using the well-known FE method; the model is updated until some condition is reached. The experimental setup gives the necessary boundary conditions for the computational model. Optimisation of an appropriate cost function minimises the discrepancy between the measured and computed displacement/strain fields. Material parameters are changed during the optimisation problem until solution with a sufficient accuracy is found.

The approach can be divided into two primary forms. The first one is the force balanced method, also denoted as FEMU-F (Cottin et al., 1984), where all the nodal displacements, as well as the prescribed forces, are known from the experiment. It is worth emphasising that for the FEMU-F analysis a direct FE method solution is not necessary. However, in many cases, the displacements are known only partially, and hence the force method is not suitable. Therefore, the displacement method, also denoted as FEMU-U, was developed as an alternative approach (Cottin et al., 1984; Farhat et al., 1993). Both methods were modified in many ways till now, and even a hybrid method combining both of them was presented (Giton et al., 2006). The chosen optimisation algorithm influences mainly the number of iterations needed to find a suitable solution and consequently the computation time. Iterative gradient-based methods are often used here, e.g., a cost function gradient is determined to find its minimum. However, this minimum may be only local due to various possible combinations of model parameters influencing the final solution.

Nevertheless, the method often needs a low number of iterations and is adequate for simpler models with a moderate number of unknown constitutive parameters. Another way might be application of a heuristic approach and, e.g., evolutionary algorithms, which might help to find the global minimum of the function and thus a more robust solution. Although this is followed by a large number of necessary FE analyses prolonging the time needed to obtain the solution, it could be beneficial for very complex models with a large number of unknown parameters in situations with heterogeneous material characteristics (Burczynski et al., 2006).

5.3.2. Virtual fields method

The development of the virtual fields method (VFM) is dated 1989. However, the theoretical background was published in a series of articles (Grédiac et al., 2002a,b, 2003) in order to target and avoid known drawbacks like a straightforward solution of multiple models or simplifications of loading boundary conditions of FEMU and other methods. The VFM takes advantage of full-field measurements of the sample and takes strains as an input. Strains are calculated from the displacement field using, e.g., DIC. It also assumes that loading conditions are known but it does not limit them. Stress is expressed by means of the unknown material parameters of the chosen constitutive model on the basis of the known strain field. Based on this, virtual fields are chosen, which is the critical issue of the method. Various approaches were developed like its analytical construction, usually by means of a polynomial function. This can also be improved by its automatization (Grédiac et al., 2002a) or piecewise definition, so that the sample does not have the same functional expression. VFM requires many assumptions to estimate suitable constitutive parameters. However, many of them can be easily included when considering typical specimens for uniaxial or biaxial tension tests, assuming a constant or linear strain distribution through the thickness. A review by Grédiac et al. (2006) describes the methodology together with applications, and a comparison with other approaches can be also found in Avril et al. (2008). The VFM, like other non-updating approaches, does require full-field strain measurements; otherwise, no solution can be found. However, a faster solution can be found with only a few assumptions, thus providing more extensive posibilities. Moreover, development of the method continues as confirmed by very recent publications on this topic (Livens et al., 2021; Mei et al., 2021a,b).

Regardless of the chosen approach for identifying constitutive parameters, it is clear that full-field approaches are necessary in experiments to incorporate the material behaviour properly. It might not be required for homogeneous materials like steel the behaviour of which is well known, but the need increases when dealing with biological tissues containing multiple structural components.

5.4. Ultimate stress/strain

The knowledge of the constitutive models for plaque components is essential as it is a necessary input for computational modelling. Here, experiments can help with their identification and, moreover, give other mechanical characteristics of the same importance, namely tissue failure properties. Once this value is known, the results from computational modelling can be compared to estimate the potential rupture risk. The ultimate values depend on the specific loading conditions, which correspond to biaxial extension in the case of arteries. Thus the ultimate values from biaxial loading are of interest. However, it is not easy to estimate the tissue strength from the commonly used biaxial tension tests as the rupture occurs at the clamps. (Davis et al., 2015; Duprey et al., 2016; Romo et al., 2014) showed a possible extraction of the ultimate stresses from a bulge-inflation test for ascending thoracic aorta aneurysms. Their approach required some assumptions (membrane state of stress) and full-field displacement measurement but it seems as an excellent approximation. Unfortunately, as mentioned already, such tests are not feasible

for the atherosclerotic tissue; thus only tension tests are commonly used to obtain ultimate values of plaque components.

The tissue strength of 300 kPa is often used as decisive for possible plaque failure as thoroughly discussed in the review by Holzapfel et al. (2014b) where the authors confirmed a lack of information on the ultimate stresses and strains. Cilla et al. (2012) proposed a vulnerability factor based on comparison of the maximum computed stresses with the critical value of 0.247 MPa referred to the experimental study by Loree et al. (1994). Fracture stress and strain in the circumferential direction for carotid atherosclerotic plaques were presented in Lawlor et al. (2011), similarly to Teng et al. (2015) who focused on the ultimate values of various components of the carotid plaque; however, almost half of the samples in Teng et al. (2015) was not included due to limitations of the used testing device. Results of a planar tension test with whole carotid plaques presented in Cunnane et al. (2016) are hardly comparable due to the plaque non-homogeneity and a more complex state of stress in planar tension. The studies were able to find ultimate stresses close to the 300 kPa boundary. Despite the number of studies mentioned in Table 5.1, only some of them presented also the ultimate values. This might be due to improper samples disabling an investigation of ultimate values due to ruptures close to the clamps. Nevertheless, the insignificance of rupture location (near the clamp or central location) was shown for carotid plaques in Cunnane et al. (2016). It is, of course, convenient to analyse rupture in the specimen centre. However, the latter study might reveal that the rupture occurs rather due to tissue structure with only insignificant location-dependent differences. Therefore, the limited sample size, disabling a proper preparation of a dog-bone shape, might not be that problematic for these characteristics.

Even though ultimate strains can provide similar information about the failure, they are rarely investigated or used for risk assessment. However, there might be a problem as the ultimate values differ greatly among studies that provide this information. While Teng et al. (2015) showed average ultimate strains of around 0.2, contradictory results were found in Lawlor et al. (2011) but also in, e.g., (Barrett et al., 2017; Mulvihill et al., 2013a) and some others from the same research group. For carotid samples based on planar tension testing of whole very complex plaques they obtained ultimate strains up to 1. Therefore, this issue requires much more investigation to clarify and suggest applicable ultimate strains. Some variance is expectable because different tests are used, as shown for thoracic aorta in Duprey et al. (2016) where ultimate engineering strains for biaxial and uniaxial test protocol were 0.37 and 0.69[15], respectively. This is approximately 20 % difference while almost eight times higher differences occur when comparing data from uniaxial tension (Teng et al., 2015) and concentric plaque-type from Barrett et al. (2016a). An *In vivo* estimation of strains (see later in section 5.7) showed that average values of 0.05 can occur for the carotid artery (Nederveen et al., 2014) during a cardiac cycle, i.e. between the systolic and diastolic pressure. Although the load difference is lower than during mechanical testing, it indicates that the strain values might be rather lower. Therefore, a proper characterisation is highly needed to have some threshold for computational modelling.

[15]This value is for circumferential direction, however, the axial direction showed a similar value of 0.63. The data was tested in Duprey et al. (2010)

5.4.1. Plaque fracture

Ultimate stress or strain can be a good indicator for possible plaque rupture. However, it is also essential to know the mechanism of rupture. There is a specific field called fracture mechanics in which crack propagation is studied. Although it has a robust background for homogenous, isotropic linear elastic or elastic plastic materials, it is relatively rarely used in the biomechanics of atherosclerosis. A plaque rupture can occur under low loads due to existing cracks or other material discontinuities. There are studies where a well-known rupture mechanism is applied to the atherosclerotic tissue. Cohesive theory of fracture of three-layered atherosclerotic plaque with artificial cracks was firstly introduced in Ferrara et al. (2008). They studied a crack development under varying conditions like a higher material resistance and geometrical variability (three models were reconstructed from MRI) and showed that the geometry itself influenced the stress distribution. In Pei et al. (2013), principles of the linear elastic fracture mechanics[16] were applied for idealized models. Therefore, they assumed that all the plaque components are linear elastic to simulate crack initiation, fatigue crack propagation and the final plaque rupture. The initial crack location was chosen in the maximum stress area, as well as in other parts of the plaque to study a variety of possible scenarios. Similarly to Ferrara et al. (2008), geometrical variations were among the most significant features influencing the growth. The crack growth description is indeed an exciting challenge, but it remains questionable

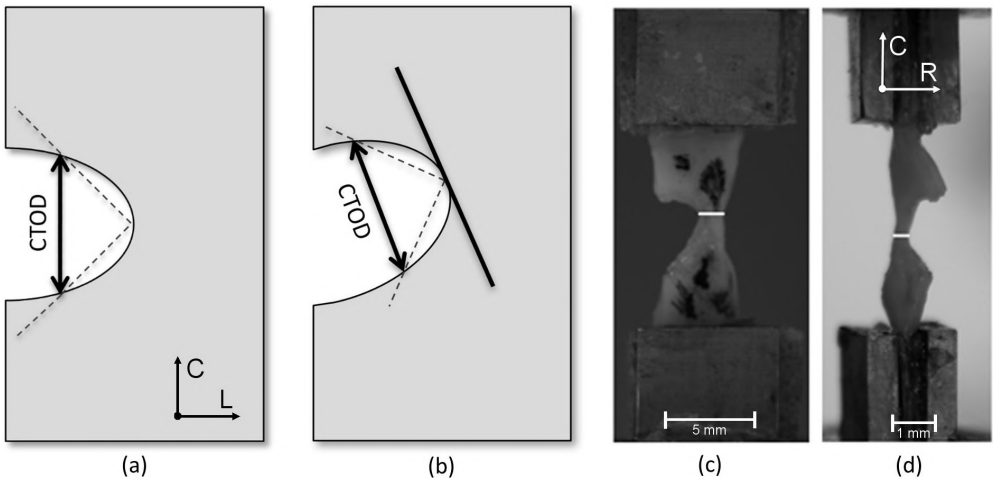

Figure 5.22: CTOD measurements depicted for atherosclerotic plaque which is calculated between intersections of the sides with 90 deg vertex centred at the crack tip . Reprinted from Davis et al. (2016b).

whether the cracks can be spotted during imaging. Moreover, all the above studies lacked experimental evidence for their models. To the best author's knowledge, there is only one experimental study related to carotid plaques by Davis et al. (2016b) who applied the crack tip opening displacement (CTOD), known from elastic-plastic fracture mechanics[17]. These metrics should describe fracture toughness. A miniature tensile experiment with a single edge notch was used for FC specimens with an initial crack (crack length between 45 - 70 % of the specimen width). The authors also included information about the FC

[16]The stress intensity factor K was used to describe status at the crack tip. A cyclic growth rate was then determined from K using Paris-Erdogan law

[17]Another metric is J-integral and both are used for problems where the plastic zone is too large for a standard linear elastic fracture mechanics. It is not mentioned there why a large plastic zone is assumed.

structure, which helped them to analyse its contribution to the fracture. However, the number of samples was limited and thus the results only indicate a trend where a higher CTOD was found for plaques with lower collagen content. This is a pioneering study pointing to an alternative way how to evaluate a rupture risk of the FC. However, it is questionable whether the above mentioned approaches apply to a heterogeneous and complex material like atherosclerotic plaque. As the pulsating blood flow acts onto the plaque, it might be relevant to introduce more complex approaches such as hydraulic fracture, which accounts for shear stresses, see Perkowska et al. (2017). However, here the evidence does not exist.

5.5. Representation of results

Regardless of the chosen experimental approach, the atherosclerotic tissue (the same applies for most soft tissue) often reveals high variation among tested samples/specimens. It is expectable as each person is unique, which applies to the tissue. Nevertheless, it is essential to experimentally investigate the behaviour of multiple samples to reveal some patterns in the behaviour. It is also crucial since the PS data are hard (or even impossible) to obtain, and thus some average response is needed. To specify a population-based model from multiple samples, averaging is often applied to specify a representative material response. However, methods used to analyse experimental data are often inadequate and may thus cause misinterpretation of the essential information. Average-mean together with a standard deviation is often used when describing the experimental data see, e.g., (Lawlor et al., 2011; Maher et al., 2009; Sommer et al., 2012) even though the data distribution was not investigated and showed high asymmetry. Ebenstein et al. (2009) characterised results of their mechanical study by box plots where highly asymmetric distribution is evident; in contradiction to this evident fact, however, they used average-mean value and standard deviation to show population behaviour, no matter that these values implicate negative initial modulus in a significant percentage of cases. Thus, this approach is not suitable for constitutive modelling of such non-linear behaviour of materials. Another commonly used approach is to model each response by a constitutive model and to calculate average values of model constants. Here, isotropic (Maher et al., 2009; Schulze-Bauer et al., 2003) as well as anisotropic models (Holzapfel et al., 2005b; Polzer et al., 2015; Sommer et al., 2012) were used without any analysis of data distribution and discussion on the appropriateness of this representation.

In contrast, Teng et al. (2014) suggested that an average model representing a set of samples should not be specified based on means or medians of its constants since their combination is not unique and there is not the only set of constants that can describe the behaviour. Moreover, they suggested that a different averaging method might cause differences in the resulting representative response. Proper representation of an average constitutive model is also important for further analyses and comparisons (Walsh et al., 2014). Akyildiz et al. (2014) compared in their review atherosclerotic tissue from various sources while averaging the stiffness at a specific level of deformation. Again, no attention was paid to the shape of data distribution, resulting in data averaging which may increase differences among studies. Therefore, a unified methodology for data analysis of the results of mechanical experiments is needed for an accurate constitutive description of population-representative mechanical behaviour and its further application in research and clinics. The problem of a proper representation has been noted recently (Vitásek et al.,

2021), although the authors focused on the abdominal aortic tissue. Their results showed remarkable differences in the response when (i) averaging the responses before the fitting process, (ii) averaging the constitutive parameters or (iii) fitting the constitutive model to all responses at once. All this should be kept in mind before fitting the constitutive model.

5.6. Constitutive models for plaques

Experimental investigation of mechanical properties is essential and requires an accurate description via a constitutive model for further computational modelling—the structure of arterial healthy and atherosclerotic tissues results in non-linear stress-strain responses with large deformations. Therefore, the hyperelastic model is preferably used. Hyperelastic material is a type of constitutive model which is ideally elastic and for which a strain-energy density function W exists as a scalar function of some strain or deformation tensor. In other words, stress-strain relation can be derived from W using

$$S_{ij} = \frac{\partial W}{\partial E^L_{ij}} = 2\frac{\partial W}{\partial C^R_{ij}}, \tag{5.3}$$

where S_{ij} are components of 2. Piola-Kirchhoff stresss tensor, E^L_{ij} are componets of Green-Lagrange strain tensor and C^R_{ij} are components of right Cauchy-Green deformation tensor.

There are several types of potentials W describing a non-linear behaviour of atherosclerotic tissue. The summary Table 5.1 lists some of them used to describe the stress-strain relationship. Therefore, this section mentions only those of preference for carotid arterial tissue, both healthy and diseased. It is important to note, that soft biological tissue is often assumed as incompressible, meaning that $J = \det \mathbf{F} = 1$, where J is volume ratio (3^{rd} invariant of $\mathbf{F}$) and $\mathbf{F}$ is deformation gradient.

5.6.1. Isotropic model

Neo-Hooke

$$W = c_{10}(I_1 - 3), \tag{5.4}$$

where $c_{10} = \frac{\mu}{2}$ is stress-like material parameter with c_{10} describing material initial stiffness while μ describes initial shear modulus, $I_1 = \lambda_\theta^2 + \lambda_z^2 + (\lambda_\theta \lambda_z)^{-1}$ is the first invariant of right Cauchy-Green tensor $\mathbf{C}$, when accounting for incompressibility $\lambda_\theta \lambda_z \lambda_r = 1$. On of the simplest hyperelastic model for rubber-like materials.

Mooney-Rivlin

$$W = \sum_{i+j=1}^{3} c_{ij}(I_1 - 3)^i (I_2 - 3)^j, \tag{5.5}$$

where c_{ij} are stress-like material parameters, I_1 and I_2 are first and second invariants of right Cauchy-Green deformation tensor $\mathbf{C}$.

Ogden

$$W = \sum_{r=1}^{N} \frac{\mu_r}{\alpha_r}(\lambda_1^{\alpha_r} + \lambda_2^{\alpha_r} + \lambda_3^{\alpha_r} - 3), \tag{5.6}$$

where λ_1,$\lambda_2$and λ_3 are principal stretches 5.2, N is number of terms ($N = 1$ was used in Barrett et al. (2009)), μ_r are stress-like parameters describing stiffness and α_r are dimensionless material parameters. The model was firstly introduced in Ogden et al. (1972).

Demiray

$$W = \frac{a}{b}\left(e^{\frac{b}{2}(I_1-3)} - 1\right), \tag{5.7}$$

where a is a stress-like material parameter and b is a dimensionless parameter defining progression of the stress-strain curve. This model was firstly used by Demiray (1972) and used for soft tissue (carotid bifurcation) in Delfino et al. (1997).

Yeoh

$$W = \sum_{i=1}^{N} c_{i0}(I_1 - 3)^i, \tag{5.8}$$

where c_{i0} are stress-like material parameters defining stiffness of material. The model was proposed in Yeoh (1993) again for rubber-like materials but found a broad use in soft tissue modelling.

Modified Mooney-Rivlin

$$\begin{aligned} W = {} & c_1(I_1 - 3) + c_2(I_2 - 3) + c_3(I_1 - 3)^2 + c_4(I_1 - 3)(I_2 - 3) \\ & + c_5(I_2 - 3)^2 + c_6(I_1 - 3)^3 + c_7(I_1 - 3)^2(I_2 - 3) \\ & + c_8(I_1 - 3)(I_2 - 3)^2 + c_9(I_2 - 3)^3 + D_1\left(e^{D_2(I_1-3)} - 1\right), \end{aligned} \tag{5.9}$$

where c_1 - c_9, D_1 and D_2 are material constants. This model description is taken from ADINA (R&D, Inc.) (Bathe, 2002) because it differs from the description e.g., from ANSYS. It is explicitly stated that constants D_1 and D_2 are primarily intended for modelling of certain biological materials. Moreover, c_3 - c_9 are available for more close fit though increasing a possible over-fitting problem. This model is widely used in structural and FSI studies of atherosclerotic plaques in the research group of D. Tang, see e.g., (Tang et al., 2008, 2009, 2017) though only with a limited number of non-zero constants (c_1, c_2, D_1 and D_2). It is worth to mention that this model is a combination of Mooney-Rivlin and Demiray models.

5.6.2. Anisotropic model

More complex material descriptions might also incorporate the tissue anisotropy, preferably by means of structural information like collagen fibre orientation and distribution. These models were generally developed for an arterial wall (and layers) though they are sometimes used also for experimental characterization of atherosclerotic plaque (Chai et

al., 2015; Heiland et al., 2013; Lisický et al., 2021b) or for all components of the computational model (Cilla et al., 2012, 2015). Nevertheless, the fibre direction and distribution is fitted phenomenologically and do not have any relevant base in histology. This is crucial as only a limited number of studies attempted to investigate collagen structure for atherosclerotic plaque. Akyildiz et al. (2017) gave a preliminary insight into this problem showing that no dominant direction of collagen fibres can be found for carotid plaques with 52 % being in circumferential, 34 % in longitudinal and 14 % radial direction.

On the other hand, Pagiatakis et al. (2015) showed that collagen fibres are aligned with the first principal stress direction (investigated through FSI analysis) which was found to be longitudinal for coronary plaques. Recently, Johnston et al. (2021) investigated the influence of collagen fibre orientation in the FC, showing that the fibre alignment in the circumferential direction plays the most critical role for plaque stability. To the best author's knowledge, these are the only relevant measurements about collagen structure for atherosclerotic plaques. Therefore, it is clear that much research should be done in this direction.

Holzapfel 2000

$$W = W_{iso} + W_{aniso} = \frac{\mu}{2}(I_1 - 3) + \frac{k_1}{2k_2}\sum_{i=4,6}\left(e^{k_2(I_i-1)^2} - 1\right), \tag{5.10}$$

where isotropic part of the model is defined by neo-Hooke model (5.4) with stress-like material parameter μ representing stiffness of the matrix. The parameter k_1 is stress-like while k_2 is dimensionless parameter referenced to the fibre properties. This model was proposed by Holzapfel et al. (2000). $I_4 = I_6 = \lambda_\theta^2 \cos^2\varphi + \lambda_z^2 \sin^2\varphi$ are invariants of right Cauchy-Green deformation tensor $\mathbf{C}$.

Holzapfel 2005

$$W = W_{iso} + W_{aniso} = \mu(I_1 - 3) + \frac{k_1}{2k_2}\left(e^{k_2\left[(1-\varrho)(I_1-3)^2 + \varrho(I_4-1)^2\right]} - 1\right), \tag{5.11}$$

where $\varrho \in \langle 0; 1\rangle$ is dimensionless parameter that can be seen as a concentration parameter representing a degree of anisotropy. The model was proposed by Holzapfel et al. (2005b) and represents composite material reinforced by a single family of collagen fibres.

GOH

$$W = W_{iso} + W_{aniso} = c_{10}(I_1 - 3) + \frac{k_1}{2k_2}\sum_{i=4,6}\left(e^{k_2(I_i^*-1)^2} - 1\right), \tag{5.12}$$

where I_i^* is defined as

$$I_i^* = \kappa I_1 + (1 - 3\kappa) I_i \tag{5.13}$$

where κ represents the fibre orientation dispersion within the fibre families and can be thought of as a measure of anisotropy. If the $\kappa = 0$, the model coincides with eq. (5.10), $\kappa = 1/3$ represents maximum dispersion with random/isotropic distribution. This model was introduced by Gasser et al. (2005), and the abbreviation stays for the three authors, Gasser, Holzapfel and Ogden. The non-collagenous matrix is characterized by the isotropic neo-Hooke model (5.4). The anisotropic part of the model represents two transversally isotropic contributions of two symmetrical collagen fibre families.

5.7. *In vivo* mechanical characteristics

Until now, most of the mentioned information on the characterization of material properties or related topics shared a similarity in the need for a tissue extracted from the body to enable testing. While it is not that problematic for carotid atherosclerotic tissue (the endarterectomy is still the most frequently used approach for the treatment), it might be harder for other tissues. Moreover, the knowledge on mechanical properties comes quite late when the intervention has already happened. Sure, if some general knowledge and relations were found and their subsequent application before intervention would prove its benefit, this approach would not be doubted. Nevertheless, to the best of author's knowledge, there is no study proving this concept yet. Therefore, also other approaches were developed for the identification of mechanical characteristics like *in vivo* evaluation of strain, enabling prediction of rupture-prone parts of a plaque. This topic is extensive, and hence only a brief introduction will be discussed here to provide the reader with some insight and to inspire further effort in this direction. Although more of them exist, some favourite methods will be discussed in combination with carotid arteries.

5.7.1. Distensibility

Before the focus switches specifically to atherosclerotic plaques, it is important to introduce approaches used for arteries without or with an only moderate plaque. Stiffening of arteries with age and disease is well known and can indicate a potential risk for the patient. Reneman et al. (1986) used the *distensibility* and cross-sectional *compliance* which can be investigated non-invasively using M-mode imaging [18]. With time it was slightly modified but a variety of applications (Hoeks et al., 1990; Reneman et al., 2005) showed a good correlation between distensibility and age, indicating important changes in the tissue. The distensibility coefficient DC $[\frac{1}{Pa}]$ is calculated using

$$DC = \frac{2(\Delta D/D_{dias})}{\Delta p}, \tag{5.14}$$

and compliance coefficient $[\frac{m^2}{Pa}]$

$$CC = \frac{\Delta D/D_{dias}}{2\Delta p} \cdot \pi D_{dias}^2, \tag{5.15}$$

where D_{dias} is diastolic diameter and ΔD is maximal increase in diameter during cardiac cycle.

Pulse wave velocity

Once the distensibility is known, it can be used to calculate another characteristic called Pulse Wave Velocity (PWV) $[\frac{m}{s}]$ using equation from Brands et al. (1998)

$$c_w = \pm\sqrt{\frac{1}{\varrho DC}}, \tag{5.16}$$

[18] A form of ultrasonography where a single scan line is emitted, received and graphically displayed.

where ϱ is the blood density (ca 1060 kg/m^3). Moreover, since the PWV is known, the mechanical properties, namely Young's modulus, can be approximated as suggested in Brands et al. (1998) by using

$$E = \frac{D\varrho c_w^2}{h}, \tag{5.17}$$

where h is the vessel wall thickness. Moreover, the authors also proposed a methodology for a local identification of PWV utilizing ultrasound, enabling a non-invasive investigation of mechanical properties. Nevertheless, the approach has many assumptions which are not fully met in the case of carotid arteries and hence the use is limited here (Apostolakis et al., 2016; Widman et al., 2012). Also, the PWV measurements require relatively high distances between two positions, i.e., for the aorta, measurements between the carotid and femoral artery is required. However, progress in this field enables a direct investigation of local properties also for carotid tissue as proposed in a feasibility study (Luo et al., 2012) indicating a possibility to detect a diseased artery. PWV gained special attention and recently entered the field of clinical routine for carotid arteries (De Buyzere et al., 2017).

5.7.2. Elastography

Once the artery is diseased, it might be impossible to use the abovementioned approaches. Therefore, some other ways were of interest. Elastography was proposed by Ophir et al. (1991) and is based on imaging the object under different levels of deformation. Afterwards, cross-correlation can be used to access the displacement of the tissue along ultrasound lines, and by a spatial derivation of displacement, strain is obtained. As with most methods for this purpose, elastography was initially aimed at tumour detection, but cardiovascular diseases quickly received attention. Especially, intravascular elastography applications were initially developed for femoral or coronary arteries with and without plaque. Despite promising results, it might find little use in clinical practice due to the main disadvantage of necessary catheterization. Consequently, a non-invasive approach was developed focused on carotid arteries due to their accessible location even for standard ultrasound devices (also, it is one of prominent locations causing cerebrovascular events). Here, two approaches are often used: longitudinal direction and cross-sectional imaging.

In longitudinal imaging, the artery is shown from the side, revealing anterior and posterior wall, see Figure 5.23. The same direction is used in assessment of intima-media thickness (IMT) performed preventively to investigate a potential presence of atherosclerosis within the artery (De Groot et al., 2008) using an external ultrasound or occasionally IVUS. As a result, radial strains are calculated. It was firstly used for the carotid artery with atherosclerosis in a preliminary study by Kanai et al. (2003) who recalculated the obtained radial strain into a circumferential elastic modulus. Higher values were obtained for healthy patients compared to those with atherosclerosis. Similar values were found later in Schmitt et al. (2007) also for carotid atherosclerotic plaques revealing exciting information about plaque size, composition and mechanical interaction between plaque components. Here, displacements (probably obtained by using image registration or a similar approach from the author's understanding) were used for strain calculations representing an important input for estimation of elastic modulus. The authors assumed an axisymmetric and homogenous wall, influencing thus the results for plaques. Real-time elastography was examined in Liu et al. (2015) as a pre-operative investigation before the endarterectomy. After that, a post-operative pathology was assessed to indicate a possible plaque vulnerability which was then compared with the results from elastography.

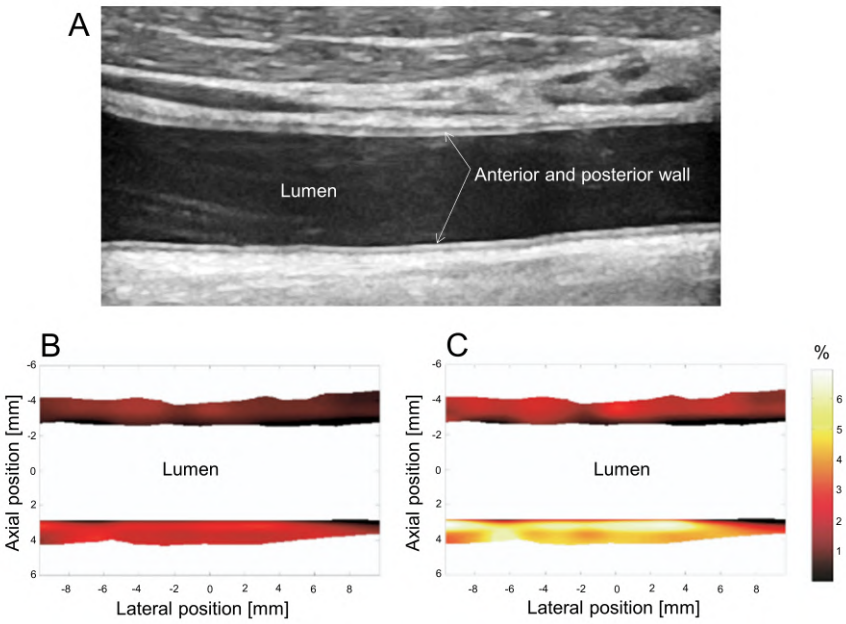

Figure 5.23: Ultrasound image of common carotid artery (A) showing anterior and posterior wall which can be analysed with longitudinal approach mentioned above. Axial strain maps under pressure gradient of 18.5 mmHg (B) and 33 mmHg (C) are shown from Schmitt et al. (2007).

Exquisite sensitivity indicates promising results for this approach. Similar results were found in comparison with high-resolution MRI, showing the feasibility of the approach for detection of large LCs and its potential for a risk assessment Naim et al. (2013). Von Mises equivalent strain was evaluated for carotid atherosclerotic tissue in Zhang et al. (2019) showing higher values for patients with cerebral infarction compared to a control group, suggesting that peak von Mises equivalent strain might be an essential indicator of the plaque vulnerability.

According to De Korte et al. (2016), principal strains should consist of components in radial and circumferential direction of the atherosclerotic plaque. This might be a problem for a cross-sectional approach, and additional modifications are needed. Using a 3D ultrasound system, Ribbers et al. (2007) evaluated two-dimensional displacement and strain fields (by recording both longitudinal and transversal sections of the artery) in order to calculate radial and circumferential strain components. Cross-sectional images were used to determine axial strain along the ultrasound beam. Generally, they showed the possibility of 2D acquisition for strain analysis and found out that higher strain concentrations occurred in atherosclerotic plaques. The two-dimensional strain tensor was also evaluated in Maurice et al. (2005) though by using Lagrangian speckle model estimator. Hansen et al. (2010) introduced an approach where radial strains are constructed from transverse cross-sectional imaging by projecting axial strains into radial. It was based on their previous work (Hansen et al., 2009) on phantoms. There are many other studies within this research group using also simulated plaques to indicate accuracy of the method (Hansen et al., 2014) in comparison with an adjusted approach which is moreover suitable also for 3D strain characterization (Fekkes et al., 2016) using FE simulations. It is important to note that the mechanical properties for the FE model were not used from elastography though obtained from a standard testing of arterial tissue (Loree et al., 1994).

5.7.3. Magnetic resonance

The versatility of MRI was already mentioned in the creation of geometry models. The same also applies in the field of *in vivo* identification of mechanical characteristics. This is very important because one modality could provide multiple important inputs for PS computational models. However, there are still limitations, mainly in the resolution, accompanying this approach when carotid arteries are investigated[19]. Whereas axial resolution was previously influential for geometry model creation, the in-plane resolution is a key disadvantage here. In order to sufficiently capture the carotid wall with thickness of around 1 mm, at least 0.5 mm in-plane resolution is needed. However, this can be very challenging as a hunt for better resolution will always be accompanied by decreasing the signal-to-noise ratio. Of course, single purpose coils are needed. Otherwise, it would not be even possible to capture the carotid artery wall. Nevertheless, there are variations of MRI which might enable the search for mechanical parameters, although the resolution will remain a problem for small arteries as carotid. Cine MRI is capable of imaging the movement over time. The imaging sequence can be synchronized with the heart rhythm. Avril et al. (2011) presented the approach for *in vitro* phantom and *in vivo* carotid artery showing its feasibility to identify elastic properties. This was further enhanced in Franquet et al. (2013b) presenting a new method called magnitude-based FEMU, where the authors combine an experimentally obtained deformation with FE simulations to obtain elastic properties from inverse analysis. It was again demonstrated on both a phantom and *in vivo* images to identify the stiffness of carotid artery with a FE model including a surrounding tissue. The authors also mentioned that an even more complex constitutive model would be reachable using this approach. Franquet et al. (2013a) verified this approach for 13 healthy subjects. Even though only a linear model was used to describe the material properties, the authors observed a change of Young's modulus representing tissue stiffening during systole, which might be necessary for non-linear models as usual for this type of tissue[20]. Koktzoglou (2013) showed that cine MRI in combination with black blood[21] could be beneficial for carotid wall movement tracking because the isotropic spatial resolution can be obtained. This was demonstrated in Speelman et al. (2016) where plaque displacements between systole and diastole were found from black blood cine MRI using image registration technique. Also, Nederveen et al. (2014) used black blood cine MRI to investigate *in vivo* strains of the carotid artery using the image registration approach. There are many other favourite MRI techniques, such as Displacement Encoding using Stimulated Echoes, enabling the movement detection and a subsequent analysis of strains though the low dimensions of carotid artery limit their use in this field. This limitation is mentioned in most MRI-based papers showing the importance of improvements of MRI devices with a potential for further analysis. As the improvements will probably take some time, it is possible at least to simulate a better resolution as it was shown in Nieuwstadt et al. (2015a) where the authors used a 2D geometry model created from histology sections for a simulated MRI and ultrasound.

[19]Not only carotid arteries but also other smaller arteries have this limitation. Nevertheless, some applications are possible for the aorta as the wall thickness is larger - around 2 mm.

[20]The authors have not forgotten to mention that additional steps are still needed as the model is minimal due to poor resolution of images.

[21]Black or dark blood is a technique where the signal from flowing blood is suppressed, rendering it as black, rather than enhanced as it is common during the so-called bright blood imaging.

This section summarized current approaches for *in vivo* identification of mechanical characteristics such as displacements, strains or stiffness. There are various approaches, but elastography using ultrasound and MRI seems to be the most promising. Most studies tried to correlate the investigated quantities with a potential plaque vulnerability or to identify its components based on their stiffness. Despite their importance, the *in vivo* mechanical characteristics describe the tissue at a specific load (often between systolic and diastolic pressure), revealing thus only a limited part of its behaviour. Some attempts were shown using FE models and the already mentioned inverse analysis to identify the constitutive model. Applications of this approach are still rare, although it shows a high potential for PS modelling. It would increase the accuracy of the models and thus also the accuracy of risk assessment. Therefore, the estimation of a constitutive model based on limited information can be a hot topic in further research. In the meantime, *ex vivo* experiments increase the knowledge about the behaviour, and a possible combination might bring necessary inputs for subsequent implementation. The author believes that someday we will reach a proper understanding of samples from interventions, which will enable a choice of suitable material model based on a known relationship with *in vivo* characteristics.

5.8. Author's contribution

Mechanical properties are essential for computational modelling. A proper understanding requires a thorough experimental investigation. More than 60 patients undergoing CEA provided samples for investigation with written consent during the author's studies. However, only 55 of the extracted samples were usable for uniaxial tension tests. Samples should be tested as fast as possible under an environment similar to the body. Accidentally, initial samples (n = 11) were collected and transported in the formaldehyde solution. Samples treated like this are fixed with a possible influence on mechanical responses. However, such a comparison was not performed till now, thus it inspired the study (see Appendix D) to take advantage of our mistake. The comparison was made with a comparable cohort of 16 samples; the total number of specimens was 26 in formaldehyde and 44 in a saline solution. Even though the testing of formaldehyde-fixed specimens was done within 24 h after the CEA, significant differences were found between the cohorts: the initial stiffness increases for formaldehyde specimens together with a reduction in variance. A subsequent study with saline fixed samples including consequently 44 patients only (after another year of sample harvesting) was performed to investigate the influence of characteristics detectable *in vivo*. The idea of the study was to find possible factors with a substantial effect on mechanical behaviour and ultimate stresses/strains. The stress-strain responses showed a typical non-linear behaviour with significant differences between female and male cohorts. Tissue strength was found significantly different between calcified and non-calcified cohorts, including female samples. Interestingly, loading direction (circumferential and longitudinal) was found significantly different only within the male group, while both directions were comparable for the female group.

Representative constitutive models were incorporated for each group enabling a more focused application during computational modelling (Appendix E). As the mechanical response is non-linear, the comparisons were performed at different stress levels. This was found essential compared to other approaches of representing multiple results together (Appendix F). In this study, the published experimental data for atherosclerotic plaques was digitised and then re-analysed, comparing representative average responses. The

compared approaches included strain-based, stress-based and constant-based averaging. Substantial differences were found among all the protocols except for nearly linear responses, but essentially the constant-based approach differed the most. The stress-based approach, taking into account data non-normality (mean vs. median), was recommended as the most rigorous approach to represent a soft tissue with significant strain stiffening.

Even though the latter factors reduced the variation among specimens, it still remained very high. The author believes that full-field measurements and inverse analysis could lead to more accurate results due to tissue heterogeneity. An alternative approach to digital image correlation, based on image registration for full-field strain analysis, was evaluated (Appendix G). The approach was validated on a set of samples including (i) complex heterogeneous deformations with sub-pixel displacements, (ii) a typical uniaxial tension test of the aorta, and (iii) indentation test of skin. The results indicated advantages compared to digital image correlation in extending the region of interest to the whole specimen when considering the natural pattern only. This might be very important for limited specimen sizes from complex atherosclerotic plaques. The incorporation is planned for a new set of samples in the following project, which is not a part of this thesis. Nevertheless, the approach is relatively easy to use because an open-source Elastix tool was used.

Residual deformation and stress

Residual stress (RS) and the related deformation will be introduced in this chapter. It is believed to represent the vital behaviour of arteries in adaptation to pathological changes in the wall structure during senescence. The vessel removed from the body cannot be considered stress free. Even though the RS may be small compared to the stress existing in the loaded configuration *in vivo*, their impact on the stress distribution is much higher due to the strain stiffening response of the tissue makes it more uniform, and thus cannot be neglected (Delfino et al., 1997; Gasser et al., 2005; Holzapfel et al., 2007; Humphrey et al., 2002). The inclusion of the RS into computational modelling is necessary since the input model geometry should be stress-free (Cilla et al., 2012; Holzapfel et al., 2014b). Various studies focused on the simulation of the RS within a specific type of artery, which was modelled using previously published geometrical parameters (Alastrué et al., 2007, 2010; Cilla et al., 2012; Liu et al., 2019; Pierce et al., 2015; Raghavan et al., 2004; Schröder et al., 2016). However, the simulation was not always based on the experimental studies related to the simulated artery type. The conventional approach of the *opening angle* is the most general approach when investigating the RS (Chuong et al., 1986; Fung, 1983; Humphrey et al., 2002). The subsequent inverse models (i.e., closing an opened segment into a closed ring) define the RS.

Most experimental evidence came from the whole wall without specific layer separation, and the complex multi-layered structure was neglected. Delfino et al. (1997) proposed an experimental and computational study for the whole carotid artery, which indicates that the highest differences in stresses between the inner and outer wall surface may be related to atherosclerosis-prone sites of the artery. Greenwald et al. (1997) investigated differences in the opening angle when the outer and inner ring were separated; this issue was also studied in Holzapfel et al. (2007) where the importance of 3D layer-specific residual deformations was investigated, and it was concluded that the only one parameter, the opening angle of the circumferential ring, is not sufficient. The deformation of an axial strip should also be included. Schulze-Bauer et al. (2002) published evidence about the crucial role of the residual stretches in the circumferential and axial strip of the femoral artery adventitia. Schulze-Bauer et al. (2003) presented some data on the residual deformation of iliac artery layers characterised only by the opening angle of the circumferential ring. An exciting finding of the negative opening angle of the intima layer was mentioned, though it resulted only from two samples, and the phenomenon was not thoroughly investigated. Holzapfel et al. (2007) proposed a systematic methodology how to investigate the 3D residual deformation for separate layers of human aortas, which was then enhanced in Holzapfel et al. (2010) with a theoretical framework with specification of the needed geometrical parameters capable to describe sufficiently a 3D RS. Sommer et al. (2010) were the first to provide an extensive investigation of the mechanical behaviour of separate carotid wall layers. They proposed experimental evidence of residual stretches and RS, which were evaluated independently with different methodology and compared

with unified access (Holzapfel et al., 2007, 2010). In the case of the residual stretches, a whole biaxial sample was used to measure lengths/radii for the axial/circumferential residual deformations in specific configurations.

In contrast, the specimens following the methodology from Holzapfel et al. (2007) were used to determine RS though represented only by a curvature parameter. Sommer et al. (2012) proposed a theoretical framework to calculate the axial stretch from the curvature published previously. However, no evidence of the 3D residual deformation was published yet for the carotid wall with separate layers; if using a systematic methodology as proposed in (Holzapfel et al., 2007, 2010), it could be then used as an input for further simulations as done, for instance, by (Pierce et al., 2015; Sigaeva et al., 2019).

6.1. Atherosclerotic plaques

Till now, only arterial wall without atherosclerosis was discussed. It is probably due to the non-cylindrical character of the plaque, making it hard to apply the approaches known from the healthy arteries. The review Holzapfel et al. (2014b) focusing on atherosclerosis does mention RS, though again only for the non-atherosclerotic tissue. As discussed above, challenges for the healthy wall still remain and even more lacks to be covered experimentally exist for atherosclerotic plaques. Only a single record was found in proceedings Pocaterra et al. (2009) where the authors observed a tiny opening of the carotid plaque from endarterectomy. A subsequent simulated closing of the segment showed an insignificant influence of RS for the plaque[22].

Some data are available for coronary plaques in Ohayon et al. (2007) who applied the opening angle approach to six lesions. The radial cut to the artery ring was always performed in the healthy part, revealing an average opening of $118 \pm 35°$. Unfortunately, none of the plaques were cut in a different place to see whether the artery would also open in the same manner when cut in the diseased part. It is important to note that the plaques contained the wall components (adventitia and media layers) for which we know that the RS exist and might cause the opening. Afterwards, they created a computational 2D model to analyse the influence of the RS, which was applied by closing the segment. Their results showed that the RS influenced dramatically the resulting stress distribution in the FC (see Figure 6.24) and the locations with highest stresses changed in some cases. The same models and approaches were used for mice samples in Broisat et al. (2011) and recently mentioned in Martiel et al. (2021), both recommending the use of circumferential RS when analysing healthy and diseased arterial tissue[23]. A similar opening angle of $120 \pm 16°$ for coronary artery was found in Kural et al. (2012) but again with including both adventitia and media unseparated. This need not to be a problem if the results are applied to a similar geometrical configuration, including wall components. However, it is not always the case as it can be seen, e.g., in Wang et al. (2017) who took the opening angle of 120° and applied it to the 3D model of a coronary artery, although modelling the plaque and wall components with the same mechanical properties. The authors again applied the approach of closing the arterial segment in order to include circumferential RS into the

[22]Some data is available in Kural et al. (2012) though the authors tested a carotid wall with only limited information on atherosclerosis. Thus it is not considered as relevant here.

[23]Closing the arterial segment using computational modelling is a complex process especially when the plaque is present. The authors of the latter paper included images of a closed segment showing some severe problems like the deformation of LC and FC into the lumen area, which is unrealistic. However, this issue was not discussed (or at least not found).

model. Their results indicated again that the RS included in the computational model might reduce extreme stresses on the FC. The closing approach in the latter study is an alternative to the analytically estimated RS and was used to validate the assumption on a perfectly circular segment in comparison with its specific shape (Raghavan et al., 2004). The lack of experimental data resulted in an application of the data from measurements of a non-diseased wall, e.g., in Williamson et al. (2003). Here, the authors applied an initial strain to receive a configuration with a smaller radial gradient and with tension on the outer surface while the inner surface is in compression. They did not find significant differences when the RS was introduced. Another computational application of RS can be seen in Cilla et al. (2012) including circumferential and axial RS for the idealised plaque confirming a significant reduction in peak stresses when the RS is included.

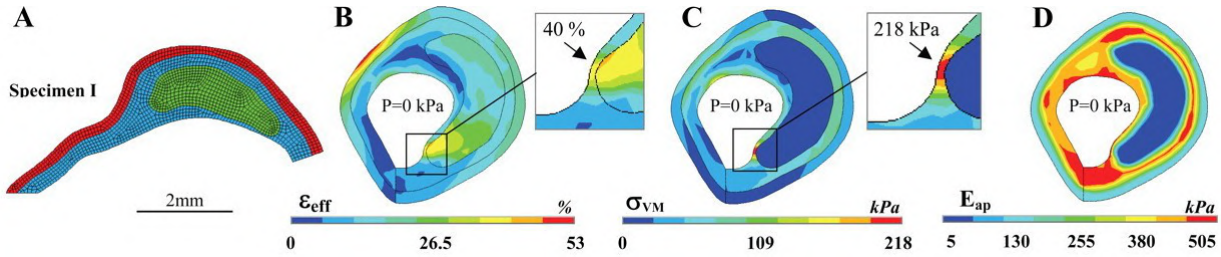

Figure 6.24: The open zero-stress segment of coronary artery (A), computed strain (B), RS (C) and apparent Young's modulus (D) were estimated by closing the whole segment. Very high RS was found in the cap region, reaching almost the tissue strength. Reprinted from Ohayon et al. (2007).

The problem of RS is very often mentioned, and its vast effect is expected for computational modelling of healthy and diseased arteries. The last section discussed the lack of practical information for both carotid wall and atherosclerotic plaques. Even though some approaches like opening angle, which is well known for healthy arteries, were applied to atherosclerotic tissue, their relevance remains questionable. Investigated plaques also contained an arterial wall and potentially influenced thus the RS distribution on FC. RS might be possibly presented in the plaque only slightly due to disease progression, and the inclusion through computationally closing the segment might result in unrealistic stress/strain distribution within the FT/FC surface. Endarterectomy samples (without outer wall components if possible, some parts of media is nevertheless presented) tested in this thesis revealed no or tiny opening of the plaque[24] confirming thus findings of Pocaterra et al. (2009). Esmaeili Monir et al. (2016) showed in their computational study that layer-specific RS of a healthy carotid artery leads to different stress distribution compared to whole artery release. Therefore, it is essential to include this when dealing with atherosclerotic plaques.

6.2. Author's contribution

Experimental investigation of layer-specific residual deformation of carotid arteries from a cadaver was performed (Appendix H). The presence of atherosclerotic plaque was rare, and the experiment was thus focused on the adventitia and media+intima layers only.

[24]The same can be seen, e.g., in Teng et al. (2015) Figure 7 B or Barrett et al. (2016b) Figure 1, for carotid atherosclerotic plaques

Two different protocols were compared: (i) layer separation after the RS is released and (ii) in reverse order. Results showed different openings for media and adventitia, where the latter remained almost closed while media opened considerably. Different residual deformation was confirmed for specific layers. High differences were found between two experimental setups with almost four time higher values for media+intima when the layer separation was done before the radial cut of circumferential sample. Moreover, interesting behaviour of adventitia was detected as the circumferential ring was closing rather than opening as expected from the literature. Similar discrepancies were found also for axial strip of adventitia which mostly did not show any deformation and remains straight. Both these findings were attempted to explain by a correlation between opening angle and a ration of thickness of media+intima and adventitia. Statistically significant negative correlation indicates that imperfect separation might influence the residual deformation and should be thus well addressed in future studies.

The experiment is nowadays incorporated with computational study of atherosclerotic plaque where the influence of RS is investigated in 2D. This study is in progress and was only included as an accepted abstract at Euromech Colloquium 2022 (Appendix I). The first configuration applies the RS via closing a whole arterial segment (adventitia, media and plaque) using a moderate opening angle. In contrast, the second configuration applies layer-specific RS by closing the segments separately. Plaque opening was relatively small based on experience from endarterectomy samples. As expected, the opening of the whole segment introduced high RS in the FC area, influencing thus PCS after subsequent application of arterial pressure. On the other hand, a neglected influence on PCS was found when layer-specific RS was introduced. The results point out the necessity of a proper experimental investigation of atherosclerotic plaques as the inclusion of RS through the whole closing segment (showing essential effect in the literature for coronary artery) might underestimate the results and thus increase the risk of fault decision when using computational modelling. Due to the low occurrence of atherosclerotic plaques from a cadaver (endarterectomy samples are insufficient as the plaque is often cut and miss the other wall components). Nevertheless, the experimental protocol (ii) showed that the layer separation before RS release is doable and thus will be applied on samples with plaque once available (project in cooperation with Department of Anatomy, MUNI is running in a time of writing this thesis). Also, the methodology for layer-specific RS inclusion was developed to follow presented preliminary results.

Conclusion

Atherosclerosis is an arterial wall disease in which a lesion forms continuously. The vessel lumen narrows, influencing a proper blood flow and thus the delivery of oxidized blood to essential organs. The lesion can be symptomatic or asymptomatic, which only becomes apparent when a problem occurs; this type is most important in clinics. Depending on the specific artery, the lesion increases the risk of severe health problems like myocardial infarction or stroke. Such events occur when the plaque ruptures, releasing its content into the blood flow and completely blocking the blood supply. These plaques are called unstable or vulnerable and their identification is essential to prevent critical events. Potential indicators of plaque vulnerability have been studied for decades. The idea is to recognize plaques of clinical interest during a control screening. The soft tissue biomechanics is trying to understand the rupture mechanics and to bring a potential tool for an early detection of unstable plaques.

The topic of the present study was very general, aiming at computational modelling of carotid arteries with atherosclerosis. An extensive literature review showed many potential directions for the research though only some were further elaborated in the original research. Even though many original studies were introduced, the main objectives can be separated into two general blocks. The first block of the study focuses on possible ways for geometry reconstruction from *in vivo* and *ex vivo* images using different modalities like computed tomography or magnetic resonance and subsequent use of the created models for plaque vulnerability assessment. The computational study showed potential shortcomings of the current way of modelling, which might be essential when peak stresses are evaluated. More specifically, the inability of a proper plaque component distinction during imaging often leads to unifications in geometry (carotid wall components), which is crucial when the blood pressure acts onto a plaque. This problem increases when additional factors are accounted for, such as considerable variation of mechanical properties. This factor was partially considered in the computational study Lisický et al. (2020) but mainly, it inspired a second block of the present study, which was experimental.

Atherosclerotic plaque samples from endarterectomy were collected during four years of the author's study in cooperation with St. Ann's hospital Brno. This enabled a thorough experimental study of the mechanical properties of plaque components, and thus improving our understanding of the diseased tissue. The included patients almost doubled the current maximum cohort size in the literature for the carotid plaques. Important *in vivo* factors were detected from the measured cohorts enabling a more targeted application in further computational studies. This, in combination with a proper representation of multiple experimental data, can be essential in plaque vulnerability assessment.

Last but not least, autopsy samples of carotid arteries from the Department of Anatomy of Masaryk University, primarily without atherosclerosis, were used to investigate the residual deformation of separated layers of arterial wall. Although the pandemic influenced the sample collection, exciting results showed that our current experimental knowledge is very limited in this field. The residual stress release, requiring also layer separation, plays a crucial role in the resulting values used as inputs for subsequent computational modelling applications and deserves thus our thorough focus.

Potentials for future work

The author believes that all parts studied within this thesis contributed to the current state of the art of biomechanics in modelling atherosclerotic tissue. However, the literature search indicated some other paths with a considerable potential that were not included. These can be of interest for further investigation and are therefore listed below with a brief description.

8.1. Influence of calcifications

Recent review Barrett et al. (2019) summarizes current knowledge on calcifications within the atherosclerotic plaques and their possible impact on plaque's mechanical properties and subsequent applications in computational modelling. The authors mentioned some exciting ideas about implementations in clinical practice. Recent study Benitez et al. (2021) investigated (using FSI) the impact of calcification on a plaque vulnerability in carotid artery. Even though the study focuses on influential factors, it might be challenging to incorporate the calcifications into a model properly. They are not present as one big stone as modelled there, which is evident from their X-ray image. Their results show significantly higher stresses for the calcified model. The non-calcified version was modelled with different material properties for the corresponding volume. The Young's modulus was set 100 times lower, and hence the change in stresses is noticeable but non-realistic. It might be misleading to model the area with calcifications as a compact continuum instead of the discontinuous micro-calcifications. These might be considered as a particle composite within the LC.

8.2. Residual stress modelling

In present thesis, a layer-specific residual deformation (investigated through the opening angle of the arterial layer segments) was confirmed for the carotid artery. The extension to a complete artery with atherosclerotic plaque is of interest because the preliminary results indicated that the layer-specific RS might not be a critical factor for an atherosclerotic plaque. The present experimental investigation might be essentially easy to adapt for the whole plaques from cadavers. Once evidence of the opening angles would be recorded, specific computational models can confirm the effect.

8.3. Collagen fibre distribution

Determination of the collagen fibre distribution within the plaques remains a valid point. Minimal information can be found in literature. Once this is properly investigated, a

question about the necessity of anisotropic constitutive modelling will be closer to being answered.

8.4. Stent deployment simulation

Some crucial factors for computational modelling were revealed in this thesis. Their importance might be reflected during a simulation of stent deployment. The created complex geometry models can be used for this purpose with mechanical properties measured here.

8.5. Machine learning in biomechanics

Machine learning attracted attention rapidly in many fields, including very close topics like computer vision. Some discussion can also be found in a recent paper Holzapfel et al. (2021) where a deep learning—a subset of machine learning—was used to predict a constitutive model of artery based on the sample microstructure. Although a minimum number of samples was used, it shows a new potential direction where results of multiple different studies might be combined to increase the model validity. Sample size restricts the use in biomechanics, but some hybrid approaches might be an exciting way for a combination with computational modelling.

8.6. *In vivo* mechanical properties

Approaches concerning *in vivo* mechanical properties were discussed in this thesis. It is possible to obtain a component-specific strain distribution during a cardiac cycle. It would also be interesting to find a connection between this characteristic and a whole non-linear function characterized by a constitutive model. Once this relation is found, a proper constitutive model can be used for computational modelling bringing the patient-specific models closer to their purpose. The identification can be further enhanced with above mentioned machine learning, taking into account also *in vivo* factors discussed during experimental investigation.

List of Figures

List of Tables

References

Acosta Santamaría, V. A. et al. (2018). "Three-Dimensional Full-Field Strain Measurements across a Whole Porcine Aorta Subjected to Tensile Loading Using Optical Coherence Tomography–Digital Volume Correlation." In: *Frontiers in Mechanical Engineering* 4.March, pp. 1–14. ISSN: 2297-3079. DOI: 10.3389/fmech.2018.00003.

Affagard, J. S. et al. (2015). "Identification of hyperelastic properties of passive thigh muscle under compression with an inverse method from a displacement field measurement." In: *Journal of Biomechanics* 48.15, pp. 4081–4086. ISSN: 18732380. DOI: 10.1016/j.jbiomech.2015.10.007.

Akyildiz, A. C. et al. (2011). "Effects of intima stiffness and plaque morphology on peak cap stress." In: *Biomedical engineering online* 10.1, p. 25.

Akyildiz, A. C. et al. (2014). "Mechanical properties of human atherosclerotic intima tissue." In: *Journal of biomechanics* 47.4, pp. 773–783.

Akyildiz, A. C. et al. (2016). "A Framework for Local Mechanical Characterization of Atherosclerotic Plaques: Combination of Ultrasound Displacement Imaging and Inverse Finite Element Analysis." In: *Annals of Biomedical Engineering* 44.4, pp. 968–979. ISSN: 15739686. DOI: 10.1007/s10439-015-1410-8.

Akyildiz, A. C. et al. (2017). "3D Fiber Orientation in Atherosclerotic Carotid Plaques." In: *Journal of Structural Biology* 200.1, pp. 28–35. ISSN: 10958657. DOI: 10.1016/j.jsb.2017.08.003.

Akyildiz, A. C. et al. (2018). "Intima heterogeneity in stress assessment of atherosclerotic plaques." In: *Interface Focus* 8.1. ISSN: 20428901. DOI: 10.1098/rsfs.2017.0008.

Alastrué, V. et al. (2007). "Assessing the use of the "opening angle method" to enforce residual stresses in patient-specific arteries." In: *Annals of Biomedical Engineering* 35.10, pp. 1821–1837.

Alastrué, V. et al. (2010). "Numerical framework for patient-specific computational modelling of vascular tissue." In: *International Journal for Numerical Methods in Biomedical Engineering* 26.1, pp. 35–51.

Apostolakis, I. Z. et al. (2016). "Piecewise Pulse Wave Imaging (pPWI) for Detection and Monitoring of Focal Vascular Disease in Murine Aortas and Carotids in Vivo." In: *IEEE Transactions on Medical Imaging* 35.1, pp. 13–28. ISSN: 1558254X. DOI: 10.1109/TMI.2015.2453194.

Auricchio, F. et al. (2011). "Carotid artery stenting simulation: from patient-specific images to finite element analysis." In: *Medical engineering & physics* 33.3, pp. 281–289.

Avril, S. et al. (2008). "Overview of identification methods of mechanical parameters based on full-field measurements." In: *Experimental Mechanics* 48.4, pp. 381–402. ISSN: 00144851. DOI: 10.1007/s11340-008-9148-y.

Avril, S. et al. (2011). "In vivo velocity vector imaging and time-resolved strain rate measurements in the wall of blood vessels using MRI." In: *Journal of Biomechanics* 44.5, pp. 979–983. ISSN: 00219290. DOI: 10.1016/j.jbiomech.2010.12.010.

Balu, N. et al. (2009). "Improvements in carotid plaque imaging using a new eight-element phased array coil at 3T." In: *Journal of Magnetic Resonance Imaging* 30.5, pp. 1209–1214. ISSN: 10531807. DOI: 10.1002/jmri.21890.

Barrett, H. E. et al. (2016a). "On the effect of calcification volume and configuration on the mechanical behaviour of carotid plaque tissue." In: *Journal of the Mechanical Behavior of Biomedical Materials* 56, pp. 45–56. ISSN: 18780180. DOI: 10.1016/j.jmbbm.2015.11.001.

Barrett, H. E. et al. (2016b). "Towards the characterisation of carotid plaque tissue toughness: Linking mechanical properties to plaque composition." In: *Acta Biomaterialia* 43, pp. 88–100. ISSN: 18787568. DOI: 10.1016/j.actbio.2016.07.042.

Barrett, H. E. et al. (2017). "Calcification Volume Reduces Stretch Capability and Predisposes Plaque to Rupture in an in vitro Model of Carotid Artery Stenting." In: *European Journal of Vascular and Endovascular Surgery* 54.4, pp. 431–438. ISSN: 15322165. DOI: 10.1016/j.ejvs.2017.07.022.

Barrett, H. E. et al. (2015). "Characterising human atherosclerotic carotid plaque tissue composition and morphology using combined spectroscopic and imaging modalities." In: *Biomedical engineering online* 14.Suppl 1, S5. ISSN: 1475925X. DOI: 10.1186/1475-925X-14-S1-S5.

Barrett, H. E. et al. (2019). "Calcifications in atherosclerotic plaques and impact on plaque biomechanics." In: *Journal of Biomechanics* 87, pp. 1–12. ISSN: 18732380. DOI: 10.1016/j.jbiomech.2019.03.005.

Barrett, S. et al. (2009). "Experimental measurement of the mechanical properties of carotid atherothrombotic plaque fibrous cap." In: *Journal of biomechanics* 42.11, pp. 1650–1655.

Bathe, K. (2002). "Theory and modeling guide." In: *Vol II: ADINA-F, ADINA R&D, Inc., Watertown, MA*.

Belloni, V. et al. (2019). "Py2dic: A new free and open source software for displacement and strain measurements in the field of experimental mechanics." In: *Sensors (Switzerland)* 19.18, pp. 1–19. ISSN: 14248220. DOI: 10.3390/s19183832.

Benitez, J. et al. (2021). "Evaluating the Impact of Calcification on Plaque Vulnerability from the Aspect of Mechanical Interaction Between Blood Flow and Artery Based on MRI." In: *Annals of Biomedical Engineering* 49.4, pp. 1169–1182. ISSN: 15739686. DOI: 10.1007/s10439-020-02655-1.

Bersi, M. R. et al. (2020). "Multimodality Imaging-Based Characterization of Regional Material Properties in a Murine Model of Aortic Dissection." In: *Scientific Reports* 10.1, pp. 1–23. ISSN: 20452322. DOI: 10.1038/s41598-020-65624-7.

Blaber, J. et al. (2015). "Ncorr: Open-Source 2D Digital Image Correlation Matlab Software." In: *Experimental Mechanics* 55.6, pp. 1105–1122. ISSN: 17412765. DOI: 10.1007/s11340-015-0009-1.

Boyd, S. K. et al. (2006). "Evaluation of three-dimensional image registration methodologies for in vivo micro-computed tomography." In: *Annals of biomedical engineering* 34.10, pp. 1587–1599.

Brands, P. J. et al. (1998). "A noninvasive method to estimate pulse wave velocity in arteries locally by means of ultrasound." In: *Ultrasound in Medicine and Biology* 24.9, pp. 1325–1335. ISSN: 03015629. DOI: 10.1016/S0301-5629(98)00126-4.

Broisat, A. et al. (2011). "Assessing low levels of mechanical stress in aortic atherosclerotic lesions from apolipoprotein E-/- mice-brief report." In: *Arteriosclerosis, Thrombosis,*

and Vascular Biology 31.5, pp. 1007–1010. ISSN: 10795642. DOI: 10.1161/ATVBAHA.111.225227.

Brown, M. S. et al. (1976). "Receptor-mediated control of cholesterol metabolism." In: *Science* 191.4223, pp. 150–154.

Brown, M. et al. (1975). "Use of mutant fibroblasts in the analysis of the regulation of cholesterol metabolism in human cells." In: *Journal of cellular physiology* 85.S1, pp. 425–436.

Buffinton, C. M. et al. (2014). "Effect of Calcification Modulus and Geometry on Stress in Models of Calcified Atherosclerotic Plaque." In: *Cardiovascular Engineering and Technology* 5.3, pp. 244–260. ISSN: 18694098. DOI: 10.1007/s13239-014-0186-6.

Burczynski, T. et al. (2006). *IUTAM Symposium on Evolutionary Methods in Mechanics: Proceedings of the IUTAM Symposium held in Cracow, Poland, 24–27 September, 2002*. Vol. 117. Springer Science & Business Media.

Burke, A. P. et al. (1997). "Coronary risk factors and plaque morphology in men with coronary disease who died suddenly." In: *New England Journal of Medicine* 336.18, pp. 1276–1282.

Cahalane, R. M. et al. (2018). "Relating the mechanical properties of atherosclerotic calcification to radiographic density: A nanoindentation approach." In: *Acta Biomaterialia* 80, pp. 228–236. ISSN: 18787568. DOI: 10.1016/j.actbio.2018.09.010.

Caro, C. et al. (1971). "Atheroma and arterial wall shear-Observation, correlation and proposal of a shear dependent mass transfer mechanism for atherogenesis." In: *Proceedings of the Royal Society of London. Series B. Biological Sciences* 177.1046, pp. 109–133.

Cathcart, M. K. et al. (1985). "Monocytes and neutrophils oxidize low density lipoprotein making it cytotoxic." In: *Journal of leukocyte biology* 38.2, pp. 341–350.

Cavinato, C. et al. (2019). "Does the knowledge of the local thickness of human ascending thoracic aneurysm walls improve their mechanical analysis?" In: *Frontiers in Bioengineering and Biotechnology* 7.JUL, pp. 1–12. ISSN: 22964185. DOI: 10.3389/fbioe.2019.00169.

Cecchi, E. et al. (2011). "Role of hemodynamic shear stress in cardiovascular disease." In: *Atherosclerosis* 214.2, pp. 249–256.

Chai, C. K. et al. (2013). "Local axial compressive mechanical properties of human carotid atherosclerotic plaques-characterisation by indentation test and inverse finite element analysis." In: *Journal of Biomechanics* 46.10, pp. 1759–1766. ISSN: 00219290. DOI: 10.1016/j.jbiomech.2013.03.017.

Chai, C. K. et al. (2015). "Local anisotropic mechanical properties of human carotid atherosclerotic plaques - Characterisation by micro-indentation and inverse finite element analysis." In: *Journal of the Mechanical Behavior of Biomedical Materials* 43, pp. 59–68. ISSN: 18780180. DOI: 10.1016/j.jmbbm.2014.12.004.

Chau, A. H. et al. (2004). "Mechanical analysis of atherosclerotic plaques based on optical coherence tomography." In: *Annals of Biomedical Engineering* 32.11, pp. 1494–1503. ISSN: 00906964. DOI: 10.1114/B:ABME.0000049034.75368.4a. arXiv: 17331558.

Chen, Y. et al. (2021). "Rupture Risk Assessment of Cervical Spinal Manipulations on Carotid Atherosclerotic Plaque by a 3D Fluid-Structure Interaction Model." In: *BioMed Research International* 2021. ISSN: 23146141. DOI: 10.1155/2021/8239326.

Cheng, G. C. et al. (1993). "Distribution of circumferential stress in ruptured and stable atherosclerotic lesions. A structural analysis with histopathological correlation." In: *Circulation* 87.4, pp. 1179–1187.

Chuong, C.-J. et al. (1986). "Residual stress in arteries." In: *Frontiers in biomechanics*. Springer, pp. 117–129.

Cilla, M. et al. (2012). "3D computational parametric analysis of eccentric atheroma plaque: influence of axial and circumferential residual stresses." In: *Biomechanics and modeling in mechanobiology* 11.7, pp. 1001–1013.

Cilla, M. et al. (2015). "A parametric model for analysing atherosclerotic arteries: On the FSI coupling." In: *International Communications in Heat and Mass Transfer* 67, pp. 29–38.

Clark, D. J. et al. (2004). "Safety and utility of intravascular ultrasound-guided carotid artery stenting." In: *Catheterization and Cardiovascular Interventions* 63.3, pp. 355–362. ISSN: 15221946. DOI: 10.1002/ccd.20188.

Coolen, B. F. et al. (2016). "Three-dimensional quantitative T1 and T2 mapping of the carotid artery: Sequence design and in vivo feasibility." In: *Magnetic Resonance in Medicine* 75.3, pp. 1008–1017. ISSN: 15222594. DOI: 10.1002/mrm.25634.

Cottin, N. et al. (1984). "On the parameter identification of elastomechanical systems using input and output residuals." In: *Ingenieur-Archiv* 54.5, pp. 378–387. ISSN: 00201154. DOI: 10.1007/BF00532820.

Cox, M. A. et al. (2008). "Mechanical characterization of anisotropic planar biological soft tissues using finite indentation: Experimental feasibility." In: *Journal of Biomechanics* 41.2, pp. 422–429. ISSN: 00219290. DOI: 10.1016/j.jbiomech.2007.08.006.

Cunnane, E. M. et al. (2016). "Mechanical properties and composition of carotid and femoral atherosclerotic plaques: A comparative study." In: *Journal of Biomechanics* 49.15, pp. 3697–3704. ISSN: 18732380. DOI: 10.1016/j.jbiomech.2016.09.036.

Dall'Ara, E. et al. (2014). "About the inevitable compromise between spatial resolution and accuracy of strain measurement for bone tissue: A 3D zero-strain study." In: *Journal of Biomechanics* 47.12, pp. 2956–2963. ISSN: 18732380. DOI: 10.1016/j.jbiomech.2014.07.019.

Davis, F. M. et al. (2015). "Pointwise characterization of the elastic properties of planar soft tissues: application to ascending thoracic aneurysms." In: *Biomechanics and Modeling in Mechanobiology* 14.5, pp. 967–978. ISSN: 16177940. DOI: 10.1007/s10237-014-0646-9.

Davis, F. M. et al. (2016a). "Local mechanical properties of human ascending thoracic aneurysms." In: *Journal of the Mechanical Behavior of Biomedical Materials* 61, pp. 235–249. ISSN: 18780180. DOI: 10.1016/j.jmbbm.2016.03.025.

Davis, L. A. et al. (2016b). "Characterization of fracture behavior of human atherosclerotic fibrous caps using a miniature single edge notched tensile test." In: *Acta Biomaterialia* 43, pp. 101–111. DOI: 10.1016/j.actbio.2016.07.027. URL: http://dx.doi.org/10.1016/j.actbio.2016.07.027.

De Buyzere, M. et al. (2017). "Carotid artery plaque and arterial stiffness: About conflicts between ultrasound and tonometry and between local and global." In: *Journal of Hypertension* 35.8, pp. 1569–1572. ISSN: 14735598. DOI: 10.1097/HJH.0000000000001394.

De Groot, E. et al. (2008). "Measurement of carotid intima–media thickness to assess progression and regression of atherosclerosis." In: *Nature clinical practice Cardiovascular medicine* 5.5, pp. 280–288.

De Korte, C. L. et al. (2016). "Review: Mechanical Characterization of Carotid Arteries and Atherosclerotic Plaques." In: *IEEE Transactions on Ultrasonics, Ferroelectrics, and Frequency Control* 63.10, pp. 1613–1623. ISSN: 08853010. DOI: 10.1109/TUFFC.2016.2572260.

De Wilde, D. et al. (2016). "Assessment of shear stress related parameters in the carotid bifurcation using mouse-specific FSI simulations." In: *Journal of Biomechanics* 49.11, pp. 2135–2142. ISSN: 18732380. DOI: 10.1016/j.jbiomech.2015.11.048.

Delfino, A. et al. (1997). "Residual strain effects on the stress field in a thick wall finite element model of the human carotid bifurcation." In: *Journal of biomechanics* 30.8, pp. 777–786.

Demiray, H. (1972). "A note on the elasticity of soft biological tissues." In: *Journal of Biomechanics* 5.3, pp. 309–311. ISSN: 00219290. DOI: 10.1016/0021-9290(72)90047-4.

Di Giuseppe, M. et al. (2020). "In Vitro Measurement of Strain Localization Preceding Dissection of the Aortic Wall Subjected to Radial Tension." In: *Experimental Mechanics*. ISSN: 17412765. DOI: 10.1007/s11340-020-00641-1.

Dohad, S. et al. (2017). "Optical coherence tomography guided carotid artery stent procedure: technique and potential applications." In: *Catheterization and Cardiovascular Interventions* 91.3, pp. 521–530. ISSN: 1522726X. DOI: 10.1002/ccd.27344.

Duprey, A. et al. (2010). "In vitro characterisation of physiological and maximum elastic modulus of ascending thoracic aortic aneurysms using uniaxial tensile testing." In: *European Journal of Vascular and Endovascular Surgery* 39.6, pp. 700–707.

Duprey, A. et al. (2016). "Biaxial rupture properties of ascending thoracic aortic aneurysms." In: *Acta Biomaterialia* 42, pp. 273–285. ISSN: 18787568. DOI: 10.1016/j.actbio.2016.06.028.

Ebenstein, D. M. et al. (2002). "Assessing structure-property relations of diseased tissues using nanoindentation and FTIR." In: *Materials Research Society Symposium - Proceedings* 711, pp. 47–52. ISSN: 02729172. DOI: 10.1557/proc-711-ff4.2.1.

Ebenstein, D. M. et al. (2009). "Nanomechanical properties of calcification, fibrous tissue, and hematoma from atherosclerotic plaques." In: *Journal of Biomedical Materials Research - Part A* 91.4, pp. 1028–1037. ISSN: 15493296. DOI: 10.1002/jbm.a.32321.

Eckstein, H.-H. et al. (2008). "Results of the Stent-Protected Angioplasty versus Carotid Endarterectomy (SPACE) study to treat symptomatic stenoses at 2 years: a multinational, prospective, randomised trial." In: *The Lancet Neurology* 7.10, pp. 893–902.

Escribano, J. et al. (2019). "Balance of mechanical forces drives endothelial gap formation and may facilitate cancer and immune-cell extravasation." In: *PLoS computational biology* 15.5.

Esmaeili Monir, H. et al. (2016). "Finite element modelling of the common carotid artery in the elderly with physiological intimal thickening using layer-specific stress-released geometries and nonlinear elastic properties." In: *Computer Methods in Biomechanics and Biomedical Engineering* 19.12, pp. 1286–1296. ISSN: 14768259. DOI: 10.1080/10255842.2015.1128530.

Falk, E. (1992). "Why do plaques rupture?" In: *Circulation* 86.6 Suppl, pp. III30–42.

Farhat, C. et al. (1993). "Updating finite element dynamic models using an element-by-element sensitivity methodology." In: *AIAA Journal* 31.9, pp. 1702–1711. ISSN: 00011452. DOI: 10.2514/3.11833.

Fekkes, S. et al. (2016). "2-D Versus 3-D Cross-Correlation-Based Radial and Circumferential Strain Estimation Using Multiplane 2-D Ultrafast Ultrasound in a 3-D Atherosclerotic Carotid Artery Model." In: *IEEE Transactions on Ultrasonics, Ferroelectrics, and Frequency Control* 63.10, pp. 1543–1553. ISSN: 08853010. DOI: 10.1109/TUFFC.2016.2603189.

Fernández-Ruiz, I. (2016). "Carotid artery stenosis—stenting or endarterectomy?" In: *Nature Reviews Cardiology* 13.4, pp. 181–181.

Ferrara, A. et al. (2008). "Numerical modelling of fracture in human arteries." In: *Computer Methods in Biomechanics and Biomedical Engineering* 11.5, pp. 553–567. ISSN: 10255842. DOI: 10.1080/10255840701771743.

Finn, A. V. et al. (2010). "Concept of vulnerable/unstable plaque." In: *Arteriosclerosis, thrombosis, and vascular biology* 30.7, pp. 1282–1292.

Fleg, J. L. et al. (2012). "Detection of high-risk atherosclerotic plaque: Report of the NHLBI Working Group on current status and future directions." In: *JACC: Cardiovascular Imaging* 5.9, pp. 941–955. ISSN: 1936878X. DOI: 10.1016/j.jcmg.2012.07.007. arXiv: NIHMS150003.

Floc'H, S. L. et al. (2009). "Vulnerable atherosclerotic plaque elasticity reconstruction based on a segmentation-driven optimization procedure using strain measurements: Theoretical framework." In: *IEEE Transactions on Medical Imaging* 28.7, pp. 1126–1137. ISSN: 02780062. DOI: 10.1109/TMI.2009.2012852.

Franquet, A. et al. (2013a). "Identification of the in vivo elastic properties of common carotid arteries from MRI: A study on subjects with and without atherosclerosis." In: *Journal of the Mechanical Behavior of Biomedical Materials* 27, pp. 184–203. ISSN: 17516161. DOI: 10.1016/j.jmbbm.2013.03.016.

Franquet, A. et al. (2013b). "A new method for the in vivo identification of mechanical properties in arteries from cine MRI images: Theoretical framework and validation." In: *IEEE Transactions on Medical Imaging* 32.8, pp. 1448–1461. ISSN: 02780062. DOI: 10.1109/TMI.2013.2257828.

Fry, D. L. (1969). "Certain histological and chemical responses of the vascular interface to acutely induced mechanical stress in the aorta of the dog." In: *Circulation research* 24.1, pp. 93–108.

Fung, Y. (1983). "On the foundations of biomechanics." In:

Gao, H. et al. (2009). "Carotid arterial plaque stress analysis using fluid–structure interactive simulation based on in-vivo magnetic resonance images of four patients." In: *Journal of biomechanics* 42.10, pp. 1416–1423.

Garcia-Garcia, H. M. et al. (2009). "Virtual histology and optical coherence tomography: From research to a broad clinical application." In: *Heart* 95.16, pp. 1362–1374. ISSN: 13556037. DOI: 10.1136/hrt.2008.151159.

Gasser, T. C. et al. (2005). "Hyperelastic modelling of arterial layers with distributed collagen fibre orientations." In: *Journal of the Royal Society Interface* 3.6, pp. 15–35. ISSN: 17425662. DOI: 10.1098/rsif.2005.0073. arXiv: 0312002v1 [arXiv:q-bio].

Gijsen, F. J. et al. (2015). "Carotid Plaque Morphological Classification Compared With Biomechanical Cap Stress: Implications for a Magnetic Resonance Imaging-Based Assessment." In: *Stroke; a journal of cerebral circulation* 46.8, pp. 2124–2128. ISSN: 15244628. DOI: 10.1161/STROKEAHA.115.009707.

Gijsen, F. J. et al. (2021). "Morphometric and Mechanical Analyses of Calcifications and Fibrous Plaque Tissue in Carotid Arteries for Plaque Rupture Risk Assessment." In: *IEEE Transactions on Biomedical Engineering* 68.4, pp. 1429–1438. ISSN: 15582531. DOI: 10.1109/TBME.2020.3038038.

Giton, M. et al. (2006). "Hyperelastic behaviour identification by a forward problem resolution: Application to a tear test of a silicone-rubber." In: *Strain* 42.4, pp. 291–297. ISSN: 00392103. DOI: 10.1111/j.1475-1305.2006.00285.x.

Glagov, S. et al. (1987). "Compensatory enlargement of human atherosclerotic coronary arteries." In: *New England Journal of Medicine* 316.22, pp. 1371–1375.

Goldstein, L. et al. (1977). "The low-density lipoprotein pathway and its relation to atherosclerosis." In: *Annual review of biochemistry* 46.1, pp. 897–930.

Gown, A. M. et al. (1986). "Human atherosclerosis. II. Immunocytochemical analysis of the cellular composition of human atherosclerotic lesions." In: *The American journal of pathology* 125.1, p. 191.

Grédiac, M. et al. (2006). "The Virtual Fields Method for Extracting Constitutive Parameters From Full-Field Measurements: a Review." In: *Strain* 42.4, pp. 233–253. DOI: 10.1111/j.1475-1305.2006.tb01504.x.

Grédiac, M. et al. (2002a). "Special virtual fields for the direct determination of material parameters with the virtual fields method. 2 - Application to in-plane properties." In: *International Journal of Solids and Structures* 39.10, pp. 2707–2730. ISSN: 00207683. DOI: 10.1016/S0020-7683(02)00128-2.

Grédiac, M. et al. (2002b). "Special virtual fields for the direct determination of material parameters with the virtual fields methods. 1 - Principle and definition." In: *International Journal of Solids and Structures* 39.10, pp. 2691–2705. ISSN: 00207683. DOI: 10.1016/S0020-7683(02)00127-0.

Grédiac, M. et al. (2003). "Special virtual fields for the direct determination of material parameters with the virtual fields method. 3. Application to the bending rigidities of anisotropic plates." In: *International Journal of Solids and Structures* 40.10, pp. 2401–2419. ISSN: 00207683. DOI: 10.1016/S0020-7683(03)00030-1.

Greenwald, S. et al. (1997). "Experimental investigation of the distribution of residual strains in the artery wall." In:

Groen, H. C. et al. (2010). "Three-dimensional registration of histology of human atherosclerotic carotid plaques to in-vivo imaging." In: *Journal of biomechanics* 43.11, pp. 2087–2092.

Grønholdt, M. et al. (1998). "Coronary atherosclerosis: determinants of plaque rupture." In: *European heart journal* 19, pp. C24–9.

Guvenir Torun, S. et al. (2021). "Multicomponent Mechanical Characterization of Atherosclerotic Human Coronary Arteries: An Experimental and Computational Hybrid Approach." In: *Frontiers in Physiology* 12.September, pp. 1–12. DOI: 10.3389/fphys.2021.733009.

Hansen, H. H. et al. (2014). "Ultrafast vascular strain compounding using plane wave transmission." In: *Journal of Biomechanics* 47.4, pp. 815–823. ISSN: 18732380. DOI: 10.1016/j.jbiomech.2014.01.015.

Hansen, H. H. et al. (2009). "Noninvasive carotid strain imaging using angular compounding at large beam steered angles: Validation in vessel phantoms." In: *IEEE Transactions on Medical Imaging* 28.6, pp. 872–880. ISSN: 02780062. DOI: 10.1109/TMI.2008.2011510.

Hansen, H. H. et al. (2010). "An angular compounding technique using displacement projection for noninvasive ultrasound strain imaging of vessel cross-sections." In: *Ultrasound in Medicine and Biology* 36.11, pp. 1947–1956. ISSN: 03015629. DOI: 10.1016/j.ultrasmedbio.2010.06.008.

Hatsukami, T. S. et al. (2000). "Visualization of fibrous cap thickness and rupture in human atherosclerotic carotid plaque in vivo with high-resolution magnetic resonance imaging." In: *Circulation* 102.9, pp. 959–964.

Heiland, V. M. et al. (2013). "Identification of carotid plaque tissue properties using an experimental-numerical approach." In: *Journal of the Mechanical Behavior of Biomedical Materials* 27, pp. 226–238. ISSN: 17516161. DOI: 10.1016/j.jmbbm.2013.05.001.

Hoeks, A. P. et al. (1990). "Assessment of the distensibility of superficial arteries." In: *Ultrasound in Medicine and Biology* 16.2, pp. 121–128. ISSN: 03015629. DOI: 10.1016/0301-5629(90)90139-4.

Hoffman, A. H. et al. (2017). "Stiffness properties of adventitia, media, and full thickness human atherosclerotic carotid arteries in the axial and circumferential directions." In: *Journal of biomechanical engineering* 139.12.

Holzapfel, G. A. et al. (2000). "A new constitutive framework for arterial wall mechanics and a comparative study of material models." In: *Journal of elasticity and the physical science of solids* 61.1, pp. 1–48.

Holzapfel, G. A. et al. (2002). "A layer-specific three-dimensional model for the simulation of balloon angioplasty using magnetic resonance imaging and mechanical testing." In: *Annals of Biomedical Engineering* 30.6, pp. 753–767.

Holzapfel, G. A. et al. (2004). "Anisotropic mechanical properties of tissue components in human atherosclerotic plaques." In: *J. Biomech. Eng.* 126.5, pp. 657–665.

Holzapfel, G. A. et al. (2005a). "Changes in the mechanical environment of stenotic arteries during interaction with stents: computational assessment of parametric stent designs." In: *J. Biomech. Eng.* 127.1, pp. 166–180.

Holzapfel, G. A. et al. (2007). "Layer-specific 3D residual deformations of human aortas with non-atherosclerotic intimal thickening." In: *Annals of biomedical engineering* 35.4, pp. 530–545.

Holzapfel, G. A. et al. (2010). "Modelling the layer-specific three-dimensional residual stresses in arteries, with an application to the human aorta." In: *Journal of the Royal Society Interface* 7.46, pp. 787–799.

Holzapfel, G. A. et al. (2014a). *Biomechanics of soft tissue in cardiovascular systems*. Vol. 441. Springer.

Holzapfel, G. A. et al. (2014b). "Computational approaches for analyzing the mechanics of atherosclerotic plaques: a review." In: *Journal of biomechanics* 47.4, pp. 859–869.

Holzapfel, G. A. et al. (2005b). "Determination of layer-specific mechanical properties of human coronary arteries with nonatherosclerotic intimal thickening and related constitutive modeling." In: *J Physiol Heart Circ Physiol* 103.4, pp. 806–808. ISSN: 00221767. DOI: 10.1152/ajpheart.00934.2004..

Holzapfel, G. A. et al. (2021). "Predictive constitutive modelling of arteries by deep learning." In: *Journal of The Royal Society Interface* 18.182, p. 20210411. DOI: 10.1098/rsif.2021.0411.

Hrubanová, A. et al. (Nov. 2020). "IMPACT OF FORMALDEHYDE ON MECHANICAL PROPERTIES OF ATHEROSCLEROTIC CAROTID ARTERIES." In: *ENGINEERING MECHANICS 2020*. Chap. 166394, pp. 210–213. DOI: 10.21495/5896-3-210.

Huang, X. et al. (2014a). "Higher critical plaque wall stress in patients who died of coronary artery disease compared with those who died of other causes: A 3D FSI study based on ex vivo MRI of coronary plaques." In: *Journal of Biomechanics* 47.2, pp. 432–437. ISSN: 00219290. DOI: 10.1016/j.jbiomech.2013.11.007.

Huang, X. et al. (2016). "3D MRI-based multicomponent thin layer structure only plaque models for atherosclerotic plaques." In: *Journal of biomechanics* 49.13, pp. 2726–2733.

Huang, Y. et al. (2014b). "The influence of computational strategy on prediction of mechanical stress in carotid atherosclerotic plaques: comparison of 2D structure-only,

3D structure-only, one-way and fully coupled fluid-structure interaction analyses." In: *Journal of biomechanics* 47.6, pp. 1465–1471.

Humphrey, J. et al. (2002). *Cells, tissues, and organs.*

Iannaccone, F. et al. (2014). "The influence of vascular anatomy on carotid artery stenting: a parametric study for damage assessment." In: *Journal of biomechanics* 47.4, pp. 890–898.

Iqbal, J. et al. (2013). "Coronary stents: historical development, current status and future directions." In: *Br Med Bull* 106.1, pp. 193–211.

Johnston, R. D. et al. (2021). "An investigation into the critical role of fibre orientation in the ultimate tensile strength and stiffness of human carotid plaque caps." In: *Acta Biomaterialia* 124.February, pp. 291–300. ISSN: 18787568. DOI: 10.1016/j.actbio.2021.02.008.

Jonášová, A. et al. (2018). "Noninvasive assessment of carotid artery stenoses by the principle of multiscale modelling of non-Newtonian blood flow in patient-specific models." In: *Applied Mathematics and Computation* 319, pp. 598–616. ISSN: 00963003. DOI: 10.1016/j.amc.2017.07.032.

Kaazempur-Mofrad, M. et al. (2003). "Cyclic strain in human carotid bifurcation and its potential correlation to atherogenesis: Idealized and anatomically-realistic models." In: *Journal of Engineering Mathematics* 47.3-4, pp. 299–314.

Kaazempur-Mofrad, M. et al. (2004). "Characterization of the atherosclerotic carotid bifurcation using MRI, finite element modeling, and histology." In: *Annals of biomedical engineering* 32.7, pp. 932–946.

Kamenskiy, A. V. et al. (2015). "Age and disease-related geometric and structural remodeling of the carotid artery." In: *Journal of vascular surgery* 62.6, pp. 1521–1528.

Kanai, H. et al. (2003). "Elasticity imaging of atheroma with transcutaneous ultrasound: Preliminary study." In: *Circulation* 107.24, pp. 3018–3021. ISSN: 00097322. DOI: 10.1161/01.CIR.0000078633.31922.8A.

Kelly-Arnold, A. et al. (2013). "Revised microcalcification hypothesis for fibrous cap rupture in human coronary arteries." In: *Proceedings of the National Academy of Sciences* 110.26, pp. 10741–10746. ISSN: 0027-8424. DOI: 10.1073/pnas.1308814110.

Kent, K. C. et al. (2010). "Analysis of risk factors for abdominal aortic aneurysm in a cohort of more than 3 million individuals." In: *Journal of Vascular Surgery* 52.3, pp. 539–548. ISSN: 07415214. DOI: 10.1016/j.jvs.2010.05.090.

Khimchenko, A. et al. (2016). "Extending two-dimensional histology into the third dimension through conventional micro computed tomography." In: *NeuroImage* 139, pp. 26–36.

Kochanek, K. D. et al. (2019). "Deaths: final data for 2017." In:

Kock, S. A. et al. (2008). "Mechanical stresses in carotid plaques using MRI-based fluid-structure interaction models." In: *Journal of Biomechanics* 41.8, pp. 1651–1658. ISSN: 00219290. DOI: 10.1016/j.jbiomech.2008.03.019.

Kok, A. M. et al. (2016). "Peak cap stress calculations in coronary atherosclerotic plaques with an incomplete necrotic core geometry." In: *BioMedical Engineering Online* 15.1, pp. 1–13. ISSN: 1475925X. DOI: 10.1186/s12938-016-0162-5.

Kok, A. M. et al. (2017). "Model-based cap thickness and peak cap stress prediction for carotid MRI." In: *Journal of Biomechanics* 60, pp. 175–180. ISSN: 18732380. DOI: 10.1016/j.jbiomech.2017.06.034.

Koktzoglou, I. (2013). "4D dark blood arterial wall magnetic resonance imaging: Methodology and demonstration in the carotid arteries." In: *Magnetic Resonance in Medicine* 69.4, pp. 956–965. ISSN: 15222594. DOI: 10.1002/mrm.24647.

Koskinas, K. C. et al. (2012). "Role of endothelial shear stress in stent restenosis and thrombosis: pathophysiologic mechanisms and implications for clinical translation." In: *Journal of the American College of Cardiology* 59.15, pp. 1337–1349.

Kural, M. H. et al. (2012). "Planar biaxial characterization of diseased human coronary and carotid arteries for computational modeling." In: *Journal of Biomechanics* 45.5, pp. 790–798. ISSN: 00219290. DOI: 10.1016/j.jbiomech.2011.11.019.

Lawlor, M. G. et al. (2011). "Experimental determination of circumferential properties of fresh carotid artery plaques." In: *Journal of biomechanics* 44.9, pp. 1709–1715.

LEE, R. T. et al. (1991). "Structure-Dependent Dynamic Mechanical-Behavior of Fibrous Caps From Human Atherosclerotic Plaques." In: *Circulation* 83.5, pp. 1764–1770. ISSN: 0009-7322. DOI: 10.1161/01.CIR.83.5.1764.

Liapis, C. et al. (2009). "ESVS guidelines. Invasive treatment for carotid stenosis: indications, techniques." In: *European journal of vascular and endovascular surgery* 37.4, pp. 1–19.

Libby, P. et al. (1991). "Involvement of the immune system in human atherogenesis: curent knowledge and unanswered questions." In: *Laboratory investigation* 64.1, pp. 5–15.

Libby, P. et al. (2015). "Requiem for the 'vulnerable plaque'." In: *European heart journal* 36.43, pp. 2984–2987.

Lionello, G. et al. (2014). "An effective procedure to create a speckle pattern on biological soft tissue for digital image correlation measurements." In: *Journal of the Mechanical Behavior of Biomedical Materials* 39, pp. 1–8. ISSN: 18780180. DOI: 10.1016/j.jmbbm.2014.07.007.

Lisický, O. et al. (2021a). "Interpretation of Experimental Data is Substantial for Constitutive Characterization of Arterial Tissue." In: *Journal of Biomechanical Engineering*. ISSN: 0148-0731. DOI: 10.1115/1.4051120.

Lisický, O. et al. (Sept. 2020). "Consideration of stiffness of wall layers is decisive for patient-specific analysis of carotid artery with atheroma." In: *PLOS ONE* 15.9. Ed. by F.-B. Tian, e0239447. ISSN: 1932-6203. DOI: 10.1371/journal.pone.0239447.

Lisický, O. et al. (2021b). "Constitutive models and failure properties of fibrous tissues of carotid artery atheroma based on their uniaxial testing." In: *Journal of Biomechanics* 129, p. 110861. ISSN: 00219290. DOI: 10.1016/j.jbiomech.2021.110861.

Lisickỳ, O. et al. (2019). "Influence of Transversal Resolution on Reconstructing Atherosclerotic Plaque Components." In: *ECCOMAS Thematic Conference on Computational Vision and Medical Image Processing*. Springer, pp. 501–508.

Liu, F. et al. (2015). "Real-time tissue elastography for the detection of vulnerable carotid plaques in patients undergoing endarterectomy: A pilot study." In: *Ultrasound in Medicine and Biology* 41.3, pp. 705–712. ISSN: 1879291X. DOI: 10.1016/j.ultrasmedbio.2014.10.007.

Liu, H. et al. (2019). "Finite element simulation of three dimensional residual stress in the aortic wall using an anisotropic tissue growth model." In: *Journal of the mechanical behavior of biomedical materials* 92, pp. 188–196.

Livens, P. et al. (2021). "Material characterization of curved shells under finite deformation using the virtual fields method." In: *Strain* March, pp. 1–18. ISSN: 14751305. DOI: 10.1111/str.12398.

Loree, H. M. et al. (1994). "Mechanical properties of model atherosclerotic lesion lipid pools." In: *Arteriosclerosis and Thrombosis* 14.2, pp. 230–234. ISSN: 10498834. DOI: 10.1161/01.atv.14.2.230.

Loree, H. M. et al. (1992). "Effects of fibrous cap thickness on peak circumferential stress in model atherosclerotic vessels." In: *Circulation research* 71.4, pp. 850–858.

Lowder, M. L. et al. (2007). "Correction of distortion of histologic sections of arteries." In: *Journal of Biomechanics* 40.2, pp. 445–450.

Luo, J. et al. (2012). "Pulse Wave Imaging (PWI) of the human carotid artery: An in vivo feasibility study." In: *The Journal of the Acoustical Society of America* 131.4, pp. 3289–3289. ISSN: 0001-4966. DOI: 10.1121/1.4708297.

MacNeil, J. A. et al. (2007). "Accuracy of high-resolution peripheral quantitative computed tomography for measurement of bone quality." In: *Medical engineering & physics* 29.10, pp. 1096–1105.

Macrae, R. A. et al. (2016). "Methods in Mechanical Testing of Arterial Tissue: A Review." In: *Strain* 52.5, pp. 380–399. ISSN: 14751305. DOI: 10.1111/str.12183.

Maher, E. et al. (2009). "Tensile and compressive properties of fresh human carotid atherosclerotic plaques." In: *Journal of biomechanics* 42.16, pp. 2760–2767.

Maher, E. et al. (2011). "Inelasticity of human carotid atherosclerotic plaque." In: *Annals of Biomedical Engineering* 39.9, pp. 2445–2455. ISSN: 00906964. DOI: 10.1007/s10439-011-0331-4.

Malandain, G. et al. (2004). "Fusion of autoradiographs with an MR volume using 2-D and 3-D linear transformations." In: *NeuroImage* 23.1, pp. 111–127. ISSN: 10538119. DOI: 10.1016/j.neuroimage.2004.04.038.

Maldonado, N. et al. (2012). "A mechanistic analysis of the role of microcalcifications in atherosclerotic plaque stability: potential implications for plaque rupture." In: *AJP: Heart and Circulatory Physiology* 303.5, H619–H628. ISSN: 0363-6135. DOI: 10.1152/ajpheart.00036.2012.

Malek, A. M. et al. (1999). "Hemodynamic shear stress and its role in atherosclerosis." In: *Jama* 282.21, pp. 2035–2042.

Man, V. (2018). "Využití experimentů pro zlepšení úrovně konstitutivních modelů tkání aortálních výdutí." cze. PhD thesis.

Manfrini, O. et al. (2006). "Sources of Error and Interpretation of Plaque Morphology by Optical Coherence Tomography." In: *American Journal of Cardiology* 98.2, pp. 156–159. ISSN: 00029149. DOI: 10.1016/j.amjcard.2006.01.097.

Markl, M. et al. (2010). "In vivo wall shear stress distribution in the carotid artery: effect of bifurcation geometry, internal carotid artery stenosis, and recanalization therapy." In: *Circulation: Cardiovascular Imaging* 3.6, pp. 647–655.

Martiel, J.-L. et al. (2021). *Importance of residual stress and basal tone in healthy and pathological human coronary arteries*, pp. 433–461. ISBN: 9780128171950. DOI: 10.1016/b978-0-12-817195-0.00019-6.

Matsumoto, T. et al. (2012). "Tensile properties of vascular smooth muscle cells: Bridging vascular and cellular biomechanics." In: *Journal of Biomechanics* 45.5, pp. 745–755. ISSN: 00219290. DOI: 10.1016/j.jbiomech.2011.11.014.

Maurice, R. L. et al. (2005). "Non-invasive high-frequency vascular ultrasound elastography." In: *Physics in Medicine and Biology* 50.7, pp. 1611–1628. ISSN: 00319155. DOI: 10.1088/0031-9155/50/7/020.

Mei, Y. et al. (2021a). "General Finite-Element Framework of the Virtual Fields Method in Nonlinear Elasticity." In: *Journal of Elasticity* 145.1-2, pp. 265–294. ISSN: 15732681. DOI: 10.1007/s10659-021-09842-8.

Mei, Y. et al. (2021b). "Introducing regularization into the virtual fields method (VFM) to identify nonhomogeneous elastic property distributions." In: *Computational Mechanics* 67.6, pp. 1581–1599. ISSN: 14320924. DOI: 10.1007/s00466-021-02007-3.

Milner, J. S. et al. (1998). "Hemodynamics of human carotid artery bifurcations: computational studies with models reconstructed from magnetic resonance imaging of normal subjects." In: *Journal of vascular surgery* 28.1, pp. 143–156.

Miniño, A. M. et al. (2002). "Deaths: final data for 2000." In: *statistics* 34, p. 36.

Moerman, A. M. et al. (2019). "An MRI-based method to register patient-specific wall shear stress data to histology." In: *PLoS One* 14.6, e0217271.

Morr, S. et al. (2014). "Carotid artery stenting: current and emerging options." In: *Medical Devices (Auckland, NZ)* 7, p. 343.

Mulvihill, J. et al. (2013a). "Mechanical, biological and structural characterization of in vitro ruptured human carotid plaque tissue." In: *Acta biomaterialia* 9.11, pp. 9027–9035.

Mulvihill, J. J. et al. (2013b). "On the mechanical behaviour of carotid artery plaques: The influence of curve-fitting experimental data on numerical model results." In: *Biomechanics and Modeling in Mechanobiology* 12.5, pp. 975–985. ISSN: 16177959. DOI: 10.1007/s10237-012-0457-9.

Naim, C. et al. (2013). "Characterisation of carotid plaques with ultrasound elastography: Feasibility and correlation with high-resolution magnetic resonance imaging." In: *European Radiology* 23.7, pp. 2030–2041. ISSN: 09387994. DOI: 10.1007/s00330-013-2772-7.

Nallamothu, B. K. et al. (2011). "Operator experience and carotid stenting outcomes in Medicare beneficiaries." In: *Jama* 306.12, pp. 1338–1343.

Napoli, C. et al. (1997). "Fatty streak formation occurs in human fetal aortas and is greatly enhanced by maternal hypercholesterolemia. Intimal accumulation of low density lipoprotein and its oxidation precede monocyte recruitment into early atherosclerotic lesions." In: *The Journal of clinical investigation* 100.11, pp. 2680–2690.

Nederveen, A. J. et al. (2014). "MRI strain imaging of the carotid artery: Present limitations and future challenges." In: *Journal of Biomechanics* 47.4, pp. 824–833. ISSN: 18732380. DOI: 10.1016/j.jbiomech.2014.01.014.

Ní Annaidh, A. et al. (2012). "Characterization of the anisotropic mechanical properties of excised human skin." In: *Journal of the Mechanical Behavior of Biomedical Materials* 5.1, pp. 139–148. ISSN: 17516161. DOI: 10.1016/j.jmbbm.2011.08.016. arXiv: 1302.3022.

Nieuwstadt, H. A. et al. (2015a). "Carotid plaque elasticity estimation using ultrasound elastography, MRI, and inverse FEA - A numerical feasibility study." In: *Medical Engineering and Physics* 37.8, pp. 801–807. ISSN: 18734030. DOI: 10.1016/j.medengphy.2015.06.003.

Nieuwstadt, H. et al. (2013). "The influence of axial image resolution on atherosclerotic plaque stress computations." In: *Journal of biomechanics* 46.4, pp. 689–695.

Nieuwstadt, H. et al. (2015b). "A computer-simulation study on the effects of MRI voxel dimensions on carotid plaque lipid-core and fibrous cap segmentation and stress modeling." In: *PloS one* 10.4.

Nieuwstadt, H. A. et al. (2014). "The Influence of Inaccuracies in Carotid MRI Segmentation on Atherosclerotic Plaque Stress Computations." In: *Journal of Biomechanical Engineering* 136.2, p. 021015. ISSN: 0148-0731. DOI: 10.1115/1.4026178.

Novák, K. (2018). "Analýza vlivu uspořádání kolagenu na mechanické vlastnosti tepen." cze. PhD thesis.

O'Reilly, B. L. et al. (2020). "An experimental and computational investigation of the material behaviour of discrete homogenous iliofemoral and carotid atherosclerotic plaque constituents." In: *Journal of Biomechanics* 106. ISSN: 18732380. DOI: 10.1016/j.jbiomech.2020.109801.

Ogden, R. W. et al. (1972). "Large deformation isotropic elasticity – on the correlation of theory and experiment for incompressible rubberlike solids." In: *Proceedings of the Royal Society of London. A. Mathematical and Physical Sciences* 326.1567, pp. 565–584. ISSN: 0080-4630. DOI: 10.1098/rspa.1972.0026.

Ohayon, J. et al. (2001). "In-vivo prediction of human coronary plaque rupture location using intravascular ultrasound and the finite element method." In: *Coronary Artery Disease* 12.8, pp. 655–663. ISSN: 09546928. DOI: 10.1097/00019501-200112000-00009.

Ohayon, J. et al. (2005). "A three-dimensional finite element analysis of stress distribution in a coronary atherosclerotic plaque: in-vivo prediction of plaque rupture location." In: *Biomechanics applied to computer assisted surgery* 37.2, pp. 225–241.

Ohayon, J. et al. (2007). "Influence of residual stress/strain on the biomechanical stability of vulnerable coronary plaques: potential impact for evaluating the risk of plaque rupture." In: *American Journal of Physiology-Heart and Circulatory Physiology* 293.3, H1987–H1996. ISSN: 0363-6135. DOI: 10.1152/ajpheart.00018.2007.

Ohayon, J. et al. (2008). "Necrotic core thickness and positive arterial remodeling index: Emergent biomechanical factors for evaluating the risk of plaque rupture." In: *American Journal of Physiology - Heart and Circulatory Physiology* 295.2, pp. 717–727. ISSN: 03636135. DOI: 10.1152/ajpheart.00005.2008.

Ophir, J. et al. (1991). "Elastography: a quantitative method for imaging the elasticity of biological tissues." In: *Ultrasonic imaging* 13.2, pp. 111–134.

Pack, E. et al. (2020). "Biaxial Stress Relaxation of Vaginal Tissue in Pubertal Gilts." In: *Journal of Biomechanical Engineering* 142.3, pp. 1–7. ISSN: 0148-0731. DOI: 10.1115/1.4045707.

Pagiatakis, C. et al. (2015). "A comparison between the principal stress direction and collagen fiber orientation in coronary atherosclerotic plaque fibrous caps." In: *Medical and Biological Engineering and Computing* 53.6, pp. 545–555. ISSN: 17410444. DOI: 10.1007/s11517-015-1257-z.

Pei, X. et al. (2013). "Fatigue crack propagation analysis of plaque rupture." In: *Journal of Biomechanical Engineering* 135.10, pp. 1–9. ISSN: 01480731. DOI: 10.1115/1.4025106.

Peña, J. A. et al. (2021). "Biomechanical characterization and constitutive modeling of the layer-dissected residual strains and mechanical properties of abdominal porcine aorta." In: *Journal of Biomechanics* 132, p. 110909. ISSN: 18732380. DOI: 10.1016/j.jbiomech.2021.110909. URL: https://doi.org/10.1016/j.jbiomech.2021.110909.

Perkowska, M. et al. (2017). "Redirection of a crack driven by viscous fluid." In: *International Journal of Engineering Science* 121, pp. 182–193. ISSN: 00207225. DOI: 10.1016/j.ijengsci.2017.09.009. eprint: 1710.01119.

Pichat, J. et al. (2018). "A survey of methods for 3D histology reconstruction." In: *Medical image analysis* 46, pp. 73–105.

Pierce, D. M. et al. (2015). "A method for incorporating three-dimensional residual stretches/stresses into patient-specific finite element simulations of arteries." In: *Journal of the mechanical behavior of biomedical materials* 47, pp. 147–164.

Pocaterra, M. et al. (2009). "Circumferential residual stress distribution and its influence in a diseased carotid artery." In: *Summer Bioengineering Conference*. Vol. 48913. American Society of Mechanical Engineers, pp. 849–850.

Polzer, S. et al. (2015). "Structure-based constitutive model can accurately predict planar biaxial properties of aortic wall tissue." In: *Acta Biomaterialia* 14, pp. 133–145. ISSN: 18787568. DOI: 10.1016/j.actbio.2014.11.043.

Polzer, S. (2012). "Deformačně napěťová analýza aortálních aneurysmat : Stress-strain analysis of aortic aneurysms." eng. PhD thesis.

Prosi, M. et al. (2004). "Influence of curvature dynamics on pulsatile coronary artery flow in a realistic bifurcation model." In: *Journal of biomechanics* 37.11, pp. 1767–1775.

Raghavan, M. et al. (2004). "Three-dimensional finite element analysis of residual stress in arteries." In: *Annals of Biomedical Engineering* 32.2, pp. 257–263.

Reneman, R. S. et al. (1986). "Age-related changes in carotid artery wall properties in men." In: *Ultrasound in Medicine and Biology* 12.6, pp. 465–471. ISSN: 03015629. DOI: 10.1016/0301-5629(86)90218-8.

Reneman, R. S. et al. (2005). "Non-invasive ultrasound in arterial wall dynamics in humans: What have we learned and what remains to be solved." In: *European Heart Journal* 26.10, pp. 960–966. ISSN: 0195668X. DOI: 10.1093/eurheartj/ehi177.

Ribbers, H. et al. (2007). "Noninvasive Two-Dimensional Strain Imaging of Arteries: Validation in Phantoms and Preliminary Experience in Carotid Arteries In Vivo." In: *Ultrasound in Medicine and Biology* 33.4, pp. 530–540. ISSN: 03015629. DOI: 10.1016/j.ultrasmedbio.2006.09.009.

Richardson, P. et al. (1989). "Influence of plaque configuration and stress distribution on fissuring of coronary atherosclerotic plaques." In: *Lancet* 334.8669, pp. 941–944.

Riou, L. M. et al. (2014). "Effects of mechanical properties and atherosclerotic artery size on biomechanical plaque disruption - Mouse vs. human." In: *Journal of Biomechanics* 47.4, pp. 765–772. ISSN: 18732380. DOI: 10.1016/j.jbiomech.2014.01.020.

Rioufol, G. et al. (2002). "Multiple atherosclerotic plaque rupture in acute coronary syndrome: a three-vessel intravascular ultrasound study." In: *Circulation* 106.7, pp. 804–808.

Romo, A. et al. (2014). "In vitro analysis of localized aneurysm rupture." In: *Journal of Biomechanics* 47.3, pp. 607–616. ISSN: 00219290. DOI: 10.1016/j.jbiomech.2013.12.012.

Rosenfeld, M. E. et al. (1990). "Macrophages, endothelial cells, and lipoprotein oxidation in the pathogenesis of atherosclerosis." In: *Toxicologic Pathology* 18.4a, pp. 560–571.

Ross, R. (1986). "The pathogenesis of atherosclerosis—an update." In: *New England Journal of Medicine* 314.8, pp. 488–500.

Ross, R. (1993). "The pathogenesis of atherosclerosis: a perspective for the 1990s." In: *Nature* 362.6423, pp. 801–809.

Ross, R. (1999). "Atherosclerosis—an inflammatory disease." In: *New England journal of medicine* 340.2, pp. 115–126.

Ross, R. et al. (1976). "The pathogenesis of atherosclerosis." In: *New England journal of medicine* 295.7, pp. 369–377.

Rothwell, P. et al. (2003). "Reanalysis of the final results of the European Carotid Surgery Trial." In: *Stroke* 34.2, pp. 514–523.
Rothwell, P. et al. (2004). "Carotid endarterectomy for asymptomatic carotid stenosis: asymptomatic carotid surgery trial." In: *Stroke* 35.10, pp. 2425–2427.
Saam, T. et al. (2005). "Quantitative evaluation of carotid plaque composition by in vivo MRI." In: *Arteriosclerosis, thrombosis, and vascular biology* 25.1, pp. 234–239.
Sadat, U. et al. (2010). "Finite element analysis of vulnerable atherosclerotic plaques: A comparison of mechanical stresses within carotid plaques of acute and recently symptomatic patients with carotid artery disease." In: *Journal of Neurology, Neurosurgery and Psychiatry* 81.3, pp. 286–289. ISSN: 1468330X. DOI: 10.1136/jnnp.2009.190363.
Salvucci, F. P. et al. (2010). "A patient-specific method for the evaluation of wall shear stress in human coronary arteries." In: *2010 Annual International Conference of the IEEE Engineering in Medicine and Biology Society, EMBC'10*, pp. 3788–3791. ISSN: 1557-170X. DOI: 10.1109/IEMBS.2010.5627565.
Schaar, J. A. et al. (2003). "Terminology for high-risk and vulnerable coronary artery plaques." In: *European heart journal* 25.12, pp. 1077–1082.
Schmidt, T. et al. (2018). "Coronary stents: history, design, and construction." In: *Journal of clinical medicine* 7.6, p. 126.
Schmitt, C. et al. (2007). "Noninvasive Vascular Elastography: Toward A Complementary Characterization Tool of Atherosclerosis in Carotid Arteries." In: *Ultrasound in Medicine and Biology* 33.12, pp. 1841–1858. ISSN: 03015629. DOI: 10.1016/j.ultrasmedbio.2007.05.020.
Schröder, J. et al. (2016). "An engineering tool to estimate eigenstresses in three-dimensional patient-specific arteries." In: *Computer Methods in Applied Mechanics and Engineering* 306, pp. 364–381.
Schulze-Bauer, C. A. et al. (2002). "Mechanics of the human femoral adventitia including the high-pressure response." In: *American Journal of Physiology-Heart and Circulatory Physiology* 282.6, H2427–H2440.
Schulze-Bauer, C. A. et al. (2003). "Passive biaxial mechanical response of aged human iliac arteries." In: *J. Biomech. Eng.* 125.3, pp. 395–406.
Sigaeva, T. et al. (2019). "Anisotropic residual stresses in arteries." In: *Journal of the Royal Society Interface* 16.151, p. 20190029.
Slager, C. et al. (2005). "The role of shear stress in the generation of rupture-prone vulnerable plaques." In: *Nature clinical practice Cardiovascular medicine* 2.8, pp. 401–407.
Solav, D. et al. (2018). "MultiDIC: An open-source toolbox for multi-view 3D digital image correlation." In: *IEEE Access* 6, pp. 30520–30535. ISSN: 21693536. DOI: 10.1109/ACCESS.2018.2843725.
Sommer, G. et al. (2010). "Biaxial mechanical properties of intact and layer-dissected human carotid arteries at physiological and supraphysiological loadings." In: *American Journal of Physiology-Heart and Circulatory Physiology* 298.3, H898–H912.
Sommer, G. et al. (2012). "3D constitutive modeling of the biaxial mechanical response of intact and layer-dissected human carotid arteries." In: *Journal of the mechanical behavior of biomedical materials* 5.1, pp. 116–128.
Speelman, L. et al. (2011). "Initial stress in biomechanical models of atherosclerotic plaques." In: *Journal of Biomechanics* 44.13, pp. 2376–2382. ISSN: 00219290. DOI: 10.1016/j.jbiomech.2011.07.004.

Speelman, L. et al. (2016). "MRI-based biomechanical parameters for carotid artery plaque vulnerability assessment." In: *Thrombosis and Haemostasis* 115.3, pp. 493–500. ISSN: 03406245. DOI: 10.1160/TH15-09-0712.

Stary, H. C. (2000). "Natural history and histological classification of atherosclerotic lesions: an update." In: *Arteriosclerosis, thrombosis, and vascular biology* 20.5, pp. 1177–1178.

Stary, H. C. et al. (1992). "A definition of the intima of human arteries and of its atherosclerosis-prone regions. A report from the Committee on Vascular Lesions of the Council on Arteriosclerosis, American Heart Association." In: *Arteriosclerosis and thrombosis: a journal of vascular biology* 12.1, pp. 120–134.

Stone, G. W. et al. (2011). "A prospective natural-history study of coronary atherosclerosis." In: *New England Journal of Medicine* 364.3, pp. 226–235.

Švancara, P. et al. (Nov. 2020). "COMPUTATIONAL MODELING OF BLOOD FLOW IN THE BIFURCATION OF HUMAN CAROTID ARTERY." In: *ENGINEERING MECHANICS 2020*. 1. Chap. 166395, pp. 480–483. DOI: 10.21495/5896-3-480.

Tang, D. et al. (2004). "Effect of a lipid pool on stress/strain distributions in stenotic arteries: 3-D fluid-structure interactions (FSI) models." In: *J. Biomech. Eng.* 126.3, pp. 363–370.

Tang, D. et al. (2005). "Quantifying effects of plaque structure and material properties on stress distributions in human atherosclerotic plaques using 3D FSI models." In:

Tang, D. et al. (2008). "A negative correlation between human carotid atherosclerotic plaque progression and plaque wall stress: In vivo MRI-based 2D/3D FSI models." In: *Journal of Biomechanics* 41.4, pp. 727–736. ISSN: 00219290. DOI: 10.1016/j.jbiomech.2007.11.026. arXiv: NIHMS150003.

Tang, D. et al. (2009). "Sites of rupture in human atherosclerotic carotid plaques are associated with high structural stresses: an in vivo MRI-based 3D fluid-structure interaction study." In: *Stroke* 40.10, pp. 3258–3263.

Tang, D. et al. (2014). "Image-based modeling for better understanding and assessment of atherosclerotic plaque progression and vulnerability: Data, modeling, validation, uncertainty and predictions." In: *Journal of Biomechanics* 47.4, pp. 834–846. ISSN: 18732380. DOI: 10.1016/j.jbiomech.2014.01.012.

Tang, D. et al. (2017). "Cap inflammation leads to higher plaque cap strain and lower cap stress: an MRI-PET/CT-based FSI modeling approach." In: *Journal of biomechanics* 50, pp. 121–129.

Tardy, Y. et al. (1997). "Shear stress gradients remodel endothelial monolayers in vitro via a cell proliferation-migration-loss cycle." In: *Arteriosclerosis, thrombosis, and vascular biology* 17.11, pp. 3102–3106.

Teng, Z. et al. (2009). "An experimental study on the ultimate strength of the adventitia and media of human atherosclerotic carotid arteries in circumferential and axial directions." In: *Journal of Biomechanics* 42.15, pp. 2535–2539. ISSN: 00219290. DOI: 10.1016/j.jbiomech.2009.07.009. arXiv: NIHMS150003. URL: http://dx.doi.org/10.1016/j.jbiomech.2009.07.009.

Teng, Z. et al. (2010). "Arterial luminal curvature and fibrous-cap thickness affect critical stress conditions within atherosclerotic plaque: An in vivo MRI-based 2D finite-element study." In: *Annals of Biomedical Engineering* 38.10, pp. 3096–3101. ISSN: 00906964. DOI: 10.1007/s10439-010-0078-3.

Teng, Z. et al. (2014). "Material properties of components in human carotid atherosclerotic plaques: A uniaxial extension study." In: *Acta Biomaterialia* 10.12, pp. 5055–5063. ISSN: 18787568. DOI: 10.1016/j.actbio.2014.09.001.

Teng, Z. et al. (2015). "The influence of constitutive law choice used to characterise atherosclerotic tissue material properties on computing stress values in human carotid plaques." In: *Journal of biomechanics* 48.14, pp. 3912–3921.

Van Engelen, A. et al. (2011). "Multi-feature-based plaque characterization in ex vivo MRI trained by registration to 3D histology." In: *Physics in Medicine & Biology* 57.1, p. 241.

Van Wijk, D. F. et al. (2015). "Increasing the spatial resolution of 3T carotid MRI has no beneficial effect for plaque component measurement reproducibility." In: *PLoS ONE* 10.7, pp. 1–15. ISSN: 19326203. DOI: 10.1371/journal.pone.0130878.

Virmani, R. et al. (2000). "Lessons from sudden coronary death: a comprehensive morphological classification scheme for atherosclerotic lesions." In: *Arteriosclerosis, thrombosis, and vascular biology* 20.5, pp. 1262–1275.

Vitásek, R. et al. (2021). "Sources of inconsistency in mean mechanical response of abdominal aortic aneurysm tissue." In: *Journal of the Mechanical Behavior of Biomedical Materials* 115, p. 104274. ISSN: 18780180. DOI: 10.1016/j.jmbbm.2020.104274.

Walsh, M. et al. (2014). "Uniaxial tensile testing approaches for characterisation of atherosclerotic plaques." In: *Journal of biomechanics* 47.4, pp. 793–804.

Wang, L. et al. (2017). "Effects of Residual Stress, Axial Stretch, and Circumferential Shrinkage on Coronary Plaque Stress and Strain Calculations: A Modeling Study Using IVUS-Based Near-Idealized Geometries." In: *Journal of Biomechanical Engineering* 139.1, pp. 1–11. ISSN: 15288951. DOI: 10.1115/1.4034867.

Widman, E. et al. (2012). "Shear wave elastography for characterization of carotid artery plaques-A feasibility study in an experimental setup." In: *IEEE International Ultrasonics Symposium, IUS*. ISSN: 19485719. DOI: 10.1109/ULTSYM.2012.0343.

Williamson, S. D. et al. (2003). "On the sensitivity of wall stresses in diseased arteries to variable material properties." In: *Journal of Biomechanical Engineering* 125.1, pp. 147–155. ISSN: 01480731. DOI: 10.1115/1.1537736.

Wong, K. K. L. et al. (2012). "Effect of calcification on the mechanical stability of plaque based on a three-dimensional carotid bifurcation model." In: *BMC Cardiovascular Disorders* 12. ISSN: 14712261. DOI: 10.1186/1471-2261-12-7.

Yamashita, K. et al. (2014). "Association between increased epicardial adipose tissue volume and coronary plaque composition." In: *Heart and Vessels* 29.5, pp. 569–577. ISSN: 16152573. DOI: 10.1007/s00380-013-0398-y.

Yang, C. et al. (2007). "In vivo/ex vivo MRI-based 3D non-Newtonian FSI models for human atherosclerotic plaques compared with fluid/wall-only models." In: *Computer modeling in engineering & sciences: CMES* 19.3, p. 233.

Yeoh, O. H. (1993). "Some forms of the strain energy function for rubber." In: *Rubber Chemistry and technology* 66.5, pp. 754–771.

Yuan, J. et al. (2015). "Influence of material property variability on the mechanical behaviour of carotid atherosclerotic plaques: A 3D fluid-structure interaction analysis." In: *International journal for numerical methods in biomedical engineering* 31.8, e02722.

Zarins, C. K. et al. (1983). "Carotid bifurcation atherosclerosis. Quantitative correlation of plaque localization with flow velocity profiles and wall shear stress." In: *Circulation research* 53.4, pp. 502–514.

Zhang, H. et al. (2019). "Von Mises Strain as a Risk Marker for Vulnerability of Carotid Plaque: Preliminary Clinical Evaluation of Cerebral Infarction." In: *Ultrasound in Medicine and Biology* 45.5, pp. 1221–1233. ISSN: 1879291X. DOI: 10.1016/j.ultrasmedbio.2019.01.007.

Zhao, J. et al. (2019). "The state of the art of two-dimensional digital image correlation computational method." In: *Engineering Reports* 1.2, pp. 1–15. ISSN: 2577-8196. DOI: 10.1002/eng2.12038.

List of abbreviations

AHA	American Heard Association
CAS	Carotid Artery Stenting
CCD	Charge-coupled Device
CEA	Carotid endarterectomy
CFD	Computational Fluid Dynamics
CT	Computed Tomography
CTOD	Crack Tip Opening Displacement
DC	Distensibility Coefficient
DIC	Digital Image Correlation
DNA	Deoxyribonucleic Acid
DOE	Design of Experiment
ECST	European Carotid Surgery Trial
ESVS	European Society for Vascular Surgery
FC	Fibrous Cap
FE	Finite Element
FEMU	Finite Element Method Updating
FSI	Fluid-Structure Interaction
FT	Fibrous Tissue
FTIR	Fourier Transform Infrared
IMT	Intima-media Thickness
IVUS	Intravascular Ultrasound
LC	Lipid Core
LDL	Low Density Lipoproteins

MI	Media + intima layer
MRI	Magnetic Resonance Imaging
NESCET	North American Symptomatic Carotid Endarterectomy Trial
OCT	Optical coherence tomography
oxLDL	oxidized Low Density Lipoproteins
PCS	Peak Cap Stress
PS	Patient-specific
PWV	Pulse Wave Velocity
RS	Residual Stress
SMC	Smooth Muscle Cells
SPACE	Stent Protected Angioplasty versus Endarterectomy
VFM	Virtual Fields Method

A. Appendix

Influence of Transversal Resolution on Reconstructing Atherosclerotic Plaque

Original research article indexed by Scopus.

O. Lisickỳ et al. (2019). "Influence of Transversal Resolution on Reconstructing Atherosclerotic Plaque Components." In: *ECCOMAS Thematic Conference on Computational Vision and Medical Image Processing*. Springer, pp. 501–508

Influence of Transversal Resolution on Reconstructing Atherosclerotic Plaque Components

Ondřej Lisický[1(✉)], Aneta Malá[2], and Jiří Burša[1]

[1] Institute of Solid Mechanics, Mechatronics and Biomechanics, Brno University of Technology, Brno, Czech Republic
161238@vutbr.cz, bursa@fme.vutbr.cz
[2] Institute of Scientific Instruments, The Czech Academy of Science, Brno, Czech Republic
malaa@ISIBrno.cz

Abstract. Assessment of atherosclerotic plaque vulnerability is nowadays closely related to computational modelling. Mechanical loading is considered as trigger for plaque rupture and requires patient specific model geometry. Here segmentation of each cross section obtained from medical imaging is used for model reconstruction. However, the number of input images depends on the chosen method. The influence of transversal resolution on surface and volume deviations is quantified in this study. The influence of smoothing process was also considered. A specimen harvested during carotid endarterectomy was imaged by *ex vivo* high-resolution 9.4 T MRI. The slice thickness varied from 1.5 mm to 0.25 mm with fixed in-plane resolution 0.078 mm. Segmented cross sections were then combined along the arterial axis. Significant differences were found in both surface and volume analyses. Smoothing was found as insignificant parameter within the slice thickness. Findings of this study show that transversal resolution influences the model, although the influence on stresses should still be investigated. *Ex vivo* imaging with a significantly better resolution may help us with understanding a plaque rupture mechanism and serve as verification for *in vivo* based models.

Keywords: Atherosclerosis · Carotid artery · Computational modelling · Magnetic resonance · Segmentation

1 Introduction

Atherosclerosis is a severe cardiovascular disease with high mortality. Cumulation of lipids leads to plaque creation which results in artery narrowing also called stenosis [1,2]. The degree of stenosis is still the only validated diagnostic criterion for risk assessment [3].

Computational modelling shows its potential to become an appropriate indicator of plaque vulnerability. Biomechanics helps us to capture its mechanical

J. M. R. S. Tavares and R. M. Natal Jorge (Eds.): VipIMAGE 2019, LNCVB 34, pp. 501–508, 2019.
https://doi.org/10.1007/978-3-030-32040-9_51

behaviour, morphological and geometrical factors which may influence its stress-strains response [4–7]. Two dimensional (2D) analyses are gradually replaced with 3D idealized and patient-specific (PS) models [8,9]. Idealized models allow us to localize critical parameters such as size of the lipid core (LC), fibrous cap thickness, etc. Both Cilla et al. [8] and then Yuan et al. [9] confirmed the influence of those components on the stress-strain state. However, PS models are considered to be more suitable for plaque vulnerability assessment [10]. However, their geometry is expressly dependent on the imaging method. There is a large number of *in vivo* methods used for plaque visualization such as intravascular ultrasound, computed tomography (preferably angiography (CT-A)), optical coherent tomography, or magnetic resonance imaging (MRI) [10]. MRI is currently taken as only non-invasive method suitable to quantify plaque components with good correlation with histology [11,12]. However, the distance between input images (transversal resolution) is still far from in-plane resolution which leads to relatively inaccurate approximation between slices in reconstructing model geometry. Nieuwstadt et al. [13] found the importance of an anisotropic resolution with a relatively better in-plane resolution to improve carotid plaque quantification. However, Nieuwstadt et al. [6] already reported that a decreased number of axial images may lead to overestimation of some plaque components included in computational model. Decrease in slice thickness may not improve plaque quantification, although it is an important parameter for 3D PS models. Model used in those papers [6,13] were based on histology. Histology is taken as a gold standard for plaque composition although the sample preparation leads to considerable specimen deformation; it disables reconstruction of the 3D geometry of artery with significant curvature [4,6]. Groen et al. [4] demonstrated a methodology of adjusting histological sections with *ex vivo* imaging for appropriate representation of a curved shape. Model geometry is crucial input for computational modelling and if we want to better understand the mechanism of plaque vulnerability we have to focus on this issue although it is still based on *ex vivo* imaging and thus not yet feasible in decision making of surgeons. This study aims at quantification of deviations between model geometries differing in transversal sampling and ways of volume creation using high resolution MRI (9.4 T), and also at evaluation of their appropriateness for computational modelling; subsequently they could become etalons for comparison with *in vivo* models.

2 Materials and Methods

2.1 Magnetic Resonance Imaging

Carotid plaque sample from patient who was scheduled for endarterectomy (man, 61 years, provided by St. Ann University Hospital with his informed consent) underwent post-operative imaging within a day after the intervention. The sample was measured in a 9.4 T NMR system (Bruker-BioSpec 94/30 USR, Ettlingen, Germany). The images were acquired in two series: the first one with the

RARE [14] technique (repetition time TR = 2500 ms, effective echo time TEeff = 10.77 ms), the second one with IR-RARE [15] (TR = 3000 ms, TEeff = 6.66 ms, inversion time TI = 950 ms). In each series, the slice thickness and the number of slices were varied: for thickness 0.25, 0.5, 0.75, 1 and 1.5 mm we used 50, 25, 16, 12, and 10 slices, respectively. Matrix size of 256×256, field of view of 20×20 mm^2, in-plane (2D) resolution of $0.078 \times 0.078\,mm^2$, and RARE-factor = 2 were used in all measurements. To achieve a sufficient image quality, we always set the interslice gaps equal to the slice thickness and obtained the missing information by a similar measurement with all slices shifted by the slice thickness.

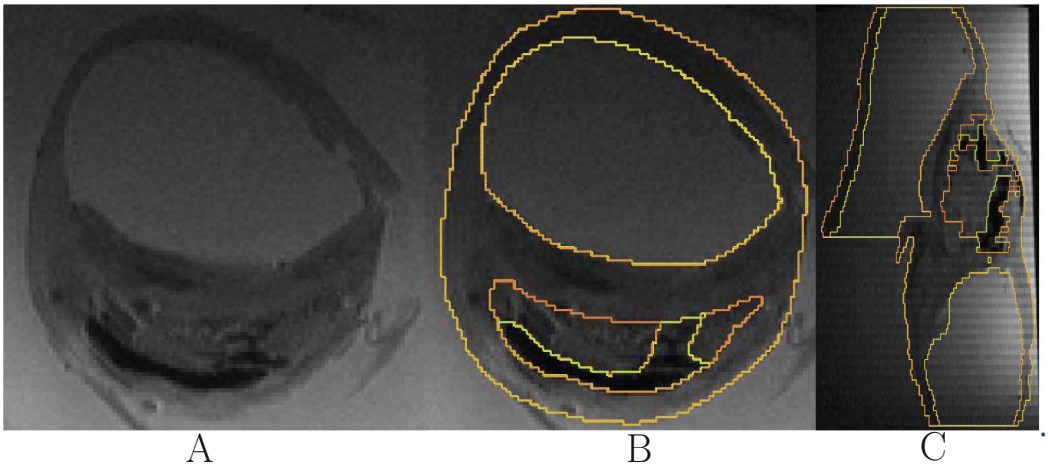

Fig. 1. *Ex vivo* MRI images of carotid plaque: (A) T1w image; (B) segmented transversal contour; (C) segmented sagittal contour

2.2 Image Segmentation and 3D Geometry Reconstruction

Each cross section was manually segmented using RETOMO software (BETA CAE Systems). Lipid core (LC), region with calcifications (CAL) and fibrous tissue (FT) were distinguished (Fig. 1). Images were segmented for each slice thickness to capture information modalities. A build-in algorithm was used to polygonize process often used to capture the object surface. High anisotropy of resolution leads to a stepped shape. The information from the image is stretched within specific slice thickness.

A smooth surface is usually presented within biological structures. As a large transversal resolution may lead to non-smooth structure, some approximation between slices is used such as NURBS [16]. In this study the Laplacian smoothing algorithm was used. Fixed parameters were used for each sample. Smooth model is also a more suitable basis for discretization.

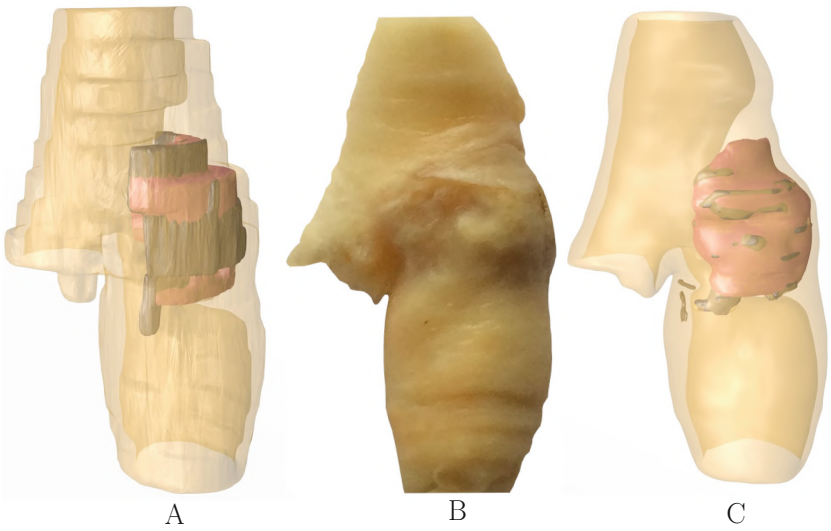

Fig. 2. 3D plaque model. Red: lipid core; grey: calcification region. (A) shows non-smoothed model based on 1.5 mm slice thickness; (B) shows the image of carotid plaque sample which was used for *ex vivo* imaging; (C) shows smoothed model based on 0.25 mm slice thickness.

2.3 Analysis

Smoothed and non-smoothed configurations were used in the following analyses. Surface deviations were defined as mean positive and mean negative differences between the reference model and the model in question. For this purpose, the smoothed model created from the 0.25 mm thick slices was chosen as reference. CAL were frequently localized as separated locations within the LC. LC and CAL were considered as connected components for surface deviation analysis. Volume of each component was also compared as another variance indicator. One way ANOVA and specifically Tukey comparison test were used to determine if there was a significant difference between the created models.

3 Results

The investigated greatly calcified atherosclerotic plaque was classified as type VII by scheme of the American Heart Association. Quantitative comparisons were performed with overall ten models, five raw models with visible stepped transitions and five after the Laplacian smoothing procedure. Figure 2 shows a view of the harvested plaque and its reference 0.25 mm smoothed model, as well as the non-smoothed model based on 1.5 mm slice thickness.

3.1 Surface Deviations

Surface deviations of the reference model compared with its non-smoothed configuration were found to be on the same order as the in-plane resolution for each plaque component. Figure 3 shows the comparison among the models.

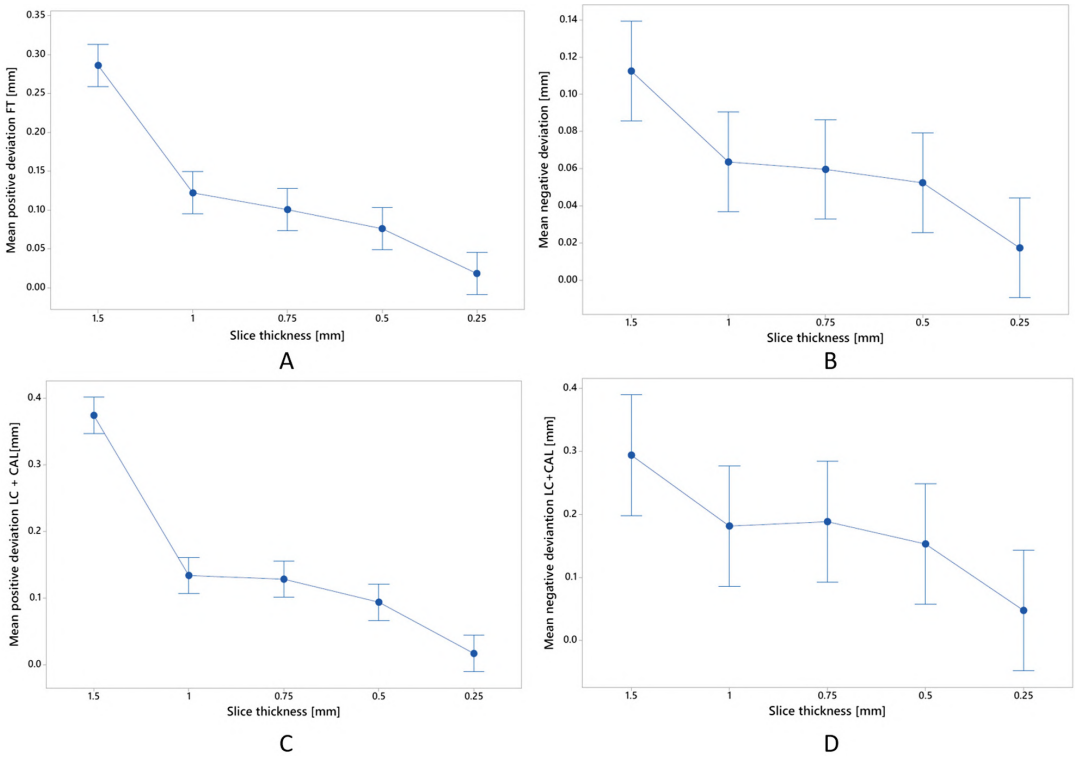

Fig. 3. Statistical analysis: (A–D) show surface deviations in dependence on slice thickness. A and B are for FT while C and D are for the joint region of CAL and LC. For all the models, both non-smoothed and smoothed models are compared with the reference model, and mean and variance are calculated from these two values. For slice thickness of 0.25 mm one of these values is zero (reference model itself).

Although differences between smoothed and non-smoothed models were insignificant (compared to vessel dimension), differences among slice thickness in both positive and negative surface deviations differed significantly ($p < 0.05$). From the graphs in Fig. 3 it is apparent that for slice thickness between 0.5 and 1 mm the differences are insignificant, while the models created on the basis of the largest (1.5 mm) and the lowest (0.25 mm) thickness differ significantly.

3.2 Volume Comparison

A volume analysis of each component confirmed significant differences among the models ($p < 0.05$). Generally, only 1 mm and 0.5 mm model may be considered as identical. Differences in volume are presented in Fig. 4.

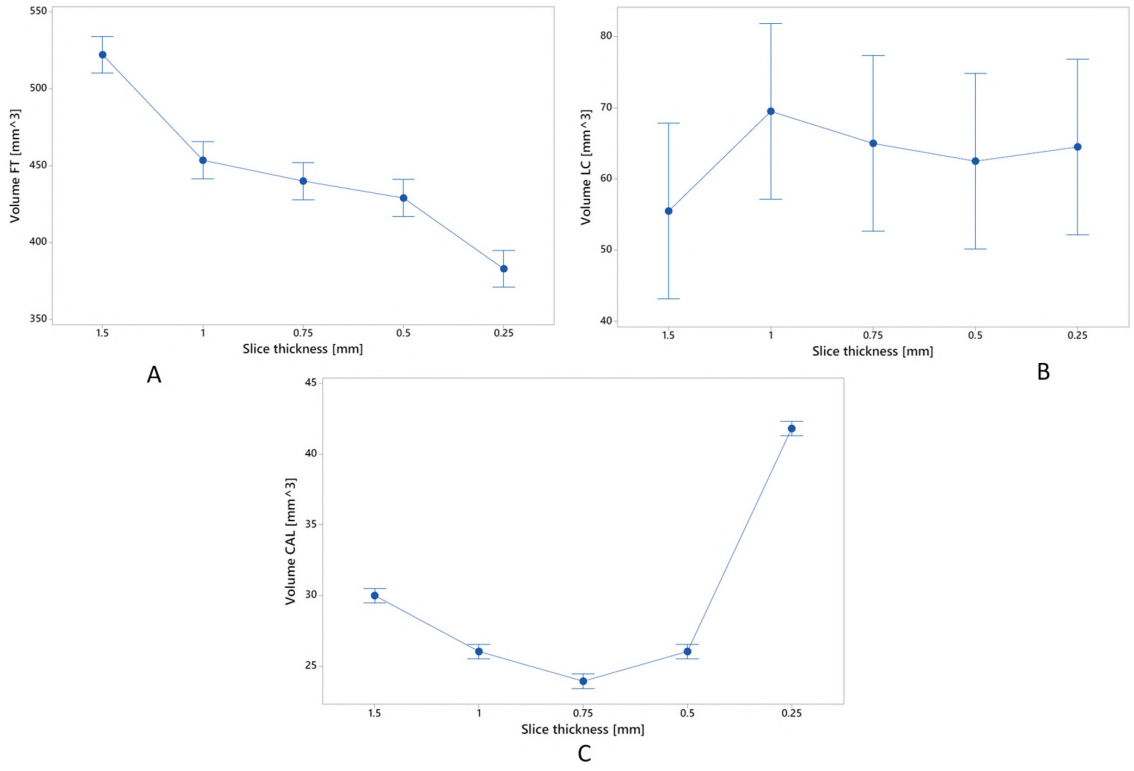

Fig. 4. Statistical analysis: (A–C) shows volume dependency on slice thickness for each component. (A) FT; (B) LC; (C) CAL.

4 Discussion

This study aimed to explore the influence of transversal resolution on the model geometry as a needed input for computational modelling in plaque vulnerability prediction. The results show that the smoothing process does not influence the model surface deviations and volume within the same slice thickness. Significant differences ($p < 0.05$) were found when comparing the models obtained with different slice thickness. However, for surface deviations these differences were on the order of 10^{-2} mm which is far below the model dimensions. Generally, the volume of FT was decreasing with decreasing slice thickness. This may be explained with the polygonization method used in this study which approximates the image content within the slice thickness linearly. LC and CAL volumes were nearly the same except for the 0.25 mm slice thickness. These results cannot be directly compared with the study of [6] since their analysis was focused on peak cap stress, although it was found that lower axial sampling has a profound influence on accuracy of the computed stresses. The sample used in this study contained a single LC. However, plaques may obtain smaller LC which may be visualized appropriately only by using lower slice thickness. Since differences between the corresponding non-smoothed and smoothed models were insignificant, it can be concluded that the used Laplacian smoothing algorithm could be used in creating the geometries for computational modelling. However, since significant differences were found among the models with different slice

thickness, its influence on stress-strain analysis is to be expected and a deeper analysis of this dependence should be performed with more samples.

This study points to necessity of choice of an appropriate input for creation of model geometry of atheroma and its further computational modelling. Post-operative extracted samples may serve as a basis for those models. The use of high resolution MRI in connection with histological slices enables us to reconstruct the model geometries more accurately than in case of using only histological slices. With further development of imaging devices and their improved resolution, such models could be created on the basis of *in vivo* imaging only in future.

Acknowledgements. This research was funded by Czech Science Foundation project No. 18-13663S and by the MEYS project (LM2015062 Czech-BioImaging).

References

1. Ross, R.: The pathogenesis of atherosclerosis: a perspective for the 1990s. Nature (1993). https://doi.org/10.1038/362801a0
2. Guyton, J.R., Klemp, K.F.: Development of the lipid-rich core in human atherosclerosis. Arterioscler. Thromb. Vasc. Biol. **16**, 4–11 (1996)
3. Lusis, A.J.: Atherosclerosis. Nature (2010). https://doi.org/10.1038/35025203
4. Groen, H.C., et al.: Three-dimensional registration of histology of human atherosclerotic carotid plaques to in-vivo imaging. J. Biomech. **43**(11), 2087–2092 (2010). https://doi.org/10.1016/j.jbiomech.2010.04.005
5. Maldonado, N., et al.: A mechanistic analysis of the role of microcalcifications in atherosclerotic plaque stability: potential implications for plaque rupture. AJP: Heart Circ. Physiol. **303**(5), 619–628 (2012). https://doi.org/10.1152/ajpheart.00036.2012
6. Nieuwstadt, H.A., et al.: The influence of axial image resolution on atherosclerotic plaque stress computations. J. Biomech. (2012). https://doi.org/10.1016/j.jbiomech.2012.11.042
7. Huang, Y., et al.: The influence of computational strategy on prediction of mechanical stress in carotid atherosclerotic plaques: comparison of 2D structure-only, 3D structure-only, one-way and fully coupled fluid-structure interaction analyses. J. Biomech. (2014). https://doi.org/10.1016/j.jbiomech.2014.01.030
8. Cilla, M., Peña, E., Martínez, M.A.: 3D computational parametric analysis of eccentric atheroma plaque: influence of axial and circumferential residual stresses. Biomech. Model. Mechanobiol. (2012). https://doi.org/10.1007/s10237-011-0369-0
9. Yuan, J., et al.: Influence of material property variability on the mechanical behaviour of carotid atherosclerotic plaques: a 3D fluid-structure interaction analysis. Int. J. Numer. Methods Biomed. Eng. (2015). https://doi.org/10.1002/cnm.2722
10. Holzapfel, G.A., et al.: Computational approaches for analyzing the mechanics of atherosclerotic plaques: a review. J. Biomech. **47**(4), 859–869 (2014). https://doi.org/10.1016/j.jbiomech.2014.01.011
11. Hatsukami, T.S., et al.: Visualization of fibrous cap thickness and rupture in human atherosclerotic carotid plaque in vivo with high-resolution magnetic resonance imaging. Circulation **102**(9), 959–964 (2000). https://doi.org/10.1161/01.CIR.102.9.959

12. Saam, T., et al.: Quantitative evaluation of carotid plaque composition by in vivo MRI. Arterioscler. Thromb. Vasc. Biol. **25**(1), 234–239 (2005). https://doi.org/10.1161/01.ATV.0000149867.61851.31
13. Nieuwstadt, H.A., et al.: A computer-simulation study on the effects of MRI voxel dimensions on carotid plaque lipid-core and fibrous cap segmentation and stress modelling. PLoS ONE **10**(4), e0123031 (2015). https://doi.org/10.1371/journal.pone.0123031
14. Hennig, J., Nauerth, A., Friedburg, H.: RARE imaging: a fast imaging method for clinical MR. Magn. Reson. Med. **3**, 823–833 (1986)
15. Bydder, G.M., Young, I.R.: MR imaging: clinical use of the inversion recovery sequence (1985)
16. Holzapfel, G.A.: A layer-specific three-dimensional model for the simulation of balloon angioplasty using magnetic resonance imaging and mechanical testing. Ann. Biomed. Eng. (2002). https://doi.org/10.1114/1.1492812

B. Appendix

Consideration of stiffness of wall layers is decisive for patient-specific analysis of carotid artery with atheroma

Original research article.
IF 3.24 (2020)

O. Lisický et al. (Sept. 2020). "Consideration of stiffness of wall layers is decisive for patient-specific analysis of carotid artery with atheroma." In: *PLOS ONE* 15.9. Ed. by F.-B. Tian, e0239447. ISSN: 1932-6203. DOI: 10.1371/journal.pone.0239447

PLOS ONE

RESEARCH ARTICLE

Consideration of stiffness of wall layers is decisive for patient-specific analysis of carotid artery with atheroma

Ondřej Lisický[1☯]*, Aneta Malá[2], Zdeněk Bednařík[3], Tomáš Novotný[4], Jiří Burša[1☯]

1 Institute of Solid Mechanics, Mechatronics and Biomechanics, Brno University of Technology, Brno, Czech Republic, **2** Institute of Scientific Instruments, The Czech Academy of Science, Brno, Czech Republic, **3** 1st Department of Pathology, St. Anne's University Hospital Brno and Faculty of Medicine, Masaryk University, Brno, Czech Republic, **4** 2nd Department of Surgery, St. Anne's University Hospital Brno and Faculty of Medicine, Masaryk University, Brno, Czech Republic

☯ These authors contributed equally to this work.
* 161238@vutbr.cz

Citation: Lisický O, Malá A, Bednařík Z, Novotný T, Burša J (2020) Consideration of stiffness of wall layers is decisive for patient-specific analysis of carotid artery with atheroma. PLoS ONE 15(9): e0239447. https://doi.org/10.1371/journal.pone.0239447

Editor: Fang-Bao Tian, University of New South Wales, AUSTRALIA

Received: February 17, 2020

Accepted: September 7, 2020

Published: September 29, 2020

Peer Review History: PLOS recognizes the benefits of transparency in the peer review process; therefore, we enable the publication of all of the content of peer review and author responses alongside final, published articles. The editorial history of this article is available here: https://doi.org/10.1371/journal.pone.0239447

Data Availability Statement: All supporting data (models, statisticas) are available on DOI: https://doi.org/10.6084/m9.figshare.12937196.

Abstract

The paper deals with the impact of chosen geometric and material factors on maximal stresses in carotid atherosclerotic plaque calculated using patient-specific finite element models. These stresses are believed to be decisive for the plaque vulnerability but all applied models suffer from inaccuracy of input data, especially when obtained *in vivo* only. One hundred computational models based on *ex vivo* MRI are used to investigate the impact of wall thickness, MRI slice thickness, lipid core and fibrous tissue stiffness, and media anisotropy on the calculated peak plaque and peak cap stresses. The investigated factors are taken as continuous in the range based on published experimental results, only the impact of anisotropy is evaluated by comparison with a corresponding isotropic model. Design of Experiment concept is applied to assess the statistical significance of these investigated factors representing uncertainties in the input data of the model. The results show that consideration of realistic properties of arterial wall in the model is decisive for the stress evaluation; assignment of properties of fibrous tissue even to media and adventitia layers as done in some studies may induce up to eightfold overestimation of peak stress. The impact of MRI slice thickness may play a key role when local thin fibrous cap is present. Anisotropy of media layer is insignificant, and the stiffness of fibrous tissue and lipid core may become significant in some combinations.

Introduction

Atherosclerosis is a cardiovascular disease causing local intimal thickening of artery wall and plaque formation. Vulnerable atherosclerotic plaques, characterized by lipid accumulation under a thin fibrous cap (FC), have attracted attention of researchers for more than two decades [1, 2]. A rupture of the plaque may cause blood clot formation and leads to the stroke in case of carotid arteries [3]. The rupture occurs when stresses induced by mechanical loading

Funding: This work was supported by Czech Science Foundation (https://gacr.cz/en/) project No. 18-13663S. The MRI service was funded by project LM2015062 "National Infrastructure for Biological and Medical Imaging (Czech-BioImaging)" of the Ministry of Education, Youth and Sports of the Czech Republic (http://www.msmt.cz/?lang=2).

Competing interests: No authors have competing interests.

Abbreviations: 2D, two-dimensional; 3D, three-dimensional; CCD, central composite design; CT, computed tomography; DoE, design of experiment; FC, fibrous cap; FE, finite element; FSI, fluid structure interaction; FT, fibrous tissue; LC, lipid core; MB, media behaviour; MRI, magnetic resonance imaging; PCS, peak cap stress; PPS, peak plaque stress; PS, patient specific; SEDF, strain-energy density function; ST, slice thickness; WT, wall thickness.

exceed the tissue strength. Thus, the peak cap stress (PCS) within the FC is believed to be the most valuable indicator of the plaque vulnerability [4–7].

Recent progress in imaging techniques and in computational modelling enables us to use patient-specific (PS) geometries for assessment of stresses. Finite element (FE) analysis [6, 8] or fluid-structure interaction (FSI) [9–12] are mostly used to analyse the impact of key factors like geometrical parameters or mechanical characteristics of the plaque and arterial wall on the stresses.

Like any diseased arterial wall, the thickened intima layer called fibrous tissue (FT) is very heterogeneous. Hence its mechanical properties vary locally within a plaque as well as among different plaques [7, 13, 14]. Therefore, analyses of plaque composition and experimental investigation of mechanical properties of its components are needed. In particular, little information is known about mechanical behaviour of lipid core (LC). Frequently its very soft behaviour is assumed in computational modelling [4, 6, 15], except for a study applying the other extreme of very high stiffness [16]. In contrast, mechanical behaviour of the vessel wall layers appears to be well supported by experiments. Uniaxial and biaxial mechanical tests of separated wall layers [8, 17, 18] enable us to describe its anisotropic behaviour even accounting for the wall structure.

Simplified 2D models used earlier in FE analyses were found to overestimate the stresses [6, 10, 19], therefore the research should focus on 3D models [20]. However, the level of these models varies. Simpler models with idealized geometry use to consider either homogeneous or layered arterial wall [4, 21], although the omission of the wall is also presented frequently [7, 10, 12]. Nowadays PS models are preferred but they suffer from lack of geometrical data and large dispersion of mechanical properties. While 2D histology sections or *ex vivo* MRI scans of autopsy samples enable us to reconstruct completely both the lumen and the vessel wall [4, 6, 8], the MRI images taken either *in vivo* [9, 12] or with samples from endarterectomy (where the plaque is resected without media and adventitia) do not enable us to capture wall boundaries. Consequently, the 3D models based on *in vivo* imaging give often contradictory results depending, for instance, on consideration of real mechanical properties of outer wall layers or FT stiffness [4, 7] or quality of the geometrical data [6, 22].

In this study, 3D PS FE models of carotid atherosclerotic artery for two patients accounting for both media and adventitia layers are used to investigate the significance of several factors in the calculation of extreme stresses in the atheroma; this should indicate their significance in further vulnerability diagnosis and enable us to propose a reasonable level of computational models. In total, five different factors related to mechanical properties or geometry of the atheroma are investigated; application of the design of experiment (DoE) concept, especially central composite design (CCD), resulted in one hundred solved computational models.

Methods

Acquiring data on geometry and structure

Ethics statement. This study was approved by the medical ethical committee of St. Anne's University Hospital in Brno (reference number 12V/2017). Written informed consent was obtained from the subject.

Magnetic resonance imaging (MRI). Atherosclerotic plaques were harvested (sample 1: man, 61 years, sample 2: man 71 years) during endarterectomy in St. Anne's University Hospital in Brno which met the following requirements: (1) the presence of at least one large LC with calcifications within, (2) undamaged and entire external surface of the FT and (3) an overall length which could be covered with a sufficient number of images using standard *in vivo* axial resolution. The samples were classified as an atherosclerotic lesion of Type VII [23].

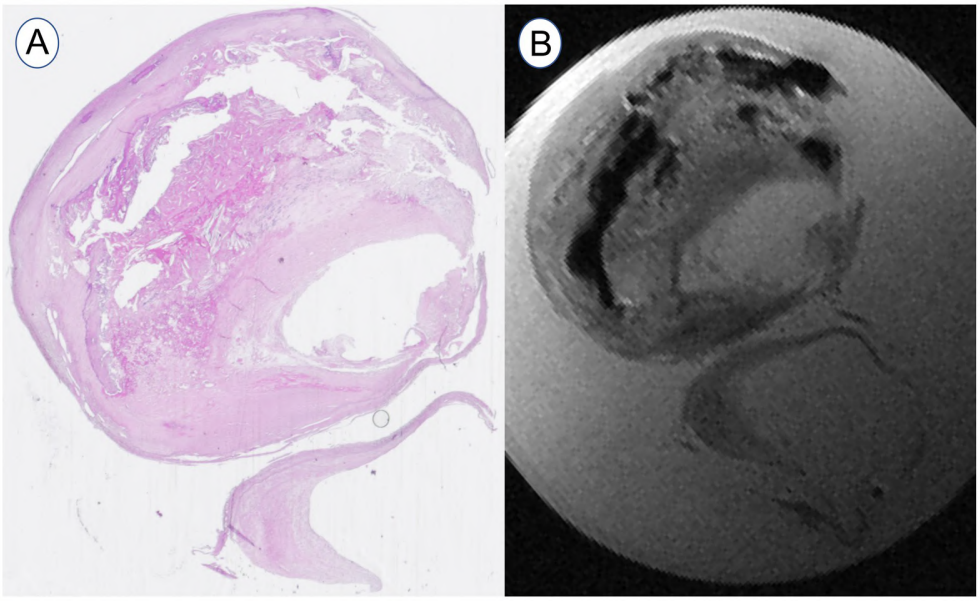

Fig 1. Example of carotid plaque bifurcation. From the histology cross-section (A) and the high-resolution MRI 9.4 T with ST = 0.25 mm (B).

https://doi.org/10.1371/journal.pone.0239447.g001

Post-operative imaging of the samples was performed with a 9.4 T MRI system (Bruker BioSpec 94/30 USR, Ettlingen, Germany). The images were acquired in two series: the first one with the RARE technique (repetition time TR = 2500 ms, effective echo time TEeff = 10.77 ms), the second one with IR-RARE (TR = 3000 ms, TEeff = 6.66 ms, inversion time TI = 950 ms). The slice thickness (ST) was set to 1.5 mm, 1 mm and 0.25 mm for the purpose of comparison. An in-plane resolution of 78 μm was constant for all measurements with the matrix size of 256x256 (see Fig 1).

Histology. After MRI the samples were fixed in 10% neutral formalin for 24 hours and then subjected to decalcification, dehydrated and embedded in paraffin. Subsequently, 3–5 μm thick tissue slices were cut off and stained with hematoxylin-eosin. Then the slices were scanned and compared with the individual MRI images to distinguish the tissue components properly (see Fig 1). However, they could not be directly used for model segmentation due to their unavoidable deformation after the histological processing [22].

3D PS model of carotid artery with atheroma

Semi-automatic segmentation of the recorded MR images was applied using RETOMO (BETA CAE Systems) to distinguish the plaque components. We focused on segmentation of the FT and LC (including the regions of calcification). As biological structures are characterized by smooth surfaces [8], the geometry was smoothed [24] with the same parameters for all the models. Since the individual vessel wall layers cannot be distinguished in the *in vivo* MRI scans and the sample harvested at endarterectomy cannot include the media and adventitia layers of the wall, the outer surface of the obtained geometry was used to create the volume of the missing layers. For this purpose, the outer surface of the specimen was offset equidistantly by 0.5 mm [11, 21] to create the outer surface of the artery wall. Although it is known the media may be degraded and non-uniformly thick under the plaque, the assumption of constant wall thickness (WT) was adopted here as an appropriate simplification and the thickness

was included into DoE as one of the investigated parameters. The reconstructed model is depicted in Fig 2.

Material models

Media was modelled as a fibre-reinforced anisotropic layer, composed of a non-collagenous matrix and two families of collagen fibres. Based on mean material response [25], its anisotropic behaviour was characterized by the following strain-energy density function (SEDF) according to [26]:

$$\Psi = \Psi_{iso} + \Psi_{aniso} = \frac{\mu}{2} + \frac{k_1}{2k_2}\left(e^{k_2(1-\rho)(I_1-3)^2+\rho(I_4-1)^2} - 1\right) \quad (1)$$

where $\mu>0$ is a stress-like parameter describing the isotropic response of the tissue, $k_1>0$ is a stress-like parameter related to the collagen fibre stiffness, the dimensionless parameter $k_2>0$ refers to the level of fibre strain stiffening,$I_1 = \lambda_r^2 + \lambda_\theta^2 + \lambda_z^2$ and $I_4 = \lambda_\theta^2\cos^2\varphi + \lambda_z^2\sin^2\varphi$ are invariants of the right Cauchy-Green deformation tensor **C** (I_4 related to stretches of two fibre families), and $\rho<0;1>$ is a concentration parameter representing a "degree of anisotropy". In the applied model, + or -φ denotes the angle between the circumferential direction and direction of each fibre family located symmetrically in the tangential plane of the tube. As the applied FE software Ansys does not offer this material option, the model was implemented via a user material subroutine.

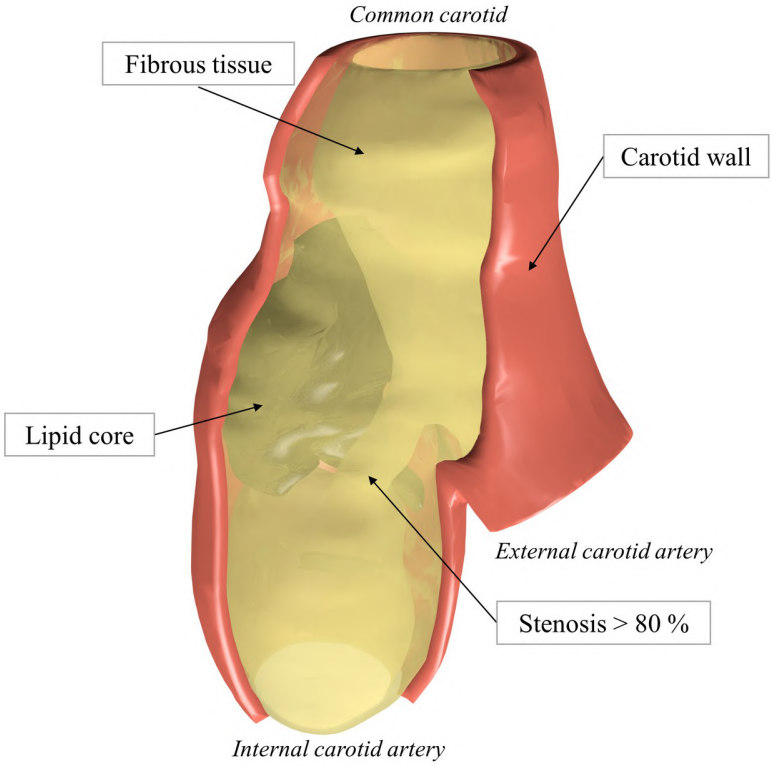

Fig 2. Illustration of the 3D PS model of the atherosclerotic carotid plaque (sample 1) obtained from endarterectomy. Carotid wall (red) shares the surface with FT.

https://doi.org/10.1371/journal.pone.0239447.g002

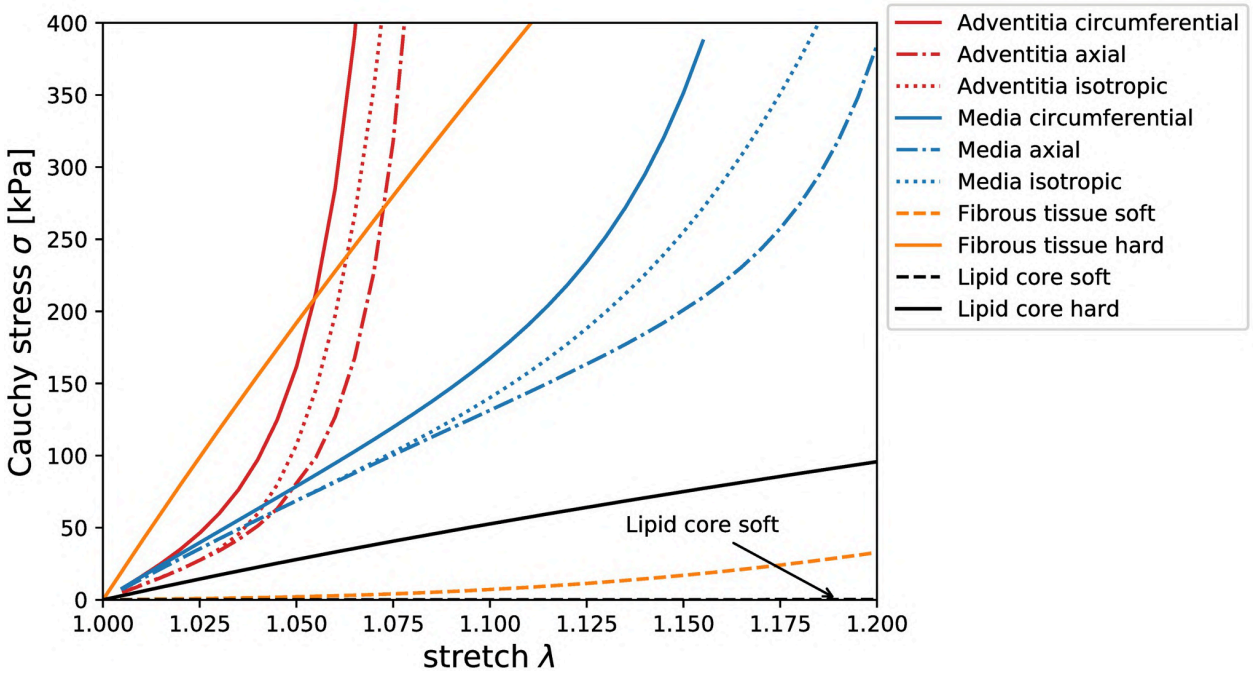

Fig 3. Stress-stretch equi-biaxial responses of the chosen constitutive models. The dotted lines show the isotropic fit of the circumferential (solid) and axial (dash dotted) anisotropic responses. The soft (dashed) and the hard (solid) isotropic responses for the FT and LC are also presented for comparison.

https://doi.org/10.1371/journal.pone.0239447.g003

The other wall layers and plaque components were modelled as incompressible, hyperelastic and isotropic since their anisotropy is low [17] compared to the inter-patient variability; this simplification is generally accepted [27]. To fit the biaxial response of the adventitia (and also of the media when modelled as isotropic for comparison), 3rd order Yeoh type SEDF [28] was used in the following form:

$$\Psi = \sum_{i=0}^{3} c_{i0}(I_1 - 3)^i \tag{2}$$

where c_{i0} are material parameters. Material responses of both layers were taken from experimental biaxial testing of each carotid component [17]. Material parameters for the wall layers were identified with considering residual stresses and stretches observed in the load-free geometry [25]. Uniaxial test data of FT [7, 13, 14] were fitted with the 2nd order Yeoh SEDF while the LC was modelled with Neo-Hookean (i.e. 1st order Yeoh) constitutive model. Material responses can be seen in Fig 3 with the used material parameters presented in Table 1.

FE model setup and boundary conditions

FE analysis was performed in FE software ANSYS 19.2. (Ansys Inc., PA, USA). The vessel wall was meshed with four/eight elements across the WT using linear 8 node hexahedral elements (SOLID185) in ICEM 19.2. (Ansys Inc. PA, USA) see Fig 5. A linear tetrahedral element (SOLID285) mesh performed in ANSA (Beta CAE) was used for the FT and LC. A bonded contact was used to join the FT with the vessel wall, while the other components were connected by shared nodes. A constant pressure value of 13 kPa (mean arterial pressure) was applied on the luminal surface of the geometry. Free ends of the vessel wall were fully

Table 1. Material parameters.

Tissue	Type	Material constants [a]				
Media	A	$\mu = 122.3$	$k_1 = 24.7$	$k_2 = 16.5$ [-]	$\varphi = 6.9$ [°]	$\rho = 0.8$ [-]
	I	$c_{10} = 122.3$	$c_{20} = 0$	$c_{30} = 337.7$		
Adventitia	I	$c_{10} = 88.7$	$c_{20} = 0$	$c_{30} = 45301.4$		
Lipid core	I soft	$c_{10} = 0.1$				
	I hard	$c_{10} = 50$				
Fibrous tissue	I soft	$c_{10} = 2.7$	$c_{20} = 20$			
	I hard	$c_{10} = 342.1$	$c_{20} = 20$			

[a]The above values are in kPa if not otherwise specified. Symbols I and A denote the isotropic and anisotropic behaviour, respectively.

https://doi.org/10.1371/journal.pone.0239447.t001

constrained. A mesh convergence analysis was performed to obtain a suitable element size for all models. A typical mesh density resulted in 24k elements for the vessel wall and 95 k for FT with LC.

Material orientation. Consideration of media layer anisotropy drew the problem of the orientation of principal material axes in each point of the model. Each element coordinate system needs to be rotated to the preferred orientation of the collagen fibres. In this study, we take advantage of the applied locally structured hexahedral mesh which enables us to define a centroid of each section and subsequently also the central line (see Fig 4). Two points of this

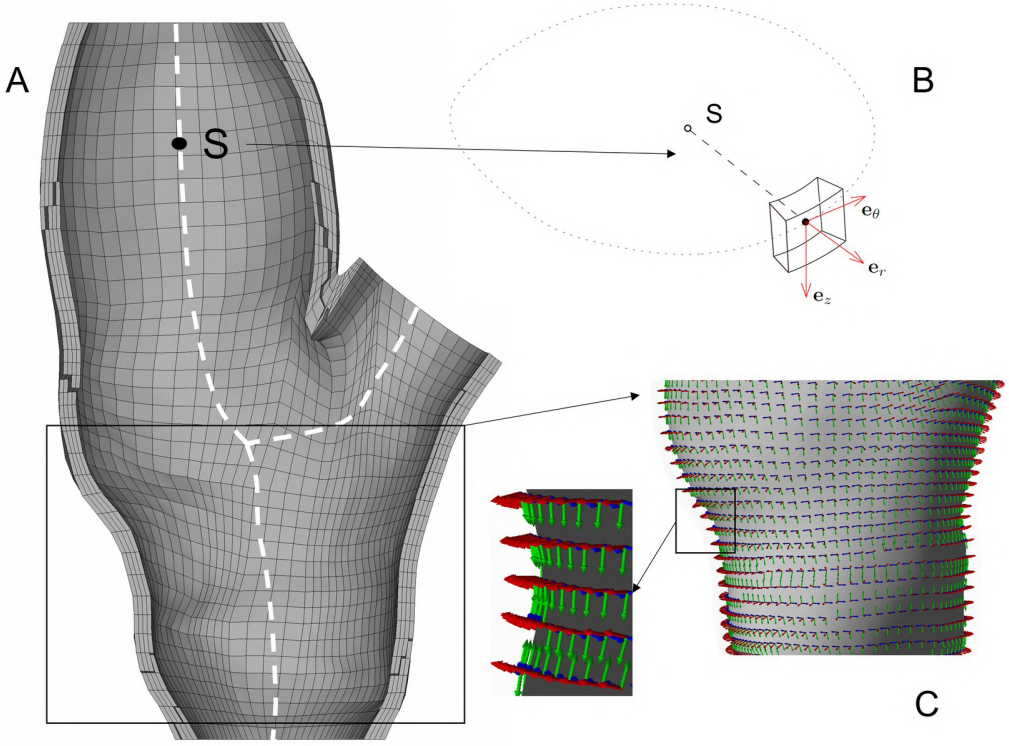

Fig 4. Computational model with principal material directions. (A) The discretized model of the vessel wall of sample 1 with hexahedral elements; the central line (white dashed) serves for definition of the axial base e_z. (B) Detailed illustration of the coordinate system of an individual element. (C) Detail of element-specific material directions within the vessel wall model; the blue, green and red arrows indicate the circumferential, axial and radial directions, respectively.

https://doi.org/10.1371/journal.pone.0239447.g004

line close to the section were used to define the local axial basis $\mathbf{e}_z$. A vector normal to the inner surface of the element located in its centroid was used as the local radial basis $\mathbf{e}_r$. After that, a cross product of those two bases resulted in the circumferential basis $\mathbf{e}_\theta$. The resulting distribution of bases determinates the principal material directions when the anisotropic constitutive model is applied.

The investigated factors and their statistical analysis

In biomechanics, all the input data for computational modelling suffer from large uncertainties or inaccuracies. This variance of input data may influence the character of the deformation and consequently, the stresses evaluated as a potential indicator of plaque vulnerability. Similarly to another biomechanical study [29], DoE with 95% confidence level was applied for this statistical analysis; specifically the CCD was chosen, to analyse (using Minitab 15 statistical software) the possible non-linear dependence of PCS on some of the five selected factors. This resulted in overall 100 computational models for the two patients, differing in their material and geometrical factors; these models afforded the input data for statistical analysis.

In the DoE methodology, a 2-factorial design was performed and thereafter augmented with a set of axial points resulting in the CCD, specifically the face-centred design. Here, the middle level of each factor is used (centre of a factorial face) enabling to estimate a possible curvature of the response. The model suitability was checked for all the fitted responses via normal distribution of residuals and a sufficient coefficient of determination ($R^2>0.8$). The first (maximal) principal stresses were adopted as stress response indicators, especially PPS and PCS [4, 6]; for all the 3D models analysed, they were evaluated in cross-sections with a 0.2 mm span. Lastly, the analysis of variance was performed within the DoE to find the significance of the individual factors and of their combinations. Except for media behaviour (MB), all the factors were set as continuous. A specific choice of factors can be found below with their range of values summarized in Table 2.

Lipid core stiffness. The LC plays a key role in the plaque vulnerability through its size or location in the plaque where the resulting distance from the lumen to the LC is characterized as FC thickness [7, 21]. However, the LC composition almost disables its mechanical testing. Thus, the stiffness of the LC was chosen as a variable factor ranging from 0.1 to 50 kPa. The lower value (related to lipids) is mostly used in computational models while the upper value was chosen to reflect the hypothesis that micro-calcifications occurring in the extracellular matrix of the LC may cause its stiffening by orders.

Fibrous tissue stiffness. Experimental data of carotid plaques [7, 13, 14] were analysed to find samples with extreme stiffness which were then fitted with the second-order Yeoh SEDF (see Fig 3). Nearly linear stress-strain response, i.e. a very low strain stiffening, was found for both the most and the least stiff plaques, thus the number of variables could be reduced. The second material parameter c_{20} (related to strain stiffening) was fixed and only the first constant c_{10} (initial stiffness) was fitted giving a sufficient quality of the fit ($R^2>0.8$).

Table 2. DoE factors. Selected factors for DoE with their chosen upper and lower limits.

Factor	Minimum	Maximum
Wall thickness [mm]	0	0.5
Slice thickness [mm]	0.25	1.5
Lipid core μ [kPa]	0.1	50
Fibrous tissue c_{10} [kPa]	2.7	342.1
Media behaviour	isotropic	anisotropic

https://doi.org/10.1371/journal.pone.0239447.t002

Media behaviour. The biaxial response of carotid media [25] was used to fit both anisotropic and isotropic constitutive models (see Fig 3). The anisotropic description was applied with the locally varying orientation of the element coordinate system.

Slice thickness. *In vivo* and *ex vivo* imaging methods differ substantially in their resolution (both axial and in-plane). Histological slices are often used for reconstruction of 2D and 3D PS plaque geometries [4, 6] since they provide a suitable in-plane resolution. However, it is very laborious to achieve a sufficient axial resolution and the deformation caused by slice preparation [20, 22] may result in distortion of the shape. Therefore, *ex vivo* MRI was used for the 3D reconstruction in this study. As only *in vivo* imaging has potential in clinical assessment of plaque vulnerability, the impact of different resolutions of the MR images was chosen as another investigated factor, since the lower axial resolution of the *in vivo* MRI may cause loss of geometrical information significant for the computational analysis [6]. This factor was set as continuous with values ranging from 0.25 (resolution of the applied *ex vivo* MRI) to 1.5 mm (a typical resolution of *in vivo* MRI).

Vessel wall thickness. The vessel WT was set from 0 to 0.5 mm [11, 21] where the lower limit represents models with identical mechanical properties for the wall and the FT [7, 12, 19], neglecting thus the impact of different properties of the outer arterial layers. This means the volume of the wall was always included in the model but with different material properties. In all the models the thickness of the wall was halved between media and adventitia. Fig 5 shows the used configurations where the vessel wall is represented with 4 elements per thickness even when the half thickness t = 0.25 mm (axial point) is considered (see Fig 5).

Since the CCD requires only continuous variables, the discrete MA factor was fixed and the DoE was performed twice with four continuous factors. The DoE results were compared using a paired t-test to investigate the significance of the MB factor.

Results

The factors significant for the statistical model are summarized in the Table 3.

An example of the numerical results of the PS model of the atherosclerotic carotid artery is presented in the form of displacements and first principal stresses for sample 1 in Fig 6. Cross-

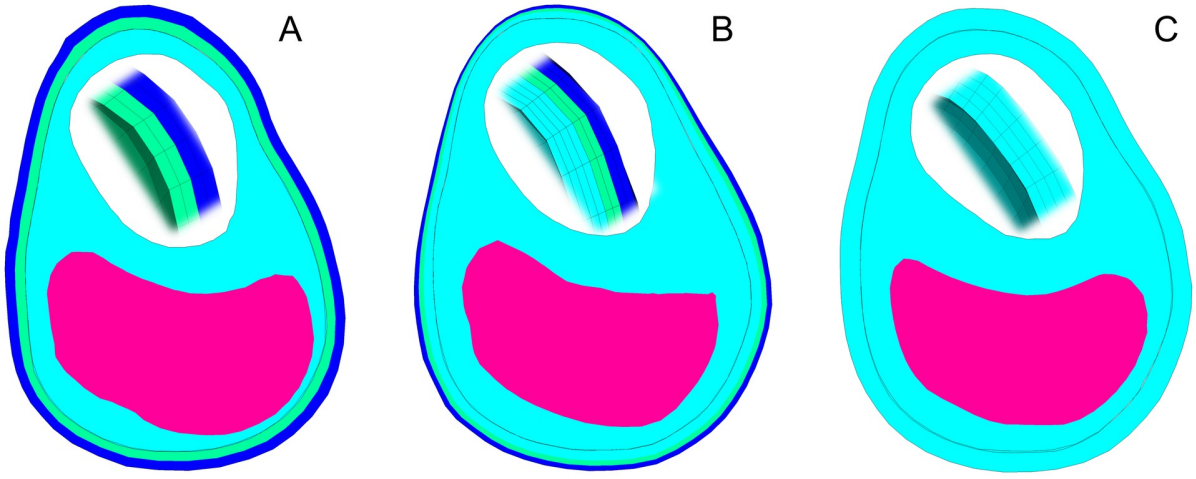

Fig 5. Cross-sections representing the model configurations. Different WT of 0.5 mm (A), 0.25 mm (B) and 0 mm (C). The adventitia (dark blue) is always represented with 2 elements, as well as the media (light green). FT (light blue) increases its volume with decreasing WT. LC representation (pink) is immutable in the same axial position and with the same ST. Details of the wall are presented in the white lumen area.

https://doi.org/10.1371/journal.pone.0239447.g005

Table 3. Analysis of variance for the PPS and PCS.

Sample 1	Peak Plaque Stress							
		Linear		Square	2-Way interaction		Model R^2	
	Factor	**WT**	FT	**WT*WT**	**WT*FT**		0.894	
	p-value	**<0.001**	0.48	**0.08**	**<0.001**			
	Peak Cap Stress							
		Linear			Square	2-Way interaction		Model R^2
	Factor	**WT**	**LC**	FT	LC*LC	**WT*LC**	**WT*FT**	**LC*FT**	0.845
	p-value	**<0.001**	**0.01**	0.117	0.124	**0.072**	**<0.001**	**0.038**	
Sample 2	Peak Plaque Stress							
		Linear				2-Way interaction		Model R^2
	Factor	ST	WT	LC	FT	WT*FT	LC*FT	0.874
	p-value	**0.025**	**0.001**	0.113	0.115	**<0.001**	0.146	
	Peak Cap Stress							
		Linear				Square	2-Way interaction		Model R^2
	Factor	**ST**	**WT**	**LC**	**FT**	**LC*LC**	WT*LC	**WT*FT**	0.823
	p-value	**0.026**	**<0.001**	**<0.001**	**0.015**	**0.018**	0.122	**<0.001**	

The table shows the statistical significance of factors included in the statistical model represented by their p-values and R^2. The statistically significant or nearly significant factors and their combinations are highlighted in bold.

https://doi.org/10.1371/journal.pone.0239447.t003

sections in the selected locations show typical stress distributions focused on the PPS and PCS. Results near the boundary conditions and the bifurcation were not considered since they may cause non-realistic artefacts (stress concentrations due to boundary conditions). The discrete media-related factor MB was found to be insignificant (probability value p = 0.99) with stresses showing a mean difference of 1 kPa between the models with isotropic and anisotropic media for both patients. Therefore, this factor was not included in the evaluations below.

Peak plaque stress

The statistical model fitted to the PPS response showed the same significance of the WT for both samples. Unlike in sample 1, ST was found significant in sample 2. Also, the interaction between FT stiffness and WT (FT*WT) was found significant in both cases. The squared effect, evaluated by the additional face-centred axial points, was significant for sample 1 in case of WT factor. The maximum was mostly localized in the narrow part of the FT component between the luminal surface and the inner surface of the vessel wall, except for the cases with lower stress concentration where the maximum was located within the FC (see detail D in Fig 6). The cube plot in Fig 7 shows the PPS responses at low and high levels of each factor. In the model with soft FT, the PPS increased on average up to five times (from 29 to 160 kPa for sample 1 and 44 to 230 kPa for sample 2) when the wall was not included. In contrast, an opposite tendency occurred when the hard FT was considered; the PPS decreased by some 30% when the wall was not included.

The highest stress concentrations (168 kPa and 313 kPa) were found in the models without the vessel wall and with the soft atheroma components, while the lowest stresses (22 kPa and 26 kPa) were found in the models with the artery wall included and with the soft FT and hard LC. The results show that similarly to the MB factor, neither LC stiffness nor FT stiffness itself has a significant impact on the PPS minimum/maximum as long as interactions are not considered. For all the responses with the artery wall included, however, Fig 7 shows 3 up to 5

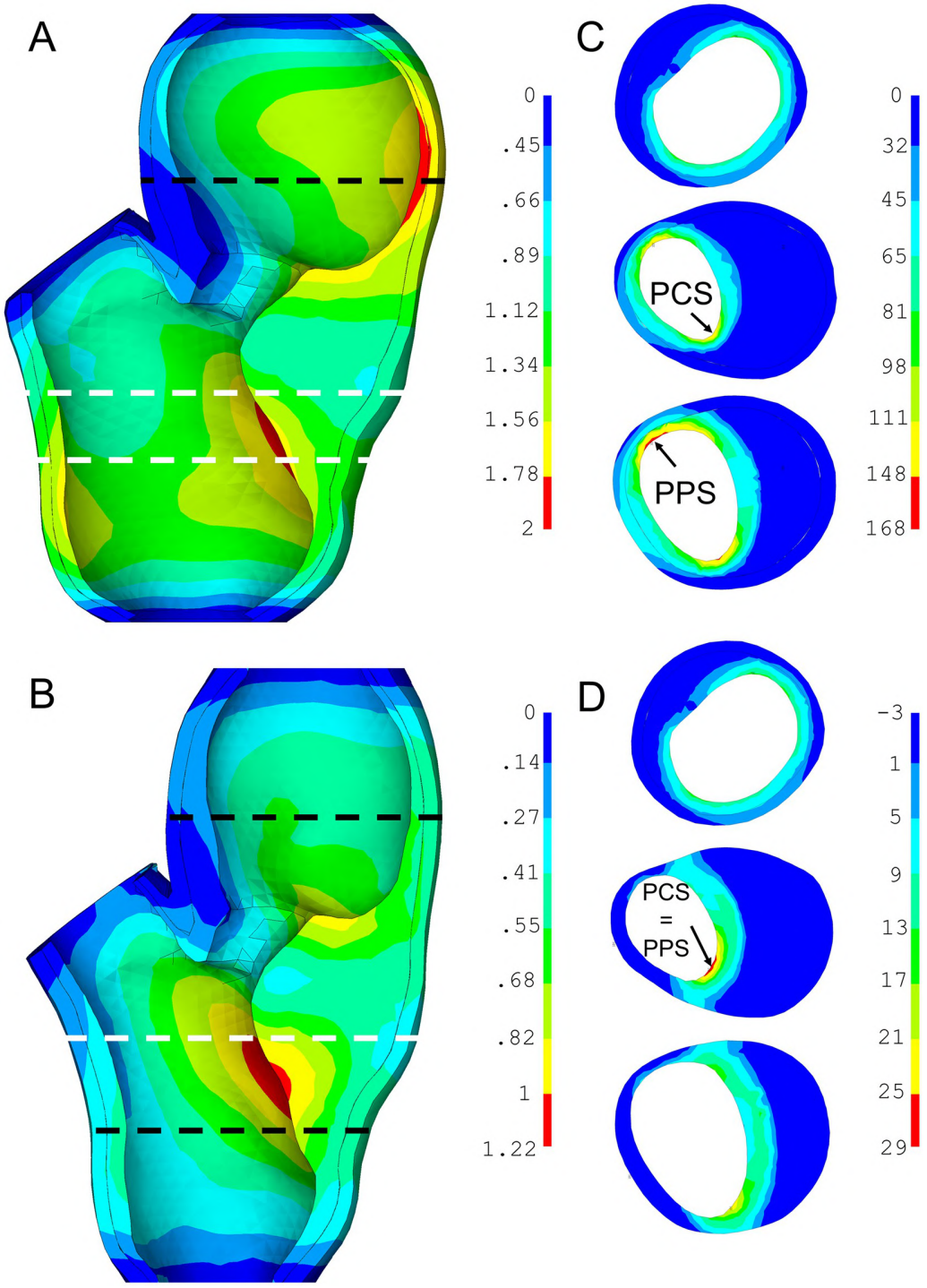

Fig 6. Contour maps of two sample 1 models. Both LC and FT being soft, differing in WT only: WT = 0 mm (A), (C) and WT = 0.5 mm (B), (D). Displacements in (A) and (B) show their 64% overestimation in model (A) with media and adventitia properties replaced by those of the FT. The maps of first principal stresses (C) and (D) show their distribution in the chosen locations (dashed lines) with the arrows indicating maximal PPS and PCS in the respective sections (white dashed lines). In the model with media and adventitia replaced by the FT, the maximal stresses are almost six times higher. Note that (D) is shown without the media and adventitia layers due to very different levels of stresses between the plaque and these layers.

https://doi.org/10.1371/journal.pone.0239447.g006

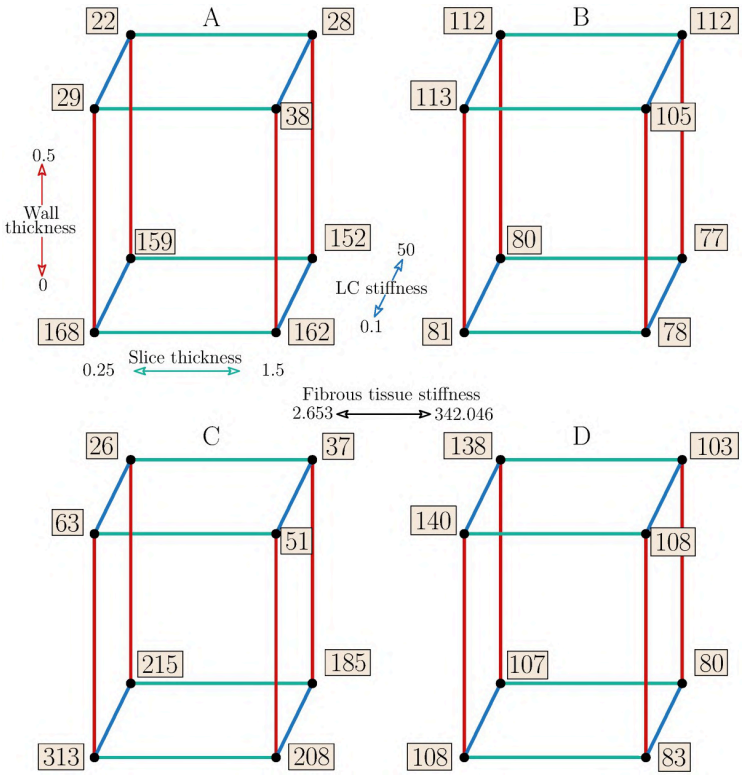

Fig 7. Cube plots of PPS values [kPa]. Patient 1 (A-B) and patient 2 (C-D). Colours represent a specific factor; red—WT, green—ST, blue—LC stiffness. Cubes A and C represent low stiffness FT while B and D high stiffness FT.

https://doi.org/10.1371/journal.pone.0239447.g007

times higher PPS values for the hard FT compared to the models with the soft FT, except for some lower ratios occurring when half WT is considered.

Peak cap stress

Maximum PCS was localized in the shoulder region of the FC in the majority of cases (see Fig 6). In contrast to PPS, the impact of the FT stiffness was found significant for sample 2, while that of the LC stiffness plays also a significant role in some cases. Also here, however, the main effect is caused by the WT and by the interaction of WT with the FT. ST and squared effect of LC factor were found significant for sample 2 although they showed only minor effect for sample 1. The PCS values at low/high levels of all the investigated factors are summarized in Fig 8. The highest PCS differences occur for the soft FT between the cases with WT = 0 and WT = 0.5, while with the hard FT the response was nearly independent of the other factors. The highest stress concentrations (153 kPa and 300 kPa) were found in the models without the vessel wall and with the soft atheroma components, while the lowest stresses (22 kPa and 25 kPa) were found in the models with the artery wall included and with the soft FT and hard LC. The maximum difference in the PCS between soft and hard components (both FT and LC) was 29 kPa vs 47 kPa and 57 kPa vs 53 kPa with the WT fully included while it amounted to 138 kPa vs 49 kPa and 300 kPa vs 50 kPa without the wall; this comparison was based on results for the minimal slice thickness only.

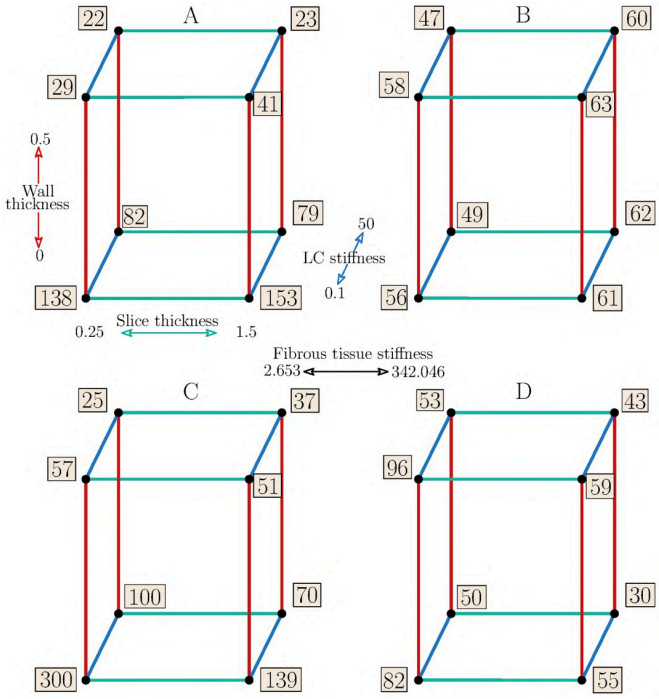

Fig 8. Cube plots of PPS values [kPa]. Patient 1 (A-B) and patient 2 (C-D). Colours represent a specific factor; red—WT, green—ST, LC stiffness—blue. Cubes A and C represent low stiffness FT while B and D high stiffness FT.

https://doi.org/10.1371/journal.pone.0239447.g008

Discussion

Credibility of computational modelling in the assessment of atherosclerotic plaque vulnerability depends on a considerable number of factors the uncertainty of which influences the calculated stress distribution throughout the plaque; evidently, their impact is worth investigating when a realistic response is required. A great number of studies focused on geometrical parameters and indicated the FC dimensions as crucial parameters for the plaque vulnerability [4, 7, 11, 21]. Even though the presented models did not fully meet the vulnerable plaque definition, it is not clear whether such plaques are the only ones which should be investigated for high stresses by computational modelling in order to examine a mechanism of rupture. Recent study Libby *et al.* [30] evaluated the current strict focus on vulnerable plaques with the conclusion that we should be prepared to address its fundamental causes in greater depth. Burke *et al.* [31] defined the limit FC thickness for vulnerable plaques <65 μm which is below the resolution of *in vivo* or even *ex vivo* imaging methods (except for e.g. μCT or histology) and so applicable analysed only to idealized studies. Moreover, stresses found in some configurations within our study exceeded a tissue threshold of 300 kPa which was discussed e.g. in Holzapfel *et al.* [20]. This indicates that either local thresholds need to be defined or that even non-vulnerable plaques from its definition might be critical for rupture risk. In this study, we focused on consideration of material properties of the vessel wall along with those of the atheroma; we used 3D PS computational models and the DoE strategy to investigate their influence on PCS and PPS.

Wall thickness

To the authors´ best knowledge, there is no current study investigating the possible impact of the wall consideration in the computational model of the atherosclerotic plaque on the stress

distribution even though the omission of the wall is very frequent in *in vivo* studies; therefore, different studies will be discussed. To consider the composition of the wall with atheroma in our study, the vessel wall was always included, although with different material properties. In Huang *et al.* [10] the authors used a PS plaque model without distinguishing between the vessel wall components. When comparable inputs are taken into consideration, the PCS maxima correlate with our findings (120 kPa vs 58 to 147 kPa represented by average values in our study depending on the FT stiffness). Yuan *et al.* [7] presented an idealized plaque model not distinguishing between the wall components but with various stiffness for each plaque component based on its mechanical tests. The decrease in the FT stiffness resulted in an increase of PCS and PPS which correlates with our findings using the configuration with WT = 0. Maximum PCS of 228 kPa was found for the configuration with a thick FC, cf. our average value of 183 kPa with comparable model inputs and independent of ST. Consideration of the wall was presented in Nieuwstadt *et al.* [6] where lower stress concentrations (mean PCS of about 60 kPa) were found compared to Yuan *et al.* [7]. Here our findings show the average PCS values of 54 kPa with a comparable LC stiffness but different FT stiffness, the effect of which was found insignificant. When we compare the discussed studies with our findings, neglecting the specific vessel wall properties leads to higher stress concentrations which may cause incorrect evaluation of PCS. This effect is reduced with a hard FT approaching the wall stiffness itself. Especially with softer FT models, however, it holds that consideration of vessel wall is decisive for the calculated stresses while the impact of its thickness variations is much less pronounced. Specifically, zero WT resulted in the overestimation of PPS and PCS by a factor of 5 up to 8 (for the soft FT and LC models).

Slice thickness

Study Lisický *et al.* [24] investigated the ST impact on magnitudes of surfaces and volumes of the atherosclerotic plaque components and found only slight impact of the ST in the whole investigated range between 0.25 to1.5 mm, with a negligible impact between 0.5 and 1 mm. In this work, we found that ST was significant for sample 2 while insignificant for sample 1. This bias might be related to the fact that, in case of sample 1 with the high ST, a minimum FC thickness was comparable with a low ST but in case of sample 2, there were huge differences between them. Here, the local minimum of the FC thickness was not captured by any of the images resulting in lower stress concentrations. In study Nieuwstadt *et al.* [6] the authors used different numbers of histological slices which resulted in low and high sampling models. Their results showed a large variation among different samplings though they concluded that the magnitude of PCS differed significantly when lower sampling was used. Higher ST of MRI or low sampling for other imaging methods may cause data loss if, for example, small LC or local thin FC are presented. Our results showed that the impact of ST should not be neglected and further investigation is needed. In conclusion, the *in vivo* MRI with its achievable axial resolution of at least 1.5 mm should be capable to distinguish critical plaque components, especially if equipped with a special carotid coil providing also a sufficient in-plane resolution as shown in studies [32, 33] although its resolution is still not capable to capture thin FC.

FT stiffness

In many experimental studies, various mechanical properties of the FT were found [7, 13, 14]. The influence of FT stiffness was examined in Akyildiz *et al.* [4] where the authors used an idealized parametric model with a Neo-Hookean (i.e. nearly linear) material model for the intima and an anisotropic material model for both the media and adventitia. The soft intima models showed a lower PCS than the stiff and intermediate intima models. In our study, the same

finding was found with the increase by a factor of 1.6 to 2 between the soft and hard FT when approximately the same inputs with full WT were used. An opposite tendency (an increase of PCS with the softer FT) was found in the Yuan *et al.* [7] but this was caused by neglecting the wall components as discussed above. In our simulations with the media and adventitia replaced by the FT, the PCS also increased 2.5 to 3.6 times between the hard and the soft FT model. The explanation of this effect may be in the stiffness of the soft FT: if it is lower by orders than the stiffness of the media, adventitia or hard FT, large deformations occurring with soft FT may induce high increase of stresses. The low and high stiffness limits of the FT used in our models show a huge variance of FT; the initial stiffness of the hard FT is ca. three times higher than those of media and adventitia while this value is lower by two orders for the soft FT. Due to the complexity of the FT structure, we can expect that the variance of its stiffness may not be random but related to some other factors characterizing different experimental groups. The two or threefold increase in the extreme stresses between the low and high FT stiffness models indicates that if we were able to classify the patients (*in vivo*, for example based on MRI) into some basic groups, the variance within each group could be significantly reduced. The presence of calcifications or even their distribution [5, 34] might serve as such an indicator. Maldonado *et al.* [34], however, presented a very low (~2%) content of micro-calcifications in the FT thus we believe their impact is within the considered range of the FT stiffness.

LC stiffness

The influence of micro-calcifications in the LC was previously discussed in [5, 34] where the authors found their high influence on the stress concentrations. Their findings indicate that thousands of micro-calcifications occur at the borders of the necrotic core or inside the LC, surrounding there some larger calcifications. Besides, the high-resolution images used in those studies indicate that modelling of calcifications as one homogeneous part [12, 16, 35] of the atherosclerotic plaque may be incorrect. Using high-resolution micro CT and histology they found that micro-calcifications are non-uniformly distributed within the FC and their amount decreases from the LC to the lumen. Grouping of these calcifications may cause artefacts in MRI and subsequent misleading evaluation of the images. In Iannaccone *et al.* [16], the whole LC was modelled in three ways: as a lipid, a fibrotic media and as a calcification. Their findings indicate that higher stresses occur when the LC is modelled as a soft lipid and correlate thus with our findings for the PCS. However, we cannot compare the results for hard LC since the LC stiffness in our models was much lower than that used in [16] where the whole LC was a ceramic-like material.

Media behaviour

Anisotropy of the arterial wall is an undisputed fact which has been investigated in the last decades and, subsequently, numerous structure-motivated constitutive models have been formulated [26, 36, 37]. However, to take advantage of these models, information on the fibrous structure of the tissue is needed. Due to lack of information on a number of collagen fibre families and on their preferred orientation and dispersion in specific arterial tissues, these models are often fitted to mechanical experiments only which make them purely phenomenological. Also in this study, the structural parameter φ was used as a phenomenological variable [25]; there it was found to be the smallest for the media layer (<10 degrees) which indicates fibres oriented dominantly in the circumferential direction. Together with the concentration parameter $\rho = 0.8$, the anisotropic behaviour of the media layer can be considered as sufficiently representative even if, due to lack of information on the anisotropy of the diseased media, we used

experimental results [8, 17] obtained partly with non-atherosclerotic tissue. The results obtained in this study indicate that the isotropic representation of the biaxial tests can be used for computational modelling of the media without significant impact on stresses in the plaque or in the FC. Nevertheless, these findings do not contradict the dominating opinion that local structural parameters of collagen fibre distribution in a specific artery and arterial layer are important for the calculation of stresses in this layer and should be investigated in detail [38].

Limitations

The FT material model may be considered as one of the main limitations of the presented study. However, no relevant data for the FT anisotropy is available, neither on its mechanical response nor on its structure. The FT extreme experimental responses selected for this study show only low strain stiffening which was captured by the second parameter of the used Yeoh SEDF. Concerning the anisotropic model of the media, the procedure applied to set its principal material directions is rigorous; their setting may be inaccurate only in very irregular parts of the geometry, such as the top of the bifurcation, where no data is available on local collagen structure. However, due to the confirmed insignificance of the media anisotropy, inaccuracies in principal directions are irrelevant. The constant pressure applied on the luminal surface might be also considered as a limitation but it was confirmed that there are no significant differences between structural and one or two-way FSI analyses [10]. Also the sample removed from the body may reduce its length and residual stresses in the tissue may be released. However, the axial pre-stretch decreases significantly with the age and thus it becomes less significant in the age group for which the atheroma is typical. Also the geometric complexity of the carotid bifurcation makes correct implementation of axial pre-stretch rather difficult, therefore it was not applied in our analyses. On the contrary, the residual stresses are believed to be a very important factor which influences the stress-strain distribution in arterial wall. In this study, the residual stresses were included in the material model of the vessel wall [25] while they were neglected in the FT and LC where, to our best knowledge, no data on their presence, magnitude, or distribution is available.

Although the geometry of the ex vivo sample may be changed, higher resolution of the MRI is substantial while distortions of the sample are negligible by virtue of its relatively high stiffness. The last limitation consists in the only two PS model geometries reconstructed in this study. Although our analyses achieved comparable statistical significance of all results (except for the MRI slice thickness which is strongly related to the complexity of geometry and its inter-patient variability), for other geometries only similar qualitative tendencies may be expected. However, a general quantitative prediction of impact of the individual factors would not be feasible, even if we made much more patient-specific calculations. Each patient has to be evaluated individually, therefore we intend to apply the presented methodology in future studies to strengthen the validity of our conclusions.

Conclusion

Our findings point out the necessity of consideration of the vessel wall stiffness in computational modelling of atherosclerotic arteries, especially when the fibrous tissue of the plaque is less stiff than the media and adventitia layers. It appears that in FE modelling of the stress response in the fibrous cap, specifically of the peak cap stress which is believed to be decisive for plaque vulnerability, the following parameters play a key role: (i) stiffness of the fibrous tissue, (ii) stiffness of the lipid core, (iii) real material properties of the media and adventitia layers of arterial wall, especially their strain stiffening which is much more pronounced than at the fibrous tissue. In contrast, anisotropy of the media layers, as well as the wall thickness itself

(if being non-zero) are less significant for maximum stresses in the fibrous cap; this fact appears encouraging for further studies based on *in vivo* MRI.

Supporting information

S1 Appendix. Verification of Ansys user subroutine for media material model.
(DOCX)

S1 Fig.
(TIF)

S2 Fig. Geometry model of patient 2. Section of sample 2 model with two large lipid cores.
(TIF)

S1 File. Ethical agreement.
(PDF)

Acknowledgments

We thank to Pavel Skácel who implemented the constitutive model needed for our study into the ANSYS software.

Author Contributions

Conceptualization: Ondřej Lisický, Jiří Burša.

Formal analysis: Jiří Burša.

Funding acquisition: Jiří Burša.

Investigation: Ondřej Lisický.

Methodology: Ondřej Lisický, Aneta Malá, Zdeněk Bednařík.

Resources: Aneta Malá, Zdeněk Bednařík, Tomáš Novotný.

Software: Ondřej Lisický.

Supervision: Jiří Burša.

Validation: Jiří Burša.

Visualization: Ondřej Lisický.

Writing – original draft: Ondřej Lisický.

Writing – review & editing: Ondřej Lisický, Aneta Malá, Zdeněk Bednařík, Tomáš Novotný, Jiří Burša.

References

1. Ross R. Inflammation or Atherogenesis. N Engl J Med. 1999; 340: 115–126.
2. Finn A V., Nakano M, Narula J, Kolodgie FD, Virmani R. Concept of vulnerable/unstable plaque. Arterioscler Thromb Vasc Biol. 2010; 30: 1282–1292. https://doi.org/10.1161/ATVBAHA.108.179739 PMID: 20554950
3. Fisher M, Paganini-Hill A, Martin A, Cosgrove M, Toole JF, Barnett HJM, et al. Carotid plaque pathology: Thrombosis, ulceration, and stroke pathogenesis. Stroke. 2005; 36: 253–257. https://doi.org/10.1161/01.STR.0000152336.71224.21 PMID: 15653581
4. Akyildiz AC, Speelman L, van Brummelen H, Gutiérrez MA, Virmani R, van der Lugt A, et al. Effects of intima stiffness and plaque morphology on peak cap stress. Biomed Eng Online. 2011; 10: 1–13.

5. Maldonado N, Kelly-Arnold A, Vengrenyuk Y, Laudier D, Fallon JT, Virmani R, et al. A mechanistic analysis of the role of microcalcifications in atherosclerotic plaque stability: potential implications for plaque rupture. AJP Hear Circ Physiol. 2012; 303: H619–H628. https://doi.org/10.1152/ajpheart.00036.2012 PMID: 22777419

6. Nieuwstadt HA, Akyildiz AC, Speelman L, Virmani R, van der Lugt A, van der Steen AFW, et al. The influence of axial image resolution on atherosclerotic plaque stress computations. J Biomech. 2013; 46: 689–695. https://doi.org/10.1016/j.jbiomech.2012.11.042 PMID: 23261242

7. Yuan J, Teng Z, Feng J, Zhang Y, Brown AJ, Gillard JH, et al. Influence of material property variability on the mechanical behaviour of carotid atherosclerotic plaques: A 3D fluid-structure interaction analysis. Int j numer method biomed eng. 2015. https://doi.org/10.1002/cnm.2722 PMID: 25940741

8. Holzapfel GA, Stadler M, Schulze-Bauer CAJ. A Layer-Specific Three-Dimensional Model for the Simulation of Balloon Angioplasty using Magnetic Resonance Imaging and Mechanical Testing. Ann Biomed Eng. 2002; 30: 753–767. https://doi.org/10.1114/1.1492812 PMID: 12220076

9. Gao H, Long Q, Graves M, Gillard JH, Li ZY. Carotid arterial plaque stress analysis using fluid-structure interactive simulation based on in-vivo magnetic resonance images of four patients. J Biomech. 2009; 42: 1416–1423. https://doi.org/10.1016/j.jbiomech.2009.04.010 PMID: 19464011

10. Huang Y, Teng Z, Sadat U, Graves MJ, Bennett MR, Gillard JH. The influence of computational strategy on prediction of mechanical stress in carotid atherosclerotic plaques: Comparison of 2D structure-only, 3D structure-only, one-way and fully coupled fluid-structure interaction analyses. J Biomech. 2014; 47: 1465–1471. https://doi.org/10.1016/j.jbiomech.2014.01.030 PMID: 24529358

11. Cilla M, Borrás I, Peña E, Martínez MA, Malvè M. A parametric model for analysing atherosclerotic arteries: On the FSI coupling. Int Commun Heat Mass Transf. 2015; 67: 29–38. https://doi.org/10.1016/j.icheatmasstransfer.2015.06.017

12. Tang D, Yang C, Huang S, Mani V, Zheng J, Woodard PK, et al. Cap inflammation leads to higher plaque cap strain and lower cap stress: An MRI-PET/CT-based FSI modeling approach. J Biomech. 2017; 50: 121–129. https://doi.org/10.1016/j.jbiomech.2016.11.011 PMID: 27847118

13. Akyildiz AC, Speelman L, Gijsen FJH. Mechanical properties of human atherosclerotic intima tissue. J Biomech. 2014; 47: 773–783. https://doi.org/10.1016/j.jbiomech.2014.01.019 PMID: 24529360

14. Walsh MT, Cunnane EM, Mulvihill JJ, Akyildiz AC, Gijsen FJH, Holzapfel GA. Uniaxial tensile testing approaches for characterisation of atherosclerotic plaques. J Biomech. 2014; 47: 793–804. https://doi.org/10.1016/j.jbiomech.2014.01.017 PMID: 24508324

15. Huang X, Yang C, Zheng J, Bach R, Muccigrosso D, Woodard PK, et al. 3D MRI-based multicomponent thin layer structure only plaque models for atherosclerotic plaques. J Biomech. 2016; 49: 2726–2733. https://doi.org/10.1016/j.jbiomech.2016.06.002 PMID: 27344199

16. Iannaccone F, Debusschere N, De Bock S, De Beule M, Van Loo D, Vermassen F, et al. The influence of vascular anatomy on carotid artery stenting: A parametric study for damage assessment. J Biomech. 2014; 47: 890–898. https://doi.org/10.1016/j.jbiomech.2014.01.008 PMID: 24480704

17. Sommer G, Regitnig P, Koltringer L, Holzapfel GA. Biaxial mechanical properties of intact and layer-dissected human carotid arteries at physiological and supraphysiological loadings. AJP Hear Circ Physiol. 2010; 298: H898–H912. https://doi.org/10.1152/ajpheart.00378.2009 PMID: 20035029

18. Kamenskiy A V., Dzenis YA, Kazmi SAJ, Pemberton MA, Pipinos II, Phillips NY, et al. Biaxial mechanical properties of the human thoracic and abdominal aorta, common carotid, subclavian, renal and common iliac arteries. Biomech Model Mechanobiol. 2014; 13: 1341–1359. https://doi.org/10.1007/s10237-014-0576-6 PMID: 24710603

19. Loree HM, Kamm RD, Stringfellow RG, Lee RT. Effects of Fibrous Cap Thickness on Peak Circumferential Stress in Model Atherosclerotic Vessels. Circulation. 1992; 71: 850–858.

20. Holzapfel GA, Mulvihill JJ, Cunnane EM, Walsh MT. Computational approaches for analyzing the mechanics of atherosclerotic plaques: A review. J Biomech. 2014; 47: 859–869. https://doi.org/10.1016/j.jbiomech.2014.01.011 PMID: 24491496

21. Cilla M, Peña E, Martínez MA. 3D computational parametric analysis of eccentric atheroma plaque: Influence of axial and circumferential residual stresses. Biomech Model Mechanobiol. 2012; 11: 1001–1013. https://doi.org/10.1007/s10237-011-0369-0 PMID: 22227796

22. Groen HC, Van Walsum T, Rozie S, Klein S, Van Gaalen K, Gijsen FJH, et al. Three-dimensional registration of histology of human atherosclerotic carotid plaques to in-vivo imaging. J Biomech. 2010; 43: 2087–2092. https://doi.org/10.1016/j.jbiomech.2010.04.005 PMID: 20444453

23. Stary HC. Natural History and Histological Classification of Atherosclerotic Lesions. Ateriosclr Thromb Vasc Biol. 2000; 20: 1177–1178. PMID: 10807728

24. Lisický O, Malá A, Burša J. Influence of Transversal Resolution on Reconstructing Atherosclerotic Plaque Components. VipIMAGE 2019. 2019. pp. 501–508.

25. Sommer G, Holzapfel GA. 3D constitutive modeling of the biaxial mechanical response of intact and layer-dissected human carotid arteries. J Mech Behav Biomed Mater. 2012; 5: 116–128. https://doi.org/10.1016/j.jmbbm.2011.08.013 PMID: 22100086

26. Holzapfel GA, Sommer G, Gasser CT, Regitnig P. Determination of layer-specific mechanical properties of human coronary arteries with nonatherosclerotic intimal thickening and related constitutive modeling. J Physiol Hear Circ Physiol. 2005; 103: 806–808. https://doi.org/10.1152/ajpheart.00934.2004 PMID: 16006541

27. Holzapfel GA, Sommer G, Regitnig P. Anisotropic Mechanical Properties of Tissue Components in Human Atherosclerotic Plaques. J Biomech Eng. 2004; 126: 657. https://doi.org/10.1115/1.1800557 PMID: 15648819

28. Yeoh OH. Some forms of the strain energy function for rubber. Rubber Chemistry and Technology. 1993. pp. 754–771.

29. Marcián P, Narra N, Borák L, Chamrad J, Wolff J. Biomechanical performance of cranial implants with different thicknesses and material properties: A finite element study. Comput Biol Med. 2019; 109: 43–52. https://doi.org/10.1016/j.compbiomed.2019.04.016 PMID: 31035070

30. Libby P, Pasterkamp G. Requiem for the "vulnerable plaque." Eur Heart J. 2015; 36: 2984–2987. https://doi.org/10.1093/eurheartj/ehv349 PMID: 26206212

31. Burke F. CORONARY RISK FACTORS AND PLAQUE MORPHOLOGY IN MEN WITH CORONARY DISEASE WHO DIED SUDDENLY. New Engl J Med Coron. 1997.

32. Hatsukami TS, Ross R, Polissar NL, Yuan C. Visualization of fibrous cap thickness and rupture in human atherosclerotic carotid plaque in vivo with high-resolution magnetic resonance imaging. Circulation. 2000; 102: 959–964. https://doi.org/10.1161/01.cir.102.9.959 PMID: 10961958

33. Saam T, Ferguson MS, Yarnykh VL, Takaya N, Xu D, Polissar NL, et al. Quantitative evaluation of carotid plaque composition by in vivo MRI. Arterioscler Thromb Vasc Biol. 2005; 25: 234–239. https://doi.org/10.1161/01.ATV.0000149867.61851.31 PMID: 15528475

34. Maldonado N, Kelly-Arnold A, Laudier D, Weinbaum S, Cardoso L. Imaging and analysis of microcalcifications and lipid/necrotic core calcification in fibrous cap atheroma. Int J Cardiovasc Imaging. 2015; 31: 1079–1087. https://doi.org/10.1007/s10554-015-0650-x PMID: 25837377

35. Kiousis DE, Rubinigg SF, Auer M, Holzapfel GA. A Methodology to Analyze Changes in Lipid Core and Calcification Onto Fibrous Cap Vulnerability: The Human Atherosclerotic Carotid Bifurcation as an Illustratory Example. J Biomech Eng. 2009; 131: 121002. https://doi.org/10.1115/1.4000078 PMID: 20524725

36. Holzapfel Gerhard A. ORW. A New Constitutive Framework for Arterial Wall Mechanics and a Comparative Study of Material Models. J Elast. 2000; 61: 1–48. https://doi.org/10.1023/A:1010835316564

37. Gasser TC, Ogden RW, Holzapfel GA. Hyperelastic modelling of arterial layers with distributed collagen fibre orientations. J R Soc Interface. 2005; 3: 15–35. https://doi.org/10.1098/rsif.2005.0073 PMID: 16849214

38. Holzapfel GA, Ogden RW. Biomechanical relevance of the microstructure in artery walls with a focus on passive and active components. Am J Physiol—Hear Circ Physiol. 2018; 315: H540–H549. https://doi.org/10.1152/ajpheart.00117.2018 PMID: 29799274

C. Appendix

Computational modeling of blood flow in the bifurcation of human carotid artery

Original research article indexed by Web of Science.

P. Švancara et al. (Nov. 2020). "COMPUTATIONAL MODELING OF BLOOD FLOW IN THE BIFURCATION OF HUMAN CAROTID ARTERY." in: *ENGINEERING MECHANICS 2020*. 1. Chap. 166395, pp. 480–483. DOI: 10.21495/5896-3-480

26th International Conference
ENGINEERING MECHANICS 2020
Brno, Czech Republic, November 24 – 25, 2020

COMPUTATIONAL MODELING OF BLOOD FLOW IN THE BIFURCATION OF HUMAN CAROTID ARTERY

Švancara P.[*], Lisický O.[**], Jagoš J.[***], Burša J.[****]

Abstract: *Computational simulations can be used to better predict the risk of atherosclerotic plaques (atheromas) formation. The study presents three-dimensional patient specific computational models of blood hemodynamic in the human carotid arteries based on finite volume method. The geometry of the arteries was created from computer tomography (CT) images. Measured mass flow rate waveform at the inlet and two-element Winkessel model at the outlets are used as boundary conditions. Blood is considered as a non-Newtonian fluid described by Carreau model and pulsating blood flow is solved by transient analysis. Time history of wall shear stress magnitude, velocity profiles in individual cross-sections and flow pattern are evaluated and discussed as they may be helpful in assessing the risk of potential development of atheroma.*

Keywords: Carotid artery, Blood, Windkessel model, Wall shear stress, Computational fluid dynamics.

1. Introduction

Atherosclerosis is responsible for nearly a third of global deaths worldwide. (Caro et al., 1971) suggested flow disturbances and low wall shear stress (WSS) as significant factors in the formation of an atherosclerotic plaque. This hypothesis was then validated by multiple studies summarized in (Malek et al., 1999). One of the approaches to investigate WSS is employing the computational fluid dynamic (CFD) simulation of the blood flow in patient specific models (Cebral et al., 2002; Gharahi et al., 2016). Problem of such simulations is to obtain accurate geometry models, determination of realistic boundary conditions, appropriate viscosity model and inclusion of the wall elasticity.

2. Methods

Geometries of the left and right carotid artery (CA) of 63 year old female patient was semi-automatically reconstructed from CT images in the RETOMO software (BETA CAE Systems); they are shown in Figs. 1a and 1c. The patient already had atheromas formed in both CAs, which were removed manually from the model so that the geometry corresponded to healthy carotid arteries. The finite volume mesh consisting of hexahedral elements was then created in software ANSYS ICEM-CFD, see Figs. 1b and 1d. To test the effect of mesh element size, three meshes with 24 809, 49 289 and 158 576 elements were created for the right CA. Fig. 2b shows an example of computed velocity profiles near the common carotid artery (CCA) inlet at systolic pressure. From the results we can see that velocity profiles differ from each other in the order of percentage units; for further simulations a mesh with 49 289 elements was used. The same element size was used for the left CA. A finite volume method was used to solve fluid dynamic problem using software ANSYS Fluent.

[*] Ing. Pavel Švancara, PhD.: Institute of Solid Mechanics, Mechatronics and Biomechanics, Brno University of Technology, Technická 2896/2; 616 69, Brno; CZ, svancara@fme.vutbr.cz

[**] Ing. Ondřej Lisický: Institute of Solid Mechanics, Mechatronics and Biomechanics, Brno University of Technology, Technická 2896/2; 616 69, Brno; CZ, 161238@vutbr.cz

[***] Ing. Jiří Jagoš: Institute of Solid Mechanics, Mechatronics and Biomechanics, Brno University of Technology, Technická 2896/2; 616 69, Brno; CZ, 145427@vutbr.cz

[****] Prof. Ing. Jiří Burša, PhD.: Institute of Solid Mechanics, Mechatronics and Biomechanics, Brno University of Technology, Technická 2896/2; 616 69, Brno; CZ, bursa@fme.vutbr.cz

doi: 10.21495/5896-3-480

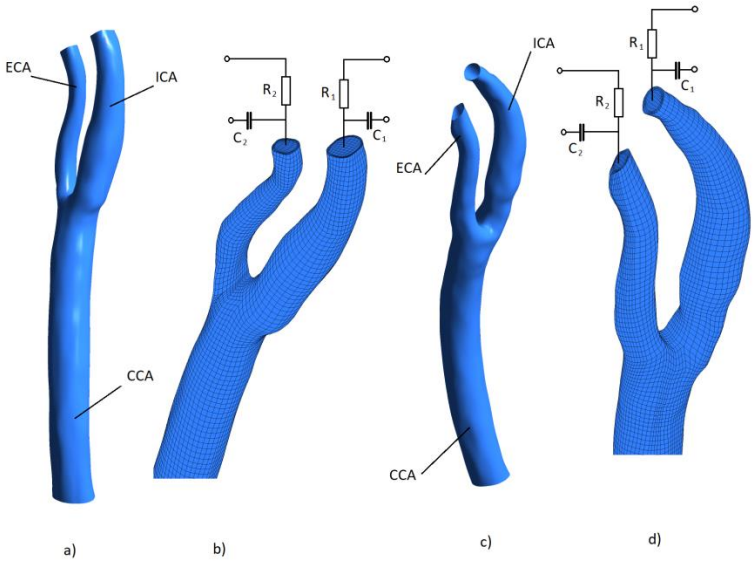

Fig. 1: a) Reconstructed geometry of the left CA; b) Detail of the finite volume mesh of the left CA with scheme of two-element Windkessel model at outlets; c) Reconstructed geometry of the right CA; d) Detail of the finite volume mesh of the right CA with two-element Windkessel model at outlets.

The waveform of mass flow rate obtained from cine phase-contrast MR flow velocity measurements (Cebral et al., 2002) was imposed at the inlet of CCA), see Fig. 2a. The downstream vascular bed was modelled with two-element Windkessel model (Shi et al., 2011) implemented in ANSYS Fluent by ANSYS customization tool Windkessel. The parameters of the outflow network were first estimated according to the pulse pressure method (Stergiopulos et al., 1999) and then iteratively tuned to achieve agreement with the waveforms of mass flow rates in internal carotid artery (ICA) and external carotid artery (ECA) published in literature (Cebral et al., 2002). Parameters used for simulations are summarized in Tab. 1.

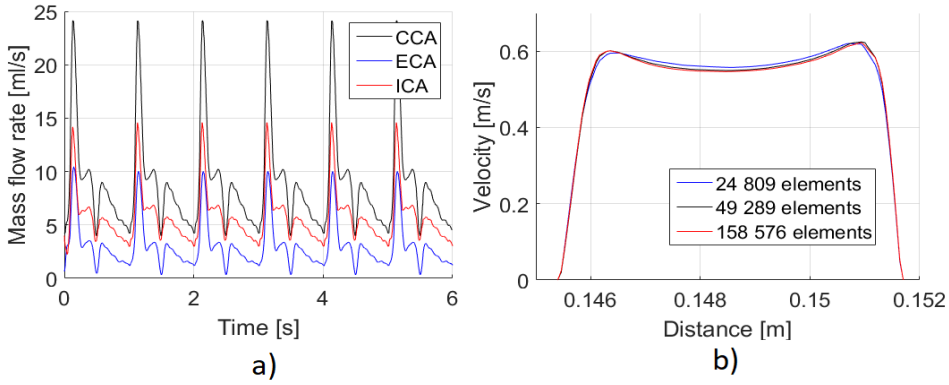

Fig. 2: a) Mass flow rate waveform used as boundary condition at CCA inlet (black) and computed mass flow rates at ECA outlet (blue) and at ICA outlet (red); b) Computed velocity profiles near left CCA inlet for different element sizes (at systolic pressure).

The blood was modelled as non-Newtonian fluid using the Carreau model for which viscosity μ_{eff} depends upon shear rate $\dot{\gamma}$ by the following equation:

$$\mu_{eff}(\dot{\gamma}) = \mu_{\inf} + (\mu_0 - \mu_{inf})\left(1+(\lambda\dot{\gamma})^2\right)^{\frac{n-1}{2}} \quad (1)$$

Where μ_0 is viscosity at zero share rate, $\mu_{\inf}$ is viscosity at infinite shear rate, λ is relaxation time and n is power index. For the present simulations the parameters $\mu_{\inf}$ = 0.0345 Pa.s, μ_0 = 0.56 Pa.s, λ=3.313 s and n = 0.3568 were used (Johnston et al., 2004). Blood flow through CA was computed by a transient analysis with a time step $\Delta t = 2\text{x}10^{-3}$ s and six periods of the cardiac cycle were solved to obtain sustained values.

Tab. 1: Parameters of two-element Windkessel models.

R_1 (ICA)	2.023e9 [kg/m^{4}s]
C_1 (ICA)	7.505e-11 [m^{4}s^2/kg]
R_2 (ECA)	3.811e9 [kg/m^{4}s]
C_2 (ECA)	8.0e-11 [m^{4}s^2/kg]

3. Results a discussion

Fig. 3a shows an example of computed streamlines with colour marked velocity magnitude for the left CA at diastolic pressure for the last solved period of the cardiac cycle. Corresponding velocity profiles in individual cross-sections near bifurcation are shown in Fig. 3b. The same results for the right CA are shown in Figs. 3c and 3d. Computed WSS magnitude distributions at diastolic pressure in global range and range up to 0.4 Pa are shown in Figs. 4a - 4c.

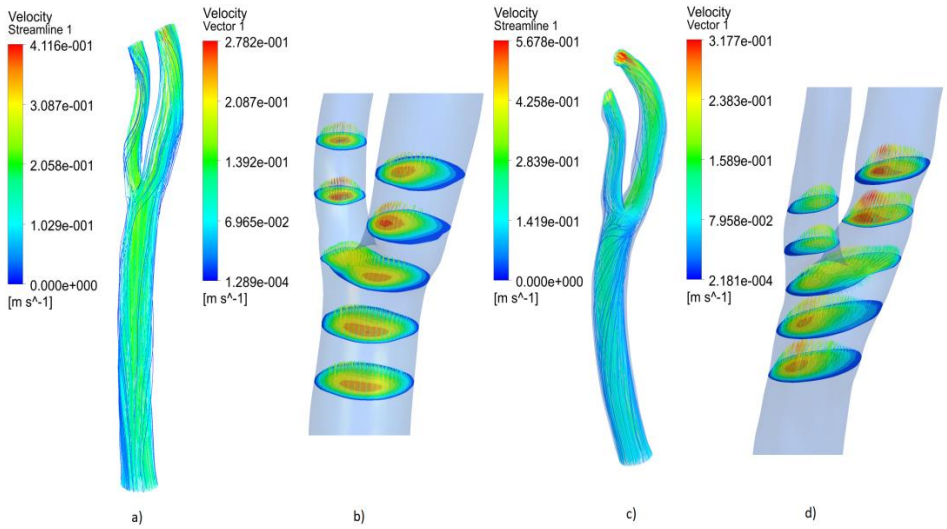

Fig. 3: Flow visualization (diastolic pressure): a) Streamlines with colour marked velocity magnitude for the left CA; b) Velocity profiles in individual cross-sections for the left CA; c) Streamlines for the right CA; d) Velocity profiles for the right CA.

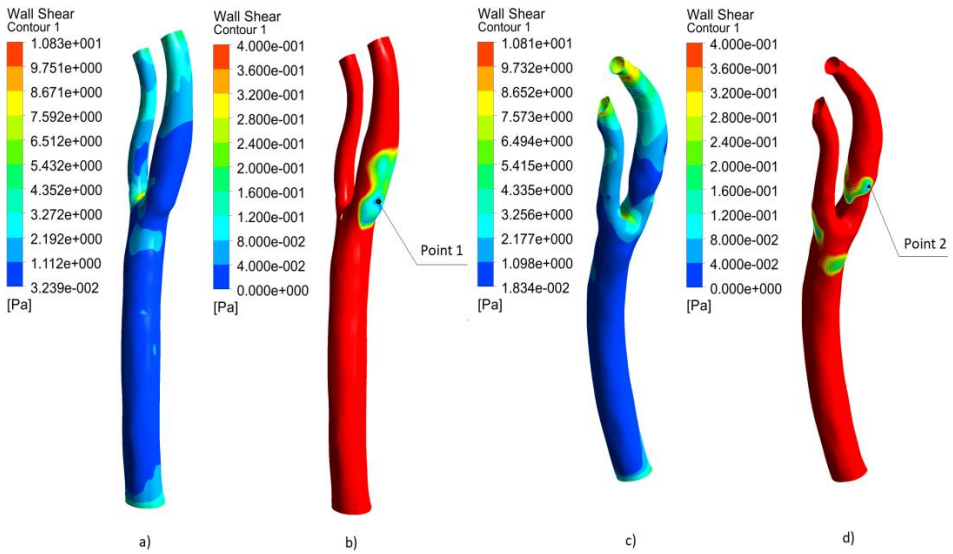

Fig. 4: Visualization of the WSS magnitude distribution (diastolic pressure): a) Left CA in global range; b) Left CA in range up to 0.4 Pa; c) Right CA in global range; d) Right CA in range up to 0.4 Pa.

The results show that on the walls of the analyzed arteries there are areas where the WSS magnitude is less than 0.4 Pa, which is low non-physiologic shear stress that could lead to development of atherosclerotic lesions (Zarins et al., 1983, Malek et al., 1999). These areas are associated with oscillatory and disturbed flow that leads to unsteady distributed flow profile. For left CA the area with low WSS magnitude (< 0.4 Pa) corresponds to the place where the atheroma began to form. For the right CA the atheroma began to form at the site of the bifurcation, which is an area surrounded by places with low WSS. Fig. 5 shows the computed time courses of the WSS magnitude at points 1 and 2 marked in Fig. 4. As we can see, the magnitude of WSS remains bellow 0.4 Pa for a significant time of the cardiac cycle. The authors are aware that the growth of the atheroma may have changed the shape of the CA and the reconstructed geometry may not fully correspond to the state before the atheroma development.

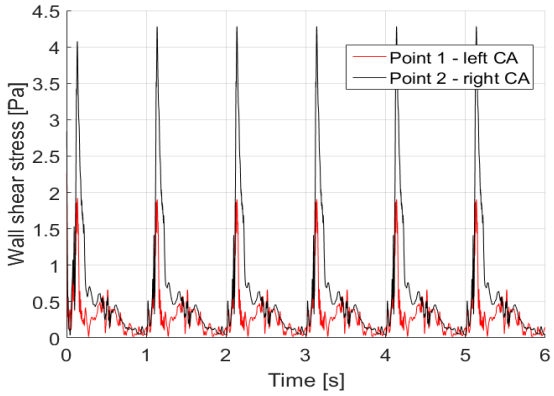

Fig. 5: Computed WSS magnitude at points 1 (left CA) and 2 (right CA).

4. Conclusions

Three-dimensional patient specific computational models of blood hemodynamic in the human carotid arteries were created. Computed results are in good agreement with physiological data published in the literature and the model is capable to predict correctly WSS magnitude, velocity profiles and flow pattern. Locations of low WSS magnitude (< 0.4 Pa) correspond well to locations where the atheroma began to form. Although the process of atheroma formation is generally more complicated and need future research, the developed model may be helpful in guiding future therapeutic strategies.

Acknowledgement

This work was supported by Czech Science Foundation project No. GA18-13663S.

References

Caro, C. G., Fitz-Gerald, J.M., Schroter, R. C. (1971) Atheroma and arterial wall shear-Observation, correlation and proposal of a shear dependent mass transfer mechanism for atherogenesis. Proceedings of the Royal Society of London. Series B. Biological Sciences, 177, 1046, pp. 109-133.

Cebral, J. R., Yim, P. J., Lohner, R. (2002) Blood flow modeling in carotid arteries with computational fluid dynamics and MR imaging. Academic Radiology, 9, 11, pp. 1286-1299.

Gharahi, H., Zambrano, B. A., Zhu, D. et al. (2016) Computational fluid dynamic simulation of human carotid artery bifurcation based on anatomy and volumetric blood flow rate measured with magnetic resonance imaging. Int J Adv Eng Sci Appl Math, 8, 1, pp. 46-60.

Johnston, B. M., Johnston, P. R., Corney, S. et al. (2004) Non-Newtonian blood flow in human right coronary arteries: steady state simulations. Journal of Biomechanics, 37, 5, pp. 709-720.

Malek, A. M., Alper, S. L., Izumo, S. (1999) Hemodynamic shear stress and its role in atherosclerosis. Jama, 282, 21, pp. 2035-2042.

Shi, Y., Lawford, P., Hose, R. (2011) Review of zero-D and 1-D models of blood flow in the cardiovascular system. Biomed Eng OnLine, 10, 33.

Stergiopulos, N., Segers P., Westerhof, N. (1999) Use of pulse pressure method for estimating total arterial compliance in vivo. Am. J. Physiol. - Hear. Circ. Physiol., 276, 2, pp. 424-428.

Zarins, C. K., Giddens, D. P., Bharadvaj, B. K. et al. (1983) Carotid bifurcation atherosclerosis. Quantitative correlation of plaque localization with flow velocity profiles and wall shear stress. Circulation research, 53, 4, pp. 502-514.

D. Appendix

Impact of formaldehyde on mechanical properties of atherosclerotic carotid arteries

Original research article indexed by Web of Science.

A. Hrubanová et al. (Nov. 2020). "IMPACT OF FORMALDEHYDE ON MECHANICAL PROPERTIES OF ATHEROSCLEROTIC CAROTID ARTERIES." in: *ENGINEERING MECHANICS 2020*. Chap. 166394, pp. 210–213. DOI: 10.21495/5896-3-210

26th International Conference
ENGINEERING MECHANICS 2020
Brno, Czech Republic, November 24 – 25, 2020

IMPACT OF FORMALDEHYDE ON MECHANICAL PROPERTIES OF ATHEROSCLEROTIC CAROTID ARTERIES

Hrubanová A.[*1], Lisický O.[1], Bartoňová P.[***1], Staffa R.[****2], Hermanová M.[*****2], Vlachovský R.[******2], Burša J.[*******1]**

Abstract: *Atherosclerosis is a life threatening cardiovascular disease causing lipoprotein accumulation within intima layer of artery wall and thus its thickening. Later stages are characterized by plaque formation with a lipid core separated from lumen by fibrous cap. In case of carotid arteries (CA), rupture of the plaque often results in a stroke. Detailed understanding of mechanical properties of atherosclerotic arteries and their components is essential for improvement of computer models used for prediction of plaque rupture. Samples of atherosclerotic CA from carotid endarterectomy were kept either in saline solution or in formaldehyde solution and then underwent uniaxial tensile testing in two directions. Statistical analysis of the obtained stress-strain responses shows that formaldehyde treatment of the tissue increases significantly the mean stiffness and reduces the dispersion.*

Keywords: Atherosclerotic plaque, Carotid artery, Mechanical properties, Uniaxial tensile test.

1. Introduction

Atherosclerosis is a progressive cardiovascular disease characterized by accumulation of lipoproteins in the inner artery wall layer – intima. Over time the lipoproteins stacked within the intima create a lesion which consists of a lipid core (LC) covered by fibrous tissue forming a new layer – fibrous cap (FC). As the disease progresses, the lesion enlarges and limits or even blocks the blood flow. The most frequent complications are detachment of a part of the lesion or rupture of the FC leading to a release of the lipid into the circulatory system and subsequent formation of blood clots. In case of common or internal CA it results in a stroke with high mortality of the patients (Fisher et al., 2005).

During this process, new components such as fibrous tissue and, in later stages, calcifications are formed within the artery wall. The layered structure of healthy artery wall is known to be heterogeneous and so are even more the specific components of atherosclerotic arteries. Hence, their mechanical properties are highly varying within the affected area (Mulvihill et al., 2013).

An arterial tissue damage occurs when stresses induced by the blood pressure loading exceed the tissue strength. The lipid core is separated from lumen by the fibrous cap, therefore detailed knowledge of mechanical properties of the fibrous cap together with the other components of the atherosclerotic plaque is fundamental for predictions of the plaque rupture risk.

Uniaxial and especially biaxial mechanical tests can help us to understand better the non-linear anisotropic mechanical behaviour of atherosclerotic tissues. Recently, biaxial tests on CAs were presented (Kamenskiy et al., 2011), (Kamenskiy et al., 2014), (Sommer et al., 2009). However, the severity of atherosclerosis was

[1] Inst. Solid Mechanics, Mechatronics and Biomechanics, Brno University of Technology, Technická 2896/2, 616 69 Brno; CZ
[2] St. Anne's University Hospital Brno and Faculty of Medicine, Masaryk University, Brno, Czech Republic
[*] Bc. Anna Hrubanová; 191418@vutbr.cz
[**] Ing. Ondřej Lisický; 161238@vutbr.cz
[***] Bc. Petra Bartoňová; 160690@vutbr.cz
[****] Prof. MUDr. Robert Staffa, PhD., 2nd Department of Surgery; robert.staffa@fnusa.cz
[*****] Prof. MUDr. Markéta Hermanová, PhD., 1st Department of Pathology; marketa.hermanova@fnusa.cz
[******] MUDr. Robert Vlachovský, PhD., 2nd Department of Surgery; robert.vlachovsky@fnusa.cz
[*******] Prof. Ing. Jiří Burša, PhD.; bursa@fme.vutbr.cz

doi: 10.21495/5896-3-210

much lower, it varied from low to medium. To our best knowledge, there are no published experimental results of biaxial testing of highly atherosclerotic arteries. In contrast, uniaxial tests were realized even with specific tissue components separated from the atheroma and the adjacent arterial wall (Holzapfel et al., 2004). Specimens studied in this paper originated from standard endarterectomy and due to severely diseased intima were also tested in uniaxial tension only. Some of the specimens were fixed in formaldehyde; as this is a standard procedure in histological analyses, the question was whether it impacts on mechanical properties of the tissue substantially.

2. Methods

2.1. Specimen extraction and preparation

All samples were acquired (with an informed consent of the patients) during endarterectomies in St. Anne's University Hospital in Brno from April to December 2019. They consisted of intima layer with atherosclerotic plaque (atheroma) and, in majority of cases, of bifurcation and part of the internal and external CA. They were tested either directly after surgery (within 24 hours), or later, after having been kept frozen at -18 °C in physiological solution, or after having been treated in formaldehyde (10% solution) for 24 hours. As it was previously shown that freezing does not influence mechanical properties of arterial tissues significantly once the specimen is unfrozen (Ebenstein et al., 2009), (O'Leary et al., 2014), we considered them in the same group as the fresh specimens.

On the day of testing, the samples were submerged in physiological solution and heated slowly to 37 °C. For each sample, presence of calcifications was evaluated. Although a standard classification (Stary, 2000) dividing atherosclerosis into 8 categories could not be used without further histological examination, presence of calcifications in most specimens indicated the lesion type VII +. To consider also the tissue anisotropy, specimens were cut off in both axial and circumferential directions; their orientation was decided primarily regarding the tissue damage. Generally, the samples were cut through the lipid core in longitudinal direction. Although the effort was to obtain the same quantity of axial and circumferential specimens, the axial incision through the sample as well as their small size caused the majority of specimens to be circumferential. In total, 70 specimens from 27 patients (18 men, 9 women) were tested with an average age of 69 years; 44 of the specimens were kept in saline (0.9% NaCl) solution and 26 specimens treated with formaldehyde.

If feasible, the fibrous cap was carefully peeled off and tested separately from the intima. However, this was possible only for few specimens (n = 3). In majority of cases, efforts of removing the FC lead to tearing the intima. Then the lipid core and calcifications were removed. For several specimens, the removal of calcifications was not possible, because calcifications were firmly fixated in the intima, so their removal caused intima to tear. The specimens were cut from sample using scalpel or, if possible, a dogbone shaped specimen was cut using a special cutting knife. In case of using scalpel, we aimed to obtain a rectangular specimen of 2 mm width.

For each specimen, information about the location within the sample, extend of calcifications and other significant factors were gathered and recorded. The thickness was measured at 3 different locations using distance indicator with 0.01 mm accuracy and the mean value of thickness was used for further analyses. During the specimen preparation, the rest of samples with other specimens were also kept in the heated physiological solution to prevent tissue drying. Directly before testing, 4 markers were made at the surface of the specimen using alcohol based or permanent marker.

2.2. Testing and evaluation

A tailored computer controlled tensile testing device (Camea s.r.o., CZ) was used to perform uniaxial tests. Two clamps were used to grip the specimen which were submerged during the test in physiological solution heated at 37 ± 0.5 °C. Deformation was evaluated off line from positions of the markers on the specimen surface captured with a CCD camera while the force was measured by an electric resistance force sensor.

Pre-tension of 0.02 N was applied to flatten the specimen (for some of the formaldehyde fixed specimens it was higher, up to 0.08 N) and uniaxial tensile test was executed until tear of the specimen. Although both longitudinal and transversal strains can be determined from four markers using software Tibixus, only the

longitudinal strain was used in the calculations. Tissue incompressibility was assumed to calculate the Cauchy stress using the following equation:

$$\sigma = \lambda \frac{F}{bt} \tag{1}$$

where F is the measured force, and b, t and λ represent width, thickness, and longitudinal stretch of the specimen, respectively.

3. Results

Each stress-strain curve was smoothened using moving average and interpolated with cubic B-spline for further analysis. Separately in both groups, which were found similar in sex and age, the curves were averaged through strains at different levels of stresses stepped by 10 kPa. All the results were checked for normality of distribution. The null hypothesis that there is no difference in strains between both groups was tested at all the stress levels using Welch's test due to non-equal variances in both groups. The null hypothesis was rejected in all cases with $p < 0.05$. Strength was not evaluated quantitatively due to the fact that in most cases (n = 51) the tear occurred at clamps. Comparison of the results in both group is presented in Fig. 1.

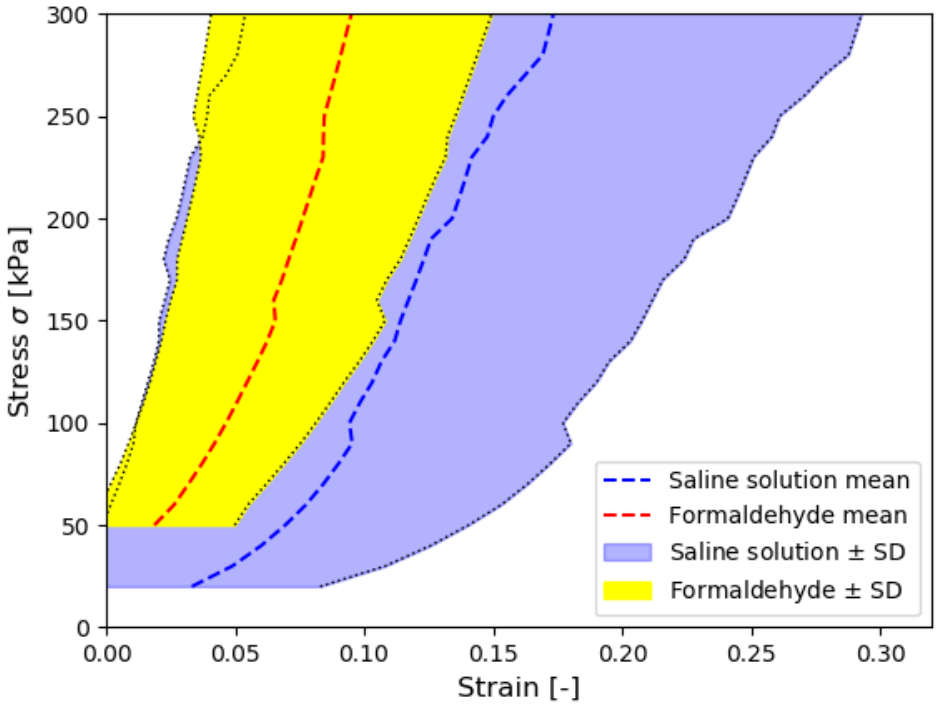

Fig. 1: Uniaxial tensile test results – mean ± SD.

4. Discussion

Knowledge of mechanical properties of specific components of atherosclerotic CA is fundamental for computational prediction of plaque rupture. In this study, the tests were performed with the extracted atheroma. The specimen gripping was realized with two 2 mm wide spring clamps, similar to clamps used in the previous research (Mulvihill, 2013). Other experiments performed with artery tissues used hooks or jaws to grip the specimens (Kamenskiy et al., 2011), (Holzapfel et al., 2004).

The acquired results confirm a substantial nonlinearity of the tissue response characterized by an increase of stiffness with increasing strain and caused by straightened collagen fibres. This phenomenon is well known for more than 60 years (Roach et. al., 1957) and was confirmed in various studies regarding CAs (Sommer et al., 2009), (Gupta et al., 1997), (Kural et al., 2012). The same tendency was evident in our experiments, while their direction dependence was not unique. Although generally the circumferential direction is stiffer in arteries due to distribution of collagen fibres (Polzer et al., 2015), in diseased arteries

the directional dependencies may be much more complex as observed in study with biaxial tensile tests of CA (Kamenskiy et al., 2011).

The measured data showed a very large dispersion in stiffness, also reported in other papers (Akyildiz et al., 2014) which, however, was substantially lower in the formaldehyde treated group. Further statistical analysis should be made to determinate possible correlations between the stress-strain response and some factors related to the origin of the tissue. To seek for such factors, we can exploit the stored data about gender, age of patients, extend of calcifications and location of the specimen within the plaque. If these correlations were found and the factors were achievable *in vivo*, they could help us to reduce the dispersion of material data and enhance thus the quality of biomechanical computational models.

5. Conclusion

The realized uniaxial tests of atherosclerotic carotid arteries tissue have shown a significant impact of formaldehyde treatment on their mechanical properties: it increases the initial stiffness and reduces the dispersion of the results compared to fresh specimens. In contrast to results of formaldehyde treated specimens, the data obtained with fresh specimens show a huge variance and indicate existence of 3 stiffness groups. As the specimens originate from various patients and locations within the atherosclerotic plaque, there might be dependencies on some specific factors obtainable *in vivo* (sex, age, direction, calcification, etc.); to identify them, a statistical analysis of a larger cohort of specimens is needed.

Acknowledgement

This work was supported by Czech Science Foundation project No. 18-13663S.

References

Akyildiz, A. C., Speelman L., Gijsen F. J. H. (2014) Mechanical properties of human atherosclerotic intima tissue. *Journal of Biomechanics*. Elsevier, 47(4), 773-783.

Ebenstein, D. M., Coughlin, D., Chapman, J., Li, C., Pruitt, L. A. (2009) Nanomechanical properties of calcification, fibrous tissue, and hematoma from atherosclerotic plaques. J. Biomed. Mater. Res. A 91, 1028-1037.

Fisher, M., Paganini-Hill, A., Martin, A., Cosgrove, M., Toole, J. F., Barnett, H. J. M., Norris, J. (2005) Carotid plaque pathology: Thrombosis, ulceration, and stroke pathogenesis. Stroke 36, 253-257.

Gupta, B. S., Kasyanov V. A. (1997) Biomechanics of human common carotid artery and design of novel hybrid textile compliant vascular grafts. *Journal of biomedical materials research*. 34(3), 341-349

Holzapfel, G. A., Sommer, G., Regitnig, P. (2004) Anisotropic Mechanical Properties of Tissue Components in Human Atherosclerotic Plaques. J. Biomech. Eng. 126, 657.

Kamenskiy, A. V., Dzenis, Y. A., Kazmi, S. A. J., Pemberton, M. A., Pipinos, I. I., Phillips, N. Y., Herber, K., Woodford, T., Bowen, R. E., Lomneth, C. S., MacTaggart, J. N. (2014) Biaxial mechanical properties of the human thoracic and abdominal aorta, common carotid, subclavian, renal and common iliac arteries. Biomech. Model. Mechanobiol. 13, 1341-1359.

Kamenskiy, A. V., Pipinos, I. I., Mactaggart, J. N., Kazmi S. A. J and Dzenis Y. A. (2011) Comparative Analysis of the Biaxial Mechanical Behavior of Carotid Wall Tissue and Biological and Synthetic Materials Used for Carotid Patch Angioplasty. *Journal of Biomechanical Engineering*. 133(11).

Kural, M. H., Cai M., Tang D., Gwyther T., Zheng J., Billiar K. L. (2012) Planar biaxial characterization of diseased human coronary and carotid arteries for computational modeling. *Journal of Biomechanics*. Elsevier, 45(5), 790-798

Mulvihill, J. J., Cunnane, E. M., Mchugh, S. M., Kavanagh, E. G., Walsh, S. R., Walsh, M. T. (2013) Mechanical, biological and structural characterization of in vitro ruptured human carotid plaque tissue. Acta Biomater. 9, 9027-9035.

O'Leary, S. A., Doyle, B. J, Mcgloughlin, T. M. (2014) The impact of long term freezing on the mechanical properties of porcine aortic tissue. J. Mech. Behav. Biomed. Mater. 37, 165-173.

Polzer, S., Gasser, C., Novák, K., Man, V., Tichý, M., Skácel, P., Burša, J. (2015) Structure based constitutive model can accurately predict planar biaxial mechanical properties of aorta wall tissue. Acta Biomater, vol. 14 (1) 133-145.

Roach, M. R.; Burton, A. C. (1957) The reason for the shape of the distensibility curves of arteries. *Can. J. Biochem. Physiol. 35*, 681-690.

Sommer, G., Regitnig, P., Koltringer, L., Holzapfel, G.A. (2009) Biaxial mechanical properties of intact and layer-dissected human carotid arteries at supraphysiological loadings. AJP Hear. Circ. Physiol. 298, H898–H912.

Stary, H. C., 2000. Natural History and Histological Classification of Atherosclerotic Lesions. Aterioscler Thromb Vasc Biol 20, 1177-1178.

E. Appendix

Constitutive models and failure properties of fibrous tissue of carotid artery atheroma based on their uniaxial testing

Original research article.
IF 2.712 (2021)

O. Lisický et al. (2021b). "Constitutive models and failure properties of fibrous tissues of carotid artery atheroma based on their uniaxial testing." In: *Journal of Biomechanics* 129, p. 110861. ISSN: 00219290. DOI: 10.1016/j.jbiomech.2021.110861

Journal of Biomechanics 129 (2021) 110861

Contents lists available at ScienceDirect

Journal of Biomechanics

journal homepage: www.elsevier.com/locate/jbiomech

Constitutive models and failure properties of fibrous tissues of carotid artery atheroma based on their uniaxial testing

Ondřej Lisický [a,*], Anna Hrubanová [a], Robert Staffa [b], Robert Vlachovský [b], Jiří Burša [a]

[a] Institute of Solid Mechanics, Mechatronics and Biomechanics, Brno University of Technology, Czech Republic
[b] 2nd Department of Surgery, St. Anne's University Hospital Brno and Faculty of Medicine, Masaryk University, Brno, Czech Republic

ARTICLE INFO

Keywords:
Atherosclerosis
Carotid artery
Fibrous tissue
Strength
Uniaxial tension

ABSTRACT

To obtain an experimental background for the description of mechanical properties of fibrous tissues of carotid atheroma, a cohort of 141 specimens harvested from 44 patients during endarterectomies, were tested. Uniaxial stress–strain curves and ultimate stress and strain at rupture were recorded. With this cohort, the impact of the direction of load, presence of calcifications, specimen location, patient's age and sex were investigated. A significant impact of sex was revealed for the stress–strain curves and ultimate strains. The response was significantly stiffer for females than for males but, in contrast to ultimate strain, the strength was not significantly different. The differences in strength between calcified and non-calcified atheromas have reached statistical significance in the female group. At most of the analysed stress levels, the loading direction was found significant for the male cohort which was also confirmed by large differences in ultimate strains. The representative uniaxial stress–strain curves (given by median values of strains at chosen stress levels) were fitted with an isotropic hyperelastic model for different groups specified by the investigated factors while the observed differences between circumferential and longitudinal direction were captured by an anisotropic hyperelastic model. The obtained results should be valid also for the tissue of the fibrous cap, the rupture of which is to be predicted in clinics using computational modelling because it may induce arterial thrombosis and consequently a brain stroke.

1. Introduction

Carotid endarterectomy is frequently indicated for severe or symptomatic arterial stenoses (Rothwell et al., 2003). In a case of vulnerable (prone to rupture) atherosclerotic plaques, however, acute events may occur also with moderate stenoses (Saam et al., 2013); assessment of the plaque vulnerability using computational modelling may reduce acute events by a more focused indication to surgery (Holzapfel et al., 2002; Kiousis et al., 2009). The credibility of computational models is contingent on realistic geometrical model considering also appropriate material models for the atherosclerotic plaque components. They are mostly modelled as isotropic (Akyildiz et al., 2011; Teng et al., 2015b) which may be caused by missing direction-dependent experimental results, as well as a lack of structural information on collagen fibre distribution.

Experiments with an autopsy sample of one iliac artery with atheroma divided into eight different components were presented in (Holzapfel et al., 2002). This data was expanded in their subsequent study (Holzapfel et al., 2004) where nine iliac arteries were tested in circumferential and longitudinal directions and fitted with an anisotropic material model. Their results show such a large inter-patient variability that the benefits of such complex division and modelling cannot be proven without comprehensive statistical analyses. However, the majority of studies (Barrett et al., 2009; Chai et al., 2014; Lawlor et al., 2011; Maher et al., 2009; Mulvihill et al., 2013; Teng et al., 2014) investigating the mechanical behaviour of fresh endarterectomy samples were not capable to divide the tissue into such a large number of components. In contrast, most authors tested only a single circumferential specimen from each patient. Information on the mechanical behaviour of the carotid artery appeared recently in (O'Reilly et al., 2020) where the authors used non-calcified samples for uniaxial tension testing in longitudinal and circumferential directions. Otherwise, only inverse FE analyses of indentation tests (Barrett et al., 2009; Chai et al., 2014) were performed. Therefore, a very limited number of studies are available to assess tissue anisotropy. Moreover, most of the presented comparisons of different plaque or wall components are based on a

* Corresponding author.
E-mail address: 161238@vutbr.cz (O. Lisický).

https://doi.org/10.1016/j.jbiomech.2021.110861
Accepted 1 November 2021
Available online 9 November 2021

single parameter, e.g. initial modulus (Chai et al., 2014; Hoffman et al., 2017) which cannot describe the nonlinear behaviour of the tissue (Kamenskiy et al., 2011; Teng et al., 2014). The review (Akyildiz et al., 2014) showed high variation among many of experimental studies focused on the mechanical response of atherosclerotic plaques in different arteries.

Structural data from electron microscopy in (Mulvihill et al., 2013) helped to show a significant relationship between the presence of calcifications and the stress/stretch values at rupture. Preoperative ultrasound can also help to divide endarterectomy samples into groups as shown in (Maher et al., 2009) with the stiffest compressive behaviour for the calcified cohort. A thorough study of the carotid plaque components important in preoperative diagnosis (Teng et al., 2014) has shown that media behaviour is comparable with the fibrous cap while being significantly different from that of the tissue with intraplaque haemorrhage. These results indicate that the description of atherosclerotic plaque in biomechanical studies may be improved using suitable constitutive models with parameters based on criteria disposable *in vivo,* as shown also in (Lisický et al., 2020).

The tissue strength of 300 kPa is often used as decisive for possible plaque failure and was thoroughly discussed in the review (Holzapfel et al., 2014) where the authors confirmed a lack of information on the ultimate stresses and strains of carotid plaques needed for biomechanical analyses. Fracture stress and strain in circumferential direction were presented in (Lawlor et al., 2011), similarly to (Teng et al., 2015a) which focused on the ultimate values of various components of carotid plaque; however, almost half of the samples were not included due to limitations of the used testing device. Results of planar tension tests with whole carotid plaques presented in (Cunnane et al., 2016) are hardly comparable due to the plaque non-homogeneity and more complex state of stress in planar tension.

The objective of this study is to obtain uniaxial stress–strain curves, including ultimate stress (strength) and strain of fibrous tissue of carotid atherosclerotic plaque and to investigate the influence of parameters detectable *in vivo* such as sex, patient's age, presence of calcifications, specimen location, and loading direction. Differences in the stress–strain characteristics are investigated at various stress levels to consider nonlinearity and asymmetric dispersion of the responses.

2. Material and methods

2.1. Sample preparation and testing

Samples of atheroma in carotid bifurcation were harvested during standard endarterectomy in St. Anne's University Hospital in Brno with the written informed consent of the patients; the study was approved by the local ethics committee. In total, 44 samples were used: 12 females (age 70.22 ± 5.27) and 32 males (70.52 ± 8.19). The samples were tested either fresh, directly after the intervention, or kept frozen at −20 °C in saline solution (0.9 % NaCl) (Ebenstein et al., 2009; Walsh et al., 2014) until testing. Before testing, the samples were heated in the saline solution to 37 °C (>30 min) and kept like this during the whole testing process. Surgical tools were used to cut out rectangular specimens 2 to 3 mm wide keeping their proper width to length ratio (Mulvihill and Walsh, 2013). The specimen thickness was averaged from measurements in 3 positions using a mechanical thickness gauge (distance indicator) with the accuracy of 0.01 mm under constant contact force of 0.18 N.

Uniaxial tension tests were performed using a tensile tester (Camea s.r.o., Czech Republic) equipped with a 20 N load cell with 0.1 % accuracy and pre-tension of 0.01 N was applied to straighten the specimen. Force and positions of four markers were recorded using a CCD camera for off-line calculation of engineering strains and stresses; their ultimate values were taken from the highest point of the stress–strain characteristic denoting the tissue fracture.

The specimens were divided into several complementary pairs of groups based on specimen orientation, sex of the donor, presence of calcifications, harvest location (near or out of lipid core) and donor age. The specimens with macro-calcifications (occurring very often for severe endarterectomy plaques) detectable by sample palpation were included in the calcified group while all the others were taken as non-calcified.

2.2. Data processing

To compare the non-linear responses of the tissues in their whole range, each stress–strain dependence was interpolated using a cubic B-spline. As proposed in (Lisický et al., 2021), the responses were averaged at specific stress-levels stepped by 10 kPa and – considering the asymmetry of data distribution – represented by strain medians as illustrated in Fig. 1.

2.3. Constitutive modelling

The fitting procedure was performed in Hyperfit (BUT, Czech Republic, http://www.hyperfit.wz.cz/) using Levenberg-Marquardt optimization algorithm maximizing the coefficient of determination R^2. Average circumferential and longitudinal responses were characterized by the following anisotropic strain-energy density function (SEDF) (Holzapfel et al., 2005):

$$\Psi = \Psi_{iso} + \Psi_{aniso} = \mu(I_1 - 3) + \frac{k_1}{2k_2}\left(e^{k_2(1-\rho)(I_1-3)^2+\rho(I_4-1)^2} - 1\right) \quad (1)$$

where μ, k_1 and k_2 are (positive) model parameters, $I_1 = \lambda_r^2 + \lambda_\theta^2 + \lambda_z^2$ and $I_4 = \lambda_\theta^2 cos^2\varphi + \lambda_z^2 sin^2\varphi$ are invariants of the right Cauchy-Green deformation tensor **C** (I_4 related to stretches of two symmetric fibre families), $\rho < 0;1 >$ is concentration parameter representing "degree of anisotropy", and ± φ denotes the angle between each fibre family and the circumferential direction.

The responses were also fitted with isotropic 3rd order incompressible Yeoh constitutive model used frequently for arterial tissues (Lawlor et al., 2011; O'Reilly et al., 2020) with the following SEDF:

$$\psi = \sum_{i=1}^{3} c_{i0}(I_1 - 3)^i \quad (2)$$

Here c_{i0} are stress-like material parameters.

2.4. Statistical analysis

Statistical analyses were performed using Minitab. The size of some samples enabled testing of several specimens, therefore a unique ID matching for specimens from each donor was used. It represented a random factor in the linear mixed-effect model (Brauer and Curtin, 2018) used to investigate the statistical significance of multiple factors on the results (strains at each evaluated stress-level, ultimate stress and strain), as well as interactions. The normal distribution of data and model residues was tested using the Shapiro-Wilk test. Significance of correlation between ultimate values and thickness (i.e., invasively evaluated parameters) was tested for each group using the Spearman correlation test; statistical significance was assumed if $p < 0.05$.

3. Results

In total, 141 specimens from 44 patients were collected and tested successfully. In general, the responses show a highly non-linear behaviour with a pronounced strain stiffening. Summary tables about the compared cohorts are available as a supplementary data. Groups in the complementary pairs showed comparable sizes except for sex. A random selection of the male samples performed to equalize the cohorts for comparison resulted in 42 male specimens (median thickness 0.98 mm)

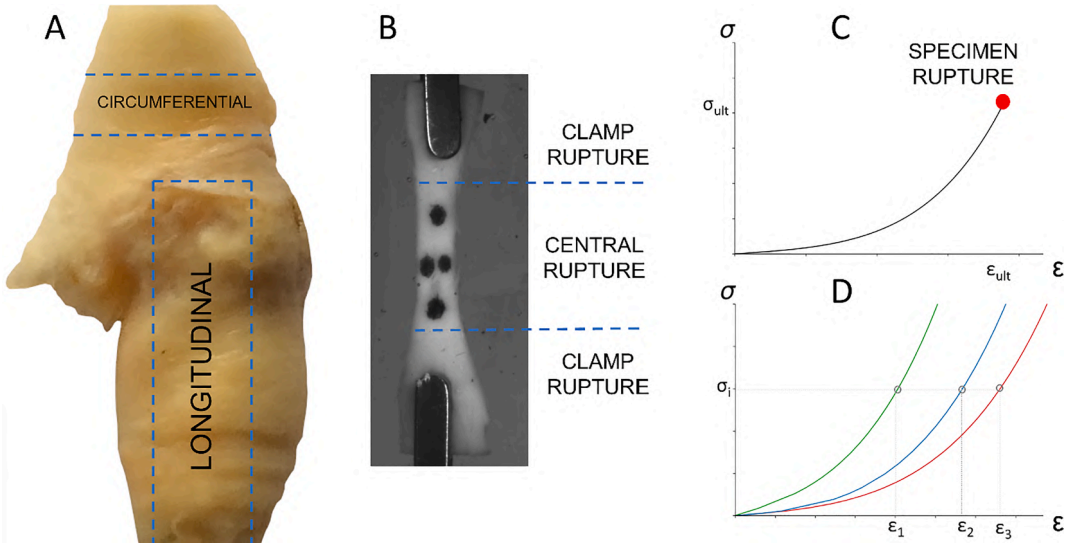

Fig. 1. Uniaxial tension tests. (A) Scheme of cutting the specimens for uniaxial tension testing from the endarterectomy samples. (B) Four markers were used to track the specimen deformation. Central rupture refers to sample fracture in the middle (unaffected) region of the specimen while clamp rupture denotes fracture near the clamps. (C) Ultimate values were recorded at specimen rupture. (D) The representative curves were obtained from median values of strains under chosen levels of stresses.

vs. 30 female specimens (median thickness 0.87 mm). In a separate investigation of these two cohorts the equalization is no longer needed, thus all specimens were used. Lipids with calcifications, inappropriate for testing, were removed from the specimens while the remaining calcifications, fixed firmly to the adjacent tissue, were left to avoid damage of the tissue.

3.1. Ultimate stress/strain

Statistically significant differences in ultimate strains were found between the female and male cohort (0.12 versus 0.19) while ultimate stresses were found comparable (0.307 versus 0.369 MPa). Fig. 2 presents results as box plots of the analysed factors separately for female and male cohorts. No factor was found significant for ultimate stress in males. However, the presence of the calcified tissue influenced the results significantly in females with the median of 0.25 MPa versus 0.335 MPa for tissue without calcifications. In the case of ultimate strains, the female cohort did not show any statistically significant factor while the loading direction was found significant for males. Here, longitudinal ultimate strains were lower compared to circumferential (0.16 versus 0.21).

Fractures occurred either near the clamps or in the central region of the specimen. Ultimate values for fracture at the centre (median thickness 1.1 mm) and near the clamp (median thickness 0.93 mm) were comparable (median stresses 0.351 vs. 0.374 MPa and median strains 0.17 vs. 0.16); thus rupture location was not considered in dividing the results into groups. Age (50–70 vs. 70–90 years) and specimen location (near the lipid core vs. out of the lipid core) have never shown statistical significance. Correlations between thickness and the corresponding ultimate values were found significant in the following cases: for females it was strain at the age group 50–70 (correlation coefficient $r_s = -0.46$, $p = 0.04$) and in the non-calcified group ($r_s = -0.53$, $p = 0.02$), while for the male cohort it was stress and strain at the age group 50–70 ($r_s = -0.3$, $p = 0.04$ and $r_s = -0.42$, $p = 0.003$, respectively) and stress ($r_s = -0.3$, $p = 0.02$) in the circumferential direction.

3.2. Stress–strain responses

Statistically significant or nearly significant differences were found at almost all stress-levels between females and males. Fig. 3 shows experimental responses with their median representations; it is evident that the female specimens correspond to the stiffest male specimens (with three exceptions of very compliant curves). This difference corresponds to their lower ultimate strains as indicated above. Corresponding material parameters are summarized in Table 1 where most of the model fits showed $R^2 \geq 0.90$.

The analysis of specific factors, performed for female and male cohort separately, showed responses without significant differences. However, significant anisotropy (influence of direction) was found in the men cohort at almost all stress-levels, except for initial values as indicated in Fig. 4. This is confirmed also by parameters of the anisotropic constitutive model in Table 2 with concentration parameter ρ being close to maximum and minimum for male and female groups, respectively. An overall comparison of the resulting responses is presented in Fig. 5.

4. Discussion

The presented study exploits samples of fibrous tissue harvested during carotid endarterectomy to quantify not only ultimate stresses and strains but all the stress–strain characteristics. These characteristics are important for its constitutive modelling and prediction of plaque rupture risk based on a comparison of the calculated stresses with the tissue strength (Holzapfel et al., 2014).

4.1. Strength

(Cilla et al., 2012) proposed a vulnerability factor based on a comparison of the maximum computed stresses with a critical value of 0.247 MPa referred to the experimental study (Loree et al., 1994). Other studies used often the threshold value of 0.3 MPa, which was thoroughly discussed in (Holzapfel et al., 2014). Our results showed a statistically significant difference only for calcified specimens (0.25 vs 0.335 MPa) in the case of the female cohort. Otherwise, comparable behaviour was found for the investigated factors (patient sex, age, loading direction, specimen location), together with their interactions. Moreover, the insignificance of rupture location (near the clamp or central location) confirmed the finding in (Cunnane et al., 2016). Most groups revealed ultimate stresses higher than the most used value of 0.3 MPa and even the value 0.247 MPa which might be relevant for calcified female sample, show thus a need for a more thorough investigation of possible influencing factors as done in our study. Comparable high results were

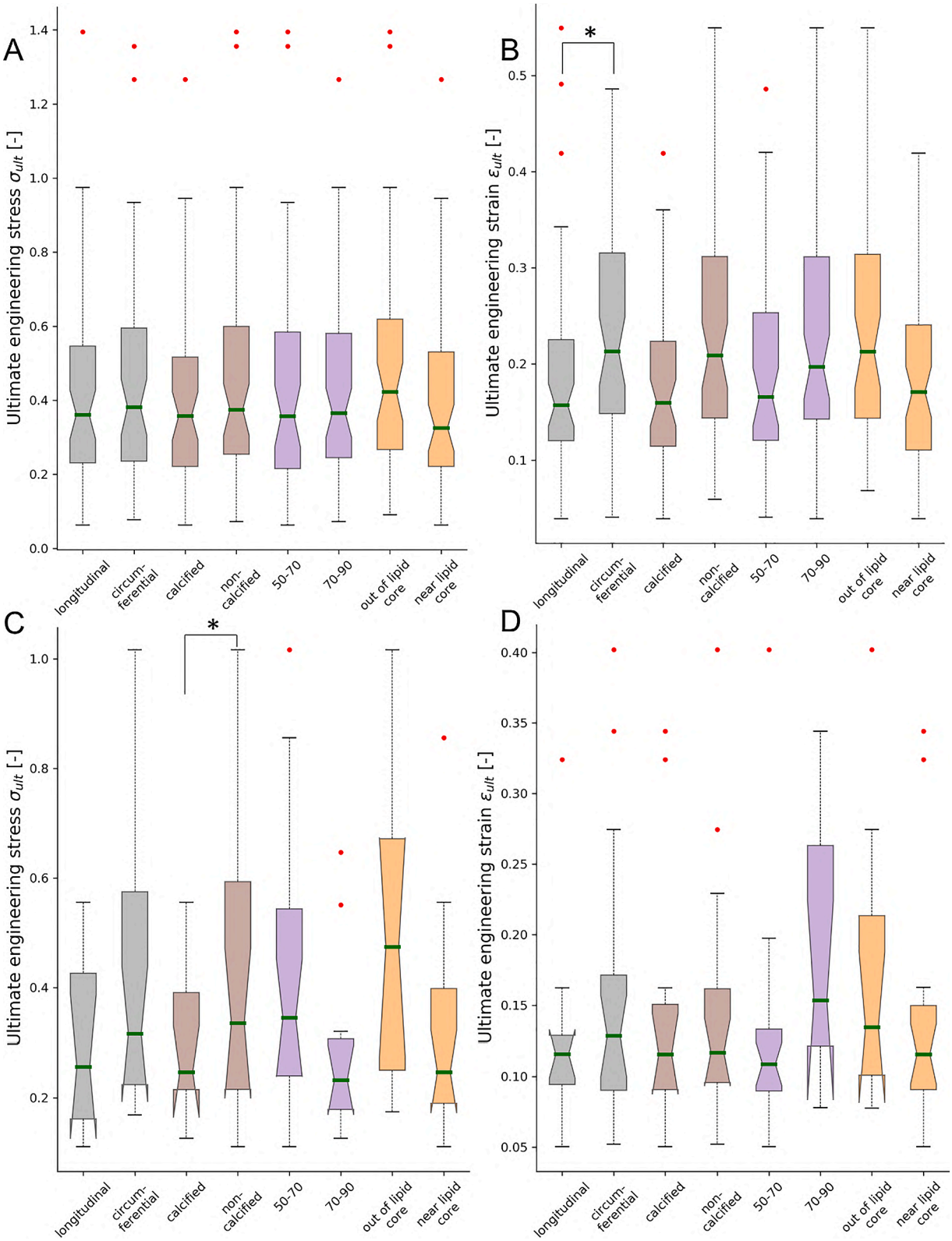

Fig. 2. Comparison of ultimate stresses (left column) and strains (right column). (A-B) represent males while (C-D) females. Data point was marked as outlier if being>1.5*IQR above the third quartile (or below the second quartile). Asterisk denotes $p < 0.05$.

found in (Lawlor et al., 2011) where the circumferential samples showed mean ultimate (Cauchy) stresses of 0.367 MPa. Teng *et al.* (Teng et al., 2015a) found statistically insignificant differences between ultimate strength for fibrous cap (median 158.3 kPa) and fibrous tissue (median 247.6 kPa) tested only in the circumferential direction. These values are significantly lower than most other results; the authors admit their ultimate values are underestimated because higher ultimate stresses could not be recorded due to frequent sliding of samples from the jaws. In (Cunnane et al., 2016), whole carotid atheromas, tested in planar extension, resulted in the strength of 0.49 MPa, supporting our outputs

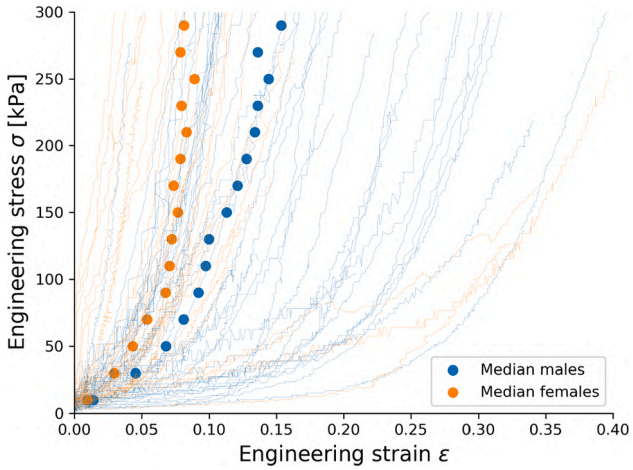

Fig. 3. Stress–strain curves for randomly selected male (blue) specimens and female (orange) specimens with median response at specific stress levels (stepped by 20 kPa in the figure).

Table 1
Material parameters [kPa] for isotropic Yeoh model. EG stands for randomly equalized sex cohort. Afterwards, the first row (also highlighted in grey backgrounds) and second row of each factor represent models for females and males, respectively.

	factor	c_{10}	c_{20}	c_{30}
EG	female	82.03	6147.4	170111.34
	male	91.14	2137.18	0.00
Sex-separated cohort	Ca	199.16	5404.39	0.00
		112.96	2053.05	0.00
	NO Ca	100.00	9268.65	50.00
		20.00	1578.29	0.00
	50–70 old	106.09	1000.00	799600.81
		65.93	2553.98	0.00
	70–90 old	100.00	4605.76	0.00
		51.43	824.12	5135.79
	near lipid core	234.55	7067.65	0.00
		110.41	1299.04	0.00
	out of lipid core	178.91	6071.77	0.00
		97.66	71.28	13118.44

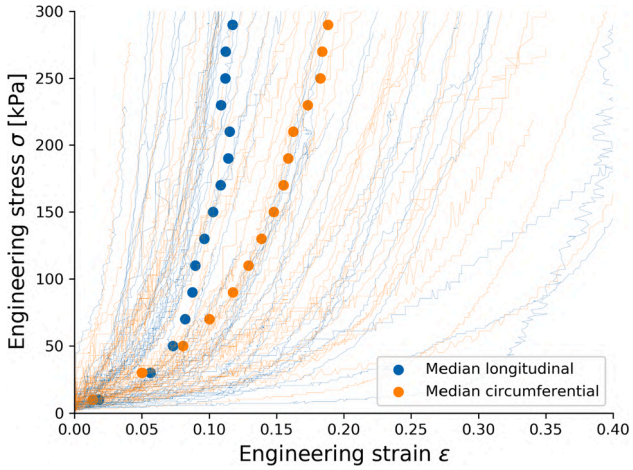

Fig. 4. Stress–strain curves in longitudinal (blue) and circumferential (orange) directions for each specimen in the male group with median responses at specific stress levels (stepped by 20 kPa in the figure).

Table 2
Material parameters for anisotropic model (Holzapfel et al., 2005).

	μ [kPa]	k_1 [kPa]	k_2 [kPa]	ϕ [rad]	ρ [-]
female	105.900	8084.160	0.100	0.776	0.500
male	113.000	559.560	1311.510	0.850	0.906

that the rupture threshold for analyses should be based on as much sample information as possible. Although the tissue strength dominates in the prediction of the plaque rupture, also other factors were proposed recently (Davis et al., 2016).

4.2. Ultimate strains

Although ultimate strains give similar information on failure and are less dependent on constitutive models, they are seldom used for evaluating plaque vulnerability. The significant difference between female and male specimens is an important finding evidenced here for the first time. The earlier stiffening of female tissue might be connected with overall lower dimensions of the plaques and thus be of interest for lowering *peri*-operative risk during carotid artery stenting (Barrett et al., 2017).

From all the investigated factors only loading direction revealed significant differences for the male group. Surprisingly, although our median ultimate stress value was comparable with the study (Lawlor et al., 2011), it was not paralleled in ultimate strains where their results showed much higher values with the mean of 0.49 vs. our median of 0.2 (for the female even smaller) in the circumferential direction. This contradiction is related to the very flat characteristics without stiffening in (Lawlor et al., 2011) but also in e.g. (Barrett et al., 2017; Mulvihill et al., 2013) for carotid samples based on planar tension test of the whole very complex plaques showing ultimate stretches up to 2. Our results are supported by comparable ultimate strains found in (Teng et al., 2015a) for the circumferential direction; their median values of 0.18 for fibrous cap and 0.21 for fibrous tissue are close to our value of 0.2. All these results are much higher than *in vivo* strains in a carotid artery with their typical value of c. 5% see (Nederveen et al., 2014). These contradictions should not be overlooked as they might have fatal consequences for designing patient-specific tools.

It was shown that mechanical properties of the fibrous cap are comparable with the fibrous tissue (Teng et al., 2015a, 2014) and both are mostly modelled using the same constitutive model. Our study has shown the significant correlation of the specimen thickness with its ultimate stresses and strains for some of the investigated groups. All these cases showed negative correlation indicating increasing ultimate values with lower specimen thickness matching also the findings for aortic aneurysm tissue (Polzer et al., 2021). In atherosclerotic arteries, this effect may be related to higher portion of soft fatty tissue in thicker specimens.

4.3. Stress strain curves

Differences with sex are quite common in biomechanics (Tong et al., 2013) and often lead to different treatment, e.g. for abdominal aortic aneurysm (Moll et al., 2011); this was confirmed in our study of atherosclerotic tissue at almost all tested stress levels for the first time. Our results show stiffer average responses for females which might be related to size differences between males and females.

Although some female samples showed high differences between circumferential and longitudinal specimens, it was not confirmed as global trend and the average responses were statistically comparable. However, the male cohort showed significant differences (see Fig. 4). This discrepancy may be related to the underlying collagen structure; a few available studies show large variability of collagen arrangement (Akyildiz et al., 2017; Pagiatakis et al., 2015). Insignificancy of loading direction was found e.g. in (O'Reilly et al., 2020); however, it cannot be

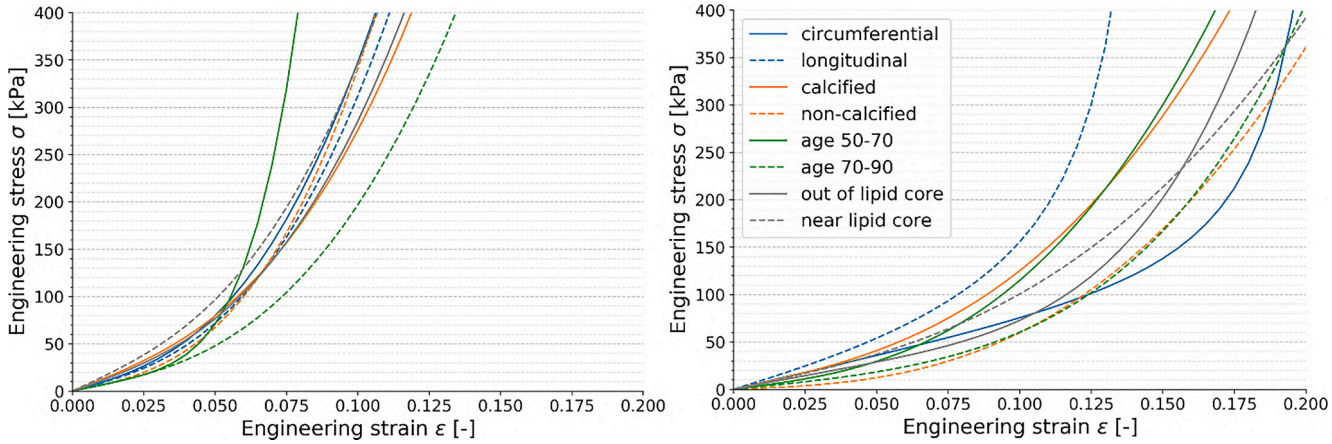

Fig. 5. Stress–strain responses of the anisotropic model (blue) and isotropic model to medians of strains at each level of stress for all groups of females (left) and males (right).

directly compared with our results due to a completely different methodology of that study (stress relaxation at almost ultimate strains or subsequent tension testing at room temperature). Moreover, the resulting average curves are presented in a limited strain range where the behaviour appears rather linear while the authors mention a highly non-linear behaviour probably similar to our male group.

Calcifications are hypothesised as an important factor for mechanical rupture of the fibrous cap (Barrett et al., 2019) but the evidence is still highly needed. As even *in vivo* imaging enables us to detect highly calcified areas it can be reasonable to aim at global representations, as presented in this study by calcified and non-calcified specimen, even if done by simple tissue palpation. Therefore, it is recommended to include this factor in further studies, while focusing on possible correlations of *ex vivo* indicators with the clinical practice (Barrett et al., 2019, 2017; Mulvihill et al., 2013).

In our statistical analysis, we focused on factors available *in vivo*. Statistical significance of most of them was not confirmed, only the revealed significant differences in responses between males and females can enable one to use the much stiffer constitutive model for females. The multiple point approach (Akyildiz et al., 2014; Lisický et al., 2021; Teng et al., 2014) gives much more focused information on the experimental data. In contrast, a comparison of single-point values like initial stiffness used in (Hoffman et al., 2017) or final tangential stiffness cannot sufficiently describe the non-linear behaviour of soft fibrous tissue and may lead to misinterpretation.

4.4. Study limitations

The size of most samples disabled testing of standard dog-bone specimens; however, the negligible difference in strength between specimens ruptured in the central and clamp regions (see 3.1) negate the influence of specimen clamping on the rupture while the rupture location is probably governed by tissue non-homogeneity. Some responses terminate earlier and thus the calculated representatives at higher stress levels tend stepwise to stiffer behaviour with subsequent termination of more compliant curves (visible at stress levels above 220 kPa, see Fig. 4, longitudinal direction). Such effect is physically unrealistic and cannot be captured with any constitutive model. However, most of curves covered whole physiological range of stresses. Preservation of arterial tissues at −20 °C does not change their mechanical response significantly (Ebenstein et al., 2009; Walsh et al., 2014). Also the assumption on tissue incompressibility is commonly applied although, slight compressibility may exist at arterial tissue (Skacel and Bursa, 2019). As only a few samples (n = 9) were large enough for cutting standard dog-bone specimens, rectangular specimens were used; this might reduce the ultimate stresses due to rupture near the clamps but this influence was shown to be small (<1 % difference between the median clamp and central rupture stress). The amount of media in the specimen was not specified histologically which may increase the dispersion of the results. Although the detection of calcifications by tissue palpation is inaccurate, it can still bring important insight to this not well-explored area, because the endarterectomy samples revealed large groupings rather than areas of micro-calcification, being more common for earlier stages of atherosclerosis (Stary, 2000). Generally, as tissue rupture is a local event, it may be influenced by non-homogeneity of the atherosclerotic artery. In contrast, the comparisons should not be significantly influenced by a missing pre-conditioning process, which was avoided due to the high dispersion of ultimate values of the investigated tissues and a consequent risk of specimen damage even under lower pre-conditioning loads. Finally, it is important to note that our study population included only voluntary donors from a single hospital who provided the written informed consent. It will be therefore important to confirm our findings also with another cohort to provide general conclusions.

5. Conclusion

To the best of the authors' knowledge, this is the first experimental study of the atherosclerotic fibrous tissue comparing ultimate stresses and strains together with the non-linear stress–strain response of longitudinal and circumferential specimens. Analysis of several factors aims at reduction of the dispersion of constitutive models and ultimate values which cannot be patient-specific in the prediction of atheroma vulnerability and rely thus on the most probable outcomes for population or a specific group. Significant differences were found between females and males in ultimate strain and in the stress–strain curves, which were much steeper (showing a stiffer response) at females (median strain value at 360 kPa stress was < 0.1) than at males (median strain value at 360 kPa stress was > 0.15). When investigating the male group separately, significant differences were also confirmed between the loading directions (for ultimate stresses and whole average responses) while the average responses were comparable for the female group. Our results enable us to use these more specific constitutive models and limit values in the prediction of fibrous cap rupture with sex as simple in vivo predictors. Comparable responses in circumferential and longitudinal directions for females might support the application of isotropic models preferred commonly in computational modelling of atheromas, while the significant differences for male indicate the need for anisotropic modelling.

CRediT authorship contribution statement

Ondřej Lisický: Conceptualization, Methodology, Software, Formal

analysis, Investigation, Writing - Original Draft, Writing - Review & Editing, Visualization. **Anna Hrubanová:** Methodology, Investigation. **Robert Staffa:** Resources, Funding acquisition. **Robert Vlachovský:** Resources, Funding acquisition. **Jiří Burša:** Formal analysis, Writing - Review & Editing, Supervision, Funding acquisition.

Declaration of Competing Interest

The authors declare that they have no known competing financial interests or personal relationships that could have appeared to influence the work reported in this paper.

Acknowledgement

This work was supported by Czech Science Foundation project No. 18-13663S.

Appendix A. Supplementary material

Supplementary data to this article can be found online at https://doi.org/10.1016/j.jbiomech.2021.110861.

References

Akyildiz, A.C., Chai, C.-K., Oomens, C.W.J., van der Lugt, A., Baaijens, F.P.T., Strijkers, G.J., Gijsen, F.J.H., 2017. 3D Fiber orientation in atherosclerotic carotid plaques. J. Struct. Biol. 200 (1), 28–35. https://doi.org/10.1016/j.jsb:2017.08.003.

Akyildiz, A.C., Speelman, L., Gijsen, F.J.H., 2014. Mechanical properties of human atherosclerotic intima tissue. J. Biomech. 47 (4), 773–783. https://doi.org/10.1016/j.jbiomech.2014.01.019.

Akyildiz, A.C., Speelman, L., van Brummelen, H., Gutiérrez, M.A., Virmani, R., van der Lugt, A., van der Steen, A.F.W., Wentzel, J.J., Gijsen, F.J.H., 2011. Effects of intima stiffness and plaque morphology on peak cap stress. Biomed. Eng. Online 10, 1–13. https://doi.org/10.1186/1475-925X-10-25.

Barrett, H.E., Cunnane, E.M., Hidayat, H., O Brien, J.M., Kavanagh, E.G., Walsh, M.T., 2017. Calcification Volume Reduces Stretch Capability and Predisposes Plaque to Rupture in an in vitro Model of Carotid Artery Stenting. Eur. J. Vasc. Endovasc. Surg. 54 (4), 431–438. https://doi.org/10.1016/j.ejvs.2017.07.022.

Barrett, H.E., Van der Heiden, K., Farrell, E., Gijsen, F.J.H., Akyildiz, A.C., 2019. Calcifications in atherosclerotic plaques and impact on plaque biomechanics. J. Biomech. 87, 1–12. https://doi.org/10.1016/j.jbiomech.2019.03.005.

Barrett, S.R.H., Sutcliffe, M.P.F., Howarth, S., Li, Z–Y., Gillard, J.H., 2009. Experimental measurement of the mechanical properties of carotid atherothrombotic plaque fibrous cap. J. Biomech. 42 (11), 1650–1655. https://doi.org/10.1016/j.jbiomech.2009.04.025.

Brauer, M., Curtin, J.J., 2018. Linear mixed-effects models and the analysis of nonindependent data: A unified framework to analyze categorical and continuous independent variables that vary within-subjects and/or within-items. Psychol. Methods 23, 389–411. https://doi.org/10.1037/met0000159.

Chai, C.K., Akyildiz, A.C., Speelman, L., Gijsen, F.J.H., Oomens, C.W.J., van Sambeek, M. R.H.M., van der Lugt, A., Baaijens, F.P.T., 2014. Local axial compressive mechanical properties of human carotid atherosclerotic plaques—characterisation by indentation test and inverse finite element analysis. J. Mech. Behav. Biomed. Mater. 43, 59–68. https://doi.org/10.1016/j.jmbbm.2014.12.004.

Cilla, M., Peña, E., Martínez, M.A., 2012. 3D computational parametric analysis of eccentric atheroma plaque: influence of axial and circumferential residual stresses. Biomech. Model. Mechanobiol. 11 (7), 1001–1013. https://doi.org/10.1007/s10237-011-0369-0.

Cunnane, E.M., Mulvihill, J.J.E., Barrett, H.E., Hennessy, M.M., Kavanagh, E.G., Walsh, M.T., 2016. Mechanical properties and composition of carotid and femoral atherosclerotic plaques: a comparative study. J. Biomech. 49 (15), 3697–3704. https://doi.org/10.1016/j.jbiomech.2016.09.036.

Davis, L.A., Stewart, S.E., Carsten, C.G., Snyder, B.A., Sutton, M.A., Lessner, S.M., 2016. Characterization of fracture behavior of human atherosclerotic fibrous caps using a miniature single edge notched tensile test. Acta Biomater. 43, 101–111. https://doi.org/10.1016/j.actbio.2016.07.027.

Ebenstein, D.M., Coughlin, D., Chapman, J., Li, C., Pruitt, L.A., 2009. Nanomechanical properties of calcification, fibrous tissue, and hematoma from atherosclerotic plaques. J. Biomed. Mater. Res. - Part A 91A (4), 1028–1037. https://doi.org/10.1002/jbm.a.v91a:410.1002/jbm.a.32321.

Hoffman, A.H., Teng, Z., Zheng, J., Wu, Z., Woodard, P.K., Billiar, K.L., Wang, L., Tang, D., 2017. Stiffness properties of adventitia, media, and Full thickness human atherosclerotic carotid arteries in the axial and circumferential directions. J. Biomech. Eng. 139, 124501 https://doi.org/10.1115/1.4037794.

Holzapfel, G.A., Mulvihill, J.J., Cunnane, E.M., Walsh, M.T., 2014. Computational approaches for analyzing the mechanics of atherosclerotic plaques: a review. J. Biomech. 47 (4), 859–869. https://doi.org/10.1016/j.jbiomech.2014.01.011.

Holzapfel, G.A., Sommer, G., Gasser, C.T., Regitnig, P., 2005. Determination of layer-specific mechanical properties of human coronary arteries with nonatherosclerotic intimal thickening and related constitutive modeling. J Physiol Hear. Circ Physiol 289 (5), H2048–H2058. https://doi.org/10.1152/ajpheart.00934.2004.

Holzapfel, G.A., Sommer, G., Regitnig, P., 2004. Anisotropic mechanical properties of tissue Components in human atherosclerotic plaques. J. Biomech. Eng. 126, 657. https://doi.org/10.1016/0025-5408(88)90092-X.

Holzapfel, G.A., Stadler, M., Schulze-Bauer, C.A.J., 2002. A layer-specific three-dimensional model for the simulation of balloon angioplasty using magnetic resonance imaging and mechanical testing. Ann. Biomed. Eng. 30 (6), 753–767. https://doi.org/10.1114/1.1492812.

Kamenskiy, A.V., Pipinos, I.I., MacTaggart, J.N., Jaffar Kazmi, S.A., Dzenis, Y.A., 2011. Comparative analysis of the biaxial mechanical behavior of carotid Wall tissue and biological and synthetic materials used for carotid patch angioplasty. J. Biomech. Eng. 133, 111008 https://doi.org/10.1115/1.4005434.

Kiousis, D.E., Rubinigg, S.F., Auer, M., Holzapfel, G.A., 2009. A Methodology to Analyze Changes in Lipid Core and Calcification Onto Fibrous Cap Vulnerability: the human atherosclerotic carotid bifurcation as an illustratory example. J. Biomech. Eng. 131, 121002 https://doi.org/10.1115/1.4000078.

Lawlor, M.G., O'Donnell, M.R., O'Connell, B.M., Walsh, M.T., 2011. Experimental determination of circumferential properties of fresh carotid artery plaques. J. Biomech. 44 (9), 1709–1715. https://doi.org/10.1016/j.jbiomech.2011.03.033.

Lisický, O., Hrubanová, A., Bursa, J., 2021. Interpretation of experimental data is substantial for constitutive characterization of arterial tissue. J. Biomech. Eng. doi 10 (1115/1), 4051120.

Lisický, O., Malá, A., Bednařík, Z., Novotný, T., Burša, J., Tian, F.-B., 2020. Consideration of stiffness of wall layers is decisive for patient-specific analysis of carotid artery with atheroma. PLoS One 15 (9), e0239447. https://doi.org/10.1371/journal.pone.0239447.

Loree, H.M., Grodzinsky, A.J., Park, S.Y., Gibson, L.J., Lee, R.T., 1994. Static circumferential tangential modulus Of human atherosclerotic tissue. J. Biomech. 27 (2), 195–204.

Maher, E., Creane, A., Sultan, S., Hynes, N., Lally, C., Kelly, D.J., 2009. Tensile and compressive properties of fresh human carotid atherosclerotic plaques. J. Biomech. 42 (16), 2760–2767. https://doi.org/10.1016/j.jbiomech.2009.07.032.

Moll, F.L., Powell, J.T., Fraedrich, G., Verzini, F., Haulon, S., Waltham, M., van Herwaarden, J.A., Holt, P.J.E., van Keulen, J.W., Rantner, B., Schlösser, F.J.V., Setacci, F., Ricco, J.-B., 2011. Management of abdominal aortic aneurysms clinical practice guidelines of the european society for vascular surgery. Eur. J. Vasc. Endovasc. Surg. 41, S1–S58. https://doi.org/10.1016/j.ejvs.2010.09.011.

Mulvihill, J.J., Cunnane, E.M., McHugh, S.M., Kavanagh, E.G., Walsh, S.R., Walsh, M.T., 2013. Mechanical, biological and structural characterization of in vitro ruptured human carotid plaque tissue. Acta Biomater. 9 (11), 9027–9035. https://doi.org/10.1016/j.actbio.2013.07.012.

Mulvihill, J.J., Walsh, M.T., 2013. On the mechanical behaviour of carotid artery plaques: the influence of curve-fitting experimental data on numerical model results. Biomech. Model. Mechanobiol. 12 (5), 975–985. https://doi.org/10.1007/s10237-012-0457-9.

Nederveen, A.J., Avril, S., Speelman, L., 2014. MRI strain imaging of the carotid artery: present limitations and future challenges. J. Biomech. 47 (4), 824–833. https://doi.org/10.1016/j.jbiomech.2014.01.014.

O'Reilly, B.L., Hynes, N., Sultan, S., McHugh, P.E., McGarry, J.P., 2020. An experimental and computational investigation of the material behaviour of discrete homogenous iliofemoral and carotid atherosclerotic plaque constituents. J. Biomech. 106, 109801. https://doi.org/10.1016/j.jbiomech.2020.109801.

Pagiatakis, C., Galaz, R., Tardif, J.-C., Mongrain, R., 2015. A comparison between the principal stress direction and collagen fiber orientation in coronary atherosclerotic plaque fibrous caps. Med. Biol. Eng. Comput. 53 (6), 545–555. https://doi.org/10.1007/s11517-015-1257-z.

Polzer, S., Man, V., Vlachovský, R., Kubíček, L., Kracík, J., Staffa, R., Novotný, T., Burša, J., Raghavan, M.L., 2021. Failure properties of abdominal aortic aneurysm tissue are orientation dependent. J. Mech. Behav. Biomed. Mater. 114, 104181. https://doi.org/10.1016/j.jmbbm.2020.104181.

Rothwell, P.M., Gutnikov, S.A., Warlow, C.P., 2003. Reanalysis of the final results of the european carotid surgery trial. Stroke 34 (2), 514–523. https://doi.org/10.1161/01.STR.0000054671.71777.C7.

Saam, T., Hetterich, H., Hoffmann, V., Yuan, C., Dichgans, M., Poppert, H., Koeppel, T., Hoffmann, U., Reiser, M.F., Bamberg, F., 2013. Meta-analysis and systematic review of the predictive value of carotid plaque hemorrhage on cerebrovascular events by magnetic resonance imaging. J. Am. Coll. Cardiol. 62 (12), 1081–1091. https://doi.org/10.1016/j.jacc.2013.06.015.

Skacel, P., Bursa, J., 2019. Compressibility of arterial wall – Direct measurement and predictions of compressible constitutive models. J. Mech. Behav. Biomed. Mater. 90, 538–546. https://doi.org/10.1016/j.jmbbm.2018.11.004.

Stary, H.C., 2000. Natural history and histological classification of atherosclerotic lesions. Aterioscler Thromb Vasc Biol 20 (5), 1177–1178.

Teng, Z., Feng, J., Zhang, Y., Sutcliffe, M.P.F., Huang, Y., Brown, A.J., Jing, Z., Lu, Q., Gillard, J.H., 2015a. A uni-extension study on the ultimate material strength and extreme extensibility of atherosclerotic tissue in human carotid plaques. J. Biomech. 48 (14), 3859–3867. https://doi.org/10.1016/j.jbiomech.2015.09.037.

Teng, Z., Yuan, J., Feng, J., Zhang, Y., Brown, A.J., Wang, S., Lu, Q., Gillard, J.H., 2015b. The influence of constitutive law choice used to characterise atherosclerotic tissue material properties on computing stress values in human carotid plaques. J. Biomech. 48 (14), 3912–3921. https://doi.org/10.1016/j.jbiomech.2015.09.023.

Teng, Z., Zhang, Y., Huang, Y., Feng, J., Yuan, J., Lu, Q., Sutcliffe, M.P.F., Brown, A.J., Jing, Z., Gillard, J.H., 2014. Material properties of components in human carotid

atherosclerotic plaques: a uniaxial extension study. Acta Biomater. 10 (12), 5055–5063. https://doi.org/10.1016/j.actbio.2014.09.001.

Tong, J., Schriefl, A.J., Cohnert, T., Holzapfel, G.A., 2013. Gender differences in biomechanical properties, thrombus age, mass fraction and clinical factors of abdominal aortic aneurysms. Eur. J. Vasc. Endovasc. Surg. 45 (4), 364–372. https://doi.org/10.1016/j.ejvs.2013.01.003.

Walsh, M.T., Cunnane, E.M., Mulvihill, J.J., Akyildiz, A.C., Gijsen, F.J.H., Holzapfel, G. A., 2014. Uniaxial tensile testing approaches for characterisation of atherosclerotic plaques. J. Biomech. 47 (4), 793–804. https://doi.org/10.1016/j.jbiomech.2014.01.017.

F. Appendix

Interpretation of Experimental Data is Substantial for Constitutive Characterization of Arterial Tissue

Original research article.
IF 2.098 (2021)

O. Lisický et al. (2021a). "Interpretation of Experimental Data is Substantial for Constitutive Characterization of Arterial Tissue." In: *Journal of Biomechanical Engineering*. ISSN: 0148-0731. DOI: 10.1115/1.4051120

Interpretation of Experimental Data is Substantial for Constitutive Characterization of Arterial Tissue

Ondřej Lisický[1]
Institute of Solid Mechanics,
Mechatronics and Biomechanics,
Brno University of Technology,
Brno 601 90, Czech Republic
e-mail: 161238@vutbr.cz

Anna Hrubanová
Institute of Solid Mechanics,
Mechatronics and Biomechanics,
Brno University of Technology,
Brno 601 90, Czech Republic

Jiří Burša
Institute of Solid Mechanics,
Mechatronics and Biomechanics,
Brno University of Technology,
Brno 601 90, Czech Republic

The paper aims at evaluation of mechanical tests of soft tissues and creation of their representative stress–strain responses and respective constitutive models. Interpretation of sets of experimental results depends highly on the approach to the data analysis. Their common representation through mean and standard deviation may be misleading and give nonrealistic results. In the paper, raw data of seven studies consisting of 11 experimental data sets (concerning carotid wall and atheroma tissues) are re-analyzed to show the importance of their rigorous analysis. The sets of individual uniaxial stress–stretch curves are evaluated using three different protocols: stress-based, stretch-based, and constant-based, and the population-representative response is created by their mean or median values. Except for nearly linear responses, there are substantial differences between the resulting curves, being mostly the highest for constant-based evaluation. But also the stretch-based evaluation may change the character of the response significantly. Finally, medians of the stress-based responses are recommended as the most rigorous approach for arterial and other soft tissues with significant strain stiffening.
[DOI: 10.1115/1.4051120]

Keywords: carotid artery, constitutive modeling, data analysis, mechanical testing, soft tissue

1 Introduction

Computational models are often used to evaluate mechanical responses of arteries either under pulsating blood flow [1–5] or under constant blood pressure [6–9]. Those techniques may contribute to prediction of rupture-prone sites in an artery or improve patient-specific tool design, which could be decisive in subsequent repeated interventions [7,8,10]. Therefore, understanding of mechanical behavior of arterial wall (and other soft tissues) is important and credibility of population-representative constitutive models represents a limitation of accuracy of computational modeling, because patient-specific data on mechanical properties are not known. Typical nonlinear stress–strain behavior of arteries caused by collagen fiber stiffening, tissue anisotropy, and heterogeneity [6,11–13] brings challenges for their representative constitutive description. Simple mechanical tests, often used for arterial tissue characterization [14–20], are useful to get insight into the material nature while more complex methods are necessary for their thorough constitutive description [21].

To specify a population-based model from multiple samples, averaging is often applied to specify a representative material response. However, methods used for analysis of experimental data are often inadequate and may thus cause misinterpretation of the fundamental information. Averaging, or mean and standard deviation are often used when describing the experimental data [16,17,22] even though the data distribution was not investigated and apparently shows high asymmetry. As no straightforward statistical method is available for direct comparison and averaging of functions (curves), a commonly used approach is to fit each response with a constitutive model and to use average values of the model constants as a representative description. Here, isotropic [16,23] as well as anisotropic models [22,24,25] were used though without any data analysis and discussion on the appropriateness of this representation. In contrast, Teng et al. [14] suggested and illustrated on a single curve that a population model representing a set of samples should not be specified on the basis of means or medians of the constants since their combination is not unique. Using a single dataset and without any comparison, they suggested that a different averaging method might cause differences in the resulting representative response. Akiyldiz et al. [15] compared atherosclerotic tissues from various sources while averaging stiffness at a specific level of deformation. Here again, no attention was paid to the shape of data distribution, resulting in data averaging, which may increase differences among studies. Therefore, a unified methodology for data analysis of the results of mechanical experiments is needed for a proper constitutive description of population-representative mechanical behavior and its further application in research and clinics.

In this study, we propose a simple methodology for evaluation of population-representative responses from mechanical tests, which is applicable for any biomechanical datasets to avoid their misinterpretation. It is applied and illustrated with data published in several studies focused on carotid wall and atherosclerotic plaque. Stress-based, stretch-based, and constant-based processing of experimental responses is realized and compared for datasets published in several available studies.

2 Methods

2.1 Data Collection. Numerous studies were found in the literature, which focus on the mechanical representation of components of the carotid artery wall and the atherosclerotic plaque. Only studies with provided raw experimental responses (curves provided) were used and classified as response-based data, in contrast to constant-based data, where the authors used a specific constitutive description of the individual responses and published only constants specific for the chosen model and their average values. Note that some studies provided both data sets. In total, 11 data sets counting 10–25 samples each were analyzed, as summarized in Table 1.

If the sample classification used in the respective study reduced highly the number of samples in a cohort (e.g., the hard tissue cohort with two representants in Ref. [17]), the data were unified and analyzed as a single dataset. As majority of data on mechanical responses concern only tension tests, compression tests were not included in the analyses. All data sets were unified and represented by stretch and Cauchy (true) stress values as it was presented in nearly all the considered papers, except for Ref. [16]. Since various representations can be seen in literature, the process of analysis may differ. The raw data are either interpolated or fitted by chosen constitutive models and then population-representative responses are sought for in different ways (see Fig. 1), as described in greater detail in Secs. 2.2 and 2.4.

[1]Corresponding author.
Manuscript received January 22, 2021; final manuscript received April 29, 2021; published online June 16, 2021. Assoc. Editor: David M. Pierce.

Table 1 Details of papers used for further analyses in this study

Study	Tissue	Test type	Number of samples	Characterization	Model
[16]	Plaque	Uniaxial tension	16	Constant-based, response-based	Mooney–Rivlin
[17]	Plaque	Uniaxial tension	14	Constant-based, response-based	Yeoh
[22]	Intact common carotid artery (CCA)	Inflation–extension	11	Constant-based	HGO 2005
	Intact internal carotid artery (ICA)		10		
[26]	Plaque	Planar tension	25	Response-based	Yeoh
[14]	Media	Uniaxial tension	65	Response-based	Modified Mooney–Rivlin (replaced by Yeoh)
	Fibrous cap	Uniaxial tension	59		
	Intraplaque hemorrhage/thrombus (iph/t)	Uniaxial tension	21		
	lipid	Uniaxial tension	38		
[27]	CCA	Biaxial tension	21	Constant-based, response-based	Four-fiber
[28]	Plaque	Uniaxial tension	16	Response-based	Yeoh

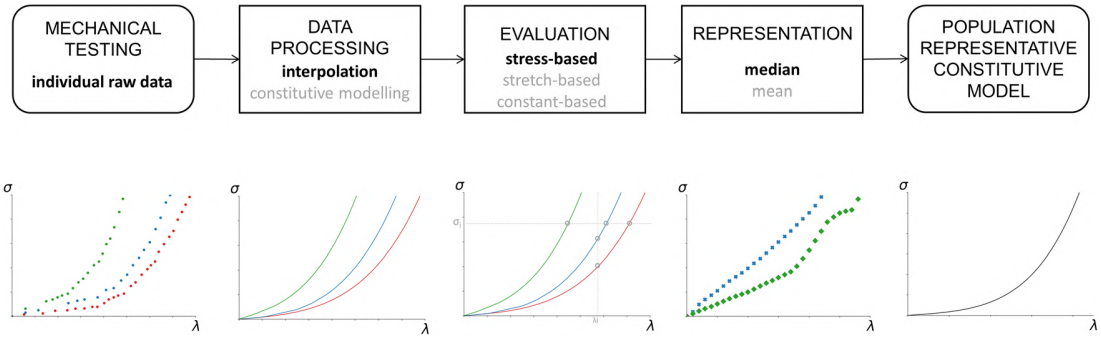

Fig. 1 Methodology flowchart. The process used in the proposed methodology for data representation and analysis. The recommended way of how to obtain the best population-representative constitutive model is highlighted in bold.

2.2 Ways of Evaluation of Representative Responses. Atherosclerotic plaque raw data sets were used from studies [14,16,17,26,28] and the curves were digitized for further processing. In contrast, for studies presenting only constants of the chosen constitutive model for each individual (see Table 1), the response of each sample was calculated using the constitutive model adopted from the original paper for all the individual sets of constants in each cohort. This was the case for the atherosclerotic plaque in Refs. [16] and [17] and for the carotid wall [22,27] where the uniaxial responses were not available.

For constant-based representation, the type of mechanical test is not relevant. If constants of a specific constitutive model were available in the original paper, they were directly used; otherwise, the presented experimental responses were fitted with the Yeoh model (see Sec. 2.3) and parameters of the individual responses were used for further data analysis (see Sec. 2.4).

For stress- and stretch-based approaches, uniaxial tension curves were used either based on the individual raw data (if available) or calculated by means of the original constitutive model using the published individual sets of model constants. These individual responses were then evaluated either for stretches at different levels of stresses (stress-based evaluation) or for stresses at different levels of stretches (stretch-based evaluation). The data sets at each stress (stretch) level were evaluated separately as described in detail below.

2.3 Constitutive Modeling. To obtain material parameters of the constitutive model for constant-based population data, a fitting procedure was performed in Hyperfit (BUT, Czech Republic[2]) software using Levenberg-Marquardt optimization algorithm, maximizing the coefficient of determination R^2. Several isotropic constitutive models (Ogden, Mooney-Rivlin, Demiray, Yeoh) were used to fit the experimental data. The third Yeoh strain-energy density function [29] in the following form:

$$\Psi \sum_{i=1}^{3} c_{i0}(I_1 - 3)^i \tag{1}$$

where c_{i0} are stress-like material parameters, provided the best fit over the range of experimental data and was also insensitive to the chosen starting point. This model was preferred for an isotropic description of arterial tissues [4,17,30,31]. The modified Mooney–Rivlin model mentioned in Ref. [14] was replaced by Yeoh due to its inappropriate quality of fit for some individual samples. Its constants were restrained by Eq. (2) as proposed in Ref. [32] to meet thermodynamic criteria; otherwise, no upper limits were used due to unknown physiological boundaries for phenomenological models.

$$c_{10} > 0, \quad -\sqrt{3c_{10}c_{30}} < c_{20} < \infty, \quad c_{30>0} \tag{2}$$

2.4 Data Analysis. Each stress–stretch dependence was interpolated using a cubic B-spline. This enables to evaluate data at any chosen levels of stress or stretch; the stress-based evaluation was done with stresses stepped by 10 kPa, while the stretch-based evaluation with stretches stepped by 0.01. Data distribution at each level was analyzed and the results were represented as mean and median values.

2.5 Statistical Analysis. To quantify the asymmetry of data distribution around the mean, the Fisher–Pearson skewness coefficient was determined at each level represented by multiple points at different stress or stretch levels using stress-based and stretch-based approaches. The average skewness coefficient was also determined for constants of constitutive model. Its value between

[2]http://www.hyperfit.wz.cz/

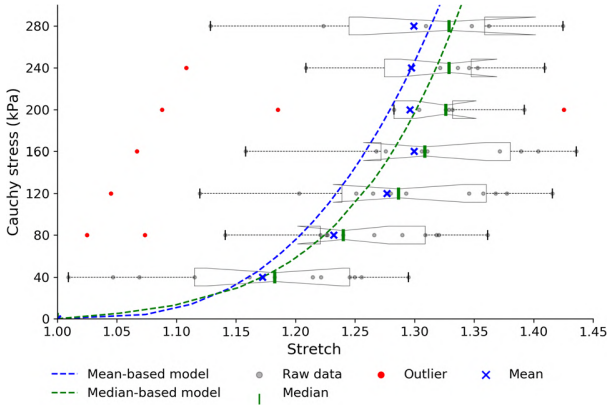

Fig. 2 Stress-based analysis of stress–stretch curves represented by box plots. Mean and median values show significant differences and are fitted with Yeoh model. Every fourth representant is shown.

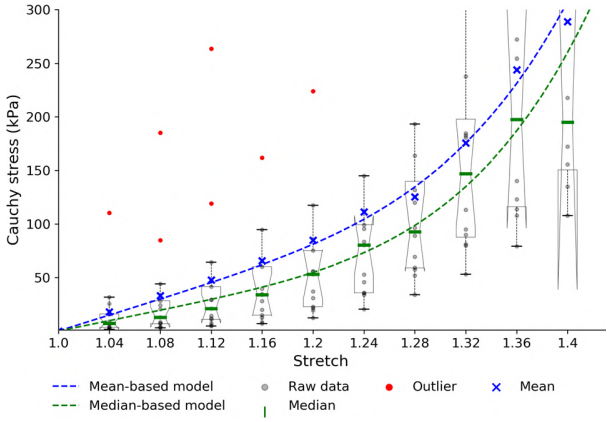

Fig. 3 Stretch-based stress–stretch curves represented by box plots. Mean and median values show significant differences and are fitted with third order Yeoh model.

−0.5 and 0.5 indicates approximately symmetric distribution, while increasing absolute value represents higher asymmetry with highly skewed distribution for absolute value higher than 1. The distributions of the representative responses from all the analyzed approaches were compared by the Anderson-Darling k-sample test with Bonferroni correction for multiple comparisons. Statistical significance was assumed if $p < 0.05$. Data point was marked as outlier if being more than 1.5 times interquartile range above the third quartile (or below the second quartile).

3 Results

This section presents graphical results from all the presented variants for the data published in Lawlor [17]; here, the experimental data were presented for each sample in the form of third-order Yeoh material constants together with a specific raw measured data. The same representation of the other studies can be found in the Supplementary Material on the ASME Digital Collection.

3.1 Stress-Based Evaluation. Figure 2 presents the data distribution by box plots for stress-based evaluation. Data distribution, in this case, was found moderately skewed resulting in significant differences between mean and median representations; in most cases, data outliers caused a significant shift of the mean. Overall results summarized in Table 2 (and graphically in Supplementary Material on the ASME Digital Collection) showed that the stress-based evaluation gave low skewness or even almost symmetrical distribution in most cases.

The range of individual experimental data, both stress and stretch, varied among samples resulting in discontinuities in the resulting characteristics. For both mean and median representations, the coefficient of determination $R^2 > 0.9$ was found in most of the cases and also the lowest value $R^2 = 0.74$ represents an acceptable fit.

3.2 Stretch-Based Evaluation. In contrast to the stress-based analysis, the data distributions were found highly skewed, and consequently significant differences occurred between mean and median values in all cases. Typical data distribution is shown in Fig. 3 and the results of skewness are summarized in the Table 2.

Results for the fitted models and comparison between mean and median representation are summarized in Supplementary Material on the ASME Digital Collection. Most of the analyzed studies resulted in almost linear behavior when stretch-based characterization with mean data was used. For both mean and median representation, the coefficient of determination $R^2 > 0.9$ was found in most of the cases and also the lowest value $R^2 = 0.67$ represents an acceptable fit. However, the responses showed more compliant behavior than those obtained for stress-based or constant-based characterization.

3.3 Constant-Based Evaluation. The constant-based representation showed the highest differences between mean and median values in almost all cases. The median curves were always more compliant and their stiffening began later then for the mean data. Distribution of constants of the constitutive model is shown in Fig. 4. Although the differences between mean and median

Table 2 Results of statistical analyses

Study	Stress-based skewness	Stretch-based skewness	Constant-based skewness	$\sigma - \lambda$	$\sigma - c$	$\lambda - c$
[16]	0.51	1.58	2.71	0.13	**0.01**	0.80
[17]	−0.65	2.41	0.68	0.60	0.21	0.10
[22] CCA	0.36	1.32	0.50	0.11	0.95	0.15
[22] ICA	0.14	0.71	0.20	0.17	0.90	**0.03**
[26]	0.81	1.00	0.74	0.65	0.95	0.96
[14] media	0.18	1.50	2.01	0.27	0.82	0.98
[14] fibrous cap	0.43	1.50	3.01	**0.02**	0.91	0.30
[14] iph/t	0.18	1.08	1.11	0.17	**0.006**	0.69
[14] lipid	0.67	1.30	2.11	0.58	0.09	0.38
[27]	−0.59	1.59	2.11	0.45	0.94	0.95
[28]	0.58	1.48	2.00	0.99	0.99	0.99

Skewness coefficient represents the average asymmetry of the data distribution for different approaches. The significance of differences between the stress- (σ), stretch- (λ) and constant- (c) based approaches is always represented by a corresponding p-value for the Anderson–Darling test. Statistically significant results are in bold.

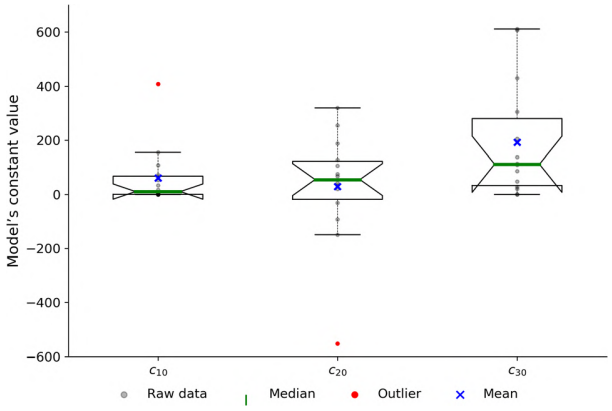

Fig. 4 Model parameters. Data distribution of material parameters of third-order Yeoh model.

values of the constants seem moderate in this case, the differences between the mean and median curves were the largest throughout the whole range. Comparison with the other two approaches is presented in Fig. 5.

As the skewness was pronounced for most of the data sets (see Table 2), an overall comparison of the representative curves based on different approaches was performed for medians. For the presented case (Lawlor [17]), the differences in distributions were lower between stress-based and stretch-based approaches, while the constant-based distribution differed more from both of them. Although statistical significance of these differences was seldom reached because of huge dispersion of all data, differences between the compared approaches are of interest, as illustrated in Fig. 5.

4 Discussion

The objective of this study was to compare different approaches to the creation of population-representative constitutive models of arterial tissues from individual experimental curves. For this purpose, we re-analyzed 11 published experimental data cohorts focusing on atherosclerotic carotid plaque components and carotid wall Three different approaches for evaluation of experimental data sets were compared: stress-based, stretch-based, and constant-based.

4.1 Input Data. Comparison of various experimental protocols used during measurement was not the aim of this work; it

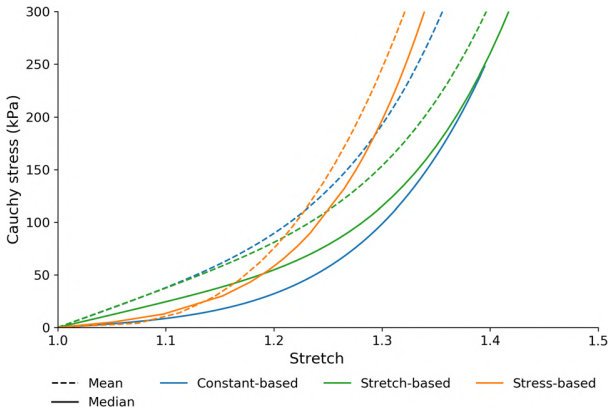

Fig. 5 Comparison of constitutive models representing population data obtained by using different approaches. Always the mean representation differs significantly from the median representation; the highest differences were found for constant-based characterization.

was done for some of the investigated studies in reviews [15,20]. In studies [26,28], the mechanical testing was performed with the whole endarterectomy sample consisting of different types of tissues; thus, the responses show behavior not typical for arterial tissues with low or even without strain stiffening. Although the largest cohort was published in both Refs. [14] and [33], it was not possible to reconstruct all the samples because more than a half of the experimental responses were not detectable in either of them. Nevertheless, the obtained data still represented suitable cohorts comparable with the other studies.

4.2 Experimental Data Characterization. The stress-based data characterization includes most individual experimental curves and preserves their pronounced strain stiffening. Also differences between the mean and median representations are the lowest, with only moderate skewness being even negligible in some cases. Our preference of this approach corresponds to Ref. [34] where the authors showed that keeping the strain stiffening is decisive for accuracy of predicted stresses. On the other hand, the stretch-based description showed very high skewness and flattens the responses, reducing thus their stiffening or even switching the tendency to softening with increasing stretch, see Refs. [14], [16], [17], [22], and [26] in Supplementary Material on the ASME Digital Collection. Their mean responses show significant differences against the median characterizations, which preserve a higher amount of strain stiffening typical for the individual responses. Moreover, shift of the strain stiffening region to significantly higher stretches was found, see, e.g., Ref. [22] ICA and Ref. [27].

The constant-based characterization appears the least appropriate for population data description. It is not only due to its high sensitivity to ambiguous constitutive model parameters but also due to the highest differences between the mean and median representations (except for ICA in Ref. [22]). Impact of the approach to data processing was low only for nearly linear stress–strain curves [26,28] but also here the mean constant-based characterization differs significantly from all the others and the differences increase with higher nonlinearity of the responses. This conclusion is in accordance with a single patient study [14] where the authors showed that multiple parameter combinations can describe the same curve. Moreover, the resulting constants might be also influenced by the initial guess (starting points) for the model, which was not discussed in the papers the constants were taken from. This may more likely happen with complex models like four-fiber or HGO, while for Yeoh model, nearly identical constants are obtained even from highly different starting points.

The comparison of different approaches in our study shows that appropriate data characterization is fundamental for the correct population-representative description of mechanical responses of soft tissues and consequently for their constitutive modeling. This holds especially for tissues with pronounced strain stiffening as typical not only for arteries but for also many other soft biological tissues. Also, the dispersion of individual data may play an important role; if the standard deviation is not much smaller than the mean, the normal Gaussian distribution predicts a significant portion of negative results. In uniaxial tension, however, negative stresses and longitudinal strains are excluded by physical principle and the same holds for many constants of constitutive models. Thus, a standard deviation comparable with the mean, as well as existence of outliers, indicates its asymmetry and, consequently, a significant difference between mean and median values. The only exception among the investigated cohorts is CCA in Ref. [22] where, however, the median curves fully coincide between stress-based and constant-based approaches and also the differences between their mean and median interpretations are low. The median stress-based characterization shows also the best correspondence to the other approaches; it is never out of their range and keeps the amount of strain stiffening of all the individual responses.

The proposed methodology is based on interpolation of each sample response, which is simple and enables further analyses. The resulting material model may be fitted with a new procedure proposed recently [35], where finite element simulations are used to reduce the errors during a testing procedure and to increase thus the accuracy of the model. Although computational models averaged from highly cited studies are often applied to analyze factors possibly important in assessing the peak stresses [36–40], our recent study [40] showed that inclusion of extremes in mechanical properties into the computational modeling might be beneficial. Moreover, combination of the results with in vivo measurements of arterial response may bring higher accuracy of the constitutive model. Although the approaches evaluating the in vivo behavior [41] of arteries offer mostly a single material-related parameter such as circumferential stiffness [42], they could be applied to reduce the high dispersion of the population-representative computational models. If we were capable to identify several groups of measured stress–strain responses and to fit specific constitutive parameters to each of them, their comparison (in the physiological range of load) with the measured in vivo stiffness could make these population–representative models closer to the unknown patient-specific response and improve thus significantly the accuracy of computational predictions.

4.3 Limitations. Although some attempts occurred to unify the test protocols and data analysis [20,35], a high variation still exists also among the studies analyzed in this paper. Unification of testing protocols [20,21] would enable direct data comparisons without recalculations needed to get comparable data from different studies. Some inaccuracies may also occur during data digitization from the published stress–strain responses and their replacement by cubic B-splines, but they do not exceed errors of measurement themselves and are negligible in comparison with the interpatient variability. Similarly, deviations of the uniaxial responses reconstructed based on constitutive models and their constants were negligible (coefficient of determination close to 1 in all cases).

The variations typical for arterial tissues might be also related to the complexity of the specimen shape and its nonhomogeneity. In all the analyzed experimental studies, the stretches were obtained by tracking two points only and represent thus a mean value for a randomly chosen part of the specimen. In contrast, more recent approaches exploit Digital Image Correlation for full-field measurements of displacements and strains and their deeper analysis may enable us to distinguish between interpatient variability and tissue nonhomogeneity [43–45]. And incorporation of multipoint responses into a representative constitutive model highlights even more the importance of rigorous statistical analyses.

Conclusion

The presented analyses show the importance of rigorous processing of experimental data for evaluation of a population-representative mechanical response of soft tissue and its constitutive model. Biomechanical data seldom show symmetric Gaussian distribution; consequently, representation of the results through mean±SD may be misleading and differ significantly from the more relevant representation based on the median. Moreover, the way of obtaining the representative stress–strain curves is also important. It was shown on the examples of carotid arteries that averaging based on stretches (or strains) and especially that based on constants of constitutive models may give results highly different from each other and especially, to change the tendencies of the stress–strain curves. The stress-based evaluation represented by median stretch at each stress level is recommended by the authors as the most rigorous way for evaluating experimental data sets to obtain the best population-representative response and its constitutive model.

Funding Data

- Czech Science Foundation (No. 18-13663S; Funder ID: 10.13039/501100001824).

Nomenclature

CCA = common carotid artery
HGO = Holzapfel Gasser Ogden model
ICA = internal carotid artery
Iph/t = intraplaque hemorrhage/thrombus
SD = standard deviation

References

[1] Xenos, M., Labropoulos, N., Rambhia, S., Alemu, Y., Einav, S., Tassiopoulos, A., Sakalihasan, N., and Bluestein, D., 2015, "Progression of Abdominal Aortic Aneurysm Towards Rupture: Refining Clinical Risk Assessment Using a Fully Coupled Fluid–Structure Interaction Method," Ann. Biomed. Eng., **43**(1), pp. 139–153.

[2] Cilla, M., Borrás, I., Peña, E., Martínez, M. A., and Malvè, M., 2015, "A Parametric Model for Analysing Atherosclerotic Arteries: On the FSI Coupling," Int. Commun. Heat Mass Transfer, **67**, pp. 29–38.

[3] Tang, D., Yang, C., Huang, S., Mani, V., Zheng, J., Woodard, P. K., Robson, P., Teng, Z., Dweck, M., and Fayad, Z. A., 2017, "Cap Inflammation Leads to Higher Plaque Cap Strain and Lower Cap Stress: An MRI-PET/CT-Based FSI Modeling Approach," J. Biomech., **50**, pp. 121–129.

[4] Teng, Z., Yuan, J., Feng, J., Zhang, Y., Brown, A. J., Wang, S., Lu, Q., and Gillard, J. H., 2015, "The Influence of Constitutive Law Choice Used to Characterise Atherosclerotic Tissue Material Properties on Computing Stress Values in Human Carotid Plaques," J. Biomech., **48**(14), pp. 3912–3921.

[5] Huang, X., Yang, C., Zheng, J., Bach, R., Muccigrosso, D., Woodard, P. K., and Tang, D., 2016, "3D MRI-Based Multicomponent Thin Layer Structure Only Plaque Models for Atherosclerotic Plaques," J. Biomech., **49**(13), pp. 2726–2733.

[6] Holzapfel, G. A., Stadler, M., and Schulze-Bauer, C. A. J., 2002, "A Layer-Specific Three-Dimensional Model for the Simulation of Balloon Angioplasty Using Magnetic Resonance Imaging and Mechanical Testing," Ann. Biomed. Eng., **30**(6), pp. 753–767.

[7] Auricchio, F., Conti, M., De Beule, M., De Santis, G., and Verhegghe, B., 2011, "Carotid Artery Stenting Simulation: From Patient-Specific Images to Finite Element Analysis," Med. Eng. Phys., **33**(3), pp. 281–289.

[8] Mortier, P., Holzapfel, G. A., De Beule, M., Van Loo, D., Taeymans, Y., Segers, P., Verdonck, P., and Verhegghe, B., 2010, "A Novel Simulation Strategy for Stent Insertion and Deployment in Curved Coronary Bifurcations: Comparison of Three Drug-Eluting Stents," Ann. Biomed. Eng., **38**(1), pp. 88–99.

[9] Nieuwstadt, H. A., Kassar, Z. A. M., Van Der Lugt, A., Breeuwer, M., Van Der Steen, A. F. W., Wentzel, J. J., and Gijsen, F. J. H., 2015, "A Computer-Simulation Study on the Effects of MRI Voxel Dimensions on Carotid Plaque Lipid-Core and Fibrous Cap Segmentation and Stress Modeling," PLoS One, **10**(4), p. e0123031.

[10] Koskinas, K. C., Chatzizisis, Y. S., Antoniadis, A. P., and Giannoglou, G. D., 2012, "Role of Endothelial Shear Stress in Stent Restenosis and Thrombosis: Pathophysiologic Mechanisms and Implications for Clinical Translation," J. Am. Coll. Cardiol., **59**(15), pp. 1337–1349.

[11] Schriefl, A. J., Zeindlinger, G., Pierce, D. M., Regitnig, P., and Holzapfel, G. A., 2012, "Determination of the Layer-Specific Distributed Collagen Fibre Orientations in Human Thoracic and Abdominal Aortas and Common Iliac Arteries," J. R. Soc. Interface, **9**(71), pp. 1275–1286.

[12] Gasser, T. C., Ogden, R. W., and Holzapfel, G. A., 2006, "Hyperelastic Modelling of Arterial Layers With Distributed Collagen Fibre Orientations," J. R. Soc. Interface, **3**(6), pp. 15–35.

[13] Holzapfel, G. A., and Ogden, R. W., 2018, "Biomechanical Relevance of the Microstructure in Artery Walls With a Focus on Passive and Active Components," Am. J. Physiol. Hear. Circ. Physiol., **315**(3), pp. H540–H549.

[14] Teng, Z., Zhang, Y., Huang, Y., Feng, J., Yuan, J., Lu, Q., Sutcliffe, M. P. F., Brown, A. J., Jing, Z., and Gillard, J. H., 2014, "Material Properties of Components in Human Carotid Atherosclerotic Plaques: A Uniaxial Extension Study," Acta Biomater., **10**(12), pp. 5055–5063.

[15] Akyildiz, A. C., Speelman, L., and Gijsen, F. J. H., 2014, "Mechanical Properties of Human Atherosclerotic Intima Tissue," J. Biomech., **47**(4), pp. 773–783.

[16] Maher, E., Creane, A., Sultan, S., Hynes, N., Lally, C., and Kelly, D. J., 2009, "Tensile and Compressive Properties of Fresh Human Carotid Atherosclerotic Plaques," J. Biomech., **42**(16), pp. 2760–2767.

[17] Lawlor, M. G., O'Donnell, M. R., O'Connell, B. M., and Walsh, M. T., 2011, "Experimental Determination of Circumferential Properties of Fresh Carotid Artery Plaques," J. Biomech., **44**(9), pp. 1709–1715.

[18] Chai, C. K., Akyildiz, A. C., Speelman, L., Gijsen, F. J. H., Oomens, C. W. J., van Sambeek, M. R. H. M., van der Lugt, A., and Baaijens, F. P. T., 2015, "Local Anisotropic Mechanical Properties of Human Carotid Atherosclerotic Plaques - Characterisation by Micro-Indentation and Inverse Finite Element Analysis," J. Mech. Behav. Biomed. Mater., **43**(10), pp. 59–68.

[19] Hoffman, A. H., Teng, Z., Zheng, J., Wu, Z., Woodard, P. K., Billiar, K. L., Wang, L., and Tang, D., 2017, "Stiffness Properties of Adventitia, Media, and Full Thickness Human Atherosclerotic Carotid Arteries in the Axial and Circumferential Directions," ASME J. Biomech. Eng., **139**(12), p. 124501.
[20] Walsh, M. T., Cunnane, E. M., Mulvihill, J. J., Akyildiz, A. C., Gijsen, F. J. H., and Holzapfel, G. A., 2014, "Uniaxial Tensile Testing Approaches for Characterisation of Atherosclerotic Plaques," J. Biomech., **47**(4), pp. 793–804.
[21] Macrae, R. A., Miller, K., and Doyle, B. J., 2016, "Methods in Mechanical Testing of Arterial Tissue: A Review," Strain, **52**(5), pp. 380–399.
[22] Sommer, G., and Holzapfel, G. A., 2012, "3D Constitutive Modeling of the Biaxial Mechanical Response of Intact and Layer-Dissected Human Carotid Arteries," J. Mech. Behav. Biomed. Mater., **5**(1), pp. 116–128.
[23] Schulze-Bauer, C. A. J., MöRth, C., and Holzapfel, G. A., 2003, "Passive Biaxial Mechanical Response of Aged Human Iliac Arteries," ASME J. Biomech. Eng., **125**(3), pp. 395–406.
[24] Holzapfel, G. A., Sommer, G., Gasser, C. T., and Regitnig, P., 2005, "Determination of Layer-Specific Mechanical Properties of Human Coronary Arteries With Nonatherosclerotic Intimal Thickening and Related Constitutive Modeling," J. Physiol. Hear. Circ. Physiol., **103**(4), pp. 806–808.
[25] Polzer, S., Gasser, T. C., Novak, K., Man, V., Tichy, M., Skacel, P., and Bursa, J., 2015, "Structure-Based Constitutive Model Can Accurately Predict Planar Biaxial Properties of Aortic Wall Tissue," Acta Biomater., **14**, pp. 133–145.
[26] Mulvihill, J. J., Cunnane, E. M., Mchugh, S. M., Kavanagh, E. G., Walsh, S. R., and Walsh, M. T., 2013, "Mechanical, Biological and Structural Characterization of In Vitro Ruptured Human Carotid Plaque Tissue," Acta Biomater., **9**(11), pp. 9027–9035.
[27] Kamenskiy, A. V., Dzenis, Y. A., Kazmi, S. A. J., Pemberton, M. A., Pipinos, I. I., Phillips, N. Y., Herber, K., Woodford, T., Bowen, R. E., Lomneth, C. S., and MacTaggart, J. N., 2014, "Biaxial Mechanical Properties of the Human Thoracic and Abdominal Aorta, Common Carotid, Subclavian, Renal and Common Iliac Arteries," Biomech. Model. Mechanobiol., **13**(6), pp. 1341–1359.
[28] Barrett, H. E., Cunnane, E. M., Kavanagh, E. G., and Walsh, M. T., 2016, "On the Effect of Calcification Volume and Configuration on the Mechanical Behaviour of Carotid Plaque Tissue," J. Mech. Behav. Biomed. Mater., **56**, pp. 45–56.
[29] Yeoh, O. H., 1993, "Some Forms of the Strain Energy Function for Rubber," Rubber Chem. Technol., **66**(5), pp. 754–771.
[30] Polzer, S., Polišenská, A., Novák, K., and Burša, J., 2019, "Moderate Thickness of Lipid Core in Shoulder Region of Atherosclerotic Plaque Determines Vulnerable Plaque—A Parametric Study," Med. Eng. Phys., **69**, pp. 140–146.
[31] O'Reilly, B. L., Hynes, N., Sultan, S., McHugh, P. E., and McGarry, J. P., 2020, "An Experimental and Computational Investigation of the Material Behaviour of Discrete Homogenous Iliofemoral and Carotid Atherosclerotic Plaque Constituents," J. Biomech., **106**, p. 109801.
[32] Bilgili, E., 2004, "Restricting the Hyperelastic Models for Elastomers Based on Some Thermodynamical, Mechanical, and Empirical Criteria," J. Elastomers Plast., **36**(2), pp. 159–175.
[33] Yuan, J., Teng, Z., Feng, J., Zhang, Y., Brown, A. J., Gillard, J. H., and Lu, Z. J. Q., 2015, "Influence of Material Property Variability on the Mechanical Behaviour of Carotid Atherosclerotic Plaques: A 3D Fluid-Structure Interaction Analysis," Int. J. Numer. Method. Biomed. Eng., **31**(8), p. e02722.
[34] Man, V., Polzer, S., Gasser, T. C., Novotny, T., and Bursa, J., 2018, "Impact of Isotropic Constitutive Descriptions on the Predicted Peak Wall Stress in Abdominal Aortic Aneurysms," Med. Eng. Phys., **53**, pp. 49–57.
[35] Fehervary, H., Smoljkić, M., Vander Sloten, J., and Famaey, N., 2016, "Planar Biaxial Testing of Soft Biological Tissue Using Rakes: A Critical Analysis of Protocol and Fitting Process," J. Mech. Behav. Biomed. Mater., **61**, pp. 135–151.
[36] Fok, P. W., and Gou, K., 2020, "Finite Element Simulation of Intimal Thickening in 2D Multi-Layered Arterial Cross Sections by Morphoelasticity," Comput. Methods Appl. Mech. Eng., **363**, p. 112860.
[37] Fan, Z. M., Liu, X., Du, C. F., Sun, A. Q., Zhang, N., Fan, Z. M., Fan, Y. B., and Deng, X. Y., 2016, "Plaque Components Affect Wall Stress in Stented Human Carotid Artery: A Numerical Study," Acta Mech. Sin. Xuebao, **32**(6), pp. 1149–1154.
[38] Deokar, R. R., and Klamecki, B. E., 2017, "Computational Modeling and Comparative Tissue Damage Analysis of Angioplasty and Orbital Atherectomy Interventional Procedures," ASME J. Med. Devices, **11**(2), pp. 021006.
[39] Iannaccone, F., Debusschere, N., De Bock, S., De Beule, M., Van Loo, D., Vermassen, F., Segers, P., and Verhegghe, B., 2014, "The Influence of Vascular Anatomy on Carotid Artery Stenting: A Parametric Study for Damage Assessment," J. Biomech., **47**(4), pp. 890–898.
[40] Lisický, O., Malá, A., Bednařík, Z., Novotný, T., and Burša, J., 2020, "Consideration of Stiffness of Wall Layers is Decisive for Patient-Specific Analysis of Carotid Artery With Atheroma," PLoS One, **15**(9), p. e0239447.
[41] Di Giuseppe, M., Farzaneh, S., Zingales, M., Pasta, S., and Avril, S., 2021, "Patient-Specific Computational Evaluation of Stiffness Distribution in Ascending Thoracic Aortic Aneurysm," J. Biomech., **119**, p. 110321.
[42] Bersi, M. R., Acosta Santamaría, V. A., Marback, K., Di Achille, P., Phillips, E. H., Goergen, C. J., Humphrey, J. D., and Avril, S., 2020, "Multimodality Imaging-Based Characterization of Regional Material Properties in a Murine Model of Aortic Dissection," Sci. Rep., **10**(1), pp. 1–23.
[43] Bersi, M. R., Bellini, C., Di Achille, P., Humphrey, J. D., Genovese, K., and Avril, S., 2016, "Novel Methodology for Characterizing Regional Variations in the Material Properties of Murine Aortas," ASME J. Biomech. Eng., **138**(7), p. 071005.
[44] Bersi, M. R., Bellini, C., Humphrey, J. D., and Avril, S., 2019, "Local Variations in Material and Structural Properties Characterize Murine Thoracic Aortic Aneurysm Mechanics," Biomech. Model. Mechanobiol., **18**(1), pp. 203–218.
[45] Davis, F. M., Luo, Y., Avril, S., Duprey, A., and Lu, J., 2016, "Local Mechanical Properties of Human Ascending Thoracic Aneurysms," J. Mech. Behav. Biomed. Mater., **61**, pp. 235–249.

G. Appendix

Evaluation of Image Registration for measuring deformation fields in soft tissue mechanics

Original research article.
Submitted in Strain, currently under review.
IF 1.848 (2020)

strain
An International Journal for Experimental Mechanics

Evaluation of Image Registration for measuring deformation fields in soft tissue mechanics

Journal:	*Strain*
Manuscript ID	Draft
Manuscript Type:	Research Article
Date Submitted by the Author:	n/a
Complete List of Authors:	Lisický, Ondřej; Brno University of Technology Faculty of Mechanical Engineering, Institute of solid mechanics, mechatronics and biomechanics; Avril, Stephane; Mines Saint-Etienne, University of Lyon, University Jean Monnet, INSERM, Saint-Etienne, France Eydan, Bastien; Mines Saint-Etienne, University of Lyon, University Jean Monnet, INSERM, Saint-Etienne, France Pierrat, Baptiste; Mines Saint-Etienne, University of Lyon, University Jean Monnet, INSERM, Saint-Etienne, France Bursa, Jiri; Vysoke uceni technicke v Brne Fakulta strojniho inzenyrstvi, Institute of Solid Mechanics, Mechatronics and Biomechanics
Keywords:	Deformation field, Digital Image Correlation, Image Registration, mechanical testing, soft biological tissue

Evaluation of Image Registration for measuring deformation fields in soft tissue mechanics

Running head title: Deformation fields with Image Registration

Ondřej Lisický[1*], Stéphane Avril[2], Bastien Eydan[2], Baptiste Pierrat[2], Jiří Burša[1]

[1] *Institute of Solid Mechanics, Mechatronics and Biomechanics, Brno University of Technology, Czech Republic*

[2] *Mines Saint-Etienne, University of Lyon, University Jean Monnet, INSERM, Saint-Etienne, France*

**Corresponding author*

E-mail: 161238@vutbr.cz

Phone: +420 605 292 174

Abstract

High-fidelity biomechanical models usually involve the mechanical characterization of biological tissues using experimental methods based on optical measurements. In most experiments, strains are evaluated based on displacements of a few markers and represents an average within the region of interest (ROI). Full-field measurements may be valuable for identifying constitutive models. The approach based on non-rigid Image Registration is proposed and compared with standard Digital Image Correlation (DIC) on a set of samples, including (i) complex heterogeneous deformations with sub-pixel displacement, (ii) a typical uniaxial tension test of aorta, and (iii) an indentation test on skin. The possibility to extend the ROI to the whole sample and the exploitation of a natural tissue pattern represents the main assets of the proposed method whereas the results show similar accuracy as standard DIC when analysing sub-pixel deformations. Therefore, displacement and strain fields measurement based on Image Registration is very promising to characterize heterogeneous specimens with irregular shapes and/or small dimensions, which are typical features of soft biological tissues.

Keywords

Deformation field, Digital Image Correlation, Image Registration, mechanical testing, soft biological tissue

1 Introduction

The expanding use of computational modelling in biomechanics [1–3], e.g., for the design of medical devices and possibly for clinical prognosis in the near future, requires appropriate knowledge of tissue behaviour. Accordingly, patient-specific medical imaging like computed tomography, magnetic resonance imaging (MRI) or intravascular ultrasound are needed for assessing the mechanical behaviour of biological tissues. MRI is a very versatile method enabling strain investigation of various tissues under load and had already been applied for tissues like myocardium [4,5], carotid artery [6], spine intervertebral disc [7] or brain [8]. The tissue deformation in latter examples was examined using Image Registration (IR) technique, which is normally used to align medical images from multiple modalities to enhance a tissue characterization though its versatility enables various applications. However, the information about *in vivo* strain cannot be easily used for constitutive model characterization, especially for soft biological tissues, often exhibiting a nonlinear behaviour under large deformations.

Various approaches used to characterise mechanical properties of soft tissues were recently reviewed [9]. The choice of a suitable method depends mostly on the available laboratory equipment and the specific application; for instance, biaxial testing requires specific testing machines and large sample specimens which may not be available with some tissues [10,11]. Another example is the inflation-extension test requiring cylinder-like specimens [12], thus hardly applicable for the aortic valve or atherosclerotic plaque [13]. Most of the experimental studies investigating mechanical properties of biological tissue assume a uniform response in the analysed area and global characteristics are obtained by tracking the displacement of e.g., few markers resulting in average deformation of the specimen [9,14] With this approach, it is straightforward to derive stress-strain curves which can subsequently be processed to identify a constitutive model.

However, the assumption of homogeneous strain and thus stress fields in the analysed area might not be met in soft tissue mechanics. The error is then transferred into the computational model and can contribute to high variation among studies with heterogeneous samples [15] and a global trend for its minimization can be seen [14]. Regional characterization of the sample during the experiment may help to capture heterogeneous fields and can be addressed by full-field methods like digital image correlation (DIC), moiré or speckle interferometry. DIC has been widely used in many biomechanical applications for decades, including e.g., human skin [16], thigh muscle [17], human ascending thoracic aneurysm wall [18], or recently for biaxial stress relaxation of tissue of vaginal mucosa [19]. An extension of this method enables analysis of surface deformation with 3D DIC [20,21] or even internal deformation of the volume with digital volume correlation (DVC) [22–24]. DIC has limitations influencing its outcomes [25] such as creation of the pattern [26] or noisy deformation field as a result of the local DIC. The latter issue is addressed by introducing global DIC enabling an investigation of continuous deformation field in combination with finite element method [27] or by introducing B-spline shape function [28,29]. However, a comparison between global FE-based DIC and local DIC [30] revealed that the local DIC outperforms its opponent when a subset size is no less than 11 pixels. Other approaches were proposed to obtain a deformation/strain field of a loaded sample describing its regional mechanical properties. Even though IR is mostly used in computer vision, Wang *et al.* [25] analysed similarities, differences and complementarity between DIC and IR. According to that study, both methods may benefit from their combination and synergy. Non-rigid B-spline IR is similar to the global DIC with a continuous deformation field, however, has less strict requirements for the pattern and even a natural surface might be sufficient. IR approach was firstly used to evaluate the compressibility of lung parenchyma in uniaxial tension test [31]. However, neither verification nor reproducibility

analyses were described in that study, although the same methodology was applied several times [32,33]. Zhu et al. [34] compared recently both methodologies with promising results on synthetic data. Another approach was used by Miga *et al.* [35] who, similarly to the IR based methods, deformed one image to fit the shape of another using finite element simulations.

In summary, even though deformation fields are crucial for soft tissue biomechanics, the use of local DIC still presents some limitations. In this study, we propose to overcome these limitations by evaluating the benefits of IR for soft tissues biomechanics.

2 Material and methods

2.1 Full-field analysis

The composition of the most soft tissue, with some exceptions like liver [33], does not show any significant surface features, and hence intensity-based IR was applied. The IR is highly dependent on the specific tissue and a customized solution might be required. Therefore, open-source Elastix [36,37] software was used to simplify the process, covering a large field of problems and ways of solution.

Sets of N recorded images (including the first undeformed image) were evaluated using the incremental approach based always on comparison of two consecutive images from the set. In the IR, the so-called moving image I_M (from the actual, i.e. i^{th} step of loading) is distorted via $\mathbf{T}(\mathbf{x})$ transformation into the reference (fixed) image I_F (recorded in the next step i+1) to find the displacements $\mathbf{u}(\mathbf{x})$ spatially aligning I_M with I_F (see Fig. 1). The optimization problem minimizing a cost function was solved using Adaptive Stochastic Gradient Descent optimization, which, in combination with a random sampler, offered high effectiveness and speed. For assessment of

alignment of both images, various similarity measures were tested, and mutual information was chosen as the most suitable one in all tested cases.

Fig. 1

Due to a common nonlinear behaviour of soft tissue, a more flexible model is required. Hence, the B-spline transform model, allowing local deformation, was used instead of the Demons algorithm applied in [34]. Therefore, images I_M and I_F were discretized into a deformable grid with B-spline control points. Displacement of each pixel defined in the undeformed state of the specimen grid was then calculated using *transformix* [36,37]. Moreover, the continuous and smooth description of deformation by the B-splines results directly in a smooth displacement field making the evaluation of strains easier. Here, directional strains were obtained by calculating central differences of the displacement field using the *gradient* function of a NumPy package. Afterwards, components E_{ij} of Green-Lagrange strain tensor were calculated as follows:

$$E_{xx} = \frac{1}{2}\left(2\frac{\partial u}{\partial x} + \left(\frac{\partial u}{\partial x}\right)^2 + \left(\frac{\partial v}{\partial x}\right)^2\right)$$

$$E_{yy} = \frac{1}{2}\left(2\frac{\partial v}{\partial y} + \left(\frac{\partial u}{\partial y}\right)^2 + \left(\frac{\partial v}{\partial y}\right)^2\right)$$

$$E_{xy} = \frac{1}{2}\left(\frac{\partial u}{\partial y} + \frac{\partial v}{\partial x} + \frac{\partial u \partial u}{\partial x \partial y} + \frac{\partial v \partial v}{\partial x \partial y}\right)$$

where u and v represent displacements in x and y directions, respectively.

A multi-resolution strategy, often used despite of its computational difficulty, was not necessary and only a single magnitude of the resolution was used without pixel size degradation. However,

this strategy can be easily implemented with Elastix when, for instance, deformations between the acquired images are too large.

2.1.1 DIC

DIC is a well-established method and was used here for a comparison of the obtained full-field measurements from experiments using the Ncorr software (local DIC) [38]. In contrast to the proposed IR approach, here the resulting displacement field, also dependent on a subset size, needs to be smoothed to evaluate the strain field. Therefore, Ncorr uses a strain window with variable radius r_ε to calculate displacement gradients. As a result, a user needs to perform multiple analyses to find an acceptable compromise in the resulting fields. Therefore, the comparison was done with a DIC setup evaluated only personally, although by following all suggestions from the user guide.

2.2 Synthetic data – heterogeneous deformations

Synthetic data are often used to investigate the performance of some approaches. For the full-field measurements, a set of samples was proposed in [39], intending to challenge DIC algorithms to see their accuracy in various scenarios. While most of the samples presented there simulate only rigid motion with varying levels of noise or distortion, there are cases (like sample 14 in [39]) introducing sub-pixel heterogeneous deformation and thus a strain field representing a real challenge for the algorithms, as stated by the authors. This sample is very often used in testing new modifications of DIC [40,41] and hence it was chosen also here to challenge the IR approach. As it is suited for DIC, it has a typical speckle pattern though with high noise, introducing uncertainties into the analysed displacements. Moreover, this sample has three variations L1, L3 and L5 differing in the applied displacement. The speckle pattern of the synthetic data together with other samples can be seen in Fig. 2.

Fig. 2

2.3 Porcine aorta – uniaxial tension

Although synthetic data provides a good basis to establish the accuracy of the methodology, it is of interest to see the performance with data typical in the field of biomechanics. Here, a uniaxial tension of porcine proximal aorta sample was tested till relatively high deformations up to 80 %. It is worth mentioning that the sample had been frozen after harvesting and was tested in air. Although this can affect the response of the tissue, the focus of this study is the evaluation of the performance of the optical method. A speckle pattern was carefully applied onto the intima surface of a dog-bone shaped circumferential specimen (width = 4 mm) using a black spray. An Instron 3343 tensile machine was used to stretch the sample with a jaw velocity of 1.3 mm/s. Images were acquired during the test with a Photron UX100 camera (resolution of 1280x1024) at a framerate of 5 i/s for further full-field analysis.

2.4 Skin sample – natural pattern

Skin mechanical characterization is an important topic of interest in biomechanics. Mechanical properties of each layer can be identified using an indentation test in combination with uni- or biaxial skin stretching. A possible way how to obtain their constitutive parameters is by using inverse analysis with full-field measurements. However, the low thickness makes it almost impossible to prepare a suitable speckle pattern for DIC. The skin sample used in this study was stained with Hematoxylin and eosin to highlight a natural pattern of the layers. As no artificial pattern was prepared, this sample was very challenging for both DIC and IR approaches. The samples are 55mm long, die-cut from abdominal skin of a 90-100 days old female pig. No pre-

stretch was applied before indentation which was performed with stainless steel probe with 4 mm diameter up to 1.93 N. The camera resolution 6000x4000.

2.5 Performance validation

A pixel-to-pixel comparison of full-field measurements was accessed as a mean absolute percentage error (MAPE) at each loading step as indicated for displacement u in horizontal direction:

$$MAPE = \frac{1}{n}\sum_{i=1}^{n}\left|\frac{u_i^{\mathrm{DIC}} - u_i^{\mathrm{IR}}}{u_i^{\mathrm{DIC}}}\right|$$

where n is number of pixels within the analysed ROI, u_i^{IR} and u_i^{DIC} are horizontal displacements evaluated using IR and DIC approaches, respectively. The synthetic data was compared with the prescribed displacement and strain functions. The performance of IR was also investigated via average structural similarity measure (SSIM) introduced in [42], by comparing the fixed and moving images after deformation, with a 21x21 sliding window and a standard deviation (SD) of 1 pixel. This measure falls between 0 and 1 where values close to 1 indicate the best structural match of both images.

3 Results

3.1 Synthetic data – small deformations

As already mentioned, this sample is challenging due to a sub-pixel heterogeneous deformation. The proposed IR approach was capable to reproduce the simulated deformation successfully for all variants. Moreover, it captured well even the highest deformation gradients. This type of data

provides a robust way to assess quality of the approach. Analogous to DIC, the setup might change the resulting displacement field and thus the strain field. In the case of DIC, the output field is influenced by the subset size r and strain window radius r_ε [38]. The trade-off between setups is well illustrated for Ncorr in Table 1 where a higher smoothing (ROI radius r=30 and r_ε =20) is needed to obtain an acceptable SD which, however, results in a higher average response. The same applies for IR as a considerable bias is presented with decreasing local error see Fig. 3.

Fig. 3

Consequently, a compromise between the mean response accuracy and the introduced variation is needed. Therefore, three different B-spline control points spacings (15, 30 and 60 pixels) were tested to indicate the necessary user interface to obtain the most suitable field. Table 1 summarizes the error in the resulting horizontal displacements and strains for both the approaches – the proposed IR and the DIC algorithms published in [38,39]. While the standard deviations in Table 1 suggest a better performance with a higher spacing of IR, it is unfortunately accompanied by a higher bias from the prescribed deformation.

Table 1

Nevertheless, even the middle spacing showed results comparable to the DIC algorithms and was therefore used for evaluation with different setups L3 and L5 (according to [39]) while L1 setup showed the best response with the spacing of 60 showing a low bias in the mean response. Fig. 4 shows the obtained results for all the three configurations of synthetic data analysed by the IR approach. Here, the mean displacement response (average of vertical points at each horizontal level) was well captured and the same applies for the calculated strains.

Fig. 4

3.2 Uniaxial tension – large deformations

The porcine specimen was tested till rupture. Every 10th image only was used for the analysis by both DIC and IR. The setup of DIC was adjusted multiple times until a trade-off between distribution of the displacement and strain fields was found. The subset radius had only a small impact on the resulting displacement distribution with maximum MAPE ~ 1 % (r = 10 vs r = 30). Similar results were obtained also with different strain window radius for smoothing, with maximum MAPE ~ 3 % between DIC strain fields with r_ε = 5 and 10. The final analysis was performed with the subset radius of 10 pixels, the strain window radius of 5 pixels and step size of 4 pixels. Moreover, large strain analysis with an automatic seed propagation was needed. Once the acceptable field characteristics were obtained, they were directly compared with the IR approach with the control point spacing of 60 pixels. Note, that only small changes were obtained with different spacings. A comparison of displacement and strain fields is shown in Fig. 5.

Fig. 5

The distribution of displacements is almost the same which is also confirmed by MAPE of 2-3 % in pixel-to-pixel comparison. The MAPE increases a bit when comparing the strain field. These results are expectable because smoothing is introduced for the local DIC. Nevertheless, the difference between the IR and DIC results is around 4 % only and the strain concentrations and strain distributions are very similar. The structural similarity was very high for all the analysed stages with SSIM values ~ 0.98 indicating a comparable capturing of the deformation field and thus confirming high accuracy of the performed IR analysis.

3.3 Skin sample

Images obtained from the indentation test were firstly modified by cutting off the indenter and the background to improve the contrast, and then filtered to highlight the natural structure needed for the analysis. As it was impossible to prepare a suitable speckle pattern for DIC, it was hardly feasible to obtain any results using Ncorr and DIC. Therefore, the performed analyses showed very high correlation coefficients within the ROI, possibly influencing the results. Moreover, some areas were automatically omitted because the correlation coefficient exceeded a cut-off value of the program. Analogous to the uniaxial sample, the displacement field was almost independent on the chosen subset region radius: maximum MAPE was around 5 % (values varied throughout loading stages) when comparing radiuses of 15, 30 and 45 for DIC. However, the impact of different smoothing radius r_ε on the evaluated strain fields was huge. When a fixed subset radius of 30 was used, the MAPE between r_ε = 5 and 10 was 80 – 170 % for horizontal strain, 50 – 100 % for vertical strain and 80 – 130 % for shear strain. Therefore, it was not possible to obtain a reasonable strain distribution within the skin sample. Consequently, no reliable reference DIC distribution could be used for comparison of IR strain fields and only displacement fields in horizontal and vertical directions were compared (with DIC subset radius of 30, step size 4 pixels).

Spacing between B-spline control points of the IR approach was set to 128 pixels in the horizontal and 64 in the vertical direction. It is important to note, that no straightforward rule could be applied with such a complex sample requiring a proper inspection of the obtained results. A comparison between the resulting full-field displacements is shown in Fig. 6. Except for initial loading stages MAPE was found around 5 % in the horizontal direction and 2 % in the vertical direction (i.e., direction of indentation), showing thus a good agreement with DIC.

Fig. 6

It was important to check also the SSIM as an additional metric for the IR and DIC comparison. Here, the values are around 0.91, which is smaller than for the uniaxial sample but still very high. Moreover, IR managed to keep the same quality even in the areas where DIC was not capable to find any results. Summaries of both MAPE and SSIM metrics are shown in Fig. 7. In the case of SSIM plotted on the whole skin sample, high values can be seen within the region evaluated by the DIC analysis. Nevertheless, some areas show lower values due to presence of a high noise and decrease thus the overall average value. These parts should be treated carefully.

Fig. 7

4 Discussion

Characterization of mechanical properties is essential in solid mechanics. Progression of atherosclerosis or formation of an aneurysm increases the tissue heterogeneity which contradicts the assumptions often used in mechanical testing and its subsequent evaluation. Additional information on tissue heterogeneity can help us to improve the tissue characterization. This study shows possible advantages of the proposed IR-based approach for mapping the deformation field in soft tissue mechanical testing. The approach provides an alternative to the well-established DIC, based on the open-source tool Elastix [36], and increases thus its potential exploitation.

A wide application of IR in computer vision, mainly for aligning clinical images of multiple modalities, inspired also the *in vivo* strain analyses between two loading stages [6–8]. As it is impossible to prepare a suitable speckle pattern needed for DIC, a full field strain evaluation depends on a natural pattern only. The results of this study showed that IR is a suitable method in mechanical experiments to obtain rigorous full-field measurements not only within the range of

small deformations, but also for large deformations and, the most importantly, with a natural pattern of a biological tissue. High accuracy was obtained for synthetic data but also in real applications found in the field of biomechanics. Fig. 4 and Table 1 show that the specific setup of both IR and DIC can highly influence the resulting fields. However, this is inevitable because some noise and the resulting errors, cannot be avoided but only minimized. A recently published study [40] compared different DIC approaches including local and global ones but also a newly proposed augmented Lagrangian DIC method which includes mesh adaptability. The authors performed also an analysis of a synthetic sample 14 from [39] (used also in this study) and showed a very high error and bias for all the approaches. Our results indicate a very good alignment with the simulated data and extend the results of [34] where the authors used Demons registration for synthetic and experimental data for uniaxial tension tests of steel, though with significant differences from the expected results at strains above 0.05. Comparison of experimental data with unknown deformation fields was done here by using DIC as a reference, although we hoped to show advantages of the proposed IR approach compared to the DIC. As there are considerable differences even among DIC analyses themselves with various parameter settings, some error was expected when validating the IR approach. Nevertheless, DIC is a well-established method and still provides proper information at some parts of the skin sample introduced here and helped us to verify the approach in combination with two metrics of registration quality. This particular example showed the advantage of our alternative approach for full-field investigations because the missing information when using DIC might be problematic for a subsequent investigation of the tissue constitutive parameters done, for instance, using inverse analysis or virtual fields methods [43,44]. Moreover, also other soft tissues showing a natural pattern may be easily analysed using this approach [31–33]. However, an additional check of the registration quality is recommended using another metric

such as SSIM used here, otherwise some unreliable deformation can be found. The potential of full-field methods is especially important for diseased soft tissues such as atherosclerotic arteries, the heterogeneity of which disables creation of a regular specimen shape [11,45–47]. In addition to material non-homogeneity, a high variation may result from non-uniform specimen thickness violating the needed assumptions of the test [48]; also these errors can be decreased by using the proposed IR approach.

4.1 Limitations

The parameters used in the current work might not be suitable generally for any possible cases as indicated e.g., by the different spacing between B-spline control points. However, the used registration tool Elastix enables an easy configuration of parameters for a wide field of applications. Although an incremental approach was used in this study, updating the undeformed image in every iteration, it might be sometimes useful to have one reference image only. In that case, a different hierarchical strategy (multi-resolution) might be preferred. Moreover, if the error is cumulated through a number of images, it might result in high differences as shown in [34]. Nevertheless, the proposed approach showed a decreasing trend in the differences against the DIC and thus no cumulative effect was suspected.

5 Conclusion

In this study, we showed that Image Registration can be beneficial for strain measurements in soft biological tissues. We verified the methodology with a challenging benchmark based on simulated data and made proofs of concept on an arterial sample in uniaxial tension and on skin under indentation. Image Registration is very interesting for samples with a natural pattern where digital

image correlation can fail due difficulties in preparing an appropriate speckle pattern. Possible extension of the evaluated region for IR compared to DIC can also be interesting for subsequent identification of constitutive parameters especially for specimens with heterogeneous strain fields where complete full-field measurements are required, eve close to the edges. We plan to apply the proposed IR analysis on a spectrum of biological tissues in the future, but also to apply it on previous experiments where images were recorded but not useable for standard DIC.

Acknowledgment

This work was supported by Czech Science Foundation project No. 21-21935S.

Reference

[1] G.A. Holzapfel, J.J. Mulvihill, E.M. Cunnane, M.T. Walsh, Computational approaches for analyzing the mechanics of atherosclerotic plaques: A review, J. Biomech. 47 (2014) 859–869. https://doi.org/10.1016/j.jbiomech.2014.01.011.

[2] O. Lisický, A. Malá, Z. Bednařík, T. Novotný, J. Burša, Consideration of stiffness of wall layers is decisive for patient-specific analysis of carotid artery with atheroma, PLoS One. 15 (2020) e0239447. https://doi.org/10.1371/journal.pone.0239447.

[3] P. Marcián, N. Narra, L. Borák, J. Chamrad, J. Wolff, Biomechanical performance of cranial implants with different thicknesses and material properties: A finite element study, Comput. Biol. Med. 109 (2019) 43–52. https://doi.org/10.1016/j.compbiomed.2019.04.016.

[4] M. Tee, J.A. Noble, D.A. Bluemke, Imaging techniques for cardiac strain and deformation: Comparison of echocardiography, cardiac magnetic resonance and cardiac computed

tomography, Expert Rev. Cardiovasc. Ther. 11 (2013) 221–231. https://doi.org/10.1586/erc.12.182.

[5] Y. Tsadok, Z. Friedman, B.A. Haluska, R. Hoffmann, D. Adam, Myocardial strain assessment by cine cardiac magnetic resonance imaging using non-rigid registration, Magn. Reson. Imaging. 34 (2016) 381–390. https://doi.org/10.1016/j.mri.2015.12.035.

[6] A.J. Nederveen, S. Avril, L. Speelman, MRI strain imaging of the carotid artery: Present limitations and future challenges, J. Biomech. 47 (2014) 824–833. https://doi.org/10.1016/j.jbiomech.2014.01.014.

[7] D.A. Reiter, F.A. Fathallah, R.T. Farouki, J.H. Walton, Noninvasive high resolution mechanical strain maps of the spine intervertebral disc using nonrigid registration of magnetic resonance images, J. Biomech. 45 (2012) 1534–1539. https://doi.org/10.1016/j.jbiomech.2012.03.005.

[8] K. Miller, K. Chinzei, G. Orssengo, P. Bednarz, Mechanical properties of brain tissue in-vivo: Experiment and computer simulation, J. Biomech. 33 (2000) 1369–1376. https://doi.org/10.1016/S0021-9290(00)00120-2.

[9] R.A. Macrae, K. Miller, B.J. Doyle, Methods in Mechanical Testing of Arterial Tissue: A Review, Strain. 52 (2016) 380–399. https://doi.org/10.1111/str.12183.

[10] G.A. Holzapfel, G. Sommer, C.T. Gasser, P. Regitnig, Determination of layer-specific mechanical properties of human coronary arteries with nonatherosclerotic intimal thickening and related constitutive modeling, J Physiol Hear. Circ Physiol. 103 (2005) 806–808. https://doi.org/10.1152/ajpheart.00934.2004.

[11] Z. Teng, Y. Zhang, Y. Huang, J. Feng, J. Yuan, Q. Lu, M.P.F. Sutcliffe, A.J. Brown, Z. Jing, J.H. Gillard, Material properties of components in human carotid atherosclerotic plaques: A uniaxial extension study, Acta Biomater. 10 (2014) 5055–5063. https://doi.org/10.1016/j.actbio.2014.09.001.

[12] G. Sommer, P. Regitnig, L. Koltringer, G.A. Holzapfel, Biaxial mechanical properties of intact and layer-dissected human carotid arteries at physiological and supraphysiological loadings, AJP Hear. Circ. Physiol. 298 (2010) H898–H912. https://doi.org/10.1152/ajpheart.00378.2009.

[13] A.C. Akyildiz, L. Speelman, F.J.H. Gijsen, Mechanical properties of human atherosclerotic intima tissue, J. Biomech. 47 (2014) 773–783. https://doi.org/10.1016/j.jbiomech.2014.01.019.

[14] H. Fehervary, M. Smoljkić, J. Vander Sloten, N. Famaey, Planar biaxial testing of soft biological tissue using rakes: A critical analysis of protocol and fitting process, J. Mech. Behav. Biomed. Mater. 61 (2016) 135–151. https://doi.org/10.1016/j.jmbbm.2016.01.011.

[15] S. V. Jett, L.T. Hudson, R. Baumwart, B.N. Bohnstedt, A. Mir, H.M. Burkhart, G.A. Holzapfel, Y. Wu, C.H. Lee, Integration of polarized spatial frequency domain imaging (pSFDI) with a biaxial mechanical testing system for quantification of load-dependent collagen architecture in soft collagenous tissues, Acta Biomater. 102 (2020) 149–168. https://doi.org/10.1016/j.actbio.2019.11.028.

[16] A. Ní Annaidh, K. Bruyère, M. Destrade, M.D. Gilchrist, M. Otténio, Characterization of the anisotropic mechanical properties of excised human skin, J. Mech. Behav. Biomed. Mater. 5 (2012) 139–148. https://doi.org/10.1016/j.jmbbm.2011.08.016.

[17] J.S. Affagard, P. Feissel, S.F. Bensamoun, Identification of hyperelastic properties of passive thigh muscle under compression with an inverse method from a displacement field measurement, J. Biomech. 48 (2015) 4081–4086. https://doi.org/10.1016/j.jbiomech.2015.10.007.

[18] C. Cavinato, J. Molimard, N. Curt, S. Campisi, L. Orgéas, P. Badel, Does the knowledge of the local thickness of human ascending thoracic aneurysm walls improve their mechanical analysis?, Front. Bioeng. Biotechnol. 7 (2019) 1–12. https://doi.org/10.3389/fbioe.2019.00169.

[19] E. Pack, J. Dubik, W. Snyder, A. Simon, S. Clark, R. De Vita, Biaxial Stress Relaxation of Vaginal Tissue in Pubertal Gilts, J. Biomech. Eng. 142 (2020) 1–7. https://doi.org/10.1115/1.4045707.

[20] F.M. Davis, Y. Luo, S. Avril, A. Duprey, J. Lu, Local mechanical properties of human ascending thoracic aneurysms, J. Mech. Behav. Biomed. Mater. 61 (2016) 235–249. https://doi.org/10.1016/j.jmbbm.2016.03.025.

[21] F.M. Davis, Y. Luo, S. Avril, A. Duprey, J. Lu, Pointwise characterization of the elastic properties of planar soft tissues: application to ascending thoracic aneurysms, Biomech. Model. Mechanobiol. 14 (2015) 967–978. https://doi.org/10.1007/s10237-014-0646-9.

[22] E. Dall'Ara, D. Barber, M. Viceconti, About the inevitable compromise between spatial resolution and accuracy of strain measurement for bone tissue: A 3D zero-strain study, J. Biomech. 47 (2014) 2956–2963. https://doi.org/10.1016/j.jbiomech.2014.07.019.

[23] V.A. Acosta Santamaría, M. Flechas García, J. Molimard, S. Avril, Three-Dimensional Full-

Field Strain Measurements across a Whole Porcine Aorta Subjected to Tensile Loading Using Optical Coherence Tomography–Digital Volume Correlation, Front. Mech. Eng. 4 (2018) 1–14. https://doi.org/10.3389/fmech.2018.00003.

[24] M.R. Bersi, V.A. Acosta Santamaría, K. Marback, P. Di Achille, E.H. Phillips, C.J. Goergen, J.D. Humphrey, S. Avril, Multimodality Imaging-Based Characterization of Regional Material Properties in a Murine Model of Aortic Dissection, Sci. Rep. 10 (2020) 1–23. https://doi.org/10.1038/s41598-020-65624-7.

[25] Z. Wang, H. Kieu, H. Nguyen, M. Le, Digital image correlation in experimental mechanics and image registration in computer vision: Similarities, differences and complements, Opt. Lasers Eng. 65 (2015) 18–27. https://doi.org/10.1016/j.optlaseng.2014.04.002.

[26] G. Lionello, C. Sirieix, M. Baleani, An effective procedure to create a speckle pattern on biological soft tissue for digital image correlation measurements, J. Mech. Behav. Biomed. Mater. 39 (2014) 1–8. https://doi.org/10.1016/j.jmbbm.2014.07.007.

[27] Y. Sun, J.H.L. Pang, C.K. Wong, F. Su, Finite element formulation for a digital image correlation method, Appl. Opt. 44 (2005) 7357–7363. https://doi.org/10.1364/AO.44.007357.

[28] P. Cheng, M.A. Sutton, H.W. Schreier, S.R. McNeill, Full-field speckle pattern image correlation with B-Spline deformation function, Exp. Mech. 42 (2002) 344–352. https://doi.org/10.1007/bf02410992.

[29] J. Réthoré, T. Elguedj, P. Simon, M. Coret, On the Use of NURBS Functions for Displacement Derivatives Measurement by Digital Image Correlation, Exp. Mech. 50

(2010) 1099–1116. https://doi.org/10.1007/s11340-009-9304-z.

[30] B. Wang, B. Pan, Subset-based local vs. finite element-based global digital image correlation: A comparison study, Theor. Appl. Mech. Lett. 6 (2016) 200–208. https://doi.org/10.1016/j.taml.2016.08.003.

[31] A. Bel-Brunon, S. Kehl, C. Martin, S. Uhlig, W.A. Wall, Numerical identification method for the non-linear viscoelastic compressible behavior of soft tissue using uniaxial tensile tests and image registration - Application to rat lung parenchyma, J. Mech. Behav. Biomed. Mater. 29 (2014) 360–374. https://doi.org/10.1016/j.jmbbm.2013.09.018.

[32] A.M. Birzle, C. Martin, S. Uhlig, W.A. Wall, A coupled approach for identification of nonlinear and compressible material models for soft tissue based on different experimental setups – Exemplified and detailed for lung parenchyma, J. Mech. Behav. Biomed. Mater. 94 (2019) 126–143. https://doi.org/10.1016/j.jmbbm.2019.02.019.

[33] A.M. Birzle, C. Martin, L. Yoshihara, S. Uhlig, W.A. Wall, Experimental characterization and model identification of the nonlinear compressible material behavior of lung parenchyma, J. Mech. Behav. Biomed. Mater. 77 (2018) 754–763. https://doi.org/10.1016/j.jmbbm.2017.08.001.

[34] C. Zhu, H. Wang, K. Kaufmann, K.S. Vecchio, Computer vision approach to study deformation of materials, ArXiv. (2019).

[35] M.I. Miga, A new approach to elastography using mutual information and finite elements, Phys. Med. Biol. 48 (2003) 467–480. https://doi.org/10.1088/0031-9155/48/4/304.

[36] S. Klein, M. Staring, K. Murphy, M.A. Viergever, J.P.W. Pluim, Elastix: a toolbox for

intensity-based medical image registration, IEEE Trans. Med. Imaging. 29 (2009) 196–205.

[37] K. Marstal, F. Berendsen, M. Staring, S. Klein, SimpleElastix: A user-friendly, multi-lingual library for medical image registration, in: Proc. IEEE Conf. Comput. Vis. Pattern Recognit. Work., 2016: pp. 134–142.

[38] J. Blaber, B. Adair, A. Antoniou, Ncorr: Open-Source 2D Digital Image Correlation Matlab Software, Exp. Mech. 55 (2015) 1105–1122. https://doi.org/10.1007/s11340-015-0009-1.

[39] P.L. Reu, E. Toussaint, E. Jones, H.A. Bruck, M. Iadicola, R. Balcaen, D.Z. Turner, T. Siebert, P. Lava, M. Simonsen, DIC Challenge: Developing Images and Guidelines for Evaluating Accuracy and Resolution of 2D Analyses, 2018. https://doi.org/10.1007/s11340-017-0349-0.

[40] J. Yang, K. Bhattacharya, Fast Adaptive Mesh Augmented Lagrangian Digital Image Correlation, Exp. Mech. 61 (2021) 719–735. https://doi.org/10.1007/s11340-021-00695-9.

[41] A. Shradhanjali, B.D. Riehl, B. Duan, R. Yang, J.Y. Lim, Spatiotemporal Characterizations of Spontaneously Beating Cardiomyocytes with Adaptive Reference Digital Image Correlation, Sci. Rep. 9 (2019) 1–10. https://doi.org/10.1038/s41598-019-54768-w.

[42] Z. Wang, A.C. Bovik, H.R. Sheikh, E.P. Simoncelli, Image quality assessment: From error visibility to structural similarity, IEEE Trans. Image Process. 13 (2004) 600–612. https://doi.org/10.1109/TIP.2003.819861.

[43] M. Grédiac, F. Pierron, S. Avril, E. Toussaint, The Virtual Fields Method for Extracting Constitutive Parameters From Full-Field Measurements: a Review, Strain. 42 (2006) 233–253. https://doi.org/10.1111/j.1475-1305.2006.tb01504.x.

[44] S. Avril, M. Bonnet, A.S. Bretelle, M. Grédiac, F. Hild, P. Ienny, F. Latourte, D. Lemosse, S. Pagano, E. Pagnacco, F. Pierron, Overview of identification methods of mechanical parameters based on full-field measurements, Exp. Mech. 48 (2008) 381–402. https://doi.org/10.1007/s11340-008-9148-y.

[45] J.J. Mulvihill, E.M. Cunnane, S.M. Mchugh, E.G. Kavanagh, S.R. Walsh, M.T. Walsh, Mechanical, biological and structural characterization of in vitro ruptured human carotid plaque tissue, Acta Biomater. 9 (2013) 9027–9035. https://doi.org/10.1016/j.actbio.2013.07.012.

[46] E.M. Cunnane, J.J.E. Mulvihill, H.E. Barrett, M.M. Hennessy, E.G. Kavanagh, M.T. Walsh, Mechanical properties and composition of carotid and femoral atherosclerotic plaques: A comparative study, J. Biomech. 49 (2016) 3697–3704. https://doi.org/10.1016/j.jbiomech.2016.09.036.

[47] H.E. Barrett, E.M. Cunnane, E.G. Kavanagh, M.T. Walsh, On the effect of calcification volume and configuration on the mechanical behaviour of carotid plaque tissue, J. Mech. Behav. Biomed. Mater. 56 (2016) 45–56. https://doi.org/10.1016/j.jmbbm.2015.11.001.

[48] O. Lisický, A. Hrubanová, R. Staffa, R. Vlachovský, J. Burša, Constitutive models and failure properties of fibrous tissues of carotid artery atheroma based on their uniaxial testing, J. Biomech. 129 (2021) 110861. https://doi.org/10.1016/j.jbiomech.2021.110861.

Fig. 8: A flowchart of IR approach used to map a full-field deformation from experimental measurements.

Fig. 9: Three samples used in the study. A is reused from [39] where artificial heterogeneous displacement field was applied. B is an aorta sample in uniaxial tension and C is a skin sample under indentation test.

Fig. 10: Horizontal displacement and strain of synthetic data Sample 14, L3 from DIC Challenge. An influence of different sizing of control points is shown for (A-B) – 15, (C-D) – 30 and (E-F) – 60. A trade-off between SD and bias to simulated data is required.

Fig. 11: Displacement (left column) and strain (right column) distribution along horizontal direction from the synthetic data of sample 14 with different setups: (A-B) - L1, (C-D) – L3 and (E-F) – L5.

Fig. 12: Comparison of displacement and strain fields obtained using DIC and IR approaches for uniaxial tension in the middle of a loading cycle.

Fig. 13: Comparison between vertical and horizontal displacement fields. DIC (top row) shows a lot of missing data due to a poor correlation coefficient while it was possible to analyse the whole sample with the IR approach (bottom row). To enable straight comparison, the colour bar scale is fixed based on DIC results. Therefore, the maximal vertical displacements in the left bottom figure are beyond the scale of DIC and depicted uniquely in purple.

Fig. 14: Comparison between DIC and IR by means of MAPE (left) and SSIM (right) metrics for the porcine (uniaxial test, in blue) and skin (indentation test, in orange) sample. In the left figure, the solid and dotted lines are related to displacements and strains, respectively. Examples of SSIM distribution are shown for both samples indicating noisy response. Some parts, mainly on the edge of the skin sample, show lower values and hence should be treated carefully.

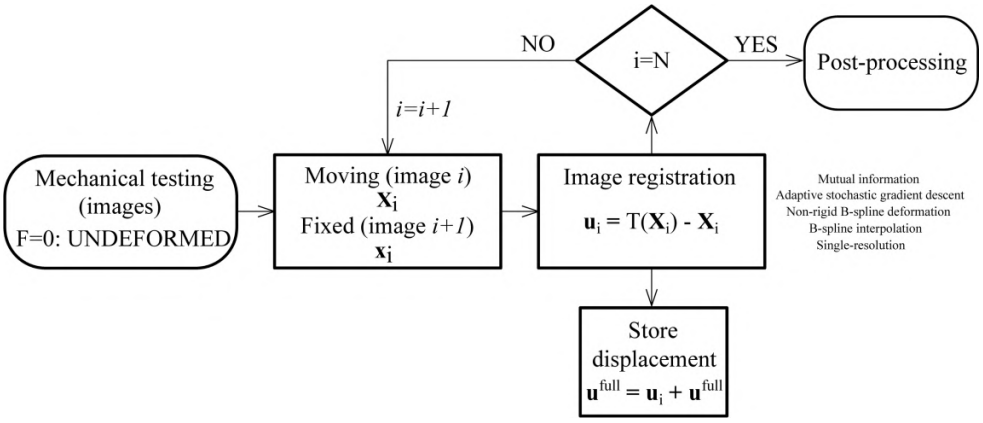

Fig. 1: A flowchart of IR approach used to map a full-field deformation from experimental measurements.

320x135mm (300 x 300 DPI)

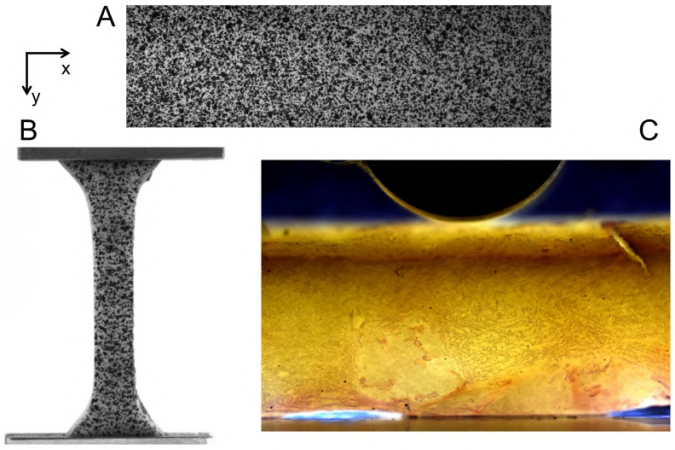

Fig. 2: Three samples used in the study. A is reused from [39] where artificial heterogeneous displacement field was applied. B is an aorta sample in uniaxial tension and C is a skin sample under indentation test.

338x190mm (300 x 300 DPI)

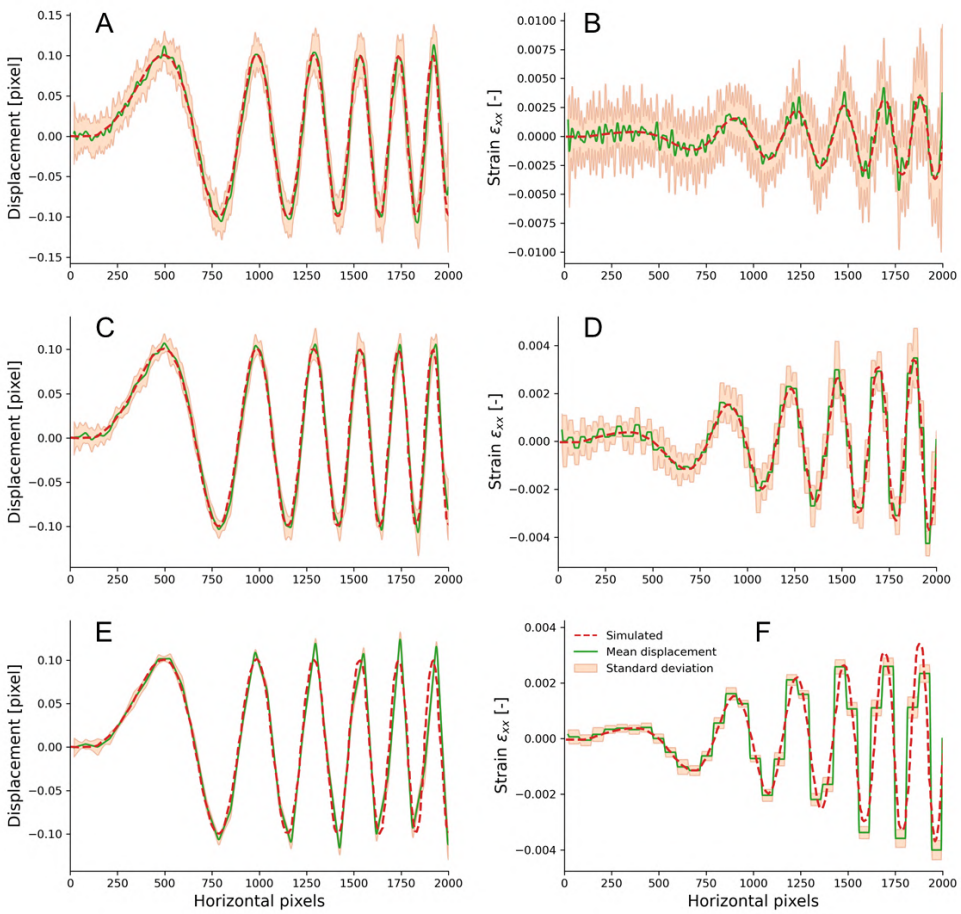

Fig. 3: Horizontal displacement and strain of synthetic data Sample 14, L3 from DIC Challenge. An influence of different sizing of control points is shown for (A-B) – 15, (C-D) – 30 and (E-F) – 60. A trade-off between SD and bias to simulated data is required.

300x300mm (96 x 96 DPI)

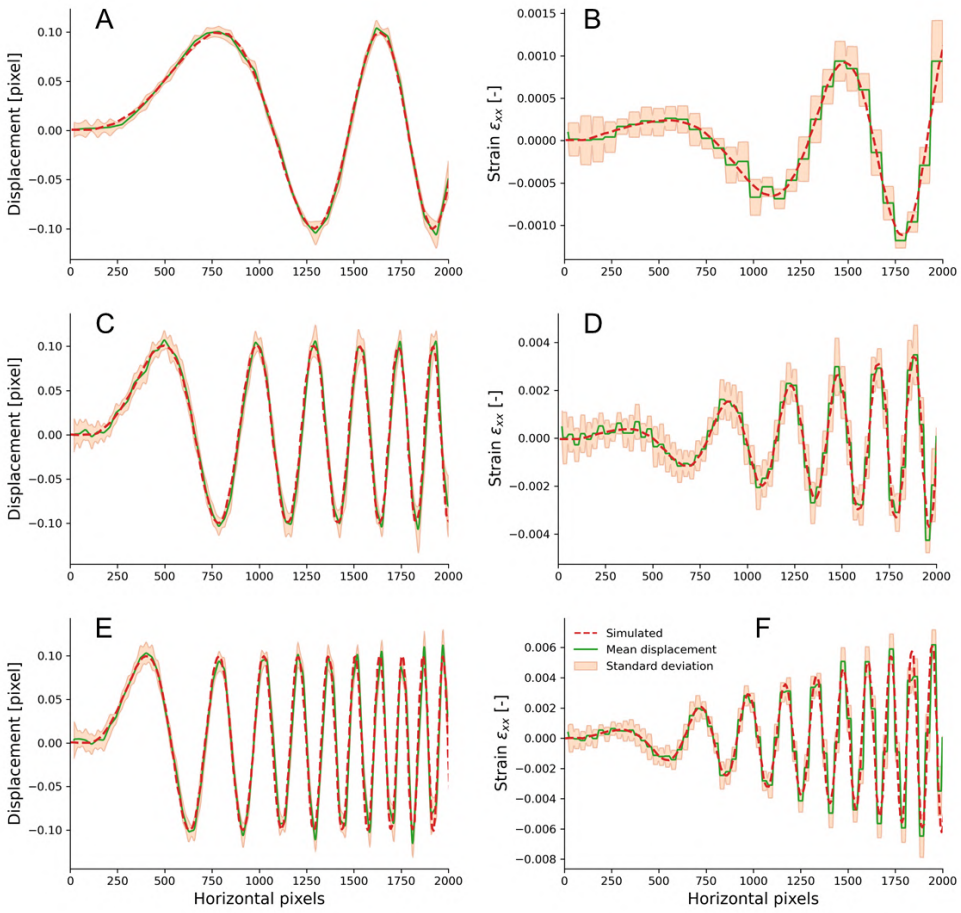

Fig. 4: Displacement (left column) and strain (right column) distribution along horizontal direction from the synthetic data of sample 14 with different setups: (A-B) - L1, (C-D) – L3 and (E-F) – L5.

300x300mm (96 x 96 DPI)

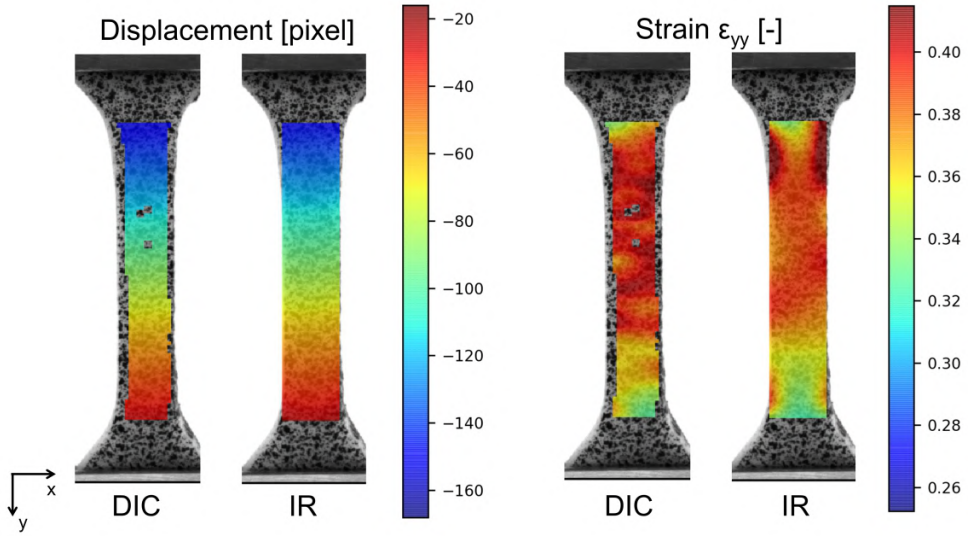

Fig. 5: Comparison of displacement and strain fields obtained using DIC and IR approaches for uniaxial tension in the middle of a loading cycle.

338x190mm (300 x 300 DPI)

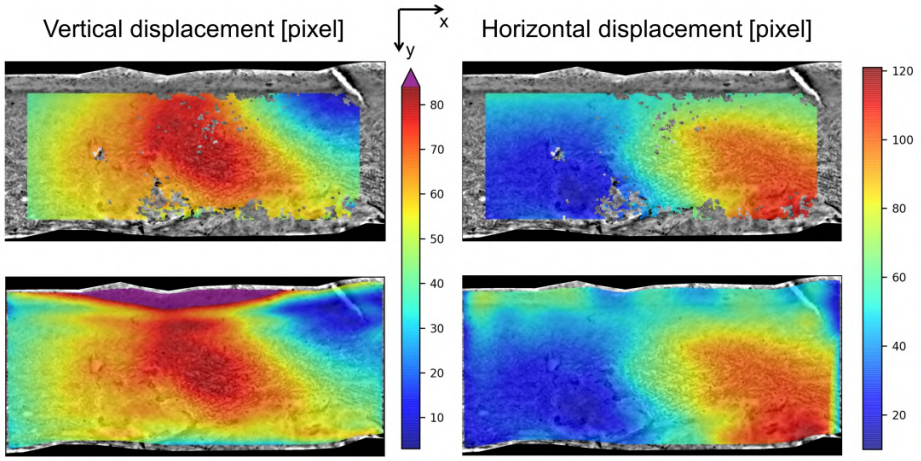

Fig. 6: Comparison between vertical and horizontal displacement fields. DIC (top row) shows a lot of missing data due to a poor correlation coefficient while it was possible to analyse the whole sample with the IR approach (bottom row). To enable straight comparison, the colour bar scale is fixed based on DIC results. Therefore, the maximal vertical displacements in the left bottom figure are beyond the scale of DIC and depicted uniquely in purple.

338x190mm (300 x 300 DPI)

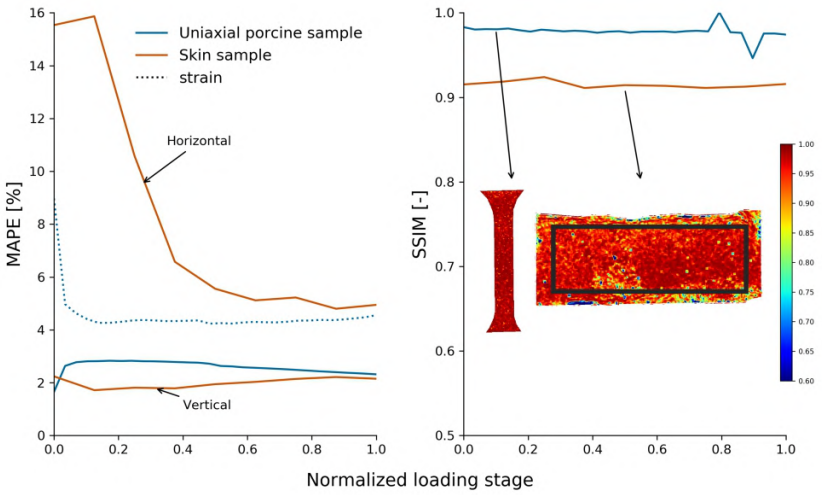

Fig. 7: Comparison between DIC and IR by means of MAPE (left) and SSIM (right) metrics for the porcine (uniaxial test, in blue) and skin (indentation test, in orange) sample. In the left figure, the solid and dotted lines are related to displacements and strains, respectively. Examples of SSIM distribution are shown for both samples indicating noisy response. Some parts, mainly on the edge of the skin sample, show lower values and hence should be treated carefully.

338x190mm (300 x 300 DPI)

		u_{xx} SD [pixel]	ε_{xx} SD [10^{-6}]
proposed IR approach	IR - 15	0.023	2559
	IR - 30	0.011	702
	IR - 60	0.006	214
Ncorr	r=10, r_ε=5	0.029	3400
	r=30 r_ε=20	0.0073	240
DIC challenge	Code A	0.005	172
	Code B	0.01	676
	Code C	0.01	578
	Code D	0.011	686
	Code E	0.015	256
	Code F	0.011	542
	Code G	0.01	429
	Code H	0.011	341
	Code I	0.012	638
	Code J	0.015	875
	Code K	0.011	551

Table 1: Synthetic data summary. SDs in the resulting displacement and strain fields analysed for the proposed IR approach in comparison with the data published for the DIC algorithms. The number x in IR - x indicate the spacing between control points. Names of DIC results have been retained from the original article.

H. Appendix

Layer-specific residual deformation and stress of carotid artery

Preliminary results including a description of Materials and Methods, Results and Discussion.

H.1. Experimental investigation - carotid artery

Experimental investigation of residual deformation of carotid arteries is substantial credibility of computational modelling. Very little information is known on a layer-specific deformation of the carotid artery (without atherosclerosis) see section 5.8. Therefore, this section provides some geometrical parameters following the protocol in Holzapfel et al. (2007) which can be then freely used as shown in Holzapfel et al. (2010). Moreover, a modification in the protocol was introduced to verify whether specific ways of layer separation influence the results and whether the separation can be done before the radial cut. If yes, we would develop an experimental approach for cases where the atherosclerotic plaque is present. The author initially thought that this section would also include atherosclerotic plaques, even though it was not included in the aims of the thesis. Unfortunately, the covid-19 pandemic influenced a sample collection from the Department of Anatomy. Nevertheless, the results are still unique and will hopefully serve for further research.

H.1.1. Materials and Methods

Common carotid arteries (both left and right) from five donors were harvested from an autopsy at the Department of Anatomy of Masaryk University in Brno. Each sample was used for research purposes with signed confirmation. Samples were preserved in a saline solution and were tested within two hours after the autopsy or frozen in -20 $°C$. Only carotids with no or minimal sign of atherosclerotic disease were included. Donors were relatively old, including male 80 years, male 88 years, male 72 years, male 73 years, and female 83 years.

Sample preparation and cleaning were done under the supervision of an experienced surgeon from St. Ann's Hospital. Loose connective tissue was carefully removed from the outer surface of the adventitia layer. The total length of samples differed from ca 1 cm to 2 cm, influencing the possibilities for the experiment. Nevertheless, the circumferential ring (denoted as ring below) was always obtained for analysis. Only the axial strip (strip below) was hard to get. Subsequently, two measurement protocols were followed see Figure H.2. The first is from Holzapfel et al. (2007) where the ring and strip were cut from an intact artery and glued pointwise with cyanoacrylate adhesive to a short plastic cylinder[1]. Thereafter, the layers are separated. In the second scenario, the adventitia layer was firstly separated from the media + intima[2] (MI), see separation in Figure H.1, and then the rings and strips were glued to the plastic cylinder. As both right and left common carotid segments were obtained, both experimental protocols were applied for the same patient. This should reduce the possible effect of inter-patient variability when comparing both protocols.

The prepared specimens were immediately put into a heated batch with 37 $°C$ 0.9 % NaCl solution. After the calibration for 30 minutes, rings were cut radially (the release of compressional RS on the inner surface and tensile RS on the outer surface manifested in

[1]Length of the plastic cylinder is somehow larger than the height of the specimen and ensures that the sample is not in contact with a pad and thus friction in the contact does not influence the opening.

[2]The intima is relatively thin for the carotid artery, and its separation was impossible without possible damage. Therefore, only two layers were measured. Surprisingly, a clear boundary was visible between adventitia and media. Also, the separation was very straightforward as it was possible to detach layers from both sides of the artery.

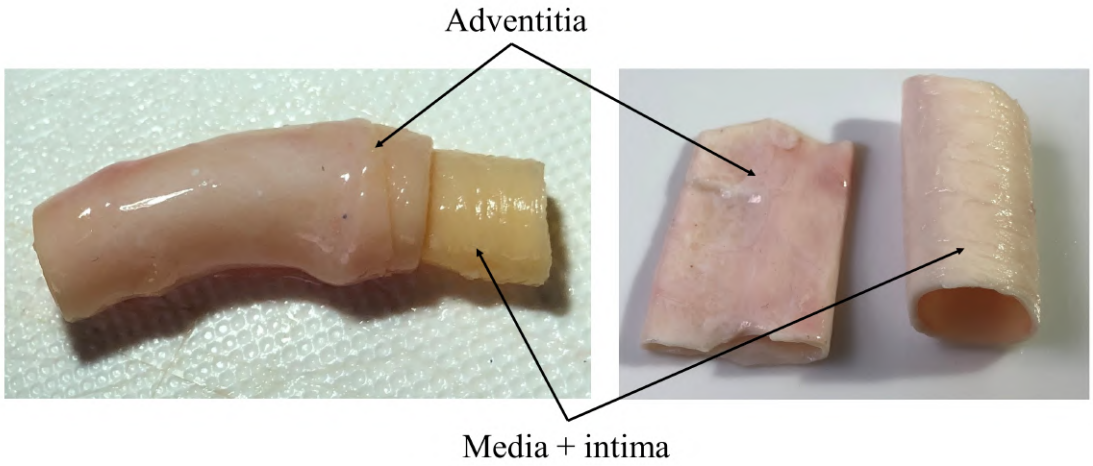

Figure H.1: Outer layer (*tunica adventitia*) separation from the MI layer. Colour differences and the boundary can be observed for all samples. The media holds its cylindrical shape after the separation while adventitia becomes flat on the air (right figure).

the ring-opening) and let in the heated bath for 16 hours. After this period, the adventitia layer was separated from the ring and strip of the experimental protocol 1 and glued to another tube. After that, specimens were in the heated batch for additional 6 hours (the times correspond to those applied in Holzapfel et al. (2007)). A digital image from a CCD camera perpendicular to the tested object was taken at each state. After the experiment, each layer was histologically examined to confirm the separation and potential destruction of the layer.

Image processing and vessel parameters

The set of images from the experiments were analysed with a semi-automatic algorithm written in python to obtain essential geometrical parameters of each segment. The segment's outer and inner boundaries were manually traced with several points and approximated with B-splines for further analysis. Images were scaled using a known diameter of the plastic cylinder. The boundary is separated into equidistant points (variable number of points), so the total length can be calculated approximately as a sum of segments between points. Curvature is calculated in each point using eq. (H.1).

$$\kappa = \frac{x'y'' - y'x''}{(x'^2 + y'^2)^{\frac{3}{2}}}, \tag{H.1}$$

where x',$y' and x''$,y'' are a first and second derivatives of a B-spline with respect to the parameter of the parametric expression, defining the segment boundary. After that a local radius was calculated as

$$r = \frac{1}{\kappa}, \tag{H.2}$$

which was then averaged for all the calculated points of each segment. The opening angle ϕ_0 was determined as an angle defined from the middle and both ending points (equidistant) of the inner boundary. The definitions of the opening angle vary among studies but can be recalculated (Humphrey et al., 2002) for comparison, assuming that the shape is circular. It is important to note that the radius rather than the opening

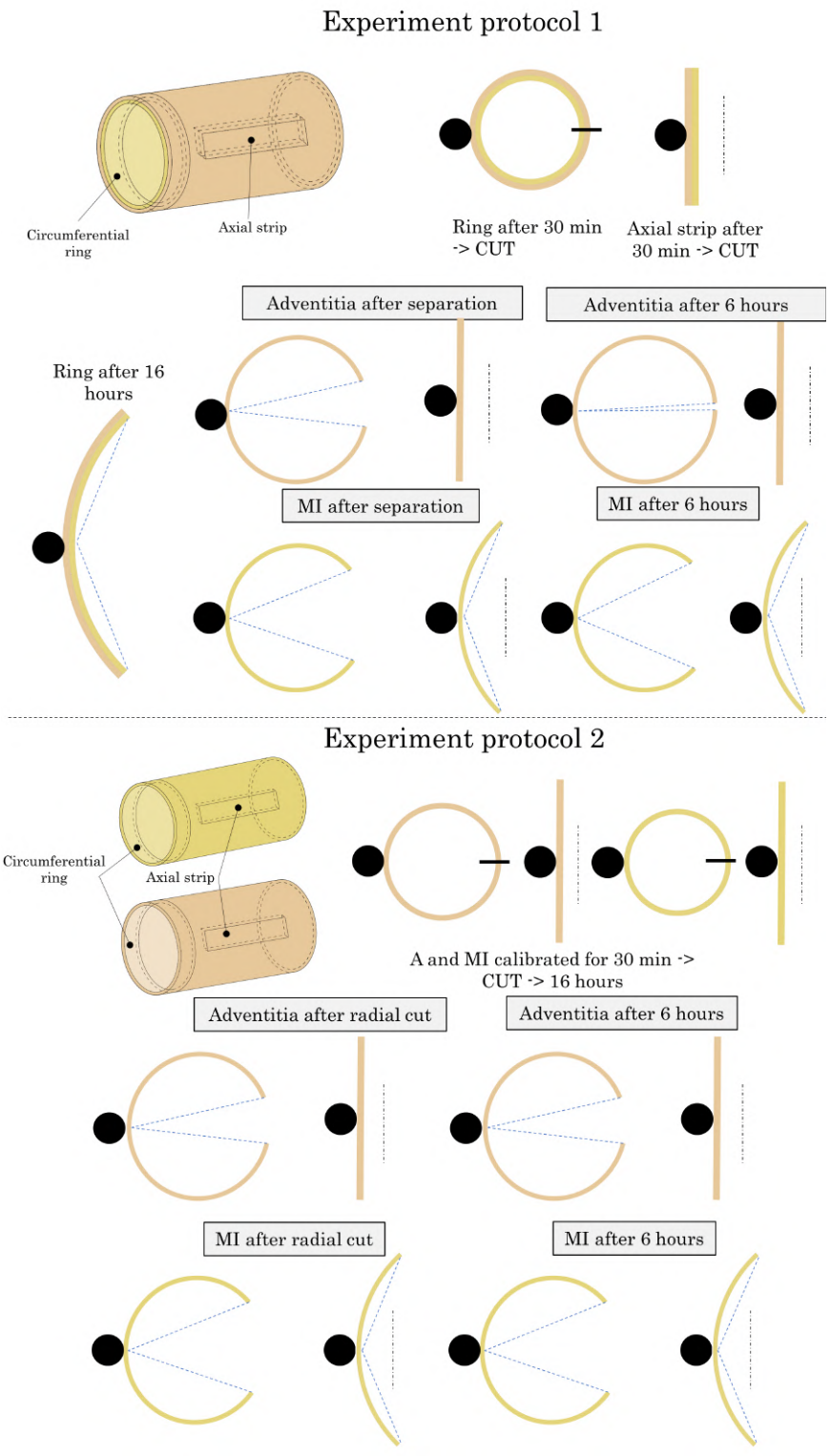

Figure H.2: Two different experimental protocols were used in this work to investigate residual deformations of carotid wall layers. Experimental protocol 1 refers to that one used in Holzapfel et al. (2007) where the separation is done after radial cut and calibration while experimental protocol 2 was designed for different RS release comparisons with the layer separation as a first step. Adventitia layer (beige) and MI layer (yellow) were calibrated, and a set of images were recorded during the 22-hour experiment. Cases where the artery axis is indicated, represent the axial specimen of the specific layer. Black circle represent the plastic cylinders being, however, much larger in reality.

angle is a characteristic quantity for a strip as the opening angle depends on the segment length. The thickness was determined locally for each point as a distance between the point at the inner boundary and the point of intersection of a normal vector with the outer boundary. Finally, a mean thickness was calculated from all local distances. To sum up, thickness, curvature (radius can be calculated using (H.2)), height, and opening angle were the parameters of interest.

Statistical analysis

The amount of patients included in the study disables a proper statistical analysis to draw a valuable conclusion; therefore, descriptive statistics were generally used, showing means ± SD for normally distributed data and median with interquartile range for skewed data. Moreover, Pearson's correlation coefficient r indicated a relationship between opening angle and sample thickness; statistical significance was assumed if $p<0.05$.

H.1.2. Results

Histological examination revealed that the separation of adventitia was not perfect, and some part of media remained. It differs from specimen to specimen, but approximately 20 % of media remains on adventitia. It was found impossible to clean the adventitia completely. The media consists of multiple sub-layers, enabling different separation locations but these sub-layers tear easily. Figure H.3 B shows extreme amount of media remaining on the adventitia (this specimen was thus not included in the analysis). Therefore, it is essential to note that the thickness of the adventitia may differ and be influenced by the presence of media. Thickness of the layers is shown in Figure H.4. The calibration in a heated bath showed that the opening is time-dependent, it is not stabilized within the first hour after cutting, however, a verification will require more samples.

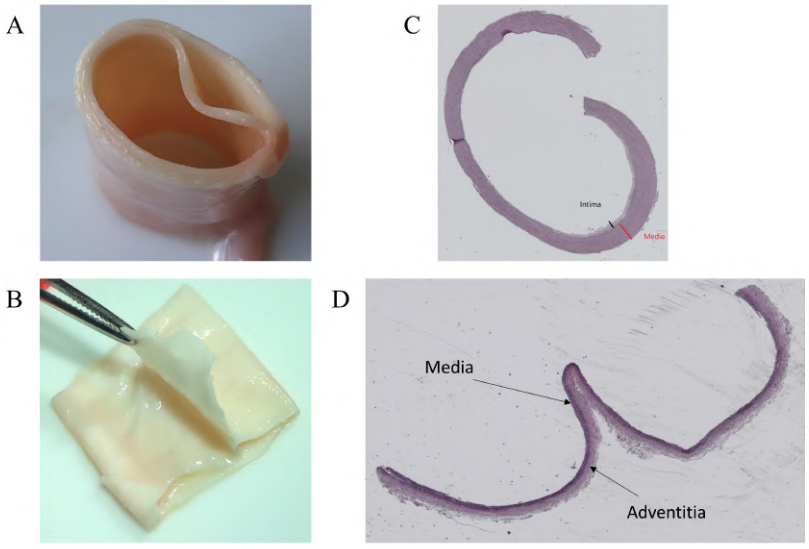

Figure H.3: An example of layer separation. The adventitia boundary was visible, enabling a straightforward separation (A). A wholesome media sub-layer and its clearing from adventitia were turned inside-out for easier access (B). Histological examination of MI (C) and adventitia with some portion of media remains on the adventitia (D).

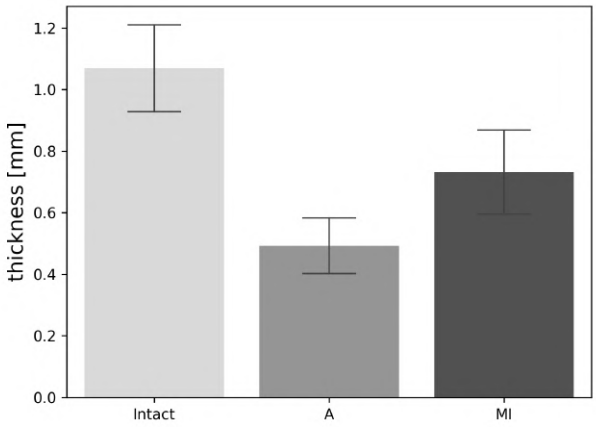

Figure H.4: Mean thickness of all investigated layers and the whole artery. The thickness of the whole artery is slightly higher than the sum of the two layers.

Circumferential ring

The summary of inner and outer curvatures is shown in Figure H.5 and opening angles in Figure H.6 for circumferential specimens. The curvature can be recalculated to radius by using eq. (H.2). The mean height was 3.94 ± 0.9 mm for adventitia, 3.94 ± 0.87 mm for MI, and 4.39 ± 0.63 mm for the whole wall.

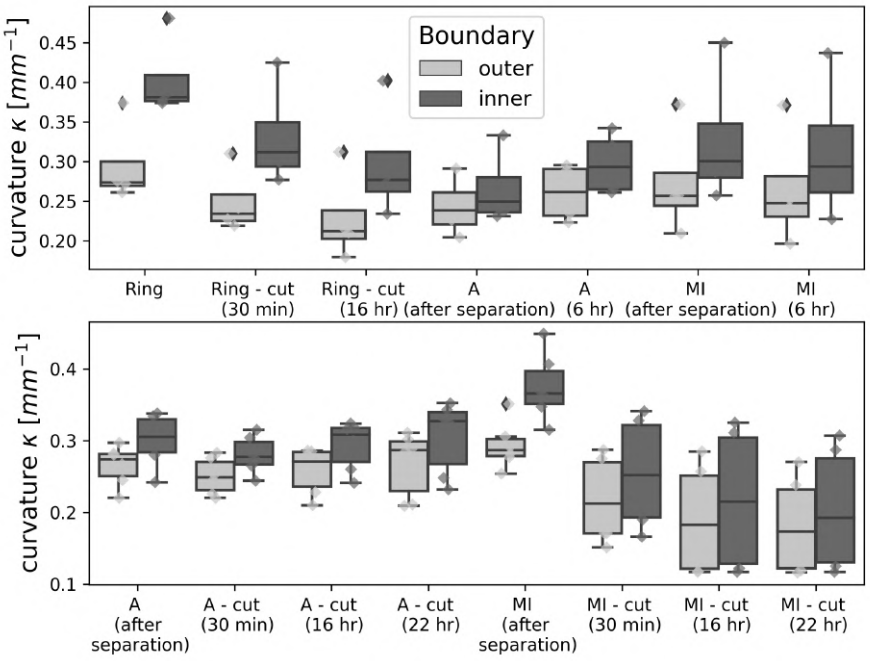

Figure H.5: Average curvatures for the inner and outer boundary of specific segments. Experimental protocol 1 - upper figure and experimental protocol 2 - lower figure.

The behaviour of adventitia was found surprising (no such a record was found in the literature) because it cannot hold its cylindrical shape on air but returned to it immedi-

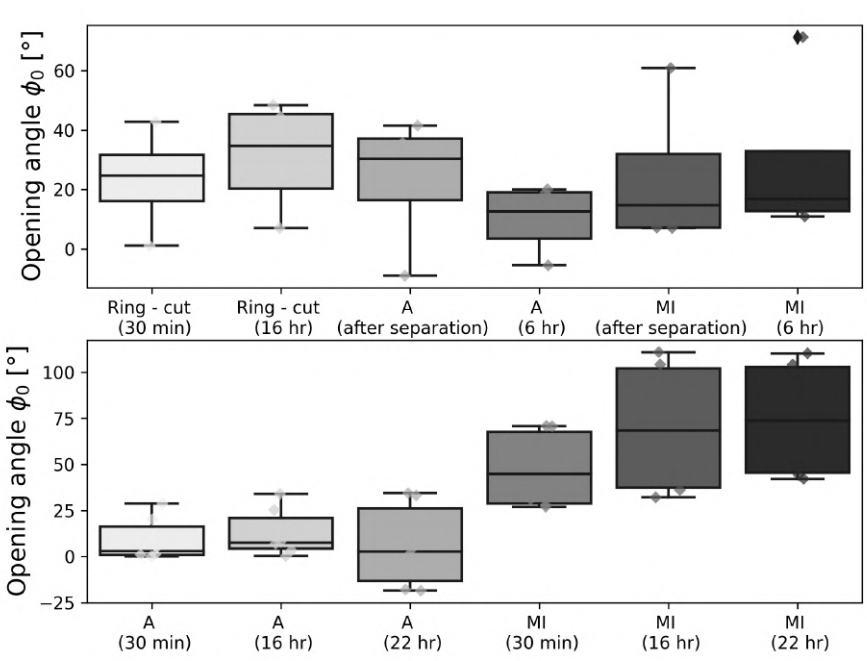

Figure H.6: Average opening angles of specific segments. Experimental protocol 1 - upper figure and experimental protocol 2 - lower figure.

ately when put into the solution[3]. Moreover, when the radial cut was performed for the ring, it mostly did not show any opening and stayed rather closed, as shown in Figure H.7 B. In some cases the ring closed even inside and a negative opening angle was recorded. It is possible that also the cases with zero opening were trying to close into negative values. However, it required manual enforcement (gently removing the contact by a radial displacement of a free end) to enable such behaviour. Unfortunately, these results were operator dependent (choice of the moving end and direction of the movement) and thus in this experiment the specimen was let free and untouched instead.

Moreover, some connective tissue remains on the outer surface of adventitia, introducing some friction and thus disabling a free movement. This rather closing behaviour was noted and can be seen in Figure H.7 B, where the free ends are mutually pushed together, distorting thus the circularity of the ring. Nevertheless, some specimens showed some opening. The visual check and thickness measurement indicated a higher portion of media remains on the adventitia layer of these specimens. A statistically significant negative correlation ($r = -0.72$, $p = 0.019$) was found between the opening angle and ratio of layer thicknesses (MI/adventitia), indicating that positive opening angles of adventitia are related to a higher portion of media on the adventitia, see Figure H.8. For adventitia with lower amount of media, the opening angle is zero or even negative.

On the other hand, MI and intact walls mostly showed the expectable opening of the ring. The opening was slightly higher for the whole artery ring compared to MI in experiment protocol 1 (see Figure H.6). However, when the layer separation was performed before cutting of the rings (experimental protocol 2), the opening of MI was higher than that of the whole wall. Unfortunately, experimental protocol 2 does not

[3]Room temperature and heated bath were tested and resulted in the same behaviour.

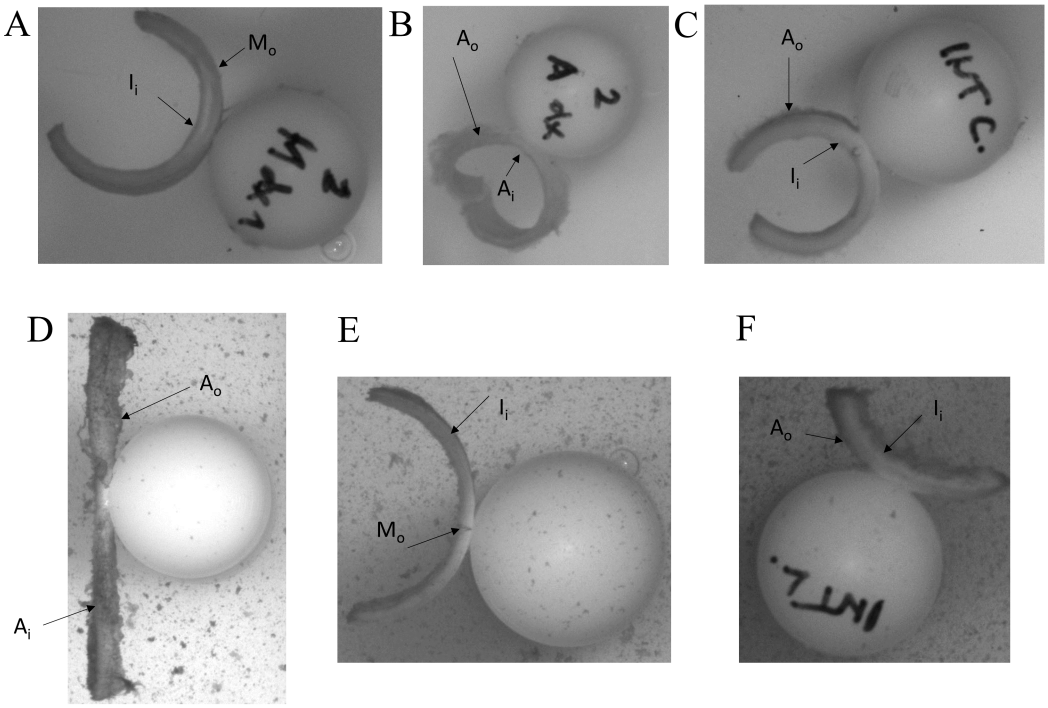

Figure H.7: This figure is an example of a typical layer behaviour, even though not from a single patient. Circumferential specimens: A - MI, B - adventitia, C - whole artery. Axial specimens: D - adventitia, E - MI, F - whole artery. Symbols A and M denote adventitia and MI specimens while subscripts i and o relate to the inner and outer surfaces of the specimen, respectively.

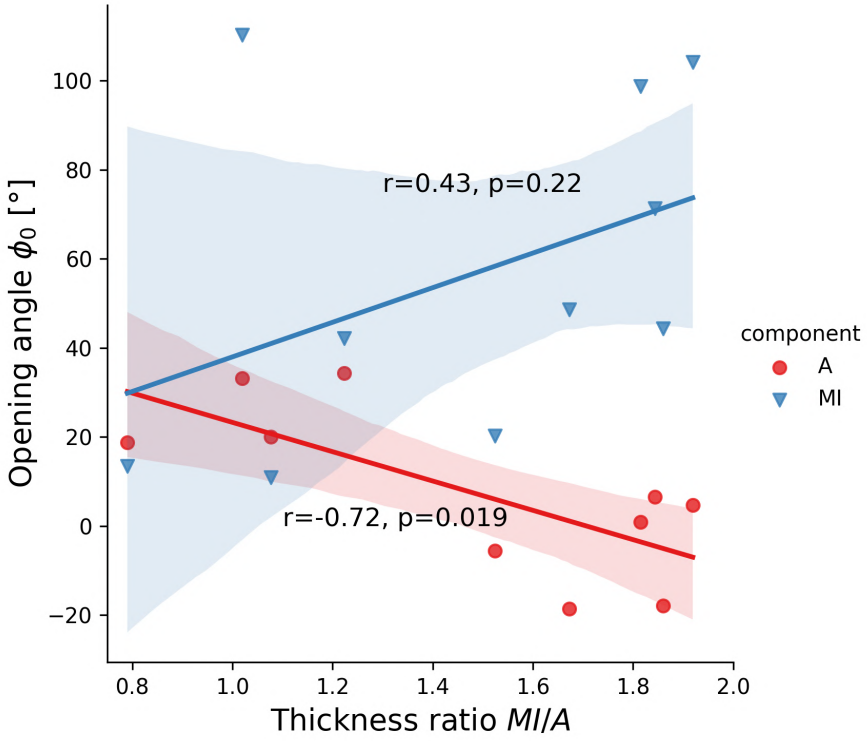

Figure H.8: Correlation between opening angle and ratio of thicknesses of MI/adventitia layers.

provide information about the whole wall, and thus the comparison is not made with the same specimen. Nevertheless, MI opening is much higher for experimental protocol 2 than for protocol 1, almost four times on average. The correlation (between thickness ratio and opening angle) was found statistically insignificant though some trend is apparent (r = 0.43, p = 0.22) and is opposite to that found for adventitia. This means that with decreasing portion of media, the opening decreases.

Axial strip

This initial study ran in parallel with the analysis of collagen fibre distribution, and the sample size was minimal. Thus it was impossible to obtain an axial strip for most of the samples, and the information is very limited. Both experimental protocols were performed for a single sample only (male 88 years). Additionally, partial information was observed for a sample of male 72 years. Results are shown in Table H.1. Adventitia revealed only negligible axial residual deformation and stayed straight (minimal curvature) for one patient (male 88) in both experimental protocols. The thickness ratio MI/adventitia was relatively, 2.11 and 1.65. However, the second patient (male 72) showed a high curvature and thus a significant bending for the adventitia axial strip. Unfortunately, the MI was ripped during separation, disabling a proper investigation of the thickness ratio. On the other hand, MI and the whole wall showed very high bending out of the vessel axis. Both situations can be seen in Figure H.7 D-F.

Table H.1: Summary table for axial residual deformation. All successfully performed tests are listed.

Experiment protocol 1

		κ_o	κ_i	t
Whole wall strip				
male 88	30 min	0.151	0.184	1.18
	16 hr	0.142	0.176	
male 72	30 min	0.145	0.184	1.12
	6 hr	0.155	0.197	
Adventitia				
male 88	separation	0.064	0.08	0.36
	6 hr	0.064	0.08	
male 72	separation	0.19	0.23	0.54
	6 hr	0.133	0.147	
Media + intima				
male 88	separation	0.163	0.186	0.76
	6 hr	0.164	0.184	

Experiment protocol 2

		κ_o	κ_i	t
Adventitia				
male 88	30 min	0.041	0.04	0.48
	16 hr	0.032	0.031	
	22 hr	0.005	0.001	
Media + intima				
male 88	30 min	0.113	0.13	0.79
	16 hr	0.114	0.131	
	22 hr	0.116	0.133	

H.1.3. Discussion

The knowledge of the mechanical behaviour of the arterial wall is essential for modelling of stresses in it. RS is generally accepted as an important factor, and its inclusion in computational models is often recommended. However, experimental evidence is minimal for specific layers of the carotid artery wall (the same applies to many others arteries). The

separation of the adventitia layer from the in principle multilayer media was performed in an experimental study Teng et al. (2009). The authors focused mainly on material strength and stress-strain characterization and mentioned some information about circumferential rings and axial strips. They did not quantify the residual deformation, e.g., by opening angle but provided only photo documentation within the article; therefore, no reasonable conclusions can be taken. The opening of the circumferential ring is mentioned for the whole wall, as well as the separated layers. One figure shows an opened adventitia segment while another figure shows zero opening. One can only speculate that they were facing similar behaviour to that reported in the present study. Moreover, it is unclear whether the figures were taken in the solution or in the air. The reported thickness of MI was 0.61 ± 0.21 mm and 0.6 ± 0.19 mm for adventitia. This indicates that a significant portion of media remained on the adventitia, thus possibly influencing the results.

A proper characterization of residual deformations of carotid wall layers was attempted in Sommer et al. (2010) who followed the experimental protocol from Holzapfel et al. (2007). The authors decided to present only curvatures without specifying the segment boundary they chose. It is therefore less accurate to compare or even represent the results. Nevertheless, it is clear that their results were also time-dependent, and, e.g., the adventitia ring showed closing (the curvature increased after 6 hr in the heated bath). The figures do not help much as the adventitia circumferential specimen is glued to a plastic cylinder (with diameter comparable to the inner wall diameter) on the inner surface, forcing thus opening and enlarging the fixed contact area. In such a configuration, the closing of the ring is impossible. Exciting results were mentioned for axial strips as the MI remains almost flat (mean curvature -0.014) while adventitia showed bending (mean curvature -0.125). The reported thicknesses were 0.47 ±0.07 mm for adventitia and 0.7 ±0.13 mm for MI, which is almost identical to measurements performed in the present study: adventitia - 0.49±0.09 mm, media - 0.73±0.13 mm. Interestingly, the authors stated that the separation of adventitia was perfect and confirmed by histology despite the Fig. 3 of that study showing comparable histological sections (comparability discussed with an experienced pathologist from St. Ann's Hospital) as the present study, see Figure H.1 D. To the best author's knowledge there is no other study mentioning residual deformations for carotid wall layers.

Our results indicate that the ratio between MI and adventitia (this can be extended to consider also intima layer if separable) is an important feature for opening angle measurement. An improper separation can influence the results, showing differences for the same type of artery as discussed above for carotid. Similar discrepancies can be seen among literature for other arteries too. Holzapfel et al. (2007) showed opening angle >180 deg (described only by a curvature) while Peña et al. (2021) published recently 40±20deg both for human abdominal aortic circumferential media ring. The influence of a proper separation can only be speculated, but the comparison in thicknesses can give a hint. Holzapfel et al. (2007) reported: adventitia - 0.41 ±0.12 mm, media - 0.59 ±0.1 mm and intima - 0.29 ±0.21 mm. On the other hand, Peña et al. (2021) reported: adventitia - 0.51 ±0.19 mm, media - 0.53 ±0.13 mm and intima - 0.13 ±0.02 mm. Unfortunately, a further comparison is disabled as one study represents the deformation only by the curvature while the other by the opening angle. Unification will be important to understand this problem well. It is advised to use more features than a single parameter that cannot be easily interpreted and especially compared with other studies.

The present study introduces preliminary results of the experimental investigation of residual deformation for human carotid artery layers. High differences were found between two experimental protocols with almost four times higher values for MI when the layer separation is done before the radial cut of the circumferential sample. An explanation of these differences represents a real challenge. Moreover, a surprising behaviour of adventitia was detected as the circumferential ring was closing rather than opening, as expected from the literature. Similar discrepancies were also found for the axial strip of adventitia, which mostly did not show any deformation and remained straight. An explanation of both of these findings was attempted by a correlation between the opening angle and a ratio of the thicknesses of MI and adventitia. Statistically significant (no generalization is intended due to low sample size) negative correlation indicates that imperfect separation might influence the residual deformation and should be thus well addressed in future studies.

I. Appendix

Layer-specific residual stress of carotid atherosclerotic plaque

Original research abstract accepted for presentation at Euromech Colloquium 627: Current challenges in soft tissue mechanics, 6-8 April 2022, Frankfurt

Layer-specific residual stress of carotid atherosclerotic plaque

Ondřej Lisický[1] & Jiří Burša[1]
[1]*Institute of Solid Mechanics, Mechatronics and Biomechanics, Brno University of Technology, Czech Republic. E-mail: 161238@vutbr.cz, bursa@fme.vutbr.cz*

Biomechanical models used for stress-strain analyses of arteries with atheroma may predict plaque rupture under mechanical loading, which is an important indicator of plaque vulnerability [1]. The input geometry of an artery is stress-free when residual stresses (RS) are released, and their incorporation may play a critical role in redistributing the stresses. A variety of approaches were introduced for arterial walls including 3D analytical distributions [2], closing the arterial segment via computational modelling [3] or volume growth [4]. The experimentally measured opening angle quantifies the amount of RS; as it differs among layers, it should be considered separately for each layer [2]. However, very limited information can be found on RS in atherosclerotic arteries. Experimental evidence was introduced for coronary arteries [3] where the radial cut released a relatively high opening angle of 118±35°. Afterwards, computational modelling was used to close the plaque showing a great impact on peak cap stress. It is important to note that both experiment and simulation were done with the whole arterial wall. In contrast, only small opening angles (see Figure 1 A) were observed in our experimental study of a large cohort of endarterectomy samples of carotid arteries [5]. It is therefore important to understand the influence of layer-specific RS when dealing with atherosclerotic tissue as the closing approach of the whole plaque with artery is often applied to introduce RS.

We studied the influence of layer-specific RS on peak cap stress using 2D idealized and patient-specific models. In the computational model, the RS were introduced through closing the segment with different opening angles and with specific hyperelastic material model obtained from the literature. The comparison was performed between the model with layer-specific RS and a configuration where adventitia, media and a plaque were closed together.

Results of this study indicate a very small impact of RS on peak cap stress when layer-specific RS are included, which reflects the negligible opening angle of the plaque and high openings of adventitia and media. On the other hand, opening the plaque together with other wall components by moderate opening angle leads to peak cap stress reduction in accordance with [2]. As the plaque growth is associated with accumulation of dead tissue, the reduction of RS in the plaque is tenable. These preliminary results show the contrast between these two approaches indicating that an unrealistic opening of the plaque might induce overestimated RS giving thus an overestimated risk of rupture.

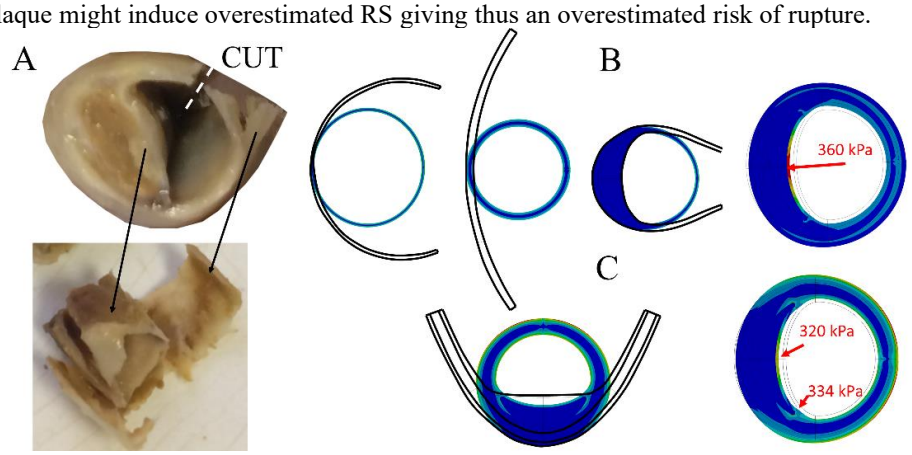

Figure 1. Endarterectomy sample cut during the intervention showing no opening (A). Layer-specific RS (B) and full wall RS (C).

References

[1] Holzapfel, G. A., et al. "Computational approaches for analyzing the mechanics of atherosclerotic plaques: a review." *J. Biomech*.47.4 (2014): 859-869.
[2] Holzapfel, G. A., and R. W. Ogden. "Modelling the layer-specific three-dimensional residual stresses in arteries, with an application to the human aorta." *J R Soc Interface* 7.46 (2010): 787-799.
[3] Ohayon, J., et al. "Influence of residual stress/strain on the biomechanical stability of vulnerable coronary plaques: potential impact for evaluating the risk of plaque rupture." *Am. J. Physiol. Heart Circ. Physiol. AM J PHYSIOL-HEART C* 293.3 (2007): H1987-H1996.
[4] Polzer, S., et al. "A numerical implementation to predict residual strains from the homogeneous stress hypothesis with application to abdominal aortic aneurysms." *Ann Biomed Eng* 41.7 (2013): 1516-1527.
[5] Lisický, O., et al. "Constitutive models and failure properties of fibrous tissues of carotid artery atheroma based on their uniaxial testing." *J. Biomech* 129 (2021): 110861.

Acknowledgement: The work has been supported by the grant project GACR No. 21-21935S.